ICE, CLOUD, and Land Elevation Satellite - 2 (ICESat-2) Project

Algorithm Theoretical Basis Document (ATBD) for Global Geolocated Photons

ATL03

Prepared By:

Tom Neumann, NASA GSFC/Code 615
Anita Brenner, NASA GSFC/Code 615
David Hancock, NASA GSFC WFF/Code 615
John Robbins, NASA GSFC/Code 615
Jack Saba, NASA GSFC/Code 615
Kaitlin Harbeck, NASA GSFC/Code 615

Goddard Space Flight Center
Greenbelt, Maryland

National Aeronautics and Space Administration

Abstract

CM Foreword

This document is an Ice, Cloud, and Land Elevation Satellite- 2 (ICESat-2) Project Science Office controlled document. Changes to this document require prior approval of the Science Development Team ATBD Lead or designee. Proposed changes shall be submitted in the ICESat-2 Management Information System (MIS) via a Signature Controlled Request (SCoRe), along with supportive material justifying the proposed change.

In this document, a requirement is identified by "shall," a good practice by "should," permission by "may" or "can," expectation by "will," and descriptive material by "is."

Questions or comments concerning this document should be addressed to:

ICESat-2 Project Science Office
Mail Stop 615
Goddard Space Flight Center
Greenbelt, Maryland 20771

Preface

This document is the Algorithm Theoretical Basis Document for the TBD processing to be implemented at the ICESat-2 Science Investigator-led Processing System (SIPS). The SIPS supports the ATLAS (Advance Topographic Laser Altimeter System) instrument on the ICESat-2 spacecraft and encompasses the ATLAS Science Algorithm Software (ASAS) and the Scheduling and Data Management System (SDMS). The science algorithm software will produce Level 0 through Level 4 standard data products as well as the associated product quality assessments and metadata information.

The ICESat-2 Science Development Team, in support of the ICESat-2 Project Science Office (PSO), assumes responsibility for this document and updates it, as required, as algorithms are refined or to meet the needs of the ICESat-2 SIPS. Reviews of this document are performed when appropriate and as needed updates to this document are made. Changes to this document will be made by complete revision.

Changes to this document require prior approval of the Change Authority listed on the signature page. Proposed changes shall be submitted to the ICESat-2 PSO, along with supportive material justifying the proposed change.

Questions or comments concerning this document should be addressed to:

Thorsten Markus, ICESat-2 Project Scientist
Mail Stop 615
Goddard Space Flight Center
Greenbelt, Maryland 20771

Review/Approval Page

Prepared by:

Thomas Neumann
Deputy Project Scientist, ICESat-2
NASA-GSFC, Code 615

Reviewed by:

Alex Gardner
NASA Jet Propulsion Laboratory

Name
<Enter Position Title Here>
<Enter Org/Code Here>

Approved by:

Name
<Enter Position Title Here>
<Enter Org/Code Here>

***** Signatures are available on-line at:** https:// /icesatiimis.gsfc.nasa.gov ***

Change History Log

Revision Level	Description of Change	SCoRe No.	Date Approved
1.0	Initial Release		

List of TBDs/TBRs

Item No.	Location	Summary	Ind./Org.	Due Date

Table of Contents

List of Figures

List of Tables

1.0 INTRODUCTION

This section provides an introduction to the ICESat-2 mission, the measurement concept of its sole instrument (ATLAS, the Advanced Topographic Laser Altimeter System), and the family of ICESat-2 data products.

1.1 Background

The ICESat-2 observatory and ATLAS instrument use a photon-counting lidar and ancillary systems (i.e. GPS and star cameras) to make three primary measurements: the time of flight of a photon from ATLAS, to the Earth, and back to ATLAS; the pointing vector at the time a photon is transmitted by ATLAS; and the position of ICESat-2 in space at the time a photon is recorded by ATLAS. This measurement approach is fundamentally different from a full-waveform lidar system (such as the 1064-nm GLAS instrument on ICESat). The ATLAS instrument transmits green (532-nm) laser pulses at 10 kHz; the ICESat-2 nominal ~500-km frozen orbit altitude yields one transmitted laser pulse every ~0.7 meter along ground tracks. Each transmitted laser pulse is split by a diffractive optical element in ATLAS to generate six individual beams, arranged in three pairs (Figure 1-1). The beams within each pair have different transmit energies ('weak' and 'strong,' with an energy ratio between them of approximately 1:4) and are separated by 90 meters in the across-track direction. The beam pairs are separated by ~3.3 kilometers in the across-track direction, and the strong and weak beams are separated by ~2.5 kilometers in the along-track direction. Figure 1-1 shows the idealized beam and footprint pattern for ICESat-2.

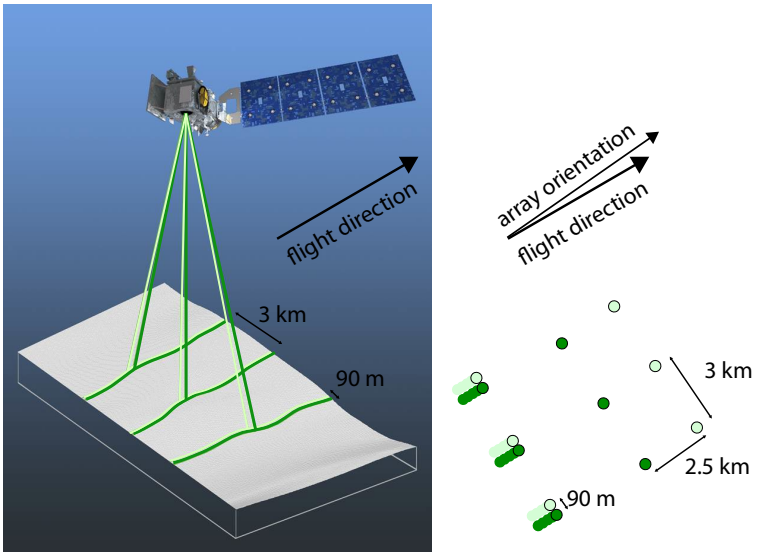

Figure 1-1. ATLAS Idealized Beam and Footprint Pattern.

The left panel (Figure 1-1) shows the beam pattern for ICESat-2, while the right panel shows the instantaneous footprint pattern generated by each transmitted laser pulse from ATLAS. Light green circles indicate footprints from the relatively low energy (weak) beams, while the dark

green circles indicate footprints from the relatively high-energy (strong) beams. As the observatory moves in the along-track direction, the aggregation of overlapping footprints form a ground track on the Earth's surface.

Approximately 10^{14} photons begin the journey from ATLAS, travelling through the atmosphere to reflect off the Earth's surface, return through the atmosphere and back into the ATLAS telescope. Of these, up to ten photons complete the journey and are recorded by the instrument electronics.

For highly reflective surfaces and clear skies, on the order of ten signal photons from a single strong beam are expected to be recorded by ATLAS for a given transmit laser pulse. At the same time, background photons from sunlight at the same 532-nm wavelength may be arriving at the detector, and some of them will also be recorded by ATLAS. Any photon that ATLAS records an arrival time for is called a photon event, regardless of the source of the photon. The number of photon events recorded by ATLAS depends on the geometry and reflectance of the Earth's surface, solar conditions, and on scattering and attenuation in the atmosphere. The number of returned photon events varies from near zero photon events per shot over very dark non-reflective surfaces, up to twelve photon events per shot over very reflective surfaces.

In order to reduce the volume of data downlinked to Earth, ICESat-2 uses on-board flight software to identify and downlink data on those photon events most likely to represent returned photons from the laser pulse while also providing data on the atmospheric conditions. Given the 10-kHz laser pulse repetition rate, there are many transmitted laser pulses en route to and from Earth at any point in time. Transmitted laser pulses are separated in flight by ~30 kilometers in one-way travel. As such, there is an inherent height ambiguity of ~15 kilometers in received photon events. Consequently, ICESat-2 can only characterize the lowest ~15 kilometers of the Earth's atmosphere. The on-board software counts photon events and generates a histogram spanning the lowest ~14 kilometers of the atmosphere with 30-m vertical bins. These atmospheric histograms aggregate the number of photon events over four hundred consecutive laser transmit pulses (an atmospheric histogram is generated every 0.04 seconds, spanning 280 meters of along-track distance). Atmospheric histograms are downlinked for the three strong ATLAS beams.

The volume and rate of photon events is large enough that ATLAS cannot assign unique time tags to every received photon event and downlink the relevant information. Instead, the flight software sets a range window of at least 500 meters and not more than 6,000 meters within which detected photons are time tagged and become photon events. The width of the window primarily depends on the surface type (e.g. ocean, land ice, land) as well as the topography (Leigh et al., 2014). Within the range window, ATLAS attaches time tags for received photons and generates altimetric histograms. The on-board software uses these histograms to identify the surface and specify which photon event data are downlinked to Earth for each beam. The band of photon time tags downlinked to Earth is called the telemetry band. The width of the telemetry band of each beam is potentially different, and is described fully in the *ATLAS Science Receiver Algorithm Description* document.

The ATL02 ATBD contains additional details on how photon times of flight are calculated. The pointing vector and observatory position in space are described by the ATBDs for Precision Pointing Determination (PPD; document_number_here), and Precision Orbit Determination (POD; document_number_here), respectively.

While the lower-level data products typically work with individual photon events, higher-level geophysical data products work with aggregations of photons in order to determine the ellipsoidal height of the Earth, canopy height and structure, and other quantities of geophysical interest. To learn more about these higher-level data products, refer to their ATBDs.

1.2 Data Product Overview

The family of ICESat-2 data products and the connections between them are shown in Figure 1-2. The ATL01 algorithm reformats and unpacks the Level 0 data from ICESat-2, then converts it into engineering units. The ATL02 processing applies instrument corrections to these data. For example, photon event time tags are corrected for the effects of temperature and voltage variations on the ATLAS electronics, and biases are removed from timing and pointing measurements. The Precision Orbit Determination and Precision Pointing Determination use data from ATL02 to determine the position of the ICESat-2 observatory as a function of time and the pointing vector of the observatory as a function of time.

ATL03 combines the data products of POD, PPD, and ATL02 to produce a Level 2 product containing geolocated ellipsoidal heights for each time tagged photon event downlinked from ATLAS. These heights are corrected for several geophysical phenomena (e.g. atmospheric refraction, tides) and are classified either as likely signal photon events or likely background photon events.

Atmospheric data products draw the raw atmospheric profiles for each strong beam from ATL02. ATL04 provides normalized relative backscatter profiles and ATL09 produces calibrated backscatter profiles, atmospheric layer heights, and related atmospheric parameters.

All Level 3A data products draw from the geolocated photon heights in ATL03 and the atmospheric parameters from ATL09. Along-track land ice ellipsoidal heights are provided in ATL06, along-track sea ice and polar ocean heights are provided in ATL07, and along-track terrestrial ellipsoidal height and related metrics for vegetation heights are provided in ATL08. Sea ice freeboard for the Arctic and Antarctic seas and associated parameters are in ATL10. Ocean heights are provided in ATL12, while inland water heights are in ATL13.

Level 3B data products are gridded products, drawing from the along-track products of Level 3A. ATL11, 14, and 15 are gridded land ice products corresponding to land ice height time series, annually gridded land ice heights, and gridded land ice height change. Sea ice gridded data for the Arctic and Antarctic are provided in ATL20 and 21, respectively. Gridded terrestrial data is provided in ATL16 while the gridded mean sea surface heights are in ATL19. Lastly, weekly and monthly gridded atmospheric data products are provided in ATL16 and 17.

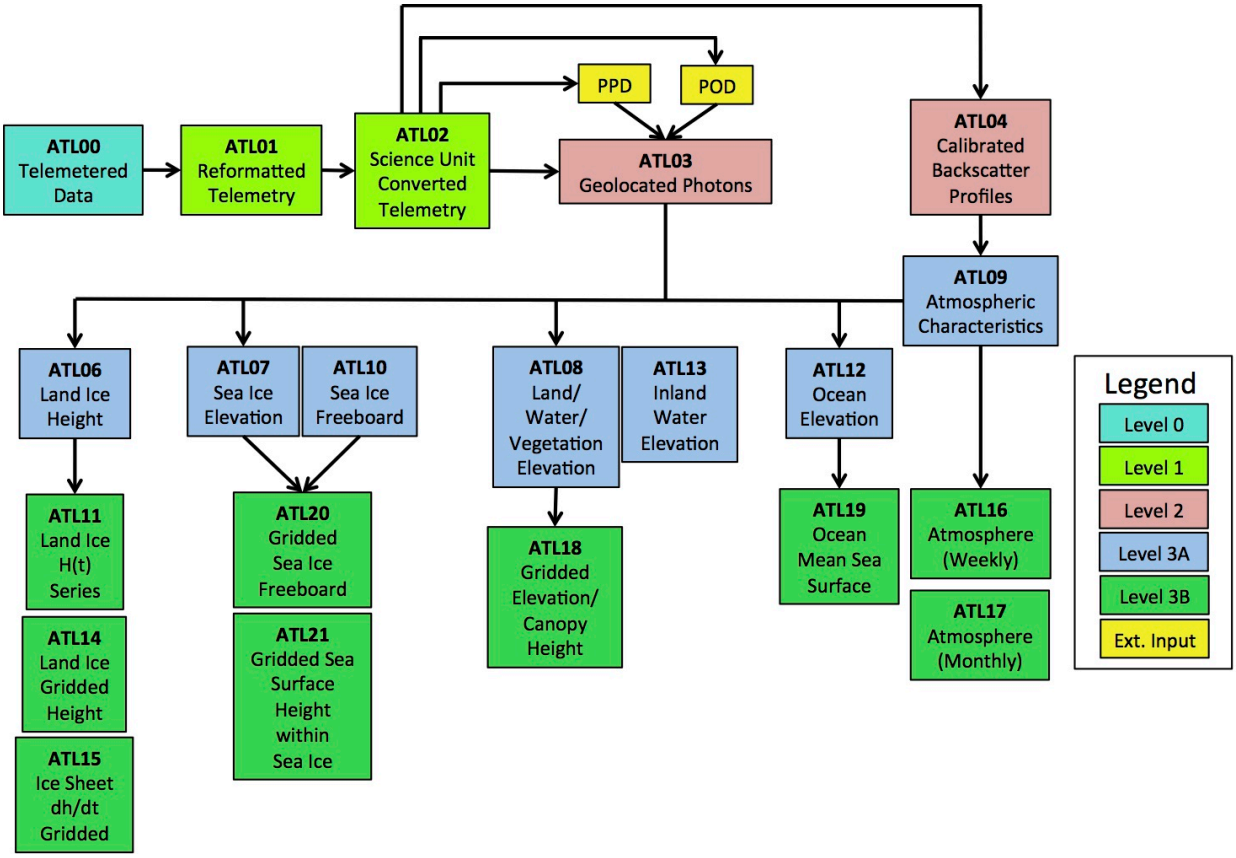

Figure 1-2. ICESat-2 Data Processing Flow.

Figure 1-2 shows the flow of ICESat-2 data from lowest to highest level of processing. The color indicates data product levels, while the text reports data product number and short name. All products (ATLxx) are generated by the Science Investigator-led Processing System (SIPS), and distributed by the National Snow and Ice Data Center (NSIDC).

2.0 ATL03 OVERVIEW AND DATA STRUCTURE

2.1 ATL03 Overview

The simplest way to describe the ATL03 data product is that it provides time, latitude, longitude, and height for each photon that ICESat-2 downlinks. The ATL03 product is the bridge between the lower level, instrumentation-specific products (ATL01/02) and the higher-level, surface-specific, science-centric products (ATL06 and above). By design, ATL03 provides a single source for all photon information needed by higher-level products (the corresponding atmospheric science Level-2 product ATL09 also feeds all the higher-level products; Figure 1-2).

Each of the surface-specific, higher-level data products, such as land ice height or sea ice freeboard, will use the geolocated signal photon events and ancillary data provided in the ATL03 product. Consequently, ATL03 provides five surface masks (land ice, sea ice, ocean, land, and inland water) to reduce the volume of data that each surface-specific along-track data product is required to process.

In addition, ATL03 classifies each photon event as either a likely signal photon event or a background photon event and provides a confidence assessment on these classifications. This classification is made by generating histograms of the number of photon events as a function of height and calculating the signal-to-noise ratio of each histogram bin. Those photon events in bins with a signal-to-noise ratio greater than a threshold are classified as signal, while other photon events are classified as background.

ATL03 applies multiple geophysical corrections to provide corrected heights for all the downlinked photon events. These corrections include the effects of the atmosphere, as well as tides and solid earth deformation. By design, each of these corrections can easily be removed by the end user from the ATL03 data products if desired. By default, they are applied to generate a best estimate of the photon height.

Lastly, ATL03 provides all other spacecraft or instrument information needed by the higher-level data products. For example, the algorithms for sea ice height and ocean height require some knowledge of the ATLAS transmitted pulse shape or the ATLAS impulse-response function. While not explicitly needed to generate the ATL03 data product, the parameters are included in the ATL03 product files to provide a single source for all subsequent data products.

ATL03 uses the product from ATL02 and the POD and PPD processes to create its output. The surface masks and geophysical corrections require a number of models and data products that have been assembled with the participation of the science community.

The output from ATL03 is described in this document, and is listed as Appendix A.

All ICESat-2 data products, including ATL03, are provided as HDF5 files (https://earthdata.nasa.gov/standards/hdf5). This file format allows similar parameters (such as instrument parameters, altimetry data, metadata, etc.) to be grouped together, and simplifies the organization of the data. The ATL03 data product is segmented into granules that each span about 1/14th of an orbit.

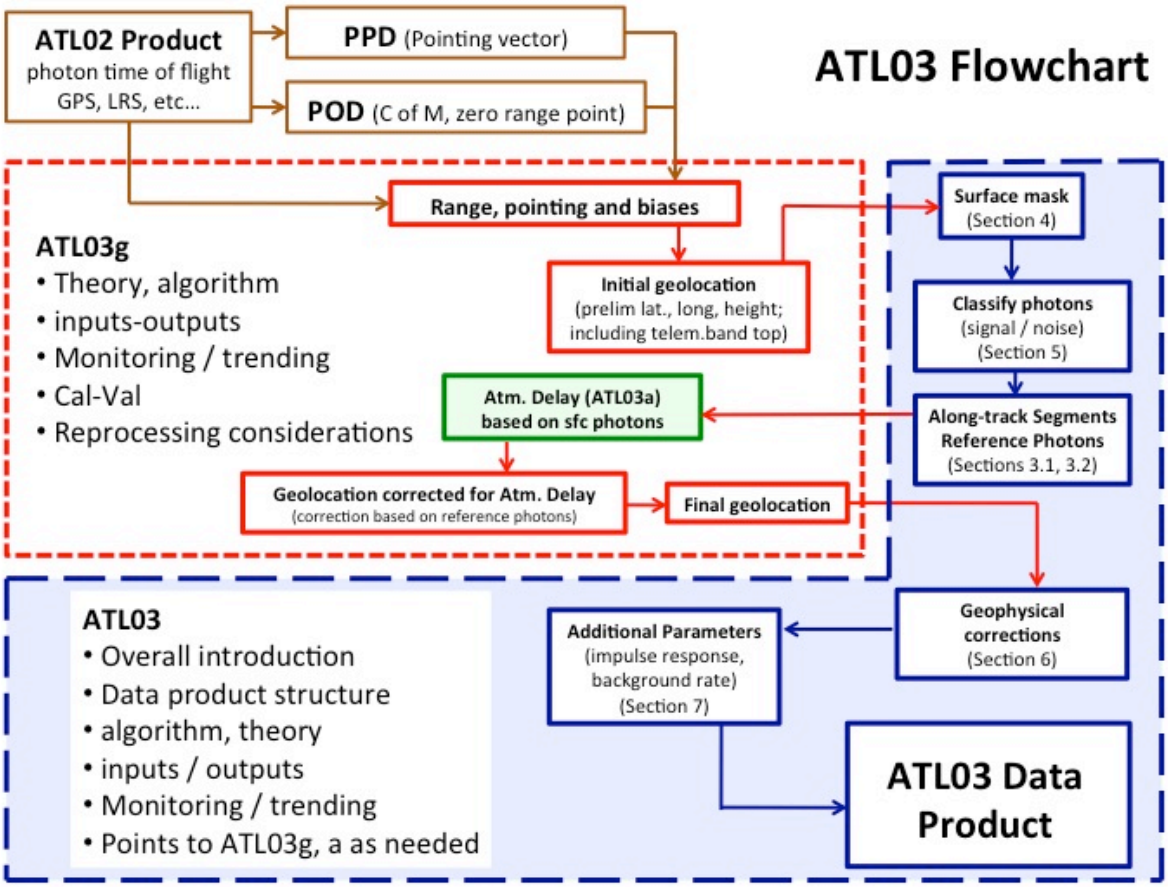

Figure 2-1. Flowchart for ATL03.

The overall ATL03 data product is described by three documents. ATL03g (elements enclosed with the red dashes) describes the process of geolocation and is summarized in section 3.0. The atmospheric delay correction is described in ATL03a (outlined in green). The elements enclosed by the blue dashes are described in this document, with the section numbers indicated.

2.2 Data Flow Within ATL03

As discussed above, the overall ATL03 process takes input from ATL02, POD, PPD and related Ancillary Files, and ultimately provides the parameters listed in Appendix A (the ATL03 data output table). Note that ATL03 and subsequent data products are only routinely generated when ATLAS is operating nominally. At all other times, ATL02 is the final data product produced. Strictly speaking, ATL03 is generated whenever the Photon Counting Electronics mode is set to 'science' (PCEx_PMF_Hk pmfmode=science) at any point within a potential ATL03 granule and laser transmit time information is available in these same periods of time. Additionally, ATL03 is generated only when all necessary pieces (ATL02, POD, PPD, and related ANC files) are available. If any of these are missing, ATL03 and higher-level products are not generated. Also note that this data flow only applies to non-transmitter echo pulse (TEP) photon

events: TEP photon events are stored in their own group on the ATL02 data product. When ATL03 is generated, Figure 2-1 provides a high-level overview of the major elements of the data flow for received photon events to produce the ATL03 data product.

The ICESat-2 geolocation along-track segment boundaries (sometimes called the ICESat-2 grid, ICESat-2 Geolocation bins, or geosegs) are described in section 3.1. This section defines a grid of points aligned with each of the 1,387 reference ground tracks (RGT) of the ICESat-2 mission. It provides a means to determine an along- and across-track distance for any point, given a latitude, longitude, and RGT number.

The PPD ATBD describes the algorithms used to determine the observatory pointing solution as a function of time, given ATL02 parameters as input. The POD ATBD describes the algorithms used to determine the position of the center of mass of the observatory as a function of time.

The primary inputs to ATL03g (functionally collected in the dashed red box in Figure 2-1) is the photon time of flight from ATL02 for each telemetered photon event, the pointing vector from PPD and the position of the observatory center of mass from POD. ATL03g uses these inputs and determines a preliminary latitude, longitude, and height above the ellipsoid for each photon in steps 1 through 7 of ATL03g, section 3.1.

In addition, ATL03g estimates the range bias for each beam, which is stored for additional analysis. The range bias estimates are used to potentially update the beam-specific time of flight biases applied in ATL02. ATL03g also estimates the pointing angle biases for each beam. These pointing angle biases are used in ATL03g and folded into a revised pointing solution.

Along with the telemetered photon events, there are a number of other parameters that also require geolocation (section 3.3). The most important is the location of the top of the telemetry bands. The telemetry band tops and widths can change every two hundred shots (often called the major frame rate) and is useful to several subsequent steps in ATL03 and higher-level products. Consequently, the range to the top of the telemetry band is treated just like a received photon event and is geolocated along with the rest of the photon events.

The preliminary ellipsoidal heights from ATL03g are then used to determine the surface type (section 4.0) of a given ground track. The surface type masks are provided at 0.05 x 0.05 degree resolution (or ~5-km resolution). Furthermore, the masks include buffer and overlap between surface types. Consequently, it is not necessary to determine the surface type of every photon individually. We use the latitude and longitude of the tops of the telemetry bands (provided at the major frame rate; every two hundred shots) as the basis to determine surface type along the granule. In the event that a particular major frame has more the one telemetry band, we assign the surface type based on the first telemetry band.

The resulting surface types and preliminary ellipsoidal heights are then passed to the signal-finding algorithm described in section 5.0. The main outputs of this algorithm are a classification for all photon events between likely background photon events and likely signal photon events (with low, medium, and high confidence). The resulting photon event classifications are then stored.

All photon events are assigned to one of the ICESat-2 geolocation along-track segments following the process described in section 3.1. The goal of this step is to discretize the cloud of photon events into a coarser group to facilitate the final geolocation step. After the photons are grouped into these segments, a reference photon for each along-track segment is identified in section 3.2. These are drawn from the signal photons (if any are present) following a heirarchical process. While the step of assigning photon events to a specific segment can be done in parallel with the photon event classification, section 3.2, Selecting the Reference Photon, requires the output from both section 3.1, The ICESat-2 Geolocation Along-Track Segments, and section 5.0, Photon Classification.

Once the reference photons have been selected, ATL03g determines the final geolocation for each photon and the associated atmospheric delays. These steps are described in step 9 of ATL03g, section 3.1 and following. This process determines the exact bounce point of the reference photons, and applies the neutral atmosphere range delay correction to all photons, yielding the best estimates of the latitude, longitude, and ellipsoidal height of every telemetered photon event along with the measurement uncertainties of these parameters.

After the geolocation process is complete, additional corrections are applied to the photon ellipsoidal heights in section 6.0, where other geophysical corrections (e.g. tides) are accounted for.

Lastly, other parameters needed by higher-level geophysical products are determined (e.g. ATLAS impulse response) in section 7.0 and added to the ATL03 output data product.

2.3 ATL03 ATBD Sections

Calculation of the latitude, longitude, and ellipsoidal height of each returned photon requires an algorithm for geolocation – the location of a given photon with respect to the surface of the Earth. The atmospheric path delay and the geolocation algorithm are described in a separate ATBD. Atmospheric path delay includes tropospheric refraction, discussed in ATL03a. The geolocation algorithm, discussed in ATL03g, draws from three sources: the ATL02 data product, the PPD pointing vector of the ATLAS boresite, and the spacecraft position relative to the Earth from the POD process.

Section 3.0 describes other issues related to geolocation, but not included in ATL03g. Namely, the ICESat-2 Geolocation along-track segments (sometimes called gelocation bins, or geolocation segments) is discussed in section 3.1 along with the algorithm to assign each photon to a segment. Section 3.2 describes how reference photons for each along-track segment that contains photons are selected, and section 3.3 describes other parameters that are also geolocated (namely, the top of the photon downlink or telemetry band).

Section 4.0 describes the surface masks used to assign each photon to one or more surface types. ATL03 defines five surface types (land ice, sea ice, land, ocean, inland water) that collectively cover the surface of the Earth. This designation provides guidance to some aspects of the photon classification algorithm (section 5.0) and guides high-level data products to the ATL03 data of interest. There is an overlap of approximately ten kilometers between adjacent surface

classifications, and therefore some regions on the Earth have multiple surface classifications. For example, areas along the edges of the Arctic Ocean will be classified as sea ice and land.

Section 5.0 describes the photon classification algorithm. This algorithm classifies each geolocated photon event as being a likely signal photon event or a background photon event. This designation can be used by higher-level data products to further reduce the data volume considered by that algorithm. The guiding philosophy of the photon classification algorithm is to avoid false negatives (i.e. signal photon events misclassified as background) at the expense of including false positives (i.e. background photon events misclassified as signal). This classification algorithm also generates a parameter to identify the degree of confidence in designating a particular photon event as signal or background.

Section 6.0 describes the geophysical corrections applied to the ATL03 data product, such as solid earth tides or dynamic ocean topographic corrections. The atmospheric refraction correction, being an integral aspect of the geolocation process, is described in detail in ATL03a. The sources of all corrections are identified here, along with their measurement uncertainties. The corrections are provided on the ATL03 product so end users can replace them, if desired. Care has been taken to ensure that the geophysical corrections and models described in section 6.0 are the same ones used during the POD process.

Section 7.0 describes parameters that are not used by ATL03, but are required by one or more higher-level data products. ATL03 provides two such parameters: the ATLAS impulse-response function, and the total count of photons time-tagged by the ATLAS instrument. Several of the higher-level data products (e.g. ATL07) use a deconvolution approach to determine the precise ellipsoidal heights of the Earth's surface by deconvolving instrument effects from the returned distribution of photons. While, in general, the time-dependent ATLAS instrument-response function is not known on orbit, this document presents an algorithm for estimating this function. In addition, several higher-level data products require an estimate of the solar background rate of photons. The photon classification in ATL03 relies on histograms of photon returns from the atmospheric colum generated and used onboard by the ground-finding algorithm. The smaller downlinked photon bandwidth (telemetry bandwidth) is generally not sufficient to generate a robust esimtate of the background count rate, but can be used if the atmospheric histograms are not available.

Section 8.0 describes data quality and browse products.

Section 9.0 contains pre-launch test data and results from the ATL03 algorithm.

Section 10.0 describes ATL03 constraints, limitations, and assumptions.

Section 11.0 summarizes the metadata groups in the ATL03 data product.

The appendices contain the table of inputs and outputs for ATL03, and the ICESat-2 ATBD lexicon, which aims to define the most commonly used terms within the ATBDs.

2.4 ATL03 Data Structure for Each Ground Track

In accordance with the HDF-driven structure of the ICESat-2 products, the top level 'Group' provides the syntax and structure for all the elements of the ATL03 product. Subsequent subsections of the ATL03 data product will characterize each of the six ground tracks associated with each reference ground track for each cycle and orbit number (see Appendix C – ATBD Lexicon). Each ground track has a different beam number and distance from the reference track, but all beams will be processed using the same sequence of steps within ATL03, except where noted otherwise. The subsections below summarize the parameters contained within each group and subgroup of the ATL03 product. The ATL03 output data product table is provided in Appendix A.

Along-track time in each group is provided by a parameter called delta_time. A user can convert to full GPS time by adding the gps_time_offset parameter found in the metadata. This common time base is based on the laser transmit times, and allows parameters at potentially different rates to be co-aligned across groups. An additional parameter (bounce_time_offset) in the geolocation group provides the time offset, at the along-track segment rate, from the transmit time, to the ground bounce point time of a reference photon. This number will usually be around 1.5 milliseconds (a result of the nominal ~500-km orbit altitude and the speed of light), and allows the user to determine the time of day a photon bounced on the surface of the Earth to an accuracy of less than 1 millisecond.

2.4.1 Group: /gtx

Each group contains the parameters for one of the six ATLAS ground tracks. As ICESat-2 orbits the Earth during science operations, sequential transmitted laser pulses illuminate six ground tracks on the surface of the Earth. All six of the ground tracks are associated with a single reference ground track. The track width for each ground track is approximately 14 meters, equal to the ATLAS footprint diameter. Each ground track is numbered according to the pattern of tracks on the ground from left to right (GT1L, GT1R, GT2L, GT2R, GT3L, GT3R, abbreviated as GTx). The labeling was chosen such that the beam names do not change when the observatory orientation changes. Consequently, the relationship between beam energy (or ATLAS spot number) and ground track name requires knowledge of the observatory orientation parameter. See Appendix C, ATBD Lexicon, for further description of these terms. Owing to HDF convention, group and parameter names are not capitalized. The parameters in the associated subgroups are described below.

2.4.1.1 Group: /gtx/heights

This group provides all parameters that are provided at the photon rate – i.e. at the rate of one value per photon for a given ground track. Examples are the ellipsoidal height, latitude, longitude, and confidence parameter for a given photon. The height, latitude, and longitude are based on the geolocation algorithm described in more detail in the ATL03g ATBD. This height includes all instrument corrections applied to the ATL02 product in addition to the geophysical

corrections described in section 6.0. By design, the geophysical corrections can be easily removed, if desired.

2.4.1.2 Group: /gtx/geolocation

This subgroup contains the outputs of the signal finding algorithm that are not provided at the photon rate, such as information related to the time interval boundaries along-track that were used to identify signal photons, or the mean and standard deviation of the background count rate used to determine thresholds for signal identification. These parameters are detailed in section 5.3, and are also described in Table 5-4.

2.4.1.2.1 Group: /gtx/geolocation/start_pulse_det

These parameters are based of data from the ATLAS start pulse detector (SPD). The SPD provides a measure of the transmitted laser energy (at 10 Hz) as well the times outgoing laser pulses crossed specific energy thresholds. These threshold crossing times provide information on the transmitted pulse shape through time. The parameters are described in section 7.1 and are provided at the along-track segment rate (~20 meters).

2.4.1.3 Group: /gtx/geophys_corr

These parameters include the best-available corrections for known geophysical phenomena that will impact ICESat-2 ellipsoidal heights of returned photons. Values for tides (ocean, solid earth, pole, load, and equilibrium), inverted barometer (IB) effects (aka dynamic atmospheric correction (DAC)), and range corrections for tropospheric delays all need to be applied with appropriate temporal and spatial resolution. These corrections are applied to the data and are included in this subgroup to allow an end user to individually remove or replace one or more of them, if desired. These parameters are all at the reference photon rate (~20 meters along-track) and are defined in section 6.0.

2.4.1.4 Group: /gtx/bckgrd_atlas

This group contains parameters to calculate the background photon rate recorded by ATLAS. The on-board software generates the altimetric histogram, which is used to determine the telemetry band of downlinked photon data (McGarry et al., 2015; Leigh et al., 2014). The altimetric histogram contains all received photon events within the altimetric (or range) window. This group contains the sum and height of the altimetric histogram (reported at 200 Hz or every 0.005 seconds) for a given ground track (or ATLAS beam; related through the orientation parameter). This group contains parameters derived from the atlimetric histogram, and related parameters from the telemetry or downlink band. These parameters are described in section 7.3, and are all posted at the 200-Hz rate.

2.4.1.5 Group: /gtx/photon_classification_output

This subgroup contains the outputs of the signal finding algorithm that are not provided at the photon rate, such as information related to the time interval boundaries along-track that were used to identify signal photons, or the mean and standard deviation of the background count rate used to determine thresholds for signal identification. These parameters are detailed in section 5.3, and are also described in Table 5-4.

2.4.2 Group: /atlas_impulse_response

Several of the higher-level data products use a deconvolution approach to further refine selection of signal photons and reject background photons. These algorithms require knowledge of the ATLAS instrument response over their algorithms' along-track aggregation distance. While the pulse spreading effects of the ATLAS instrument are expected to change slowly over time, changes in the outgoing laser pulse shape are likely to vary over shorter timescales. In the two subgroups, we provide parameters from two different sources to evaluate change in the ATLAS impulse response function.

2.4.2.1 /atlas_impulse_response/pce1_spot1 or /pce2_spot3

The second group of parameters are derived from photon events detected via the transmitter echo path (TEP). These photons are picked off from the transmitted laser pulse, and routed into the ATLAS receiver, for two of the ATLAS strong beams. These data provide a means to monitor the internal timing bias of ATLAS, as well as the instrument impulse response for beams with the TEP data. The parameters are generated as often as sufficient TEP data exists in the granule (typically occurs about every five granules or so); otherwise data from the prior granule is retained in the current granule. In addition to single-valued parameters, a histogram of the TEP photons are provided and the TEP photon event arrival times are also provided in tep_hist_times, so that a user can conduct their own analysis of the tep arrival times. These parameters are described in section 7.2.

2.4.3 Group: /ancillary_data/atlas_engineering

This group contains parameters primarily from ATL02 that provide insight into the ATLAS transmit pulse, receiver and other ATLAS parameters needed for higher-level data products.

2.4.3.1 Group: /ancillary_data/atlas_engineering/transmit

This group contains parameters related to the ATLAS transmitter, including the laser, transmit optics and the like. These parameters are generally passed from ATL02 to ATL03 and so are defined in detail in the ATL02 ATBD.

2.4.3.2 Group: /ancillary_data/atlas_engineering/receiver

Similarly, this group contains parameters related to the ATLAS receiver, such as metrics for the receiver sensitivity. These parameters are generally passed from ATL02 to ATL03 and so are defined in detail in the ATL02 ATBD.

2.4.4 Group: /ancillary_data/calibrations

This group contains information about the ATLAS calibrations data products that are necessary for the generation of upper-level data products. Many of these products were generated using pre-launch test dat and ground support equipment that are not available with on-orbit operations. Where possible, calibration products are updated on orbit. Each product is in it's own subgroup and the values of the parameters are valid for the time spanned by the granule. These calibrations are described in section 7.6 and subsections thereof.

2.4.5 Group: /ancillary_data/tep

This group contains parameters related to the ATLAS transmitter echo path, or TEP. The TEP is an optical path that provides a means to calibrate ATLAS time of flight internally, and is described in detail in ATL02. Briefly, photons following the optical path of the TEP begin at the laser, travels to the laser sampling assembly where part of the transmitted laser pulse is sampled, and then via a fiber optic cable to the optical filter assembly to the detector array assembly. Two of the three ATLAS strong spots have TEP photons available; parameters derived form these photons are valid for the duration of the ATL03 granule. For a more thorough description of the TEP, see section 7.2.2, or the ATL02 ATBD.

2.4.6 Group: /ancillary_data/gtx/signal_find_input

This group contains the setup parameters for the signal finding algorithm (Table 5-2 in section 5.3). Several parameters are common to all ground tracks, although the values for many of these parameters are laser energy dependent (strong vs. weak) and surface-type dependent, and so will be ground track-specific. They are provided once per granule to allow an unambiguous connection between the output of the signal finding algorithm (captured in the group /gtx/photon_classification_output) and the parameters that were used for a given granule.

2.4.7 Group: /orbit_info

This group contains parameters that are constant for a granule, such as the RGT number and cycle, the spacecraft orientation, and a handful of ATLAS parameters that are needed by higher-level data products.

2.4.8 Group: Quality Assessment

This group contains quality assessment data. This may include QA counters, QA along-track data, or QA summary data.

2.4.8.1 Group: Quality Assessment, Along-Track

This group contains parameters for the assessment of the ATL03 along-track data products.

2.4.8.2 Group: Quality Assessment, Packet Count

This group contains statistics on packet counts within a given ATL03 granule.

2.4.8.3 Group: Quality Assessment, Summary

This group contains a summary of data quality assessment.

2.4.9 Group: Metadata

Summarizes the metadata for the ATL03 product. The metadata will contain human-readable, grouped HDF5 attributes with sufficient content to generate the required ISO19319 XML representation of ISO19115.

2.5 ATL03 Granules

ATL03 granules contain some distance of along-track data, formatted as described in appendix A. One orbit of data is broken up into 14 granules. The granule boundaries (or granule regions) limit the granule size (less than 4 GB) and where possible simplify the formation of higher level data products by limiting the number of granules needed to form a particular higher level product. Granule boundaries are along lines of latitude and are depicted in figure X, and described below.

Region 1 extends from the ascending node equatiorial crossing to 27 degrees north latitude along ascending tracks. This region includes all along-track geolocation segments (section 3) that are entirely south of 27 degrees north latitude.

Region 2 extends from 27 degrees to 59.5 degrees north latitude along ascending tracks. This region includes all along-track geolocation segments (section 3) that span the line of 27 degrees north latitude (i.e. follow sequentially after those geolocation segments in region 1) and are entirely south of 59.5 degrees north latitude.

Region 3 extends from 59.5 degrees to 80 degrees north latitude along ascending tracks. This region includes all along-track geolocation segments (section 3) that span the line of 59.5 degrees north latitude (i.e. follow sequentially after those geolocation segments in region 2) and are entirely south of 80 degrees north latitude.

Region 4 extends from 80 degrees north latitude along ascending tracks to 80 degrees north latitude on the descending track after passing over the northernmost limit of the orbit. This region includes all along-track geolocation segments (section 3) that span the line of 80 degrees north latitude (i.e. follow sequentially after those geolocation segments in region 3) and are entirely north of 80 degrees north latitude on the descending track.

Region 5 extends from 80 degrees to 59.5 degrees north latitude along descending tracks. This region includes all along-track geolocation segments (section 3) that span the line of 80 degrees north latitude (i.e. follow sequentially after those geolocation segments in region 4) and are entirely north of 59.5 degrees north latitude.

Region 6 extends from 59.5 degrees to 27 degrees north latitude along descending tracks. This region includes all along-track geolocation segments (section 3) that span the line of 59.5 degrees north latitude (i.e. follow sequentially after those geolocation segments in region 5) and are entirely north of 27 degrees north latitude.

Region 7 extends from 27 degrees north latitude to the equator along descending tracks. This region includes all along-track geolocation segments (section 3) that span the line of 27 degrees north latitude (i.e. follow sequentially after those geolocation segments in region 6) and are entirely north of the equator.

Region 8 extends from the equator to 27 degress south latitude along descending tracks. This region includes all along-track geolocation segments (section 3) that span the descending equatorial crossing (i.e. follow sequentially after those geolocation segments in region 7) and are entirely north of 27 degrees south latitude

Region 9 extends from 27 degrees to 50 degrees south latitude along descending tracks. This region includes all along-track geolocation segments (section 3) that span the line of 27 degrees south latitude (i.e. follow sequentially after those geolocation segments in region 8) and are entirely north of 50 degrees south latitude.

Region 10 extends from 50 degrees to 79 degrees south latitude along descending tracks. This region includes all along-track geolocation segments (section 3) that span the line of 50 degrees south latitude (i.e. follow sequentially after those geolocation segments in region 9) and are entirely north of 79 segrees south latitude.

Region 11 extends from 79 degrees south latitude along descending tracks to 79 degrees south latitude along ascending tracks after crossing the southernmost point of the orbit (nominally 88 degrees south latitude). This region includes all includes all along-track geolocation segments (section 3) that span the line of 79 degrees south latitude (i.e. follow sequentially after those geolocation segments in region 10) and are entirely south of 79 degrees south latitude on the ascending track.

Region 12 extends from 79 degrees to 50 degrees south latitude along ascending tracks. This region includes along-track geolocation segments (section 3) that span the line of 79 degrees south latitude (i.e. follow sequentially after those geolocation segments in region 11) and are entirely south of 50 degrees south latitude.

Region 13 extends from 50 degrees to 27 degrees south latitude along ascending tracks. This region includes along-track geolocation segments (section 3) that span the line of 50 degrees south latitude (i.e. follow sequentially after those geolocation segments in region 12) and are entitrely south of 27 degrees south latitude.

Region 14 extends from 27 degrees south latitude to the equator along ascending tracks. This region includes along-track geolocation segments (section 3) that span the line of 27 degrees south latitude (i.e. follow sequentially after those geolocation segments in region 13) and extend to the equatorial crossing, as described in section 3.

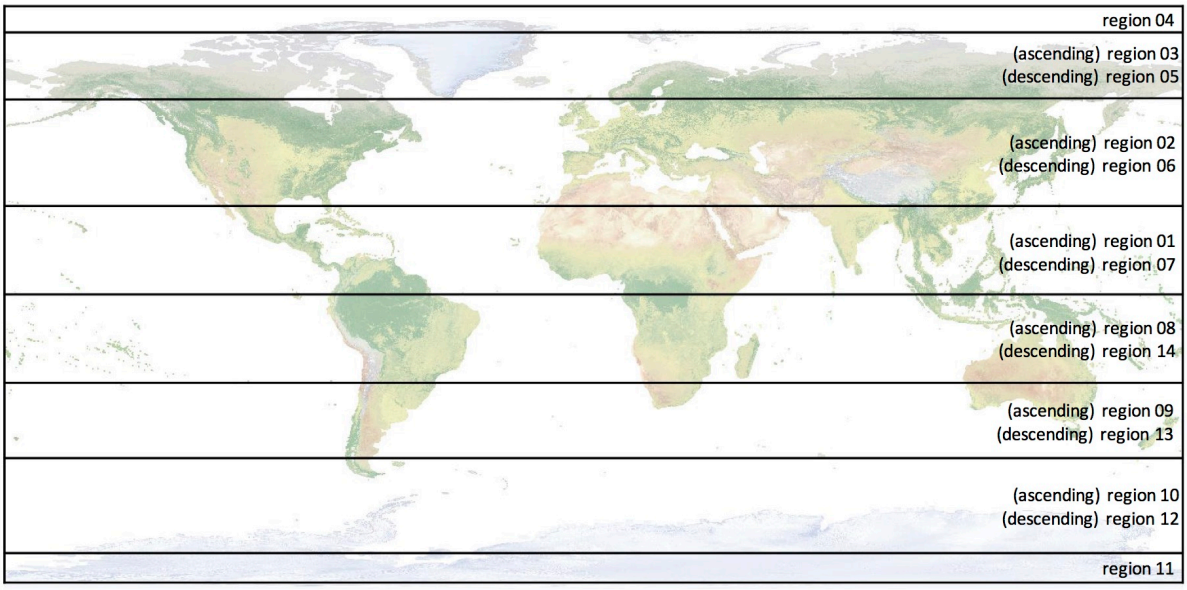

Figure 2-2. ATL03 granule regions and demarcations for those regions.

3.0 GEOLOCATION

Analysis of altimetry data to meet the ICESat-2 science requirements demands an accurate determination of the laser spot location on the Earth's surface. The geolocation of the laser spot with respect to the Earth's center of mass (or geocenter) is determined by both the orbital location of ATLAS in an appropriate reference frame and the direction of the laser beams described in the same reference frame. With these position and direction vectors and the photon path range, the location of each measured photon event can be calculated in geodetic coordinates (geodetic latitude, longitude, and height above the WGS-84 ellipsoid) along with associated measurement uncertainties.

The geolocation procedure is documented in a separate ATBD (ATL03g, Geolocation). That document provides: 1) a general theoretical overview of the algorithms, processing steps, and procedures required to geolocate the ATLAS received photons, 2) a detailed geolocation algorithm and processing flow specifically designed for the ICESat-2 mission, and 3) a description of the application of the atmospheric path delay correction. The details of the atmospheric path delay computation are provided in ATL03a. The algorithm description for the direct and crossover altimeter measurement models, and residual analysis for geolocation parameter estimation (calibration and validation), is provided in the POD and geolocation calibration documents.

3.1 The ICESat-2 Geolocation Along-Track Segments

The photon event data in ATL03 is ultimately presented in geodetic spherical coordinates as geodetic latitude, longitude and photon event height above the WGS-84 ellipsoid (or ellipsoidal height). ATL03g provides the details of the geolocation algorithm, which we briefly summarize here. Each individual photon event is initially geolocated without the correction for atmospheric path delay. These geolocated photons are then provided to the signal finding algorithm (described in section 5.0). The signal characterized photons are then binned in ~20 m along-track segments that are fixed to the Reference Ground Track (RGT) in predetermined locations. A reference photon is selected (section 3.2, below) from the photon events classified as likely signal photons. These segments are referred to as the along-track geolocation segments, also known as geolocaiton segments or geosegs in this and related documents. The atmospheric path delay (described in ATL03a) and its derivatives with respect to ellipsoid height are computed for the reference photon. The geodetic spherical coordinates of all the photons within the segment are then corrected for atmospheric path delay using the reference photon computed information.

Placement of the geolocated photons into along-track geolocation segments includes identifying the RGT segment number for each photon and computing the segment-centric cartesian coordinates for each photon from the geodetic spherical coordinates. These segment-centric cartesian coordinates are X distance from the segment start boundary in the along-track vector direction, Y distance perpendicular to the segment along-track vector to the surface of the ellipsoid at the photon location, and ellipsoid height of the photon return (which is the same as the ellipsoid height in the geodetic spherical coordinates). The ICESat-2 geolocation along-track

segments are derived to provide the ~20m segments in the along track direction for the purpose of computing the segment-centric cartesian coordinates. In addition, there are many other calculations that benefit from a mapping between geodetic spherical and segment-centric cartesian coordinates. In order to standardize this across data products, this section of ATL03 provides such a mapping.

It is worth noting that the along-track geolocation segment is a rectangular coordinate system defined using the RGT as y = 0 for each 20-m along track segment, and the beginning of the segment as x = 0. When the observatory is pointed to the RGT, this means that photon along-track (x) values range from 0 m to approximately 20 m, and the across-track (y) values go from approximately -3.3 km to +3.3 km. As explained below, the boundaries between consecutive along-track geolocation segments (i.e. where x resets from a maximum value (~20 m) to 0 m) are not co-linear due to the curvature of the ground tracks on the surface of the earth. Consequently, while the length of the along-track segments along the RGT are nominally 20m, for the left and right pairs of ground tracks the along-track segments could be greater than or less than 20m depending on the curvature of the ground tracks on the surface of the earth.

3.1.1 Preparing the Geolocation Segment Database

The first step in the photon geolocation binning is to prepare the geolocation segment database. The database requires the full RGT and interpolation times for each reference track (found in ANC22, see POD Facility ICD) to allow 20 m segment endpoints to be computed for each RGT. ANC22 is generated once, prior to launch, and is used to assign each received photon event to a segment, even if ATLAS is pointed away from the RGT (e.g. pointing at targets of opportunity or off-pointing in the mid-latitudes).

The RGT file (ANC22) contains ECF cartesian coordinate positions located on the WGS-84 ellipsoid every 1 second that define each of the 1387 ICESat-2 reference tracks. Therefore, the file contains ECF X, Y, Z at 1Hz. Time is not stored because each point is 1 sec from the previous point. All points have an associated reference track id number (0-1387). For every ascending node (AN) crossing, the reference track id number increments by 1. The first data point begins at 0 before the RGT has begun, just before the 1st AN. The interpolation time vector for a given reference track is formed using start and stop times in addition to a delta time variable for each reference track in the RGT. This interpolation vector allows the 20 m segment endpoints to be quickly computed for any track. The start and stop time for each track in the RGT has both integer and fractional seconds relative to the 0 second point in the RGT. Therefore, these times provide the data necessary to interpolate the RGT data to get the ECF cartesian positions of the start and stop of each reference track. The delta time variable represents the average time to travel ~20 m for that particular reference track. Therefore, this delta time is used to interpolate the RGT file to quickly compute ECF cartesian positions of all the segment endpoints for a reference track.

The procedure for creating the interpolating time vector for a reference track *i* (an entry in ANC22) is as follows:

1. Load up reference ground-track ECF positions that have reference track ids equal to *i*. Load up one data point (ECF position) before the first (before AN) position and one data point after the last (past next AN) position.
2. An elapsed time variable is created for these loaded data points that starts at 0 sec and increments by 1 sec for each data point.
3. Compute the time for each AN by interpolating. Store these as the *ith* reference track start and stop times. This is the time where the reference track starts and ends relative to the elapsed time variable created in step 2.
4. Calculate mean ground-track velocity by computing the distance between every data point and averaging. Taking the 20 m segment length and dividing by this mean velocity gives an approximate delta time step. This time step needs to be adjusted to create an integer number of segments between the reference track's start and stop time. The reference track start time, stop time, and delta time are then stored for the *ith* track.

The delta time step along with the start and stop times produces an interpolating time vector for each track that enables the computation of ~20 m segments with cm variation. The reference track ECF positions need to be loaded up exactly as in step 1, and the elapsed reference track time vector needs to be created exactly as in step 2. Using the interpolation time vector, elapsed time vector and loaded ECF positions, ~20 m segment endpoints are created. These segment positions fall within 3.5e-7 m of the ellipsoid.

3.1.2 Computing the segment number and segment-centric coordinates for each geolocated photon

The geolocation process described in ATL03g provides a method to calculate the bounce point of any photon. By using the initial geolocation of the reference photon (selection of the reference photon is described in section 3.2), the geolocation of all photons within a geolocation segment are determined. However, in order to correctly geolocate the non-reference photons, the geolocation segment of each photon must be established. This is accomplished using the bounce point (BP), and RGT number of each photon.

Given RGT track *K*, geodetic latitude, longitude and ellipsoid height of the j^{th} photon bounce point (BP); the segment number and segment-centric cartesian coordinates for BP *j* can be computed as follows:

1. Compute all 20 m segment endpoint positions for a reference track number *K*.

1.1. Load up 1 Hz RGT ECF positions that have reference track ids *K* from the RGT file (ANC22). Load up one additional data point (ECF position) before the first (before AN) position and one more data point after the last (past next AN) position. The interpolating time vector to produce 20 m segment endpoints can be formed from delta time, start and stop time variables also loaded from ANC22 for reference track *K*.

1.2. An elapsed time variable is created for the 1 Hz position data that was loaded up in Step 1 that starts at 0 sec and increments by 1 sec for each RGT point.

1.3. Using the interpolation time vector, elapsed time vector and loaded RGT ECF positions, ~20 m segment endpoint ECF positions are interpolated.
1.4. Cubic spline interpolation is used to compute segment ECF endpoint positions.
1.5. The last segment endpoint is discarded and the 1st segment endpoint of the next reference track is used to enforce neighboring (sequential) reference tracks share the exact same segment endpoint coordinates.

2. Compute distance between BP *j* and 1 Hz reference track positions and select 20 m segment endpoints (Fig. 3.1)

2.1. Photon bounce point geodetic spherical coordinates latitude, longitude and height (ϕ, λ, h) are converted into ECF coordinates that have topography removed (h=0) and are located on the same reference ellipsoid as the RGT (WGS-84). Define distance N:

$$N = \frac{a_e}{1-e^2 \sin\phi \sin\phi}$$

Where $a_e$and e^2 are the Earth's semi-major axis and eccentricity squared respectively. Then the ECF Cartesian coordinates (x, y, z) are computed as:

$$\begin{bmatrix} x \\ y \\ z \end{bmatrix} = \begin{bmatrix} (N+h)\cos\phi\cos\lambda \\ (N+h)\cos\phi\sin\lambda \\ (N(1-e^2)+h)\sin\phi \end{bmatrix}$$

2.2. Initially, the general location on the reference track, which is closest to the bounce point, is determined using the 1 Hz positions. The coordinate with the smallest computed absolute distance and its immediate neighboring points (for a total of 3) cover a spatial distance of approximately 15-16 km and are approximately a straight line along the reference ellipsoid.
2.3. All 20 m segment endpoint positions with a time stamp within or equal to 1 sec of the closest 1 Hz position are selected for further computations. See Figure 3.1.
2.4. The BP and selected 20 m endpoint positions are used to calculate the distance between them. The closest three endpoints contain the closest two geo-segments to the BP. The closest segment is first selected to check if it contains the BP.
2.5. Note: Additional attention is required for bounce points near the equator of an ascending node because they could actually belong to the previous or next RGT.

3. Select geo-segment number and compute segment-centric Cartesian coordinates.

3.1. Two segment boundary angles θ_1, θ_2 (see Figure 3.2) are computed for the closest geo-segment. These are the angles between the line that passes through the segment endpoint and BP, and the line spanning the segment endpoint positions (segment along-track vector). Let the selected geo-segment be bin k with segment endpoint coordinates given in Earth Centered Fixed frame as Bin_{ECF}^{k} and Bin_{ECF}^{k+1}. The first segment endpoint k is the one that occurs earliest in the RGT, and $k+1$ follows.

The geo-segment along-track unit vector is computed as:

$$\hat{s}^k = \frac{Bin_{ECF}^{k+1} - Bin_{ECF}^{k}}{\left\| Bin_{ECF}^{k+1} - Bin_{ECF}^{k} \right\|}$$

The two unit vectors formed from the geo-segment endpoint coordinates and the photon bounce point are given as:

$$\hat{r}^k = \frac{BP_{ECF}^{j} - Bin_{ECF}^{k}}{\left\| BP_{ECF}^{j} - Bin_{ECF}^{k} \right\|}, \quad \hat{r}^{k+1} = \frac{BP_{ECF}^{j} - Bin_{ECF}^{k+1}}{\left\| BP_{ECF}^{j} - Bin_{ECF}^{k+1} \right\|}$$

The boundary angles (radians) are then found by simply using the dot product:

$$\theta_1 = \cos^{-1}(\hat{r}^k \cdot \hat{s}^k), \quad \theta_2 = \cos^{-1}(\hat{r}^{k+1} \cdot -\hat{s}^k)$$

3.2. For a BP to be binned the condition to be satisfied is $\theta_1 <= 90^o$ and $\theta_2 <= 90^o$, or the max of the two angles = θ: $\theta <= 90^o$

3.3. When the above condition is uniquely satisfied geo-segment *k* with reference track id *K* is assigned to photon BP *j*. The geo-segment along track, and across track components are then easily computed from the angles and vectors computed in the above steps as:

$$dist\_ph\_along = \cos\theta_1 \left\| BP_{ECF}^{j} - Bin_{ECF}^{k} \right\|$$
$$dist\_ph\_across = \hat{w}^k \cdot \left(BP_{ECF}^{j} - Bin_{ECF}^{k} \right)$$

Where the cross track unit vector, $\hat{w}^k$ is computed from using the up and geo-segment along-track unit vectors. The up unit vector, $u_{\widehat{up}}$ is computed bu using BP *j*'s latitude and longitude coordinates.

$$u_{\widehat{up}} = \begin{bmatrix} cos\lambda cos\phi \\ sin\lambda cos\phi \\ sin\phi \end{bmatrix}, \quad \hat{w}^k = \frac{u_{\widehat{up}} \times \hat{s}^k}{\left\| u_{\widehat{up}} \times \hat{s}^k \right\|}$$

The total along track distance from the equator to photon BP *j* can be computed by summing up all the geo-segment absolute lengths (they are variable) before the k^{th} geo-segment and adding the current along track component of the k^{th} geo-segment.

$$segment\_dist\_x = \sum_{i=1}^{k-1} \left\| Bin_{ECF}^{i+1} - Bin_{ECF}^{i} \right\| + dist\_ph\_along$$

4. **Special cases**

4.1. The assumption that the reference track search area (step 2.2) is a straight-line is only approximate. Neighboring segments share approximately the same boundary wall (see Figure 3-3), but every wall is calculated independently for each segment and no constraints are enforced. Analysis shows that all geo-segment boundary walls are less than 1" (arcsecond) offset. So there exist a few cases where a BP may not be assigned a geo-segment (**$90^o \leq \theta \leq 90^o$+1"**) and another case where a BP could be assigned to two segments (**90^o-1" $\leq \theta \leq 90^o$"**). If this happens then additional computations are needed.

4.2. θ is calculated for the next closest segment and the segment with the smallest value that also meets the condition **$\theta < 90^o$+1"** is assigned the BP.

4.3. A message is printed so the user knows that the additional computation was necessary, or in the case no segment is assigned to the BP.
4.4. The result is an assignment for every photon to exactly one geo-segment bin.

5. Other output parameters

Two other output parameters are generated at this step. The *segment_ID* parameter is a seven digit number that uniquely identifies each along track segment, and is written to the /gtx/geolocation/ group at the along-track geolocation segment rate (i.e. ~20m along track). The four digit RGT number can be combined with the seven digit segment_ID number to uniquely define any along-track segment number. Values are sequential, with 0000001 referring to the first segment after the equatorial crossing of the ascending node.

The parameter *segment_length* is also written to the /gtx/geolocation/ group at the along-track geolocation segment rate. This parameter indicates the length of the along-track segments, in meters, corresponding to the segment_ID parameter discussed above. Nominally these are ~20m, but they can vary between 19.8m and 20.2m.

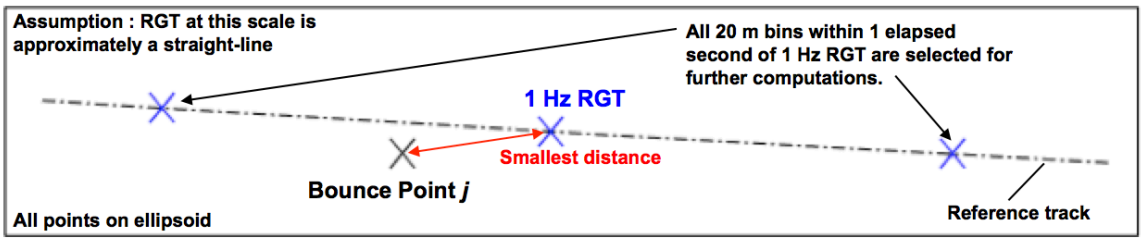

Figure 3-1. Finding the 1-Hz RGT Track Points and Segments to Search.

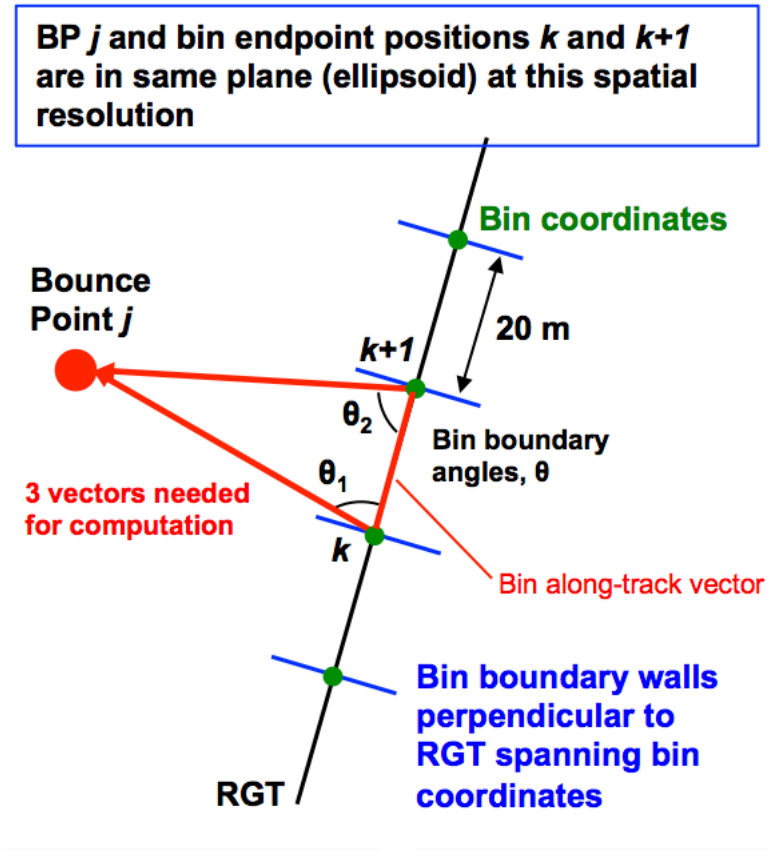

Figure 3-2. Computing the Segment Angles.

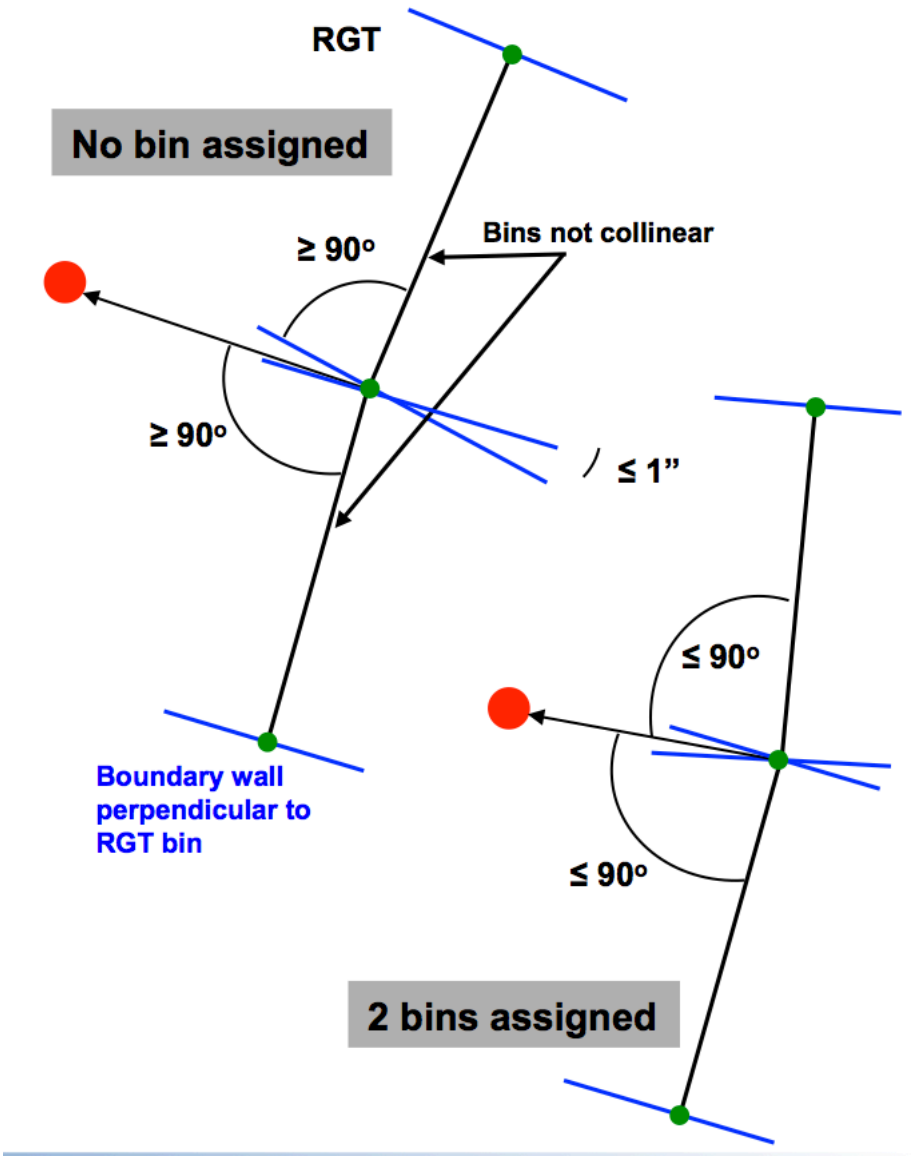

Figure 3-3. Special Cases.

3.2 Selecting the Reference Photon

As noted in ATL03g, instead of geolocating each individual received photon event, reference photons are identified for every geolocation along-track segment. These reference photons are geolocated and other photons in the same along-track segment are geolocated by determining the distance to the reference photon and gradients in the atmospheric path delay calculated in

ATL03a. We use the classified photons to determine a reference photon for a given along-track segment.

1. If more than four high-confidence signal photons are present in a given along-track segment, the reference photon is the high-confidence signal photon within 1 meter of the center of the along-track segment (i.e. within 9.5 meters from each segment end point). If more than two high-confidence signal photon pass this criteria, the reference photon is the photon with the median ellipsoidal height. If only two high-confidence signal photons pass this criteria, the reference photon is the photon with the higher ellipsoidal height.

2. If there are fewer than three high-confidence signal photons in a given along-track segment but there are four or more medium-confidence signal photons, the reference photon is the medium-confidence photon within 1 meter of the center of the along-track segment (i.e. within 9.5 meters from each segment end point). If more than two medium-confidence signal photon pass this criteria, the reference photon is the photon with the median ellipsoidal height. If exactly two medium-confidence signal photons pass this criteria, the reference photon is the photon with the higher ellipsoidal height.

3. If there are fewer than three high- or medium-confidence signal photons in a given along-track segment but there are four or more low-confidence signal photons, the reference photon is the low-confidence photon within 1 meter of the center of the along-track segment (i.e. within 9.5 meters from each segment end point). If more than two low-confidence signal photons pass this criteria, the reference photon is the photon with the median ellipsoidal height. If exactly two low-confidence signal photons pass this criteria, the reference photon is the photon with the higher ellipsoidal height.

4. If there are fewer than three high-, medium-, or low-confidence signal photons in a given along-track segment, but more than 3 classified photons (i.e. the sum of the number of high-, medium-, and low-confidence signal photons is 4 or greater), the reference photon is the classified photon within 1 meter of the center of the along-track segment (i.e. within 9.5 meters from each segment end point). If more than two classified photons pass this criteria, the reference photon is the photon with the median ellipsoidal height. If exactly two classified photons pass this criteria, the reference photon is the photon with the higher ellipsoidal height. This case is designed to cover situations where there are more than three classified photons, but fewer than 4 of any specific classification.

5. If there are no high- medium- or low-confidence signal photons in a given along-track segment, the reference photon is the photon within 1 meter of the center of the along-track segment (i.e. within 9.5 meters from each segment end point). If more than two photons pass this criteria, the reference photon is the photon with the median ellipsoidal height. If there are exactly two photon events that pass this criteria, the reference photon is the photon with the higher ellipsoidal height.

6. If there is only one photon in a given along-track segment, and criteria #4 is not met, the reference photon is the solitary photon in the along-track segment.

7. It is necessary to check that the arrival times of the reference photons are strictly monotonic increasing. For example, it is possible for there to be two photon events from a single laser pulse that are geolocated into two adjacent segments. Check that the arrival time of the $n+1^{th}$ reference photon is strictly greater than the arrival time of the n^{th} reference photon. If this test fails, assign the n+1 reference photon to the preceeding segment, and the $n+1^{th}$ segment has no reference photon. Record the number of instances that this happens in a granule, and the number of photons left in the $n+1^{th}$ bin after this reassignment step for QA purposes (parameters are named ref_photon_fail and ref_photon_fail_remaining). This latter parameter should always equal zero.

At this point, there should be a unique, or no, reference photon selected for each along-track segment. Store the ID of this reference photon for further analysis in the geolocation process. For each reference photon, determine the index of the reference photon, and store it as reference_photon_index in the /gtx/geolocation/ group. This index is a shortcut that identifies the jth reference photon within the n photons on a particular ATL03 granule. Similarly, identify the index of the first photon in the along-track geolocation segment and store it's value as ph_index_beg in the same group.

Determine the number of photons in a given along-track geolocation segment, and store this value in the segment_ph_cnt parameter in the /gtx/geolocation/ group.

In the event that there are no photons (and therefore no reference photon) in a given along-track geolocation segment, segment_ph_cnt is set to zero, and all other values that depend on the existence of a reference photon are set to invalid values. Similarly, other parameters such as the latitude, longitude, and delta_time values are best estimates.

3.3 ATLAS Range Bias Correction and Uncertainty

The primary measurement of the ICESat-2 mission is the height of the earth's surface. Therefore, careful consideration is needed to evaluate and quantify potential sources of measurement bias (time of flight bias, or range bias), and account for the bias in the ATL03 photon heights. In addition, we evaluate the uncertainty in that bias, and determine both the bias and the bias uncertainty. In this section, we present the logic and data flows used to determine the likely sources of bias and bias uncertainty, as well as the concept to evaluate the range bias using on-orbit data after launch. We have chosen to present these concepts in this document, as the plan draws from ATL02, POD, PPD, ATL03a, and ATL03g to produce the height bias correction term (parameter name here) and the uncertainty in that bias correction (parameter name here).

3.3.1 Range bias determination

The location of each detected photon for a given beam, relative to the ICESat-2 observatory, is determined by the ATL03g geolocation algorithm. The pointing direction of each beam is determined by the Precision Pointing Determination algorithm, using primarily data from the Laser Reference System (LRS) on ATLAS. Each beam shares a common origination point at the ATLAS diffractive optical element (DOE), where the single laser beam from one of the two ATLAS lasers is split into the 6 beams: 3 weak and 3 strong. The location of the DOE is measured in the ICESat-2 Master Reference Frame (MRF), which provides a common frame for the relative locations of the components of ATLAS (such as the DOE) and the ICESat-2 Observatory (such as the observatory center of mass). The schematic of the measurement is outlined in Figure 3-4.

The zero-range distance of ATLAS was measured during integration to account for the optical and electrical path lengths within ATLAS. Essentially, the zero-range distance measurement consisted of comparing the ATLAS-measured range to a target at an independently measured series of distances from ATLAS. These distances were measured for many permutation of ATLAS settings and configurations (e.g. primary and redundant detectors, primary and redundant start pulse detectors, etc…) and are documented in the ATLAS pre-launch calibration CAL-08. The zero-range distances are shown schematically as the lengths of the green vectors in Figure X. The uncorrected zero range points (ZRP) are shown as the green dots in Figure X; these points move tangentially up to a few millimeters as the beams are steered with the beam-steering mechanism to keep the laser spots aligned with the telescope.

The transmitter echo pulse (TEP; see Section 7.x for a complete description) provides the means to internally calibrate changes in the ATLAS range by selecting a small fraction of the outgoing laser light and optically routing that light into the ATLAS detectors. By observing changes in the time of flight of photons following the TEP, we can characterize changes in the internal ATLAS range bias on-orbit. This TEP-based range correction (orange vectors in figure X) is added to the uncorrected zero range points (green dots in figure x) along the beam directions to determine the corrected zero range points (orange dots in figure x). Note that the TEP-based range correction could either be a positive or negative.

The corresponding data flow for both the rapid and final ATL03 product is presented in Figure 3-5. ATL02 provides surface-return times of flight for all detected photons in the telemetry window and TEP times for likely TEP photons. The two times of flight are in distinct groups on the ATL02 data product. The surface return times of flight are passed from ATL02 to the geolocation algorithm (ATL03g), converted to range, and then eventually to photon height. In parallel, the TEP times of flight of the likely TEP photons are passed to the Instrument Support

Facility (ISF). Here, TEP photons are analyzed to generate the TEP-based range bias offset in meters. We note that not every ATL02 granule will have likely TEP photons, as described in Section 7.x. Whenever such TEP photons as likely present, these corrections for the two beams with the TEP optical path are passed from the ISF to the POD/PPD facility via ANC13. These TEP-based corrections are based on a comparison of pre-launch sets of TEP data under the relevant instrument configuration with those collected on-orbit.

When one or more threshold crossing time from the Start Pulse Detector is missing, an additional time of flight error must be accounted for. Correcting for this additional bias requires use of the Start Pulse Coefficient Table (which is nominally updated only when the laser transmit energy changes and/or the threshold crossing levels are changed) and the time of flight flag parameter (TOF_flag) from ATL02. The Start Pulse Coefficient Table is routinely provided by the ISF to the POD/PPD facility via ANC13. The TOF_flag parameter is generated at the photon rate and identifies the scenario (i.e. nominal is all threshold crossings present, and the other cases correspond to one or more missing start pulse components). Instruction for the use of the Start Pulse Coefficient Table and TOF_flag parameter will come from Tony or Meg and will be summarized here. It should involve reducing this term from the photon rate to 1 value per second. We expect anything other than the nominal case (where all expected threshold crossing times are present) to be rare.

The POD/PPD facility uses the TEP-based range bias term in a model for a range-bias correction in meters for each beam that is generated once per second. This model combines the TEP-based corrections from the ISF, pre-launch data analysis of the zero-range point for each beam (based on ATLAS Cal-08), and a model for how the TEP varies around an orbit (based on commissioning data tracking the TEP continuously for several orbits). This model will be updated as additional on-orbit data become available. When the Start Pulse Coefficient Table is used, the TEP-based range bias is combined with the TOF-flag-based correction in quadrature to produce a single range bias value for each beam at the 1-second rate. These corrections are included in the ANC04 ancillary data product that is passed from the POD/PPD facility to the SIPS where ATL03 is produced.

For the rapid processing of ATL03, the ANC04 file contains static values of the range-bias correction for each beam, based on lower fidelity models. The higher fidelity model described above requires additional processing time and is only included on the final ATL03 product.

The complete ATL03 processing flow is described above in Section 2. For the purposes of the range bias correction, ATL03 ingests the photon time of flight data from ATL02 and the range-bias corrections from ANC04 to produce our best estimate of photon range in the geolocation

processing. The value of the range bias correction is provided on the ATL03 data product as ***/gtx/geolocation/range_bias_corr*.**

3.3.2 Range bias uncertainty

We acknowledge that the range bias correction described above will not be perfect and seek to characterize the uncertainty in that calculation. There are three main sources of range bias uncertainty:

(a) uncertainty in the TEP-based bias estimate generated from the TEP determined at the ISF, σ_{TEP}. This term is driven by the uncertainty in determining the centroid of a realization of TEP photons, largely due to the transmit pulse shape variations and photon statistics. We expect this term to be very small.

(b) uncertainty in the model for how the TEP varies around an orbit, σ_{bias}. This model will be based on data collected during commissioning and will be re-evaluated periodically during the mission. The purpose of this model is to estimate the variation of the range bias for each beam between realizations of the TEP in the ATL02 data. This term captures the model uncertainties in predicting the range bias for each beam. When the TEP is available, we expect the model uncertainty for the two beams with the TEP to be zero.

(c) uncertainty in the atmospheric delay correction, σ_{atm}. The atmospheric delay (combining wet and dry tropospheric effects) is described in ATL03a. This range correction is based on imperfect atmospheric models of temperature and humidity and has a residual error that is determined in the ATL03a processing.

From a data flow standpoint, the ISF produces σ_{TEP} for each realization of the TEP along with the TEP-based bias correction. The POD/PPD facility generates σ_{bias} for each beam at the same rate as the model-based range bias correction. This is passed along with ANC04 to the SIPS. The third term (σ_{atm}) is generated during ATL03a processing and is combined in quadrature with the other two terms during geolocation processing to produce a single height uncertainty estimate. This estimate is provided at the along-track geolocation segment rate as ***sigma_h*.**

3.3.3 Range bias model evaluation

The preliminary model for the range bias variation around an orbit and through time is based on pre-launch data on the range bias and range bias variation for each beam, the orbit angle, and the

solar angle with respect to the solar array. During commissioning, the model will be updated using on-orbit data to condition (or replace) the preliminary model, using cross-over data.

During commissioning, we will collect TEP data continuously for one orbit each day during the first of two 10-day calibration periods. These TEP measurements will be turned into a time series of range bias by the ISF and provided to the POD group. These TEP-based variations in range bias will be correlated to the orbit angle and beta prime and create an updated model for the variation of the range bias of the strong beams with the TEP.

In addition, we will aggregate 10 days of ATL03 data, during nominal operating conditions and excise short latency (< 24 hours) cross-over data between ascending and descending tracks. By using the high-confidence and medium confidence likely signal photons (described in Section 5), we will compare the elevations measured between the ascending and descending passes over a given cross over for each of the six beams.

The residual height differences between the two strong beams monitored by the TEP will be considered the true height residual. Using the variation from the TEP-monitored beams, we will update the range-bias correction model for the other non-TEP monitored beams by simultaneously solving for all model parameters for each of the 6 beams. By comparing the model predictions of the TEP-monitored beams, with the measurements of the cross over residuals of these beams, we will iteratively update the model parameters to drive the height residuals toward zero. This process will be repeated any time the laser or detector side is changed from the primary to the redundant side.

The effectiveness of this approach will depend on understanding how range bias variations in the TEP-monitored beams translate to the non-TEP monitored beams from pre-launch calibration activities. This analysis will be done in the POD/PPD facility, using final ATL03 data. Provided that an improved range-bias correction model can be generated, the new model will be reviewed and implemented during re-processing and will result in a new version of ATL03, with improved range-bias corrections.

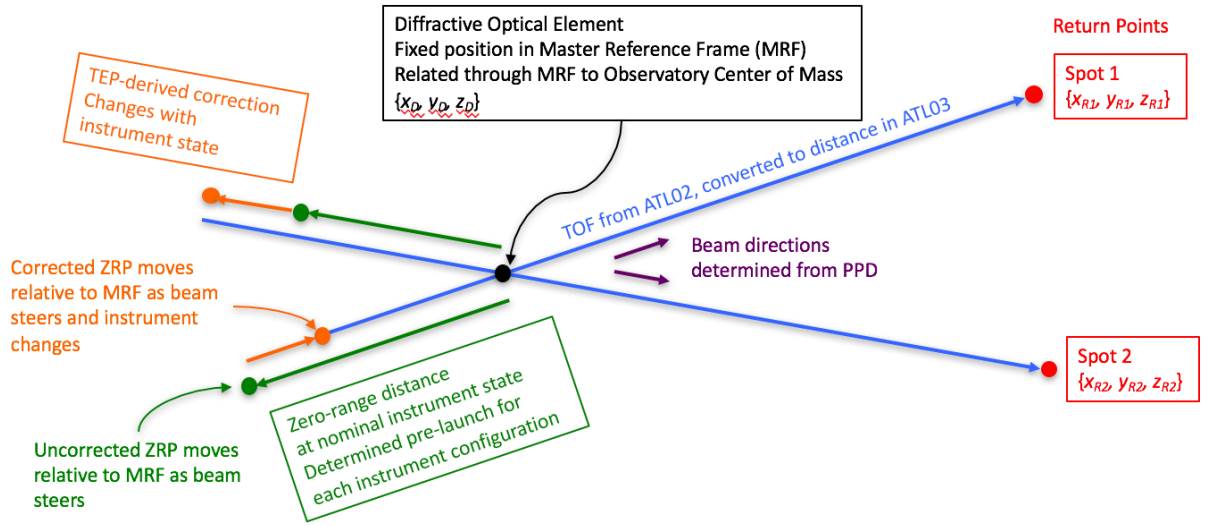

Figure 3-4. Schematic of nominal zero range distance and TEP-based correction for zero range measurement.

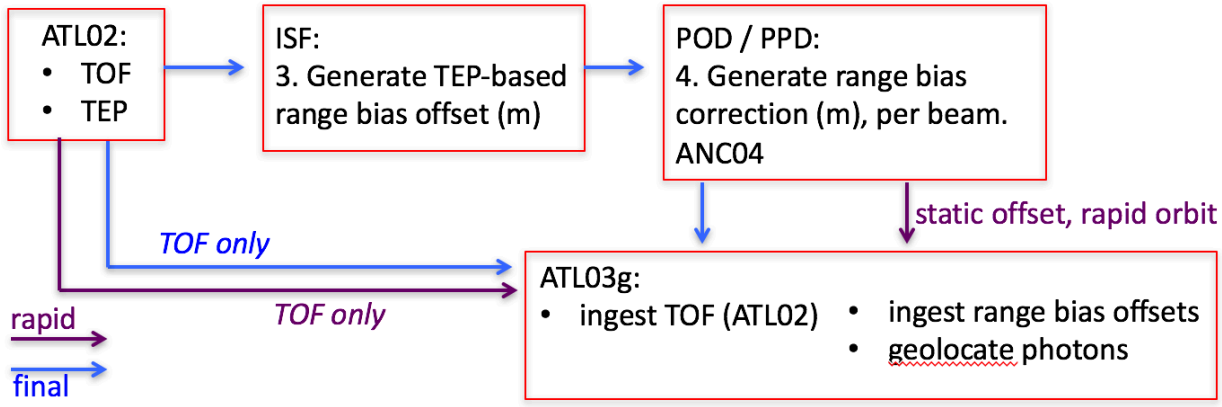

Figure 3-5. Schematic of the data flow to determine bias-corrected photon ranges.

3.4 Other Geolocated Parameters

In addition to the telemetered photon data, other parameters are treated as though they are photons in order to calculate their ellipsoidal height.

In order to generate histograms and related statistics of the telemetered photon data, the signal finding algorithm in section 5 requires the ellipsoidal height of the top of the telemetered bands of photons as well as the widths of the telemetered bands. Therefore, the tops of the telemetry

bands will also be geolocated to determine the latitude, longitude, and heights associated with each band. The heights of each geolocated telemetry band and its width are required for the signal finding algorithm (section 5) to assure all histogram bins are fully within the telemetry bands. In addition, the latitude and longitude of the telemetry bands are used to query the surface masks described in section 4 to determine the surface types traversed by a given granule.

The relevant parameters from ATL02 to derive the ellipsoidal height of the telemetry bands are the sum of the range window start (alt_rw_start) and the downlink band offset (alt_band_offset1(2) in the /pacx/altimetry/ group on ATL02 for strong and weak beams) for each beam. This will provide the delay, in seconds, to the start of the telemetry bands for all received photons in a given major frame. The range to the top of the telemetry band is determined by multiplying that delay by the speed of light divided by two. This range is then geolocated per ATL03g as are all other telemetered photon data. The along-track time associated with a given telemetry band ellipsoidal height is the first laser transmit time of the major frame, such that the telemetry band changes are synchronous with the edges of major frames. The resulting parameters are called tlm_top_bandx, and are in the ATL03 group /gtx/bckgrd_atlas. The parameter tlm_height_bandx, described in section 7.3.2, is also in this group.

Similarly, the top of the altimetric histogram will also be geolocated to provide an estimate of the ellipsoidal height of the top of the altimetric histogram. As described in section 7.3.1, the altimetric histogram is used to generate 50-shot sums of the counts in the histogram. These 50-shot sums are used in section 7.3.1 to derive an estimate of the background count rate and related metrics. The relevant parameter from ATL02 is <insert parameter name here>. As above, this is a time in seconds, from a given laser fire in a major frame. This value is converted to a range by multiplying by the speed of light divided by two, and then geolocated as per ATL03g. The resulting parameter is called bckgrd_hist_top, and is in the group /gtx/bckgrd_atlas.

Note that some of the parameters in the /gtx/bckgrd_atlas/ group are generated at 50 Hz (e.g. the major frame rate) while others are at 200 Hz (such as the 50-shot sum of the altimetric histogram). As described in section 7.3, the lower rate data has duplicate values in order to post all parameters in this group at 200 Hz.

At times, it may be necessary to know or use the ground bounce time of the reference photon. ATL03 provides the bounce_time_offset parameter in the /gtx/geolocation group. The bounce_time_offset is the difference between the transmit time and the ground bounce time of a reference photon. It is calculated from the delta_time array in the /gtx/geolocation group (which provides the transmit time of the reference photon, measured in seconds from the atlas_sdp_gps_epoch), the absolute time reference for a given granule, and the absolute bounce point time (t_B(i); from ATL03g Eq. 3.1.4) of the reference photon, as:

bounce_time_offset = bounce_point_time – (delta_time + atlas_sdp_gps_epoch)

This formulation assumes that the elapsed time from the observatory to the ground is identical to the elapsed time from the ground to the observatory. The value of bounce_time_offset is always positive. The ATL03g geolocation algorithm uses this approximation (see ATL03g, Section 3.1 and Section 3.6).

All other parameters in the ATL03 data product generated by the geolocation process are listed in Appendix A (data product group: /gtx/geolocation; posted at the along-track segment rate of approximately twenty meters) and are described in ATL03a and ATL03g.

4.0 SURFACE MASKS

4.1 Introduction

The goal of providing a set of gridded surface masks (for land ice, sea ice, land, ocean, and inland water) is to reduce the volume of data processed to generate surface-specific higher-level ICESat-2 data products. For example, the land ice surface mask directs the ATL06 land ice algorithm to consider data from only those areas of interest to the land ice community.

In order to protect against errors of omission in these masks, a buffer has been added to the best estimate of the geographic bounds of the regions of interest. Consequently, the grids do not perfectly tessellate the surface of the Earth but have overlap on the order of tens of kilometers in most regions. This means that a given latitude and longitude point could appear in two or more surface masks, and two or more higher-level data products. Differences among the algorithms used by higher-level data products for a multiply-classified granule of ATL03 are expected. For example, many permafrost areas are included in the land, land ice, and inland water masks and will be included in the associated ATL08, ATL06, and ATL13 data products, although they will all take as input the same ATL03 granule.

The masks are provided to the SIPS as text files of latitude, longitude, and a flag (=1 if the grid node contains the surface of interest), and are stored and accessed by SIPS as ANC12-01. The exception is the inland water mask, which is provided as a .tif file, and is stored and accessed by SIPS as ANC12-02. These grids are under configuration management (CM) control and the relevant document numbers are provided.

For each surface type, the technical details and code used to generate the grid are also under CM control and the relevant document numbers are provided. To the extent possible, the input data used are also under CM control.

As described above and in section 5.4.1.2, the surface type is determined at the major frame rate, or at 50 Hz. We recommend using the latitude and longitude of the geolocated top of the telemetry band as the basis for querying the surface type masks described below. On the output ATL03 data product, the surf_type parameter is posted at the along-track segment rate at reference photon locations. In order to map from one to the other, we use inclusive resampling, where the value at the reference photon location is the combination of values at the major frame locations before and after the reference photon location. If either end point indicates a particular type (i.e. type=sea ice == true), then the value at the reference photon location is that type as well. When no telemetry band is downlinked from the observatory, the surf_type array will consist only of false values (i.e. 0s) indicating that no data was telemetered for that major frame.

4.2 Land Ice

The ATL03 land ice mask is a 0.05°x0.05° logical mask that is used to isolate records to be processed using the land ice algorithms. The mask is fully described in (document number / pointer here).

4.2.1 Data Sources

4.2.1.1 Antarctica

Helen Fricker and Geir Moholdt supplied a set of polygons defining the Antarctic continent and surrounding islands, including ice shelves. A 40-km buffer was added to the Antarctic dataset to account for future movement of the ice front.

4.2.1.2 Greenland

The Greenland Ice Mapping Project used Landsat 7 and RADARSAT-1 data to generate a DEM, an ice-cover map, and an ocean mask (Howat et al., 2015). The GIMP ocean mask is available at resolutions of 15 m, 30 m, and 90 m. The 15-m mask was too large to work with, so the 30-m resolution GIMP ocean mask was used. The non-ocean portion of this mask defined the Greenland land mass. This procedure was used rather than working from the GIMP Greenland ice mask so that the entire land surface would be included in the land ice mask. The land mask for Greenland was futher augmented as needed with the non-water tiles of the MOD44W global water mask.

4.2.1.3 GLIMS

The Global Land Ice Measurements from Space (GLIMS) database consists of a single shapefile with roughly 119,000 polygons. It was downloaded from http://glims.org on 2016 Oct 4. The data release date is 2015 Jul 28.

4.2.1.4 RGI

Version 5.0 of the RGI (Pfeffer et al., 2014) consists of a set of shapefiles with multiple polygons in each. They were downloaded from `https://www.glims.org/RGI/rgi50_dl.html` on 2016 Sep 30. The date release data is 2015 Jul 20.

4.2.1.5 Permafrost

A map of permafrost regions in the Northern hemisphere was downloaded from NSIDC (`http://nsidc.org/data/docs/fgdc/ggd318_map_circumarctic/index.html`) on 2013 Feb 7. The flat lat/lon version (geographic projection) of the grid was used. This map has a resolution of 0.5°. The data are also available in polar-stereographic projections with a resolution of 12.5 and 25 kilometers, but these versions are simply reprojections of the 0.5° grid, with no additional information (Kevin Schaefer, NSIDC, pers. comm.). Since the final product is in geographic coordinates, the lat/lon grid is easier to work with. We were unable to locate a similar permafrost map for the southern hemisphere.

4.2.1.6 Other sites

In addition, three non-ice covered sites were added to the ATL06 land ice mask in order to facilitate cal-val studies of relatively flat, relatively bright surfaces. These include the areas around Lake Bonneville, White Sands Missile Range, and Salar de Uyuni.

4.2.2 Mask Generation

Step 1: The Greenland, RGI, and GLIMS datasets were converted to binary masks.

Step 2: The Scripps Antarctic polygons were converted to a mask, and a 40-km buffer was added to the Antarctic dataset to account for future movement of the ice front.

Step 3: The permafrost map (**`llipa.byte`**) was converted to a 0.05°x0.05° mask.

Step 4: The four unbuffered masks (Greenland, RGI, GLIMS, permafrost) were combined into one mask.

Step 5: A 10-km buffer was added to the combined mask, except for the southern region of South America, where a 20-km buffer was used to try to capture permafrost regions.

Step 6: The buffered Antarctic mask was combined with the buffered mask from step 5 to generate the final land ice mask (Figure 4-1).

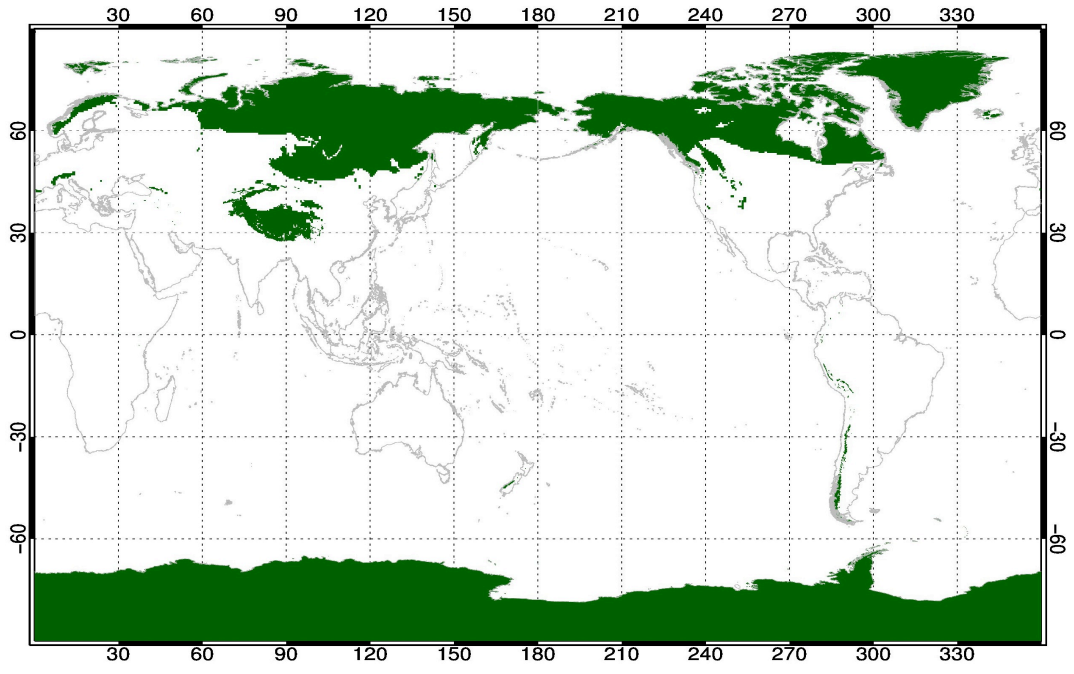

Figure 4-1. Final Buffered Land Ice Mask.

4.3 Sea Ice

The ATL03 sea ice mask is a 0.05°x0.05° logical mask that is used to isolate records to be processed using the sea ice algorithms. The mask is fully described in (document number / pointer here).

4.3.1 Data Sources

4.3.1.1 SSMI/SMMR Monthly Sea Ice Maps

The ATL03 sea ice mask was generated primarily from the 25-km resolution SSMI/SMMR monthly sea ice concentration maps available from NSIDC. These maps cover the period 1978 Oct through 2012 Dec, with change dates of 2013 Feb 6 and 2013 Jun 14. The mask includes some areas of inland water known to freeze seasonally such as Lake Superior and Lake Baikal.

4.3.1.2 Antarctica

The Antarctic sea ice mask uses the 2004 MODIS Mosaic of Antarctica (MOA) (http://nsidc.org/data/moa/) coastline to determine the southern extent of Antarctic sea ice.

4.3.1.3 Greenland

The Greenland sea ice mask uses the MODIS Mosaic of Greenland (MOG) (http://nsidc.org/data/nsidc-0547) to define the landward edge of sea ice around Greenland.

4.3.2 Mask Generation

Step 1: The monthly maps were first combined into one maximum sea ice concentration map for the Arctic and one for the Antarctic.

Step 2: Each 25-km resolution cell in the composite grids with a sea ice concentration ≥10% was subdivided into a grid of 51x51 evenly spaced (in projected space) test points, with the outer columns and rows lying along the edges of the cells. The polar-stereographic coordinates were converted to latitude and longitude, and these lat/lon were then converted to indices into a global 0.05°x0.05° grid, and the associated tiles were flagged.

Step 3: A 10-km buffer was added to this mask by marking any tile as sea ice that lies within 10 kilometers of a sea ice tile.

Step 4: The buffered map, and the area along the 2004 MODIS Mosaic of Antarctica (MOA) coastline show a number of anomalies. These were adjusted in a two-step process.

- Step 1: Areas that were incorrectly flagged as sea ice were unflagged. Each tile containing an Antarctic coastline point was flagged as sea ice, as were all tiles within 10 kilometers of each point.

- Step 2: Some areas that should have been flagged were further than 10 kilometers from the coastline. The region along the Antarctic coastline was examined in detail and the coordinates of these areas were noted. Then all of them were flagged.

The final sea ice mask is shown in Figure 4-2.

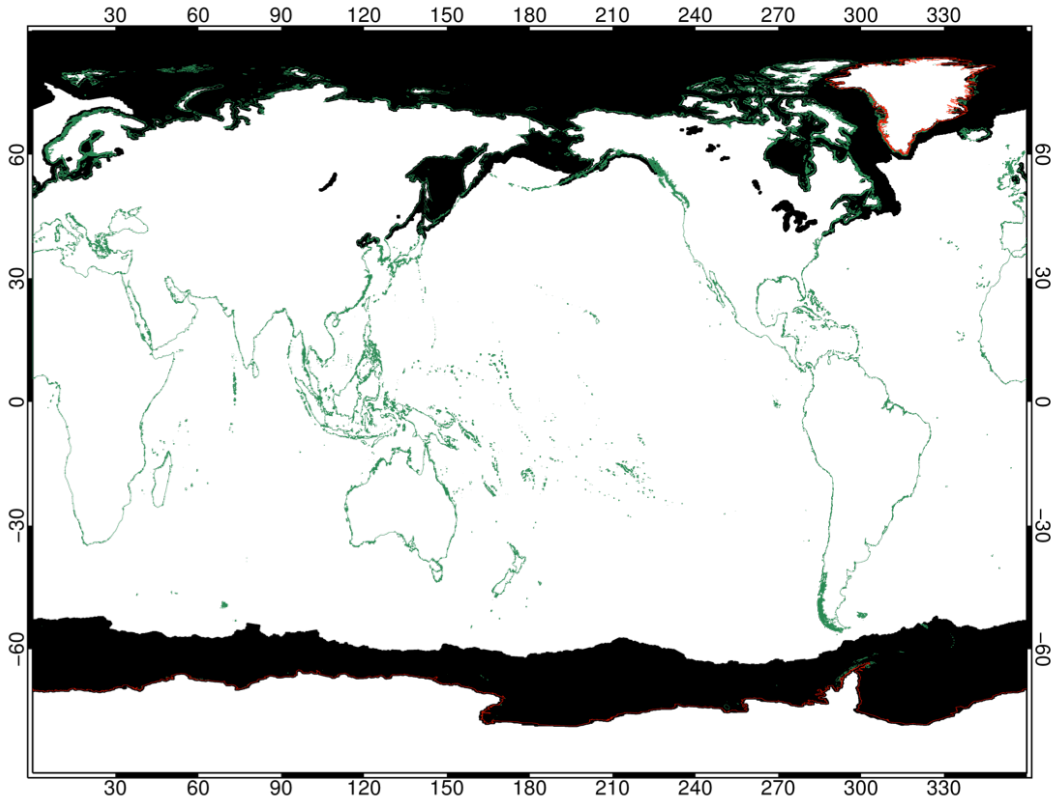

Figure 4-2. Final Buffered Sea Ice Mask.

4.4 Land and Ocean

The ATL03 land and ocean masks are 0.05°x0.05° logical masks that will be used to isolate records to be processed using the land and ocean algorithms, respectively. The source material for both of the masks is the same. These masks are fully described in (document number / pointer here).

4.4.1 Data Sources

4.4.1.1 IBCAO

The International Bathymetry Chart of the Arctic Ocean (http://www.ngdc.noaa.gov/mgg/bathymetry/arctic/) is a 500-m resolution DEM covering the Arctic area north of latitude 60°N. Version 3.0 of this DEM was released 2012 Jun 8 (Jakobsson

et al., 2012). Jamie Morison converted this to a 0.05°x0.05° DEM (pers. comm.) for use in this global mask.

4.4.1.2 MOD44W

The MODIS 250-m resolution water mask (Carroll et al., 2009) was downloaded from the land process data center (https://lpdaac.usgs.gov/products/modis_products_table/mod44w) on 2013 Dec 24. This dataset consists of 318 HDF-EOS files in MODIS sinusoidal projection, each tile covering an approximately 10°x10° region. Tiles that are entirely water are not included in the dataset.

4.4.1.3 GSHHG

The Global Self-consistent, Hierarchical, High-resolution Geography Database (Wessel and Smith, 1996) (http://www.soest.hawaii.edu/pwessel/gshhg/) is a set of polygons defining shorelines globally. The highest resolution ("full") version of the level 1 shorelines was used. Level 1 consists of boundaries between land and ocean. Other levels give boundaries of lakes, islands in lakes, and ponds on islands in lakes. The database was downloaded in shapefile format from ftp://ftp.soest.hawaii.edu/gshhg/gshhg-shp-2.2.4.zip on 2014 Feb 4. The GSHHG land/ocean shorelines are based on the World Vector Shoreline (http://shoreline.noaa.gov/data/datasheets/wvs.html), with an accuracy of 50 to 500 meters.

4.4.2 Mask Generation

Step 1: Generate land and water masks from the ICBAO DEM. Any tile with ellipsoidal height ≤0 was flagged as water and any tile with ellipsoidal height ≥0 was flagged as land.

Step 2: The MOD44W water mask was read in tile by tile. For every pixel with valid latitude, longitude, and flag, if the flag indicated water, the corresponding tile in the 0.05°x0.05° water mask was set. Similarly, for every pixel with valid latitude, longitude and flag, if the flag indicated land, the corresponding tile in the 0.05°x0.05° land mask was set. The MODIS sinusoidal projection is based on a sphere with a radius of 6371007.181 m. Latitude and longitude were calculated using software provided by Nicolo DiGirolamo.

Step 3: A list of missing MOD44W water mask files was generated. Any 0.05°x0.05° tile falling into one of these missing files was flagged as water. Latitude and longitude were calculated using software provided by Nicolo DiGirolamo.

Step 4: The full-resolution GSHHG shoreline was converted to a land mask with a resolution of 0.05°x0.05°. Its inverse was used as a GSHHG water mask.

Step 5: The masks from the three sources were combined to generate the composite water and land masks. For the water mask, any tile that was flagged in the MOD44W or IBCAO water mask, or not flagged in the GSHHG land mask, was flagged in the composite mask. For the land mask, any tile that was not flagged in the MOD44W or IBCAO, or was flagged in the GSHHG land mask, was flagged in the composite mask.

Step 6: The MOD44W water mask includes inland water. To remove it, a shrunken version of the GSHHG land mask was generated by unflagging any tiles along a 10-km wide strip around each GSHHG polygon. Any tiles flagged in this shrunken mask were unflagged in the water mask to make the ocean mask.

Step 7: Per the request of the ATL12 data product lead (Jamie Morison), a 10-km buffer was added to the composite ocean mask (Figure 4-3), and all tiles north of 84° were flagged.

Per the request of the ATL08 data product lead (Amy Neuenschwander), a 25-km buffer was added to the composite land mask (Figure 4-4), and all tiles south of 85.5° were flagged.

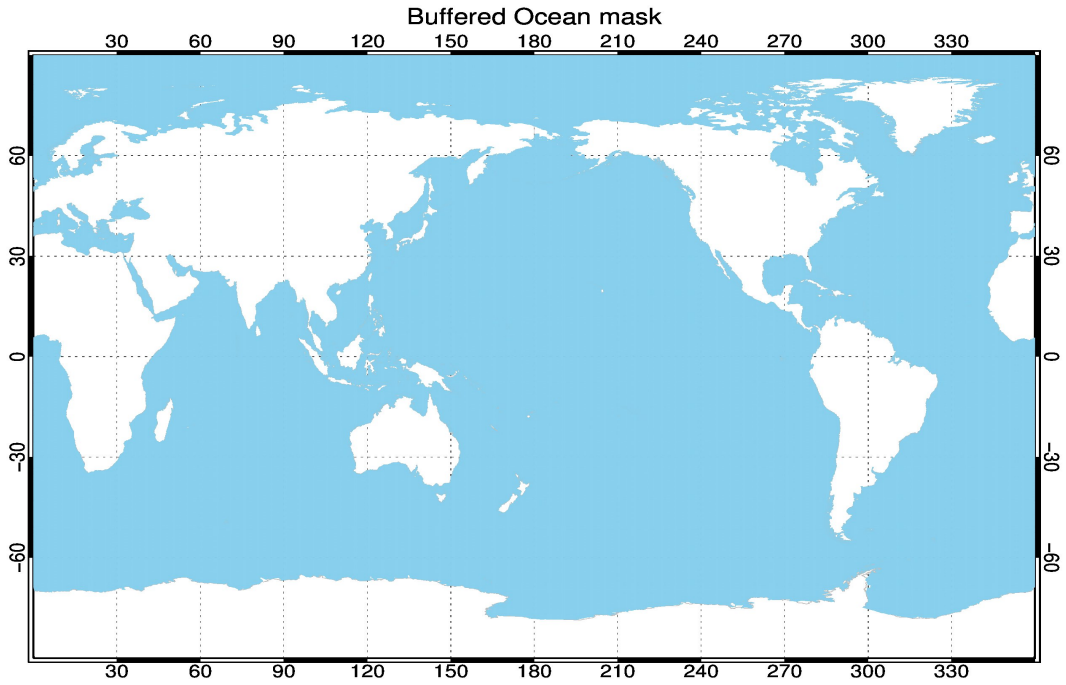

Figure 4-3. Buffered Ocean Mask.

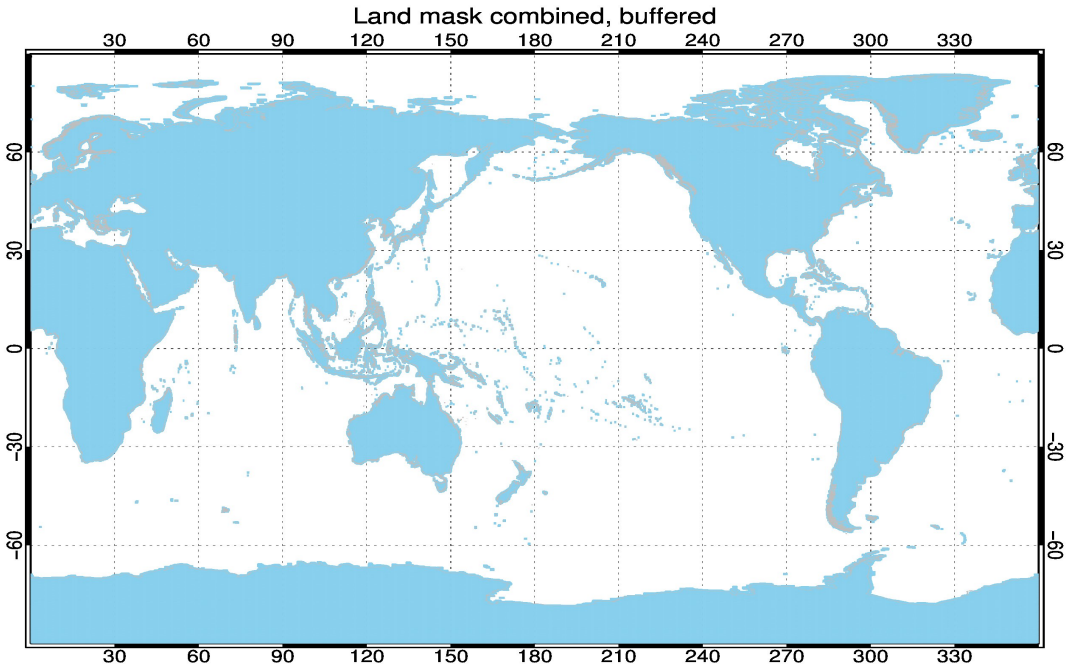

Figure 4-4. Buffered Land Mask.

4.5 Inland Water

The ATL03 Inland Water Mask is a 0.01°x0.01° logical mask that will be used to isolate records to be processed using the inland water algorithm for ATL13. For use in the program, it was generated as a set of tif files each covering 90° latitude and 5° longitude. These masks are fully described in (document number / pointer here).

4.5.1 Data sources

4.5.1.1 MOD44W

The MODIS 250-m resolution water mask (Carroll et al., 2009) was downloaded from the land DAAC (https://lpdaac.usgs.gov/products/modis_products_table/mod44w) on 24 Dec 2013. This dataset consists of 318 HDF-EOS files in the MODIS sinusoidal projection, each granule covering an approximately 10°x10° region. Granules that are entirely water are not included in the dataset; all missing granules in the MOD44W dataset are for ocean regions, not inland water regions, so they are not needed for this mask.

4.5.1.2 GSHHG

The Global Self-consistent, Hierarchical, High-resolution Geography Database (Wessel and Smith, 1996) is a set of polygons defining shorelines globally. The highest resolution ("full")

version of the level 1 shorelines (boundaries between land and ocean) was used. Other levels give boundaries of lakes, islands in lakes, and ponds on islands in lakes. The GSHHG land/ocean shorelines are based on the World Vector Shoreline (http://shoreline.noaa.gov/data/datasheets/wvs.html), which has an accuracy of 50 to 500 meters. The accuracy of the internal shorelines (lakes, islands in lakes, etc.), which are based on the CIA World Data Bank II (http://www.evl.uic.edu/pape/data/WDB) is an order of magnitude worse (500 meters to 5 kilometers); these were not used for the masks. Version 2.2.2 of GSHHG was downloaded from http://www.soest.hawaii.edu/pwessel/gshhg/ on 16 Jan 2014.

4.5.1.3 Named Marine Water Bodies (NMWB)

This is a global dataset from ESRI, consisting of 234 discrete, named water body shapes, not including interior water bodies. These data were trimmed to 78 shapes after download to exclude bodies larger than Hudson Bay (oceans, etc.) at ~920,000 km^2. The original data can be found at: http://mappingcenter.esri.com/index.cfm?fa=arcgisResources.gisData.

4.5.1.4 Global Lakes and Wetland Database

A global dataset of lakes and wetlands, based on Lehner and Doll (2004) is available here (https://worldwildlife.org/pages/global-lakes-and-wetlands-database). These datasets are provided as shape files. The Level 1 data product contains water bodies with areas greater than 50 km^2, and the Level 2 data product contains permanent water bodies greater than 0.1 km^2. Level 1 was downloaded on 30 August 2013; Level 2 on 28 August 2013.

4.5.1.5 Alaskan Lakes Database

Maps generated from Landsat images (Sheng, U California; Water depicted as of 2000) of 38,000 Lakes in Alaska. There are three levels of Alaskan Lakes identified: Level 1 are lakes greater than 10 km^2 in area; Level 2 lakes are greater than 1 km^2; and Level 3 lakes are greater than 0.1 km^2. http://data.eol.ucar.edu/codiac/dss/id=106.346. This dataset was downloaded on 18 February 2014.

4.5.1.6 Ephemeral Lakes

The mask includes the center coordinates of approximately two hundred of the largest global ephemeral lakes (i.e. non-permanent lakes). Current version as of 11 March 2014 was received from Charon Birkett on that date. (Birkett and Mason, 1995; updated).

4.5.1.7 Circum-Arctic Map of Permafrost and Ground Ice Conditions

We used the spatial and temporal extent of permafrost in the Northern Hemisphere as determined by Brown, et al. (1997), located here at http://www.arcgis.com/home/item.html?id=c7f215ed7fa149538f0542ba3839588f. This dataset was downloaded on 18 March 2014 through ESRI, which provided a ready-to-use ArcGIS

layerpack as part of the download. The underlying raw data was included in the download contents and was verified to match the NSIDC version available through FTP.

4.5.2 Mask Generation

4.5.2.1 Shapefile Generation

The ArcGIS Toolbox in ESRI ArcMap 10.1 was used to do all of the distance-based buffering and final shapefile generation. The procedure was applied to the following input datasets, resulting in one or more shapefiles containing polygons defining the regions in each case:

- The **GSHHG Version 2.2.2 coastline** was processed using a 10-km buffer.
- The **Global Wetlands Database, levels 1 and 2** were processed using a 250-m buffer (equivalent to the MOD44W pixel-size).
- The **Alaskan Lakes dataset, levels 1, 2, and 3** were processed using a 250-m buffer.
- The **Named Marine Water Bodies** dataset was reduced to include only water bodies the size of Hudson Bay (920,000 km^2) and smaller. Then a 1-km buffer was used for the processing.
- The **Ephemeral Lakes** data were received as point-based data. The data were buffered into circles of 1 degree diameter.
- The largest extent in the **Permafrost database** was used. This was deemed to be sufficiently inclusive that additional buffering was not needed.

4.5.2.2 MOD44W Masks

The MOD44W water mask was read in granule by granule. A 1-pixel (nominally 250x250m) buffer was added around each water pixel, and the granules were saved in the same coordinate system as the original files. Because the Antarctic mask was generated from polygons, the southern limit of the mask was set at 60°S, and because the northern tier mask was to include all land, and thus be defined by the GSHHG shorelines, the northern limit was set at 60°N. Thus the data that were buffered initially covered the MODIS granules from v=3 to v=14. The first pass through these data did not include row v=14. Instead of reprocessing all the data, this row was processed separately.

The MOD44W water mask granules were read one at a time. Latitudes and longitudes were computed for the SW corner of all pixels using software provided by Nick DiGirolamo, and the appropriate pixels in a 0.01°x0.01° grid were flagged. If the input pixel extended across more than one output pixel, all appropriate output pixels were flagged. This procedure was repeated for row v=14 of the MODIS grid, and the resulting mask was added to the mask generated from row v=3 to 13 granules.

4.5.2.3 Northern and Southern Tier Inland Water Mask

The buffered 0.01°x0.01° resolution GSHHG land mask was used to generate an inland water mask for the northern tier by unflagging all pixels between latitudes 60S and 60N. Then the southern tip of Greenland was added back in.

4.5.2.4 Combine the MOD44W and GSHHG Masks

The masks generated in sections 4.5.2.2 and 4.5.2.3 were combined. The MOD44W water mask was intersected with the GSHHG land mask to remove oceans, seas, and bays, and the Paleoarctic/Antarctic mask was added (in union with) to the combined mask.

4.5.2.5 Global Mask Generation

The seven 0.01°x0.01° resolution masks based on the shapefiles generated in ArcGIS (v 10.1) were combined with the 0.01°x0.01° resolution mask based on MOD44W and GSHHG by taking the union of all masks.

4.5.2.6 Final Mask Gen<eration

The global mask was broken into 144 separate .tif files, each covering 90° latitude and 5° longitude, for use by the ATL03 production software. The file names reflect the region covered. An attempt was made to generate these files as Geotiff files, but there appears to be a problem with at least one of the Geotiff parameters, so the file names and known resolution should be used when working with them. Sample file name: **`iwmask_-90_0_000E_005E.tif`**. The latitude range is given first (-90_0), followed by the longitude range (0E-5E).

The final mask is shown in Figure 4-5.

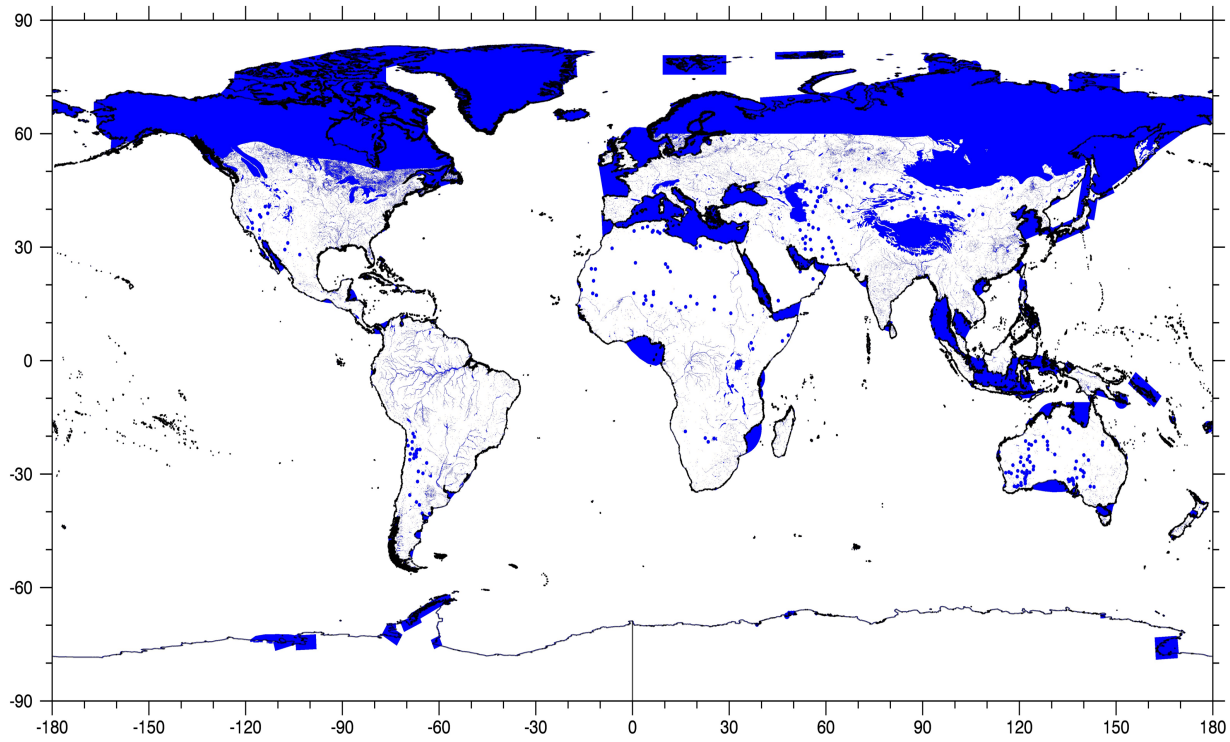

Figure 4-5. Inland Water Mask.

5.0 PHOTON CLASSIFICATION

Atmospheric conditions permitting, transmitted laser light from ATLAS reaches the Earth's surface as pulses of down-traveling photons. At the ground, photons are scattered once, or many times, by surface interactions, such as with vegetation or snow and ice grains, and depart in every direction, including back towards ATLAS. Based on performance models, the arrival times of up to twelve received photons per transmitted laser pulse return to the ATLAS telescope's focal plane and are recorded by the detector electronics. At the same time, background photons from sunlight are continually entering the telescope when the surface is illuminated by the sun, and the arrival times of these are also recorded. The number and distribution of the returned photons depends on the geometry and reflectance of the Earth's surface, on scattering and attenuation in the atmosphere, and, for the background photons, on the solar angle. Any photon that is time tagged by ATLAS, regardless of source, is referred to as a photon event. Based on pre-launch test data, photon events due to instrument noise are a small fraction of time-tagged photons, and are indistinguishable from solar background photons.

A primary objective of the ICESat-2 data processing is to correctly discriminate between signal photon events and background photon events. This is done as a series of three steps with progressively finer discrimination. First, onboard algorithms reduce the volume of data downlinked to the Earth by generating histograms and determining which photon events are most likely to contain the desired surface echo. The downlinked band of photon events varies according to surface type, surface roughness, and the precision with which the surface is already known. For example, the ellipsoidal height of the ocean is known much more precisely than the ellipsoidal height of rough mountainous terrain. It is possible that there will be more than one downlinked band of photon events for a given along-track interval, for example if the on-board algorithm identifies two distinct bands of heights that may contain surface echoes.

Second, ATL03 classifies each downlinked photon event as being either likely signal or background. This algorithm is described in detail in this section. The goal of this photon classification is to reduce the volume of data that the subsequent higher-level data products must analyze. Finally, these surface-specific higher-level data products generate precise ellipsoidal heights from the identified signal photon events. These precise, surface-specific heights are used to satisfy the ultimate goals of the ICESat-2 mission.

5.1 Introduction

ICESat-2 will telemeter time tags for all photon events that fall within the downlink bands, which are surface type and terrain dependent. The downlink bands contain both signal and background. The goal of this algorithm is to identify all the signal photon events while classifying as few as possible of the background photon events erroneously as signal. If the rate of background photon events is known, then the algorithm can identify likely signal photon events by finding regions where the photon event rate is significantly larger than the background photon event rate. The telemetry band is limited (30 meters to ~2000 meters), so the downlinked photon data is not optimal for calculating a robust background count rate. However, for

atmospheric research, ICESat-2 telemeters histograms of the sums of all photons over four hundred laser transmit pulses (0.04 seconds; ~280 meters along-track) in 30-m vertical bins for ~14 kilometers in height that includes the atmosphere, surface echoes, and extends below the Earth's surface. These histograms are referred to as atmospheric histograms. After removing the relatively few bins that may contain signal photon events from these atmospheric histograms, the algorithm uses the remaining bins to estimate the background photon event rate (section 5.4.1.1). Nominally, the atmospheric histograms will only be downlinked for the strong beams. When the atmospheric histogram is not available, the photon cloud itself is used to determine the background count rate.

The algorithm uses the resulting background rate estimate to calculate a signal threshold. It then generates a histogram of photon ellipsoidal heights (heights above the WGS-84 ellipsoid) and distinguishes signal photons from background photons as those that pass a series of tests dependent on the signal threshold. Data from each ground track is considered independently for the ellipsoidal histogramming procedure. Over sloping surfaces, the surface photons can be spread over a range of heights so that they are not readily found with ellipsoidal histogramming. To identify these, a histogram is generated relative to the surface profile as defined by the surrounding ellipsoidally-identified signal photon events. This procedure is referred to as slant histogramming. For the strong beams, if a large break in signal photons is still evident, there is an option to perform variable slope slant histogramming to find any remaining signal photon events. Since the signal to noise ratio is larger for the strong beam than the weak beam, the strong beam provides a better definition of the surface than the weak beam. The ground tracks of a strong and weak beam pair are essentially parallel to each other, and separated by ~90 meters in the across-track direction, so the slopes of the resultant surface profiles should be very similar. Therefore for the weak beam of each pair, the algorithm uses the surface profile found in the strong beam to guide slant histogramming in the weak beam.

Authors of each of the higher-level surface-specific ICESat-2 ATBDs that draw on the ATL03 data product have provided guidance regarding the fidelity to which the ATL03 algorithm needs to discriminate signal and background photon events. In general, each higher-level data product requires ATL03 to identify likely signal photon events within +/- 10 meters of the surface. Since this algorithm uses histograms, the vertical resolution at which signal photons are selected is directly proportional to the histogram bin size. All photons in any one bin are either classified as signal or background events. One of the goals of the algorithm is to use the smallest bin size for which signal can be found, to classify photons at the finest resolution possible. Our test cases show that this resolution in all but very weak signal conditions meets or exceeds the needs of the higher-level data products. This smallest bin size varies as a function of surface slope and background count rate.

Once identified, the algorithm generates a flag for each photon event indicating whether the algorithm determined a given photon event to be signal or background, as well as the parameters used to classify photons. As requested by the science team, additional photon events are flagged surrounding those selected as signal to insure that the photon events classified as signal span a minimum of twenty meters vertically. The flag distinguishes between photon events that were

added as a buffer and those that were identified as signal, and indicates the level of confidence in the classification.

The output parameters are defined in Table 5-4 and are indicated throughout this document in ***bold italics***. Table 5-1, Table 5-2, and Table 5-3 respectively contain the input variables from external data sources, parameters used to drive the algorithm, and intermediate variables generated and used within the algorithm.

5.2 Overview

This algorithm is based on the assumption that background photon events recorded by ATLAS follow a Poisson distribution, which has been supported by analysis of MABEL (the airborne ICESat-2 simulator; McGill et al. 2010) photon-counting data. (Tom wrote this for an RFA response in 2013. Not sure how to cite this. This should get a CM number as well.) Therefore, this algorithm uses Poisson statistics to find outliers to this distribution, which are designated as possible signal photon events. The algorithm makes this discrimination on the basis of histograms, where photon events are aggregated into along-track and vertical bins. Background photon events are randomly distributed among the bins (according to Poisson statistics) while signal photons cluster into one or a few bins. The algorithm is driven by input parameters, many of which are surface type dependent, to optimize signal definition while minimizing execution time.

Figure 5-1 shows photons from one MABEL green channel over the Greenland ice sheet during the daytime, with along-track distance on the x-axis and ellipsoidal height on the y-axis. The signal and noise levels in this example are similar to what we expect for the ATLAS strong beam. Each photon event is plotted as a point and because there are so many photon events from the surface, the surface appears as a thin black line. Variations in the background count rate are apparent; these are due to changing atmospheric conditions and surface reflectivity. Note that over sloping surfaces, the signal photon density decreases as the returns are spread out.

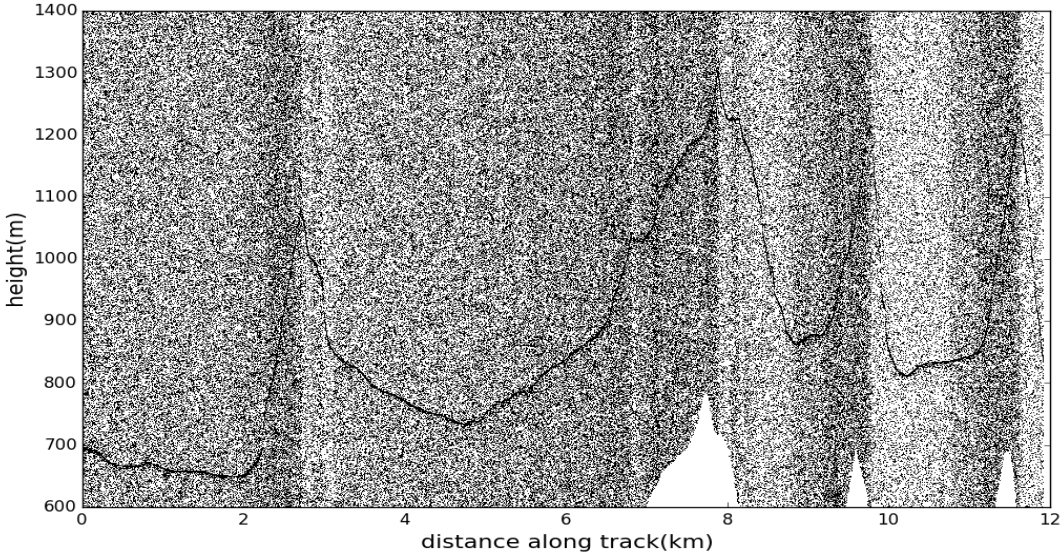

Figure 5-1. Example MABEL data collected near the edge of the Greenland ice sheet. April 2012, near local noon. This is one of several hundred granules used to develop and test the algorithm.

Surface slopes present one of the main challenges for identifying signal photon events (e.g. Figure 5-1). Ideally, one would histogram the photon event heights relative to the direction of the slope of the surface so all the signal photons would be combined into one bin. However, the surface slope over the integration span is not known *a priori*. As a first step, the algorithm histograms the photon event heights relative to the ellipsoid. The algorithm steps through the data granule in uniform time increments, Δtime. For each Δtime, the algorithm histograms the photon events over an integration time, δt, at a vertical resolution, δz. The algorithm automatically adjusts δt and δz (section 5.4.2.4) until the algorithm either identifies vertical bins that contain more photon events than a threshold based on the background count distribution, or the algorithm reaches a pre-defined limit on δt and δz (Table 5-2) without identifying any bins that contain signal photon events for a given Δtime. This automatic adjustment allows the algorithm to maintain the highest resolution possible in terms of the histogram bin dimensions when identifying signal photon events. After the algorithm identifies possible signal photon events it then selects additional bins to ensure all signal photon events are included.

Generating histograms relative to the ellipsoid can spread the signal photon events into several bins over sloping surfaces, making it less likely that bins containing signal photon events will be correctly identified by the algorithm. However, signal photon events over low-slope regions are readily identified with ellipsoidal-based histograms.

Figure 5-2 shows the results from the ellipsoidal histogram step for the segment shown in Figure 5-1. Note that some of the surface apparent in Figure 5-1 was not found in regions with steeper slopes. However, the algorithm does produce a rough approximation of the surface height

profile. For fairly flat surfaces, ellipsoidal histogramming should identify all of the signal photon events. Over surface types where significant slopes may be present, two more steps are performed. First, the algorithm performs running linear fits to the surface height profile determined by ellipsoidal histogramming to define the local surface slope, α, and histograms the photon heights relative to α to search for signal returns along a linear trend determined by the adjacent surface slopes. Figure 5-3 shows the additional signal photon events found with this step, referred to in this document as "slant" histogramming plotted in black.

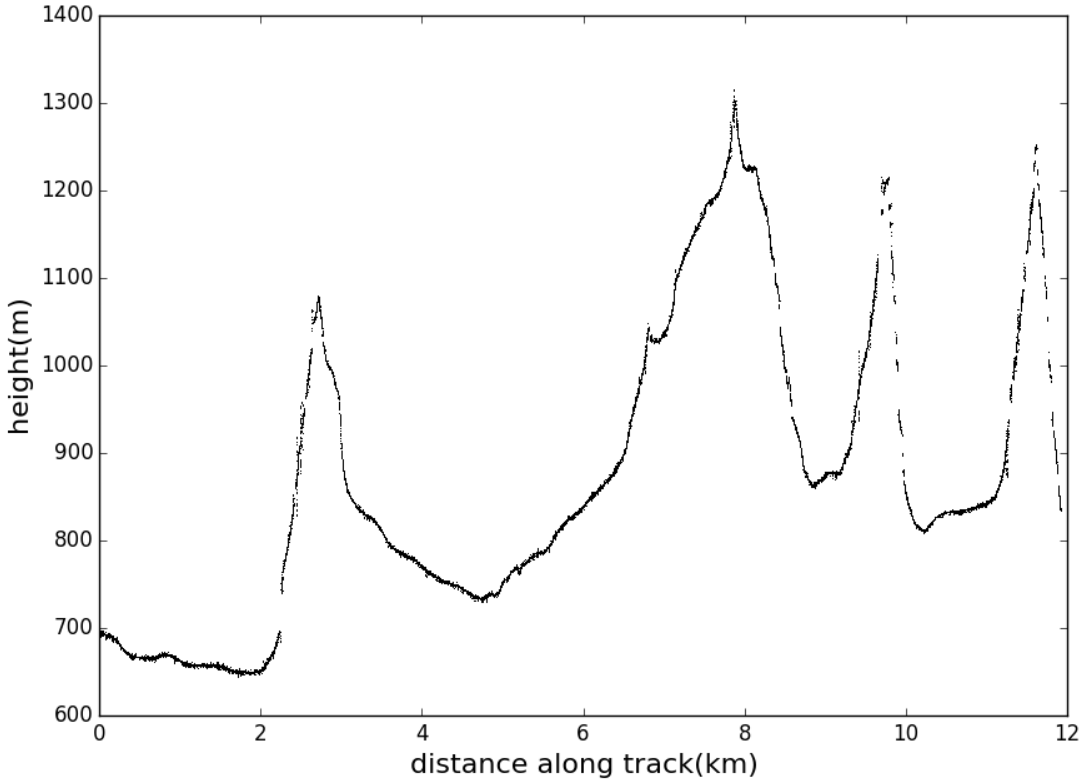

Figure 5-2. Likely Signal Photon Events after Ellipsoidal Histogram.

Next, if large time gaps still exist (greater than Δtime_gapmin), it may not be appropriate to assume that the surface slope is linear. In these cases, the algorithm generates slant histograms using a variable surface slope at each time increment, Δtime, within these gaps to try to identify any additional signal photons. For the MABEL granule shown here, there were no large gaps so variable slope slant histogramming was not needed.

The algorithm generates a confidence parameter for each likely signal photon event to indicate if the photon was classified with high, medium, or low confidence based on the signal to noise ratio of each histogram bin. The algorithm includes an option to perform an nσ edit on a running linear fit to the identified signal to remove outliers.

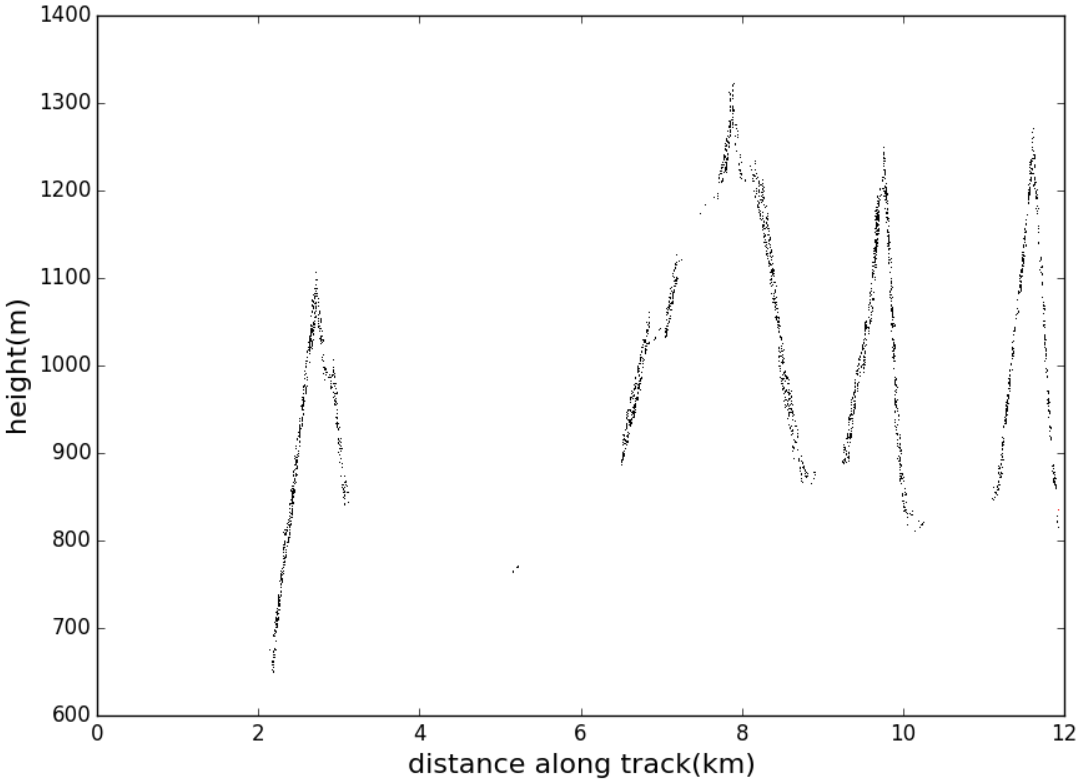

Figure 5-3. Additional Signal Photon Events.
Identified via slant histogramming. Black indicates photons found from slant histogramming using the slope from the profile defined by ellipsoidal histogramming.

Additional surrounding background photons are added if the identified signal photons for a Δtime do not meet a minimal height span requirement, Htspanmin. Higher-level data products currently require the region identified as signal spans at least 20 meters vertically. The final results for this profile are shown in Figure 5-4, color coded by confidence (blue = high; green = medium, red = low, black = padding) which when compared to Figure 5-1 appears to identify all the returns reflected from the surface.

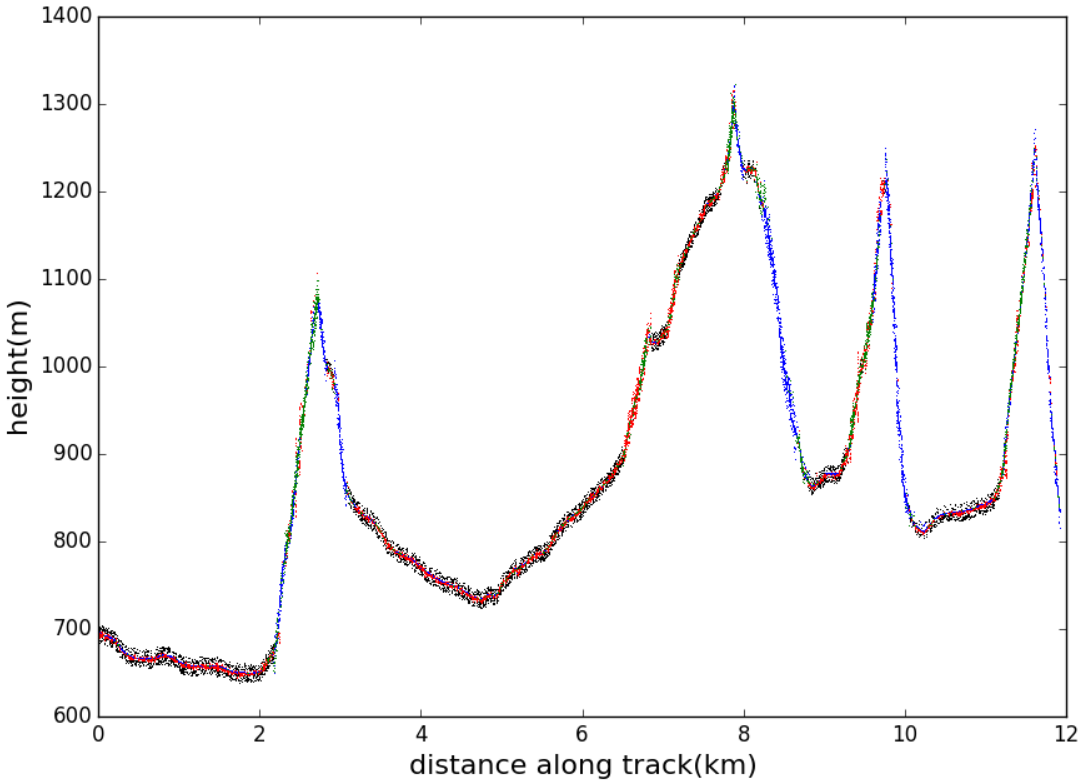

Figure 5-4. Final Classified Likely Signal Photons.
Confidence level - high (blue, 29153 photons), medium (green, 12587 photons), low (red, 4292), padding (black, 3393 photons).

The figures above illustrate the algorithm performance on a segment of MABEL data over land ice. As the algorithm development progressed, it became clear that different surfaces, and different beam energies required different parameter values in order to best identify likely signal photon events and minimize the number of false positives. As described in detail in a companion document (document title, number here), we optimized the parameter settings according to surface type (land, ocean, sea ice, land ice, inland water) and beam energy (strong and weak). Consequently, many parameters in Table 5-2 are surface type or beam energy dependent.

The likelihood of identifying likely signal photons varies as a function of background rate. We simulated a surface and varied the background photon rate to determine the sensitivity of the photon classification algorithm to background photon rate. In Figure 5-5, the simulated surface is shown on the left with two different background rates. On the right of Figure 5-5, we summarize the results of seven simulations. In general, the surface is classified with high confidence up to a few MHz of background photon events. As the background photon rate increases, the fraction of medium and low-confidence photons increases. Above approximately

10 MHz, there are relatively few high-confidence photons identified, and the surface becomes mainly classified with low-confidence. It is worth noting that the algorithm determines a similar total number of likely signal photons as the background rate increases, when the numbers of high-, medium-, and low-confidence photon events are summed, although the relative fraction of each classification changes.

Although the surface used in this example is relatively simple, we expect this example to be a useful example for similarly simple surface topologies, such as the ocean, sea ice, or ice sheet interior. For other more complex surfaces, the background rates where high- or medium-confidence photon events dominate will likely be lower, and low-confidence photon events will likely dominate.

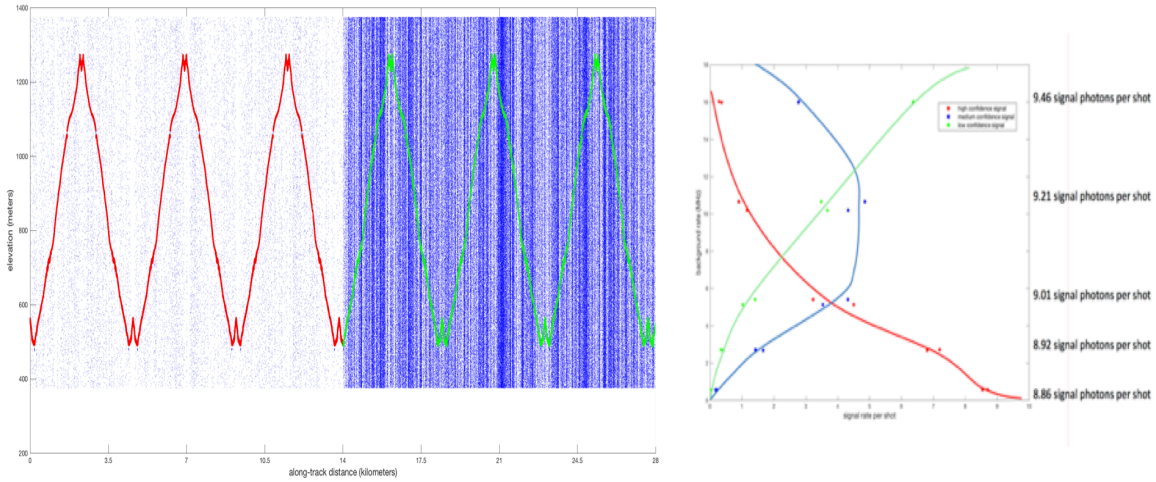

Figure 5-5: Figure on the left shows a simulated photon cloud with X MHz of background photon events on the left half and Y MHz on the right. Likely signal photons are color-coded as in Figure 5-4. Figure on the right shows the distribution of low- medium- and high-confidence photon events as a function of background rate. The photon confidence level decreases as the background rate increases.

5.3 Definitions of Variables used in Algorithm

The variables used in this algorithm are divided into four sets. Table 5-1 reports input variables from external data sources (e.g. ATL02). Table 5-2 lists parameters required to drive the algorithm (written to the ATL03 data product once per granule). Many of these parameters are constants (according to our pre-launch simulations), while others are either beam- or surface-type dependent. In order to simplify the implementation of this algorithm, as well as provide a consistent data format for end users, each parameter in table 5-2 is dimensioned by surface type

and beam (i.e. 5x6). Table 5-3 (intermediate variables, neither input nor output). Table 5-4 (output variables written to the ATL03 data product).

Input Variables for Photon Classification Algorithm

Name	Description	MABEL File Source Parameter Name	ATL02 Source Parameter Name	Notes
H_p	Photon height array	'/photon/channelnnn/elev' where nnn = channel number	/PCEx/ALT_tlm/RX_ranges rx_range	
H_{ATM}	Atmospheric histograms	'/atmosphere/histogram/channelnnn/histogram'	/PCEx/ATM_tlm/ATM_hist atm_s_bins	
Ha	Atmospheric histograms	identical to H_{ATM} if the atmospheric histogram is downlinked, otherwise it is formed from the photon cloud		
Ta_start	Array of start times associated with each Ha	'/atmosphere/delta_time_start'	/PCEx/ATM_tlm/ATM_hist delta_time	
Ta_stop	Array of stop times associated with each Ha	'/atmosphere/delta_time_stop'	Difference between the current and next delta_time. If greater then .05 sec diff then use 0.04 sec (or last delta).	
T_p	Photon time array	'/photon/channelnnn/delta_time' where nnn= channel number	/PCEx/ALT_tlm/RX_ranges delta_time	
Tw_{TOP}	The height of the top of the telemetry window maximum height for each band	'/altimetry/dem_drm/elev_top_window'	/PCEx/ALT_tlm/mf_data alt_s_rw_s alt_w_rw_s	
Tw_{WIDTH}	The width of the telemetry window for each band	'/altimetry/dem_drm/elev_bot_window'	/PCEx/ALT_tlm/mf_data alt_s_rw_w alt_w_rw_w	
Tw_start	Array of start times associated with each element of Tw_{TOP} and Tw_{WIDTH}	'/altimetry/delta_time_start'	/PCEx/ALT_tlm/mf_data delta_time	
Tw_stop	Array of stop times associated with each element of Tw_{TOP} and Tw_{WIDTH}	'/altimetry/delta_time_stop'	Created by differencing the current and next delta_time. If greater than .03 sec diff then use 0.02 sec (or last delta)	

Table 5-1. Input Variables for Photon Classification Algorithm.

Parameters Needed to Drive the Algorithm; Input Parameters

Name (units)	Variable Type	Dimension[1]	Description	Default[2]
αmax (rad)	R*4	(5, 6)	Maximum slope allowed for slant histogram; if larger than this then don't attempt to fill gap	[0.9, 0.9, 0.9, 0.9, 0.9] [0.9, 0.9, 0.9, 0.9, 0.9] [0.9, 0.9, 0.9, 0.9, 0.9] [0.9, 0.9, 0.9, 0.9, 0.9] [0.9, 0.9, 0.9, 0.9, 0.9] [0.9, 0.9, 0.9, 0.9, 0.9]
αinc (rad)	R*4	(5, 6)	Coarse increment by which to vary the surface slope, α, when filling large gaps	[0.05, 0.05, 0.05, 0.05, 0.05] [0.05, 0.05, 0.05, 0.05, 0.05] [0.05, 0.05, 0.05, 0.05, 0.05] [0.05, 0.05, 0.05, 0.05, 0.05] [0.05, 0.05, 0.05, 0.05, 0.05] [0.05, 0.05, 0.05, 0.05, 0.05]
Δtime (seconds)	R*4	(5, 6)	Time increment at which to step through the photon cloud in a granule; histograms will be	[0.00971, 0.00857, 0.00286, 0.00286, 0.00286]

[1] Dimensions for all parameters are 5x6, to accommodate for different surface types (dimension = correspond to land, ocean, sea ice, land ice, inland water, in that order), and different values for each beam energy (dimension 6; first, third and fifth values are for the strong beams; second, fourth and sixth are for weak beams). If you prefer to work in ground tracks, use the orientation parameter to convert these arrays accordingly (see section 7.5) where 1, 3 and 5 are strong beams, and 2, 4 and 6 are weak beams. In the output data table, values are found in the ground-track-specific group /ancillary_data/gtx/signal_find_input, where the gtx notation used elsewhere in this data product is followed.

[2] Default values based on tests with MABEL data over land, ocean, sea ice and land ice, and inland water. Parameters in seconds are expected to be appropriate for ICESat-2, although are derived from MABEL data.

Name (units)	Variable Type	Dimension[1]	Description	Default[2]
			formed at each Δtime to identify signal photon events	[0.012, 0.00857, 0.00286, 0.00514, 0.01086] [0.00971, 0.00857, 0.00286, 0.00286, 0.00286] [0.012, 0.00857, 0.00286, 0.00514, 0.01086] [0.00971, 0.00857, 0.00286, 0.00286, 0.00286] [0.012, 0.00857, 0.00286, 0.00514, 0.01086]
Δtime_gapmin (seconds)	R*4	(5, 6)	Time in seconds of the minimum size of a gap in the height profile over which to use variable slope slant histogramming	[0.00971, NA, NA, 0.00286, NA] [0.00971, NA, NA, 0.00286, NA] [0.00971, NA, NA, 0.00286, NA] [0.00971, NA, NA, 0.00286, NA] [0.00971, NA, NA, 0.00286, NA] [0.00971, NA, NA, 0.00286, NA]
Δt_linfit_edit (seconds)	R*4	(5, 6)	Time span over which to perform a running linear fit to identified signal when editing outliers	[0.19429, 0.17143, 0.05714, 0.05714, 0.05714] [0.24000, 0.17143, 0.05714, 0.10286, 0.21714] [0.19429, 0.17143, 0.05714, 0.05714, 0.05714] [0.24000, 0.17143, 0.05714, 0.10286, 0.21714] [0.19429, 0.17143, 0.05714, 0.05714, 0.05714] [0.24000, 0.17143, 0.05714, 0.10286, 0.21714]
nslw (n/a)	R*4	(5, 6)	The multiplier of δzmax2sl used to define half the value of the height window used for slant	[20, 20, 20, 20, 20] [20, 20, 20, 20, 20]

Name (units)	Variable Type	Dimension[1]	Description	Default[2]
			histogramming relative to the surface defined by the linear fit to the surrounding photons at slope, α	[20, 20, 20, 20, 20] [20, 20, 20, 20, 20] [20, 20, 20, 20, 20] [20, 20, 20, 20, 20]
nslw_v (n/a)	R*4	(5, 6)	The multiplier of δzmax2sl used to define half the value of the height window used for slant histogramming relative to the surface when varying the surface slope, α, to fill large gaps	[20, 20, 20, 20, 20] [20, 20, 20, 20, 20] [20, 20, 20, 20, 20] [20, 20, 20, 20, 20] [20, 20, 20, 20, 20] [20, 20, 20, 20, 20]
δt_{min} (sec)	R*4	(5, 6)	Minimum time interval over which photons are selected to histogram	[0.00971, 0.00857, 0.00286, 0.00286, 0.00286] [0.01200, 0.00857, 0.00286, 0.00514, 0.01086] [0.00971, 0.00857, 0.00286, 0.00286, 0.00286] [0.01200, 0.00857, 0.00286, 0.00514, 0.01086] [0.00971, 0.00857, 0.00286, 0.00286, 0.00286] [0.01200, 0.00857, 0.00286, 0.00514, 0.01086]
δt_{max} (sec)	R*4	(5, 6)	Maximum time interval over which photons are selected to histogram	[0.10286, 0.02286, 0.01143, 0.02286, 0.05714] [0.10286, 0.02286, 0.01143, 0.02286, 0.05714] [0.10286, 0.02286, 0.01143, 0.02286, 0.05714] [0.10286, 0.02286, 0.01143, 0.02286, 0.05714] [0.10286, 0.02286, 0.01143, 0.02286, 0.05714] [0.10286, 0.02286, 0.01143, 0.02286, 0.05714]

Name (units)	Variable Type	Dimension[1]	Description	Default[2]
δz_{min} (meters)	R*4	(5, 6)	Minimum height bin size for histogramming for first sweep	[0.6, 0.7, 0.4, 0.8, 0.7] [0.6, 0.7, 0.4, 0.7, 0.7] [0.6, 0.7, 0.4, 0.8, 0.7] [0.6, 0.7, 0.4, 0.7, 0.7] [0.6, 0.7, 0.4, 0.8, 0.7] [0.6, 0.7, 0.4, 0.7, 0.7]
δz_{max2} (meters)	R*4	(5, 6)	Maximum height bin size for histogramming for second sweep	[13, 5, 2, 5, 5] [13, 5, 2, 5, 5] [13, 5, 2, 5, 5] [13, 5, 2, 5, 5] [13, 5, 2, 5, 5] [13, 5, 2, 5, 5]
δz_{BG} (meters)	R*4	(5, 6)	Width of a height bin in each atmospheric histogram, Ha, if calculating Ha from the photon cloud	[1, 1, 1, 1, 1, 1] [1, 1, 1, 1, 1, 1] [1, 1, 1, 1, 1, 1] [1, 1, 1, 1, 1, 1] [1, 1, 1, 1, 1, 1] [1, 1, 1, 1, 1, 1]
Addpad	L*1	(5, 6)	Boolean: if true (=1), then identify addtional photons as padding to achieve htspanmin at each Δtime; if false(=0), then do not	[1, 1, 1, 1, 1] [1, 1, 1, 1, 1] [1, 1, 1, 1, 1] [1, 1, 1, 1, 1] [1, 1, 1, 1, 1] [1, 1, 1, 1, 1]
e_a	R*4	(5, 6)	Multiplier of Ha_σ used to determine which bins in Ha may contain signal photon events	[2.5, 2.5, 2.5, 2.5, 2.5] [2.5, 2.5, 2.5, 2.5, 2.5] [2.5, 2.5, 2.5, 2.5, 2.5] [2.5, 2.5, 2.5, 2.5, 2.5] [2.5, 2.5, 2.5, 2.5, 2.5] [2.5, 2.5, 2.5, 2.5, 2.5]

Name (units)	Variable Type	Dimension[1]	Description	Default[2]
e_linfit_slant	R*4	(5, 6)	Multiplier of σ_linfit, the standard deviation of the residuals between the actual photon events used to estimate the surface using a linear fit; all photons with height > e_linfit_slant × σ_linfit are edited from the next iteration of the fit	[4, 4, 4, 4, 3.5] [4, 4, 4, 4, 3.5] [4, 4, 4, 4, 3.5] [4, 4, 4, 4, 3.5] [4, 4, 4, 4, 3.5] [4, 4, 4, 4, 3.5]
e_linfit_edit	R*4	(5, 6)	Multiplier of standard deviation of linear fit to signal photons used to edit out noise during running linear fit edit of outliers	[3, 3, 3, 3, 3] [3, 3, 3, 3, 3] [3, 3, 3, 3, 3] [3, 3, 3, 3, 3] [3, 3, 3, 3, 3] [3, 3, 3, 3, 3]
e_m	R*4	(5, 6)	Multiplier of standard deviation of the number of background photon events per bin used in determining whether signal photons exist	[4, 7, 3.5, 5.5, 5.5] [4, 7, 4.5, 5.5, 5] [4, 7, 3.5, 5.5, 5.5] [4, 7, 4.5, 5.5, 5] [4, 7, 3.5, 5.5, 5.5] [4, 7, 4.5, 5.5, 5]
e_m_mult	R*4	(5, 6)	Multiplier of e_m used to determine Th_{sig2}, threshold for singular bins	[3, 3.5, 2, 2.5, 3] [3, 3.5, 2, 2, 2] [3, 3.5, 2, 2.5, 3] [3, 3.5, 2, 2, 2] [3, 3.5, 2, 2.5, 3] [3, 3.5, 2, 2, 2]
Ledit	L*1	(5, 6)	Binary (logical) flag: if true (=1), then perform an n σ edit on a running linear fit to identified signal to remove outliers	[0, 0, 0, 1, 0] [0, 0, 0, 1, 0] [0, 0, 0, 1, 0] [0, 0, 0, 1, 0] [0, 0, 0, 1, 0] [0, 0, 0, 1, 0]

Name (units)	Variable Type	Dimension[1]	Description	Default[2]
Lpcbg	L*1	(5, 6)	Binary (logical) flag: if true (=1), always use the photon cloud to calculate the background photon rate; if false, only use the photon cloud in the absence of the atmospheric histogram	[0, 0, 0, 0, 0] [0, 0, 0, 0, 0] [0, 0, 0, 0, 0] [0, 0, 0, 0, 0] [0, 0, 0, 0, 0] [0, 0, 0, 0, 0]
lslant	L*1	(5, 6)	Binary (logical) flag: if true (=1), then perform slant histogramming for the strong beam; if false (=0), do not	[1, 0, 0, 1, 0] [1, 0, 0, 1, 0] [1, 0, 0, 1, 0] [1, 0, 0, 1, 0] [1, 0, 0, 1, 0] [1, 0, 0, 1, 0]
Htspanmin	R*4	(5, 6)	Minimum height span for each time interval of photons with confidence flag > 0; if the height span is < htspanmin, then all photons not previously selected within +/- htspanmin/2 of the median height of the signal photons selected are marked with a confidence flag of 1	[20, 20, 20, 20, 20] [20, 20, 20, 20, 20] [20, 20, 20, 20, 20] [20, 20, 20, 20, 20] [20, 20, 20, 20, 20] [20, 20, 20, 20, 20]
min_fit_time_fact	I*2	(5, 6)	The factor to multiply Δtime by to obtain the minimum time over which to fit a line to a height profile to calculate the local slope using running linear fits.	[3, 4, 10, 10, 10] [3, 4, 10, 6, 3] [3, 4, 10, 10, 10] [3, 4, 10, 6, 3] [3, 4, 10, 10, 10] [3, 4, 10, 6, 3]
nδz1	I*2	(5, 6)	The number of δz values used for first δz interval δz_{min} and δz_{max1}	[5, 5, 5, 5, 5] [5, 5, 5, 5, 5] [5, 5, 5, 5, 5] [5, 5, 5, 5, 5] [5, 5, 5, 5, 5] [5, 5, 5, 5, 5]

Name (units)	Variable Type	Dimension[1]	Description	Default[2]
nδz2	I*2	(5, 6)	The number of δz values used for second δz interval δz_{max1} and δz_{max2}	[2, 2, 2, 2, 2] [2, 2, 2, 2, 2] [2, 2, 2, 2, 2] [2, 2, 2, 2, 2] [2, 2, 2, 2, 2] [2, 2, 2, 2, 2]
Nbinmin	I*2	(5, 6)	Minimum number of bins in a histogram required for the algorithm to be able to process the histogram	[5, 5, 5, 5, 5] [5, 5, 5, 5, 5] [5, 5, 5, 5, 5] [5, 5, 5, 5, 5] [5, 5, 5, 5, 5] [5, 5, 5, 5, 5]
Nphotmin	I*2	(5, 6)	The minimum number of photons over which to perform a linear fit to estimate the surface profile across a gap	[6, 6, 6, 6, 6] [6, 6, 6, 6, 6] [6, 6, 6, 6, 6] [6, 6, 6, 6, 6] [6, 6, 6, 6, 6] [6, 6, 6, 6, 6]
R	R*4	(5, 6)	Minimum ratio of max number of photons in histogram bin to mean noise value that must exist to consider a bin a signal bin	[2.5, 2.5, 2.5, 2.5, 2.5] [2.5, 2.5, 2.5, 2.5, 2.5] [2.5, 2.5, 2.5, 2.5, 2.5] [2.5, 2.5, 2.5, 2.5, 2.5] [2.5, 2.5, 2.5, 2.5, 2.5] [2.5, 2.5, 2.5, 2.5, 2.5]
r2	R*4	(5, 6)	Minimum ratio of maximum number of photons in any one bin of contiguous signal bins to maximum number of photons in largest bin required in order to accept a group of signal bins as real signal	[0.8, 0.7, 0.7, 0.8, 0.8] [0.8, 0.7, 0.7, 0.8, 0.8] [0.8, 0.7, 0.7, 0.8, 0.8] [0.8, 0.7, 0.7, 0.8, 0.8] [0.8, 0.7, 0.7, 0.8, 0.8] [0.8, 0.7, 0.7, 0.8, 0.8]

Name (units)	Variable Type	Dimension[1]	Description	Default[2]
snrlow	R*4	(5, 6)	Signal to noise ratio below which all selected signal has low confidence	[40, 40, 40, 40, 40] [40, 40, 40, 40, 40] [40, 40, 40, 40, 40] [40, 40, 40, 40, 40] [40, 40, 40, 40, 40] [40, 40, 40, 40, 40]
snrmed	R*4	(5, 6)	Signal to noise ratio above which all selected signal has high confidence. Selected signal with signal to noise ratio between snrlow and snrmed is marked as medium confidence	[100, 100, 100, 100, 100] [100, 100, 100, 100, 100] [100, 100, 100, 100, 100] [100, 100, 100, 100, 100] [100, 100, 100, 100, 100] [100, 100, 100, 100, 100]

Table 5-2. Parameters Needed to Drive the Algorithm; Input Parameters.

Parameters Calculated Interally Within the Algorithm

Name	Units	Description	Section
α	radians	Local surface slope	5.4.2.5.2
δt	seconds	Generic notation for integration time over which photon events are selected for a histogram	5.4.2.4
δt_{ATM}	seconds	Time duration spanned by each atmospheric histogram	5.4.1.1
δt_{BG}	seconds	Integration time over which the background rate is determined; when the atmospheric histograms are available, this time corresponds to 280m along track; the same duration is used if the background rate is determined from the photon cloud.	5.4.1.1
δt_{inc}	seconds	Increment that δt_{PC} should be increased by when increasing the integration time over which photon histogramming will occur for one time interval, Δtime	5.4.2.1

Name	Units	Description	Section
δt_{PC}	seconds	The integration time over which a photon cloud histogram is created, centered around t_n	5.4.2.1
δt_{PC}_use	seconds	Actual time span over which photons exist for δt_{PC} such that δt_{PC}_use = δt_{PC} if there are no missing telemetry windows within δt_{PC}, otherwise δt_{PC}_use= Σ t for the portions of all telemetry windows that exist within δt_{PC}	5.4.2.2
δz	meters	Width of height bins in a histogram	5.4.2.4
δz_{ATM}	meters	Width of a height bin in each atmospheric histogram, H_{ATM}	5.4.1.1
δz_{BG}	meters	Width of a height bin in each atmospheric histogram, Ha – nominally 30 meters set if using telemetered histogram, set to δz_{NS} if calculating the atmospheric histogram from the photon cloud.	5.4.1.1
δz_{max1}	meters	Maximum height bin size for histogramming for first pass = δz_{min} + (δz_{max2} - δz_{min}) / 2	5.4.2.4
δz_{min2}	meters	Minimal height histogram size used in second set of dz values	5.4.2.4
δz_{PC}	meters	The height bin size of a photon cloud histogram	5.4.2.1
μ	N/A	Mean of a distribution	5.4.1.1
μ_{bg}_δz_{pc}_δt_{PC}	photon events	The mean background photon count for the specific time interval time_h_b to time_h_e and height bin size δZ_{pc}	5.4.2.2
μt	photon events	The mean of a distribution that is the combination of two individual distributions	5.4.2.2
σ	N/A	Standard deviation of a distribution	5.4.1.1
σ_{bg}_δz_{pc}_δd_{PC}	photon events	The standard deviation of the background count scaled to δz_{PC} and δd_{PC}	5.4.2.2
C0 (number of linear fits in segment)	meters	The bias coefficient of the estimated surface profile formed by a linear fit to signal photons	5.4.2.5, 5.4.3
C1 (number of linear fits in section)	meters of ht per sec along granule	The slope coefficient of the estimated surface profile formed by a linear fit to signal photons	5.4.2.5, 5.4.3
Ta_start (Number of atmospheric histograms)	seconds	Time of the start of an atmospheric histogram	5.4.2.2.1
Ta_stop (Number of atmospheric histograms)	seconds	Time at the end of an atmospheric histogram	5.4.2.2.1
T_{beg}	meters	The time relative to the beginning of the pass associated with the time, time_h_b	5.4.3.3.3

Name	Units	Description	Section
T_{end}	meters	The time relative to the beginning of the pass associated with the time, time_h_e	5.4.3.3.3
Timebeg_seg [isurf,Nseg(isurf)]	seconds	The time of the beginning of a contiguous segment, Nseg(isurf), for surface type, isurf	5.4.1.2
Timeend_seg [isurf,Nseg(isurf)]	seconds	The time of the end of a contiguous segment, Nseg(isurf), for surface type, isurf	5.4.1.2
Tsl_{beg}	seconds	The time in a slant reference frame measured from the beginning of the pass to time_h_b, the beginning of the integration time used for one slant histogram	5.4.3.3.3
Tsl_{end}	meters	The time in a slant reference frame measured from the beginning of the pass to time_h_e, the end of the integration time used for one slant histogram	5.4.3.3.3
Tsl_p (Number of photon events in the photon cloud)	meters	H_p rotated through the local surface slope, α, into the slant reference frame.	5.4.3.3.3
dz_{inc1}	meters	Value to increase δz_{PC} by when varying it from δz_{min} to δz_{max1}	5.4.2.4
dz_{inc2}	meters	Value to increase δz_{PC} by when varying it from δz_{max1} to δz_{max2}	5.4.2.4
E_{gap} (ngaps)	meters	The estimated surface profile over a gap	5.4.3.2
Ha (number of atmospheric histograms)	photon events	Two-dimentional array containing atmospheric histograms (either from telemetry or calculated from the photon cloud) for each $\delta t_{BG,}$ time interval	5.4.1.1
Ha_σ (number of atmospheric histograms)	photon events	Array containing the standard deviation of the number of photon events per height bin in each atmospheric histogram; associated times are Ta_start, Ta_stop arrays	5.4.1.1
Ha_μ (number of atmospheric histograms)	photon events	Array containing the mean of the number of photon events per height bin in each atmospheric histogram; associated times are Ta_start and Ta_stop arrays	5.4.1.1
Ha_bg (number of atmospheric histograms)	photon events	An atmospheric histogram after the bins that may contain signal photon events have been removed; contains only bins with background photon events	5.4.1.2
Ha_bg_σ (number of atmospheric histograms)	photon events	Array containing the standard deviation of the number of background event photons in each δz_{BG} height bin for each δt_{BG} along the granule; associated times are in the Ta_start and Ta_stop arrays	5.4.1.3
Ha_bg_μ (number of atmospheric histograms)	photon events	Array containing the mean number of background event photons in each δz_{ATM} height bin for each δt_{ATM} along the granule; associated times are in the Ta_start and Ta_stop arrays	5.4.1.3
Ha_bg_μ_tn_δt_{ATM}_ δz_{ATM}	photon events	The mean of the number of background photon events, corresponding to a specific time time_n, integration time, δt_{ATM}, and height bin size, δz_{ATM}	5.4.2.2.1

Name	Units	Description	Section
Ha_bg_σ_tn_δt_{ATM}_ δz_{ATM}	photon events	The standard deviation of the number of background photon events, corresponding to a specific time time_n, integration time, δt_{ATM}, and height bin size, δz_{ATM}	5.4.2.2.1
$Hmin_{BG}$	meters	Minimum of heights to use in histogram	5.4.1.1.1
$Hmax_{BG}$	meters	Maximum of heights to use in histogram	5.4.1.1.1
Isegbeg [isurf,nseg(isurf)]	N/A	The index of the beginning of a contiguous segment (nseg(isurf)) within surf_type, for surface type isurf	5.4.1.2
Isegend [isurf,nseg(isurf)]	N/A	The index of the end of a contiguous segment (nseg(isurf)) within surf_type, for surface type isurf	5.4.1.2
Nb_Ha _bg (number of atmospheric histograms)	N/A	Array containing the number of bins used in each atmospheric histogram to calculate the background count statistics; associated times are in Ta_start and Ta_stop arrays	5.4.1.1.14
Hx (nbin)	meters	The height associated with the beginning of each height bin in a histogram	5.4.2.1.3
Hz (nbin)	photon events	The number of photon events in each height bin of a histogram	5.4.2.1.3
Indxsig_beg(ngrp)	N/A	Beginning index in the histogram, Hz, of a group of signal bins selected	5.4.2.3.2
Indxsig_end(ngrp)	N/A	Ending index in the histogram, Hz, of a group of signal bins selected	5.4.2.3.2
nbin	N/A	The number of height bins in a histogram	5.4.2.1.1
N_{sig}	N/A	The number of bins containing signal photon events identified in a histogram	5.4.2.3.1
Ngrp	N/A	The number of groups of contiguous signal bins found in a histogram	5.4.2.3.2
Nseg (isurf)	N/A	The number of contiguous segments in the granule for each surface type	5.4.1.3
Pmax (ngrp)	photon events	The maximum number of photon events in one bin in each signal group identified	5.4.2.3.2
Sigbins (Nsig)	N/A	The indices in the histogram, Hz, of bins identified as containing signal photon events	5.4.2.3.1
SNR	N/A	The ratio of the number of photon events in a histogram bin to μ_{bg}_δz_{pc}_δt_{PC}, the mean of the background photon event count.	5.4.2.3.1
Tbegcoef (number of linear fits in a segment)	seconds	The beginning time for each linear fit; the time of the first photon used in the linear fit	5.4.2.5.1

Name	Units	Description	Section
Tendcoef (number of inear fits in a segment)	seconds	The end time for each linear fit; the time of the last photon used in the linear fit	5.4.2.5.1
tbeg_lf (number of linear fits used for editing outliers)	seconds	The beginning time of segment where additional signal photon outlier editing using a linear fit is performed at the end of the slant histogramming algorithm	5.4.3
tend_lf (number of linear fits used for editing outliers)	seconds	The beginning time of segment where additional signal photon outlier editing using a linear fit is performed at the end of the slant histogramming algorithm	5.4.3
time_beg	seconds	The time of the earliest photon telemetered, used as the beginning of the profile	5.4.1.1.1
time_end	seconds	The time of the last photon telemetered, used as the end of the profile	5.4.1.1,1
Timebeg_seg (isurf,nseg)	seconds	The time of the beginning of each contiguous segments of surface type isurf	5.4.1.2
Timeend_seg (isurf,nseg)	seconds	The time of the end of each contiguous segments of surface type isurf	5.4.1.2
$time\_h_b$	seconds	The beginning time over which to select photon events for a specific histogram	5.4.2.1
$time\_h_e$	seconds	The end time over which to select photon events for a specific histogram	5.4.2.1
Timebeg_use (number of running linear fits in a segment)	seconds	The beginning time for each linear fit; the time of the first photon used in the linear fit	5.4.2.5.1
Timeend_use (number of running linear fits in a segment	seconds	The end time for each linear fit; the time of the last photon used in the linear fit	5.4.2.5.1
Th_{sig}	photon events	The signal threshold for a given histogram in photon event counts per height bin, calculated from the background photon rate of the atmospheric histograms	5.4.2.2
Th_{sig2}	photon events	The signal threshold for a given histogram in photon event counts per height bin used to test for spurious false positive signal events identified.	5.4.2.3.3
$time\_{n}$	seconds	Time of the midpoint of time increment n, where n goes from 1 to $(time\_{end}-time\_{beg})/\Delta time$	5.4.2
Z_{beg}	meters	The height value, calculated from the estimated surface, E_{gap} or H(t) corresponding to $time\_h_b$	5.4.2.5.2

Name	Units	Description	Section
Z_{end}	meters	The height value, calculated from the estimated surface, E_{gap}, or H(t) corresponding to time_h_e	5.4.2.5.2
Zh_{min}	meters	Height minimum over which the photon cloud is histogrammed for a given t_n	5.4.2.1
Zh_{max}	meters	Height maximum over which the photon cloud is histogrammed for a given t_n	5.4.2.1
$Zhsl_{min}$	meters	Height band minimum over which the photon cloud is histogrammed in a slant reference frame for t_n	5.4.2.5.2
$Zhsl_{max}$	meters	Height band maximum over which the photon cloud is histogrammed in a slant reference frame for t_n	5.4.2.5.2
$Zsig_{min}$(unlimited, $n\Delta t$)	meters	The minimum value of the height window over which signal photon events are selected from a single surface for a given time, t_n as determined by ellipsoidal histogramming	5.4.2.3.5
$Zsig_{max}$(unlimited, $n\Delta t$)	meters	The maximum value of the height window over which signal photon events are selected from a single surface for a given time, t_n as determined by ellipsoidal histogramming	5.4.2.3.5
Zsl	meters	The photon heights after rotation to a slant reference frame through angle α	5.4.2.5.2
Zsl_{beg}	meters	The heights, calculated from an estimated surface, E_{gap}, or H(t) in a slant reference frame corresponding to time_h_b, the beginning of the integration time used for one slant histogram	5.4.2.5.2
Zsl_{end}	meters	The heights, calculated from a estimated surface, E_{gap}, or H(t) in a slant reference frame corresponding to time_h_e the end of the integration time used for one slant histogram	5.4.2.5.2

Table 5-3. Parameters Calculated Interally Within the Algorithm.

Parameters Output from Signal Finding Algorithm

Name (dimension)	Description	Units	ATBD Section
All values from table 5-2 used to drive the algorithm.			
Parameters output for each photon event selected:			

Name (dimension)	Description	Units	ATBD Section
Conf (number of photon events in the cloud, n[3])	Confidence level for each photon event (0: noise, 1: added to pad likely signal photon events, 2: low confidence signal, 3: medium confidence signal, 4: high confidence signal)	N/A	5.4.1.3, 5.4.2.3.5
Histogram parameters output for each time interval, Δtime, when signal photon events were selected. The parameters are from the histogram used to find the majority of the signal photons in Δtime. Some parameters are surface-type specific. If a granule has multiple surface types, there will be multiple arrays of parameters below.			
$tint_{beg}$ (number of Δtime intervals in granule, n)	Beginning time of the interval relative to the beginning of the granule	seconds	5.4.1.3
δt_{PC} (number of Δtime intervals in granule, n)	Integration time over which the signal photon cloud events were selected	seconds	5.4.1.3
δz_{PC} (number of Δtime intervals in granule, n)	Height bin size of the histogram	meters	5.4.1.3
$\mu_{bg}\_\delta z_{pc}\_\delta t_{PC}$ (number of Δtime intervals in granule, n)	Mean background photon count for the specific integration interval time_h_b to time_h_c and height bin size δz_{PC}	counts	5.4.2.2
$\sigma_{bg}\_\delta z_{pc}\_\delta t_{PC}$ (number of Δtime intervals in granule, n)	Standard deviation of the background photon count for the specific integration interval time_h_b to time_h_c and height bin size δz_{PC}	counts	5.4.2.2

Table 5-4. Parameters Output from Signal Finding Algorithm.

5.4 Algorithm Implementation

The ATL03 data product is organized by ground track orientation on the ground, with ground tracks 1L and 1R forming pair one, ground tracks 2L and 2R forming pair two, and ground tracks 3L and 3R forming pair three. Since the spacecraft can have one of two orientations, the relative positions of strong and weak beams change, depending on this orientation (section 7.5). Using the spacecraft orientation parameter (/orbit_info/sc_orient) we assume the relative position of strong and weak beams are known. The spacecraft orientation is changed in order to maximize solar illumination of the solar panels approximately twice a year. As noted above, each ground track is processed separately and the steps of the algorithm are different depending on the beam

[3] The second dimension of many of these arrays (n) corresponds to the number of unique surface types in a granule. Parameters without a second dimension are not surface-type dependent.

energy or strength. If a granule spans a spacecraft rotation, then this algorithm needs to be implemented separately on the portions that occur before and after the rotation. For the rest of this discussion in section 5.4 it is assumed that the beam strength remains strong or weak for a given ground track for the whole granule.

The algorithm is driven by parameters, many of which are surface type or beam strength dependent. Thoughout section 5.4 the type of dependency is indicated by (isurf), (ibeamstrength), or both after the parameter the first time it is discussed. Each ground track is processed separately, but processing for the weak beam uses the results from the neighboring strong beam, so the strong beam of each pair must be processed first.

The algorithm begins by calculating those variables that are generated once for each ground track (section 5.4.1). This includes the background rate (section 5.4.1.1), surface types traversed and contiguous segment boundaries within each surface type (section 5.4.1.2), and initialization of the signal finding output parameters for this ground track (section 5.4.1.3). In the event that the surf_type parameter indicates null values for all surface types in a major frame, this indicates that there are no telemetered photons for that major frame, and the algorithm in section 5.4 moves on to the next major frame.

The background count rate is required in order to calculate a threshold value to determine if photon events in a particular histogram bin are signal or background (section 5.4.1.1). While the background rate could be expressed in photons per second, since this algorithm is histogram-based, the algorithm expresses the background rate by the mean, Ha_bg_μ, and standard deviation, Ha_bg_σ, of the number of background photon events of the histogram bins. The values of Ha_bg_μ and Ha_bg_σ are therefore a function of the bin size, $\delta z_{BG,}$ and along-track integration time, δt_{BG}, of the histogram used for the background calculation Ha_bg. For the strong beams, the atmospheric histogram (spanning ~14 kilometers vertically) is used to calculate Ha_bg. For weak beams the atmospheric histogram is not telemetered so the downlinked photons are used to calcualte Ha_bg. As described above, the downlink band is relatively narrow, (30 meters to ~2000 meters) and depends on the surface type and terrain variation. The atmospheric histograms, Ha, whether telemetered or formed from the downlinked photons, may or may not contain signal photons (clouds, specular surfaces, etc.), but will always contain background counts.

Because the signal finding algorithm is driven by surface-type dependent parameters and searches for a continuous height profile, the surface types traversed by the ground track must be determined (section 5.4.2). These surface-type dependent parameters include the number Nseg(isurf) of contiguous segments, the boundaries in time (or major frame count if available) of each contiguous segment (segments denoted by iseg), Timebeg_seg(isurf, iseg) and Timeend_seg(isurf,iseg). The signal finding algorithm (section 5.4.2) is then applied to each segment separately.

The final step performed at the ground track level is to initialize the signal finding output for that ground track (section 5.4.1.3). For each surface type, each segment of a ground track is processed separately through the signal finding steps of the algorithm (section 5.4.2).

The algorithm determines the signal photon events for each time increment of Δtime(isurf) by first forming and evaluating histograms formed with respect to the ellipsoidal surface. At each Δtime the algorithm creates a histogram of the ellipsoidal photon event heights for a given integration distance, $\delta t_{PC,}$ using a height bin size of δz_{PC} (section 5.4.1.2). Possible signal bins are selected by comparing them to a signal threshold, Th_{sig}, which is calculated from Ha_bg_μ and Ha_bg_σ, after they are appropriately scaled to the specific δt_{PC} and δz_{PC} values used for the ellipsoidal histogram (section 5.4.2.2). The selection of the signal bins (section 5.4.2.3) is not simply based on this threshold test, but follows a more complicated methodology, which reduces false positives while also selecting any possible signal from surrounding bins that did not pass the threshold test but may contain signal.

For each time increment, Δtime, the algorithm varies the integration time, δt_{PC} and height bin size, δz_{PC} (section 5.4.2.4), until either signal bins are identified or the upper limits of δt_{PC} and δz_{PC} are reached. This automated adaptation to the specific characteristics of each surface profile is key to selecting all signal photon events while minimizing the number of background photon events erroneously selected as signal.

If the background count rate is so small that to use it as a threshold would cause the algorithm to accept all photons as signal, the algorithm first tries to increase δt_{PC} and δz_{PC} (section 5.4.2.4) as described above. If this situation still exists at the largest values of δt_{PC} and δz_{PC} then the algorithm takes the bins with the maximum number of photons as the signal bins along with adjacent bins that contain photons (section 5.4.2.3).

After an initial height profile is formed, a histogram relative to a slope is performed to identify any missed signal photons that were spread out over the slopes (section 5.4.2.5). The process is slightly different for strong and weak beams. All additional signal photon events found are then merged with the previously identified signal photon events.

The lslant parameter determines subsequent steps for the strong beam segments. If lslant(isurf) is set to one (e.g. land or land ice), two signal-finding steps are performed. First, additional signal is sought by histogramming the photon heights relative to the surface defined by a set of running linear fits to the signal photons identified by ellipsoidal histogramming (section 5.4.2.5.1). This is referred to as slant histogramming. Second, if gaps in the profile greater than Δtime_gapmin are still present, the algorithm identifies the time intervals over which these gaps occur (section 5.4.2.5.3) and then performs slant histogramming over the time interval of each identified gap, systematically varying the slope along which the histogram is formed to find additional signal (section 5.4.2.5). This step is referred to as variable slope slant histogramming. If lslant(isurf) is set to zero, we assume the Earth's surface is essentially flat (e.g. sea ice, ocean) and slant histograming is not performed.

For weak beam segments, one additional signal-finding step is performed after ellipsoidal histogramming. Using the final surface profile defined by the neighboring strong beam, the algorithm forms running linear fits to determine local surface slopes and performs slant histogramming relative to these local slopes. Variable slope slant histogramming is not performed for the weak beam, since it is assumed that if a gap still exists that could not be filled by variable slope slant histogramming on the nearby strong beam, then there is no signal in the

gap that would be detected by the weak beam. This step requires geographically correlating the strong and weak beams.

After identifying likely signal photon events, there is an option (Ledit(isurf)) to perform an nσ edit to a running linear fit over the signal photon events to remove outliers (section 5.4.3). Next, the algorithm selects additional photons, if necessary (as directed by addpad(isurf)) to ensure the height span of the signal photons is greater than or equal to Htspanmin(isurf) (section 5.4.4). This helps ensure that photons from secondary surface returns are also flagged (e.g. from vegetation or buildings) even if they have not passed the threshold tests.

The algorithm assigns a confidence flag value to each individual telemetered photon event. This flag is initialized to zero and then set to the highest confidence level (2-4) assigned to that photon from either the ellipsoidal or slant histogramming processes or set to one if it was added as padding to assure the minimal height span is achieved. Additionally, for each Δtime interval that contains signal photons, ATL03 includes the time of the beginning of the interval, the integration time span, and the histogram bin size, used for the majority of the photon events selected for that interval and the background noise statistics.

As explained in the related document *Optimization of Signal Finding Algorithm*, the default values for each surface type (land, ocean, sea ice, land ice, inland water) and where appropriate, beam strength, have been derived based on MABEL data. Of the parameters in Table 5-2, those that are associated with time (i.e. Δtime and δt_{max}) have been scaled for use with ATLAS data. For example, most MABEL data has 1,000 laser pulses fired every 40 meters along-track (MABEL's laser pulse rate was typically 5 kHz at an average along-track velocity of 200 m/sec). For ATLAS, we expect ~57 laser pulses every 40 meters (at the ATLAS pulse repetition rate of 10 kHz and spacecraft velocity of 7 km/sec). Our initial estimates for time-based parameters are based on these considerations, along with the radiometric differences between the instruments (e.g. MABEL returned approximately 1 signal photon every ~50 laser pulses over the interior of Greenland, while ATLAS is predicted to return ~10 signal photons per laser pulse over the interior of Greenland for the strong beams, and ~2 signal photons per laser pulse over the interior of Greenland for the weak beams). We expect that these values will need to be revisted shortly after launch.

The processing steps for each of the beam strengths are summarized below with a reference to the appropriate section where the methodology is described in detail. Except for calculation of the background photon rate, the algorithm steps are run independently for each contiguous segment of each surface type using surface type or beam strength dependent input parameters.

Strong Beam Signal Finding Processing:

- Calculate the background photon rate from the atmospheric histogram (section 5.4.1.1)
- Determine the surface types this beam traverses and the contiguous segment boundaries for each surface type (section 5.4.1.2)
- Initialize arrays for signal finding output (section 5.4.1.3)
- Select photon event using ellipsoidal histograms (section 5.4.2.1-5.4.2.4)
- Perform slant histogramming (land and land ice) for segments where lslant(isurf) = 1

  - Determine local surface slopes by running linear fits to the signal found from ellipsoidal histogramming (section 5.4.2.5.1)
  - Perform slant histogramming relative to the slope defined by the signal photons found with ellipsoidal histogramming (section 5.4.2.5.2)
  - Identify remaining along-track gaps in signal photons greater than Δtime_gapmin (section 5.4.2.5.3); if they exist perform slant histogramming over the gaps, varying the surface slope (section 5.4.2.5)
- Perform nσ editing to remove outliers on request (ledit = 1) (section 5.4.3)
- Add padding if necessary to select a minimal height span of photons at each Δtime (section 5.4.4)

Weak Beam Signal Finding Processing:

- Calculate the background photon rate from either the atmospheric histogram from the neighboring strong beam (after alignment in the along-track direction) or from the telemetered photon cloud (section 5.4.1.1). Although the strong beam is ~90m across track from the weak beam, the atmospheric histogram spans 4x this distance in the along track direction. Since the ground tracks are random with respect to surface reflectivity changes on the surface of the earth, the along-distance generates little additional uncertainty compared with the along-track averaging distance.
- Determine the surface types this beam traverses and the contiguous segment boundaries for each surface type (section 5.4.1.2)
- Initialize arrays for signal finding output (section 5.4.1.3)
- Signal photon event selection using ellipsoidal histograms (section 5.4.2.1-5.4.2.4)
- Determine local surface slopes by running linear fits to the neighboring strong beam surface (section 5.4.2.5.1)
- Perform slant histogramming relative to the strong beam surface slope (section 5.4.2.5.2)
- Perform nσ editing to remove outliers on request (ledit(isurf) = 1) (section 5.4.3)
- Add padding if necessary to select a minimal height span of photons at each Δtime (section 5.4.4)

5.4.1 Variables calculated once per granule

The steps defined in this section are performed for each ground track once per granule. They include the calculation of the background photon rates (section 5.4.1.1), the number of surface types traversed by the ground track and the boundaries of each contiguous segment for each surface type (section 5.4.1.2), and the initialization of signal finding output parameters (section 5.4.1.3).

5.4.1.1 Background Photon Mean and Standard Deviation Calculation

If the atmospheric histogram, $H_{ATM,}$ (referred to as an atmospheric profile in ATL04 and 09), is downlinked in the telemetry then it will be used to determine Ha for the background photon

count calculation unless the flag Lpcbg is set to True. Nominally, the atmospheric histogram is telemetered only for the strong beams. However, the atmospheric histogram from a neighboring strong beam is also used to determine the background rates for the weak beam after care is taken to align the weak and strong beams, unless the Lpcbg flag is set to True for the weak beams. If the atmospheric histogram is not present or not used, then the background histogram Ha is formed using the photon cloud forming bins of height, δz_{BG}, over time spans, δt_{BG} (section 5.4.1.1.1). Furthermore, if atmospheric histograms incompletely span the time period represented by a histogram, use the photon cloud to determine background rates for the histogram in question. When calculating Ha from H_{ATM}, $\delta z_{BG} = \delta z_{ATM}$ and $\delta t_{BG} = \delta t_{ATM}$.

The goal of this section is to calculate the mean (Ha_bg_μ), and standard deviation (Ha_bg_σ), of the number of background photon events per histogram bin for each of the k histograms in Ha after removing possible signal bins.

First calculate Ha, either from the photon cloud (section 5.4.1.1.1) or from H_{ATM} (section 5.4.1.1.2). Calculate Ha_μ and Ha_σ using all bins (section 5.4.1.1). Second, remove any bins that may contain signal (section 5.4.1.1.2) and then calculate Ha_bg_μ and Ha_bg_σ from these remaining bins (section 5.4.1.1.3). Ha_bg_μ, and Ha_bg_σ, contain the mean and standard deviation, respectively, of the number of background photon events per height bin size, δz_{BG}, collected over the time interval, δt_{BG}.

5.4.1.1.1 Calculation of Ha from the Photon Cloud

To calculate the background rate from the photon cloud, we assume the following are given:

- T_P, the arrival time in seconds for each photon event, p.
- H_P, the ellipsoidal height for each photon event from preliminary geolocation.
- $Tw_{TOP}(2,m)$, the ellipsoidal height of the top of the telemetry window, m, for each telemetry band. This can change at the major frame rate, or every two hundred shots.
- Tw_start(m), the start time in seconds from the beginning of the granule for telemetry window, m. This value corresponds to $Tw_{TOP}(2,m)$.
- Tw_stop(m), the stop time in seconds from the beginning of the granule for telemetry window, m. This value corresponds to $Tw_{TOP}(2,m)$.
- $Tw_{WIDTH}(2,m)$, the width of telemetry window m in meters for each band.
- δz_{BG}, the bin height of each bin, k, in Ha (k,m). This is a constant, nominally 1m.
- m, the number of telemetry windows, where each window can have up to two bands
- nband(m) - the number of bands for each window, m.

Next, the algorithm calculates:

$$Time\_beg = \min(T_p)$$

$$Time\_end = \max(T_p)$$

And calculates an 'atmospheric' histogram Ha(m), of the same along track duration as the nominal atmospheric histogram (280m along-track or δt_{ATM}) for each of the m telemetry windows:

1) First, it calculates the vertical height limits of each band.
2) Second, given the vertical span of each histogram bin, δz_{BG}, it calculates the number of whole bins and resets the maximum height limit to eliminate fractional bins.
3) Finally it calculates the number of photon events in each histogram bin.

For computing efficiency, Ha is composed of up to 1000 bins, each of span δz_{BG}. The algorithm loops through each telemetry window, m:

For iband = 1, nband(m) calculate the vertical height limits $Hmin_{BG}(iband)$ and $Hmax_{BG}(iband)$ over which to histogram, adjusting $Hmax_{BG}(iband)$ to eliminate fractional histogram bins.

$$Hmin_{BG}(iband) = TW_{TOP}(iband,iw)\text{-}TW_{WIDTH}(iband,iw)$$

$$Hmax_{Bg}(iband) = TW_{TOP}(iband,iw)$$

Redefine $Hmax_{Bg}(iband)$ if needed to produce bins of size δz_{BG}.

$$nbins(iband) = fix\{(Hmax_{Bg}(iband)- Hmin_{BG}(iband))/\delta z_{BG}\}$$

$$Hmax_{Bg}(iband) = Hmin_{BG}(iband) + nbins(iband) * \delta z_{BG}$$

where fix{} truncates to the lowest whole integer

If the telemetry bands are wider than can be accommodated by 1000 bins of fixed width δz_{BG}, the algorithm populates the bins using the lowest elevation telemetry band first, and as much of the higher elevation telemetry band, from the bottom to the top, as can be accommodated. The top portion of some higher elevation telemetry bands may not be used at times. In prelaunch testing, it was found that excluding photons in the upper part of the higher elevation telemetry band resulted in negligible impacts to the resulting background statistics and photon classification.

Now, select all photon events for each iband that fall within the time and height limits.

find ip: all indices in T_P where:

$$T_P(ip) \geq Tw\_start(m) \text{ and } T_P \leq Tw\_stop(m)$$

$$\text{and } H_P(ip) \geq Hmin_{BG}(iband) \text{ and } H_P(ip) \leq Hmax_{Bg}(iband)$$

Ha(iband)= the histogram of all $H_P(ip)$ from bin width of δz_{BG}

If there are two bands that contain photons then create a combined histogram Ha(m) where:

Ha(m) = Ha(band 1) + -1 + Ha(band 2)

A bin with the value of -1 (or some other fill value) is put in the middle between the individual band histograms. The purpose of this separation is to prevent the exclusion of the last bin of the first histogram in the calculation of the statistics described in 5.4.1.1.2 if the first bin of the second histogram is calculated to contain signal.

If there is only one band that contains photons: Ha(m) = Ha(iband)

and set Ta_start(m) = Tw_start(m)

Ta_stop(m) = Tw_stop (m)

5.4.1.1.2 Calculation of Ha and Related Parameters from the Atmospheric Histogram

The atmospheric histogram telemetered, H_{ATM}, is formed by information from four hundred shots. The elevation span, $Tw_{WIDTH,}$ is the same for all atmospheric histograms, however the elevation to the top of the histogram, Tw_{TOP}, is set at the major frame rate (two hundred shots) so it can change between major frames. If Tw_{TOP} is different for the two major frames that form the atmospheric histogram, when the two histograms are summed to create the telemetered $H_{ATM,}$ some of the bins at the lower and upper elevations of H_{ATM} may contain information from only two hundred shots. These bins need to be discarded such that Ha (m) = H_{ATM} (i,m) using only bins i that contain the sum of four hundred shots.

5.4.1.1.3 Calculation of Ha_μ and Ha_σ of the Number of Photons Events in Ha

Now that Ha has been formed from either the photon cloud or the atmospheric histogram, the algorithm proceeds to calculate Ha_μ and Ha_σ of the number of photon events in each histogram, Ha(nbin, m), where nbin = number of bins in each histogram, Ha, of width δz_{BG} and m= histogram number where there is one histogram for each δt_{BG} seconds of time.

1) Calculate the mean,
   Ha_μ(k) = ($\sum_{n=1}^{n=nbin}$ Ha(n,m))/nbin
2) Calculate the standard deviation,
   Ha_σ(m)= $\sqrt{(\frac{1}{nbin-1}) \sum_{n=1}^{n=nbin} (Ha(n,m) - Ha\_\mu(m)) \wedge 2}$

5.4.1.1.4 Calculate Ha_bg, the bins in Ha that do not contain signal

For each m, calculate the bin indices in Ha(i,m), for bins likely do not contain signal based on:

1) Ha_bg(m) = Ha(i) where Ha(i,k) < Ha_μ (m) + $e_a \times$ σ (m) and for all i, where Ha (i,m) is not contiguous to a bin meeting this criteria. The input parameter e_a is as defined in Table 5-2 as the multiplier of Ha_σ used to determine which bins in Ha may contain signal photon events.

2) Nb_Ha_bg(m) = the number of background count bins selected

5.4.1.1.5 Calculate the Background Ha_bg_μ and Ha_bg_σ

Calculate the mean and standard deviation of the remaining bins as:

Ha_bg_μ(m) = Σ_i (Ha_bg(i,m))/Nb_Ha_bg(m)

$$Ha\_bg\_\sigma(m) = (1/(N\_bg(m)-1) \times \Sigma i(Ha\_bg(i,m)-Ha\_bg\_\mu(m))^2)^{1/2}$$

Note that Ha_bg_μ (m) and Ha_bg_σ (m) are specific to δz_{BG}, and the time span over which Ha_bg (nbin,k) was formed (δt_{BG}).When determining the signal threshold using them, these need to be scaled to the δz_{PC} and δt_{PC} used in the signal finding histograms described in section 5.4.2.

5.4.1.2 Surface Type Determination

The surface type for a given segment is determined at the major frame rate, as described in section 2.0, and is a two-dimensional array surf_type(n, nsurf), where n is the major frame number, and nsurf is the number of possible surface types (currently five) such that surf_type(n,isurf) is set to 0 or 1 indicating if surface type isurf is present (1) or not (0), where isurf=1 to 5 (land, ocean,sea ice, land ice, and inland water) respectively.

The surface type is defined using the masks described in section 4.0. Note that the masks are created for each of the surface types separately and there are many locations where they overlap, by design. For example, locations over land ice are also flagged as land, and sea ice is also flagged as ocean.

The surface type masks in section 4.0 are provided as logical masks, on geographic grids. In order to produce the Surf_type parameter, the algorithm determines geographic location of the major frame boundaries (every 200 shots, or ~140 meters along-track) of each ground track. The masks in section 4.0 are then interrogated using the major frame boundaries to determine Surf_type(n, nsurf) as defined above.

In addition, the algorithm determines which surface types are present in a given granule, and stores the along-track time boundaries of each surface type,

Timebeg_seg(isurf,Nseg(isurf)) for isurf = 1,5

Timeend_seg(isurf,Nseg(isurf)) for isurf = 1,5

Nseg(isurf) is defined as the number of contiguous segments of each surface type

in order to select the appropriate parameters in the signal finding section of the algorithm (section 5.4.2).

5.4.1.3 Initialization of Signal Finding Output Parameters

The signal finding output parameters are listed in Table 5-4. As noted in section 5.4.1.1, ***Ha_bg_μ*** and ***Ha_bg_σ*** are output for each ground track. The confidence level of each photon, ***conf(n,nsurf)***, is also output, where n is the photon number, nsurf indicates the surface type from 1 to 5. The surface type dependency is necessary since the parameters driving the signal selection process are surface-type dependent.

The values of conf vary from 0 to 4 where 0 = noise, 1 = padding (section 5.4.4); 2 = low confidence level signal, 3 = medium confidence level signal, and 4 = high confidence level signal.

The confidence level for each photon and each surface type is initialized to zero (noise). If a surface type is not traversed for a specific photon then the conf value for all photons of that surface type remains zero.

For each surface type, there are three other parameters output each dimensioned by (ntime):

Tint_beg(ntime); the along-track times of the beginning of each time increment

$\boldsymbol{\delta t_{PC}(ntime)}$; the integration times used for each time increment

$\boldsymbol{\delta z_{PC}(ntime)}$; the histogram bin height used for each time increment,

where ntime = (time_end - time_beg) / Δtime(isurf) along the granule.

Since Δtime is surface-type dependent, it is suggested that a separate surface type group be output under photon signal output with separare arrays for these three parameters. If a surface type is not traversed by the ground track then that group would then be missing. For each surface type, the above three arrays should be initialized to an invalid value (e.g. -999999.0)

For each pair of beams, the algorithm first processes all segments of the strong beam, since the results from the strong beam will be used in some of the steps for processing the weak beam.

All the following steps for finding signal photons are performed for each segment in Nseg(isurf) of each surface type separately since many of the input parameters are surface type or beam strength dependent.

5.4.2 Select Signal Photons

The algorithm proceeds through each segment in time increments of Δtime(isurf). For each time, $time_{\_n}$, from $time_{\_n}$ = Timebeg_seg(isurf,Nseg(isurf)) + Δtime(isurf)/2, to Timeend _seg(isurf,Nseg(isurf))- Δtime (isurf)/2. The last time increment may be less than Δtime since it has to end at Timeend_seg(isurf,Nseg(isurf)) For the rest of this discussion we will be leaving off the isurf and Nseg dependencies for clarity. The algorithm steps and corresponding sections are:

1) Create a histogram with respect to the ellipsoid of all the photon heights, H_p, using a discrete a time interval surrounding $time_{\_n}$, δt_{pc}, and a discrete height bin size, δz_{pc} (section 5.4.2.1).
2) Calculate a threshold value, Th_{sig}, from the background count parameters Ha_bg_σ and Ha_bg_μ, that corresponding to the time interval, $time_{\_n} - \delta t_{pc}/2$ to $time_{\_n} + \delta t_{pc}/2$ and bin size δz_{pc} (section 5.4.2.2).
3) Find bins where the counts meet the signal bin criteria which is a function of Th_{sig} and additional checks designed to select all feasible signal photons and a minimal number of background photons (section 5.4.2.3). Once signal bins are identified for a value of $time_{\_n}$, select all photon events occurring in these signal bins for the time interval $time_{\_n}$ - Δtime/2 to $time_{\_n}$ + Δtime/2 and flag them as signal photon events (section 5.4.2.3.5). Though this is a sub-section of section 5.4.2.3, the additional attention is warranted, as this is where signal photon events are classified. Increment $time_{\_n}$, and return to step 1 (section 5.4.1.1) to repeat the process for the next Δtime interval.

4) If no signal bins are identified, increase δtpc and δzpc and repeat steps 1-3 above until signal bins are identified or maximum values of δt and δz are exceeded (section 5.4.2.4).
5) After all signal photons are identified from the ellipsoidal histogramming, identify additional signal photons using slant histogramming (section 5.4.2.5). Steps to follow are beam-strength dependent. As mentioned above, process each segment of each surface type separately, processing the strong beam segment of a pair first.
    a) Strong beams, where lslant(isurf) is set to one (e.g. land and land ice):
        1. Form a height profile from the signal photon events identified by ellipsoidal histogramming (section 5.4.2.5.1)
        2. Perform signal finding using slant histogramming at surface slopes derived from i above (section 5.4.2.5.2)
        3. Look for remaining gaps > Δtime_gapmin (isurf) (section 5.4.2.5.3)
        4. Perform signal finding using variable slope slant histogramming over gaps > Δtime_gapmin (section 5.4.2.5)
    b) Weak beams:
        1. Form a height profile from the signal photons identified for the strong beam in the pair (section 5.4.2.5.1)
        2. Perform signal finding using slant histogramming at surface slopes from i above (section 5.4.2.5.2)
6) Remove outliers, if requested, by ledit(isurf) (section 5.4.3).

5.4.2.1 Histogram Photon Heights - Ellipsoidal Histogramming

These steps generate a histogram of the photons for each time_n in the groundtrack segment for a specific surface type, where $time\_{n}$ corresponds to the actual time associated with one Δtime increment. The first value of time_n is Timeseg_beg + Δtime/2. The $time\_{n}$ parameter is incremented by Δtime until $time\_{n}$ is greater than or equal to Timeseg_end. The first step is to determine the histogram integration time, δt_{PC}, and height bin size, δz_{PC}, which begin at their lowest values, and are updated using the methodology described in section 5.4.2.4. Next, set the beginning and end time of the integration time span over which photons will be selected for histogramming ($time\_h_b$ and $time\_h_e$) where $time\_h_b$ = max ($time\_{n}$ - $\delta t_{PC}/2$, Timeseg_beg) and $time\_h_e$ = min ($time\_{n}$ + $\delta t_{PC}/2$, Timeseg_end), to account for the segment start and end times.

At each $time\_{n}$ the algorithm classifies the photons within a time interval Δtime. The relationship between the time interval, Δtime, and the integration time, δt_{PC}, is depicted in Figure 5-. The salient points are that in order to identify signal photons in a given time interval (Δtime) the algorithm begins by histogramming just those photons in the Δtime interval. If signal is not found, δt_{PC} increases by δt_{inc}, to include photons before and after the time interval of interest (i.e. to the left and right of time_4 in Figure 5-).

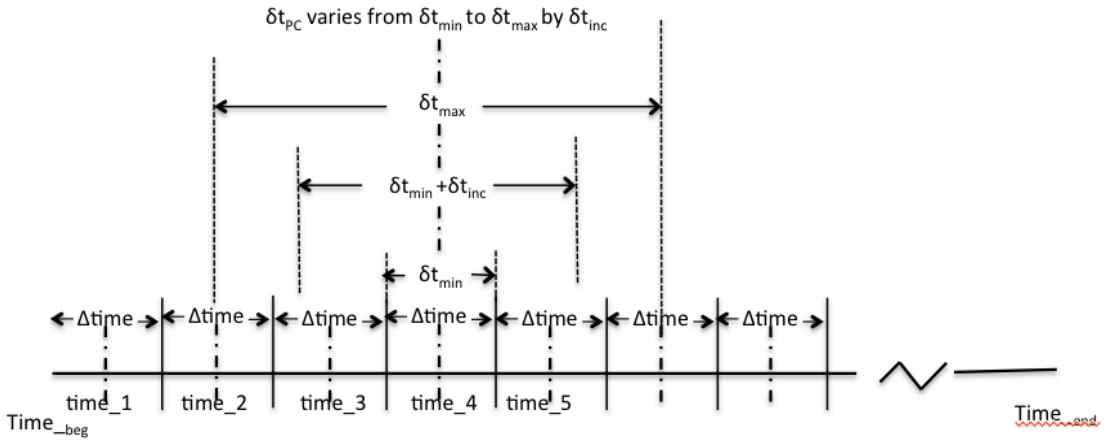

Figure 5-6. A data granule is segmented in increments of Δtime.

For every time_$_n$ the integration time, δt_{PC} and the histogram bin size, δz_{PC} are varied (section 5.4.2.4 and Figure 5-5) until signal is found or the maximum values of both δt_{PC} and δz_{PC} are reached. Note that although δt_{PC} can be larger than Δtime, only photon events within time_$_n$ - Δtime/2 and time_$_n$ + Δtime/2 are classified.

There can be up to two separate telemetry bands, nb, downlinked for each telemetry window, iwin. Additionally there can be multiple full or partial telemetry windows, nwin, included in the integration span, δt_{PC}, since the telemetry window changes at the major frame interval (200 shots or 0.02 seconds). There can also be times when no telemetry windows are downlinked.

For each telemetry band, nb, for each window, iwin, within δt_{PC} the algorithm determines the height intervals Zhmin(iwin,nb) and Zhmax(iwin,nb). The actual height interval over which to form the histogram for time increment j Zhmin(j) and Zhmax(j) is formed by taking the maximum of Zhmax(iwin,nb) and the minimum of Zhmin(iwin,nb) in order to include all telemetered photon events. If two bands are present it will also include bins with no photon events but this circumstance will not affect the algorithm. Below, the times associated with each window and photon event are used to determine the telemetry windows covered by δt_{PC}. If the major frame number is given for both that could be used instead of time in the implementation of this algorithm.

a) Calculate the height limits Zhmin and Zhmax from the telemetry band limits, ***Twtop(n,nb)/Twwidth (n,nb)*** and the corresponding times, $Tw_{start}(n)$ and $Tw_{stop}(n)$:
    a. First select which telemetry windows fall within the histogram integration distance such that

    iwin = all telemetry windows n where

    ($time\_h_b \geq Tw_{start}(n)$ and $time\_h_b \leq Tw_{stop}(n)$) or

    ($time\_h_e \geq Tw_{start}(n)$ and $time\_h_e \leq Tw_{stop}(n)$) or

    ($time\_h_b < Tw_{start}(n)$ and $time\_h_e \geq Tw_{stop}(n)$)

b. $Zh_{max} = \max(Tw_{top}(iwin,nb))$ over all iwin
c. $Zh_{min} = \min(Tw_{min}(iwin,nb))$ over all iwin

where $Tw_{min}(iwin,nb) = Tw_{TOP}(iwin,nb) - Tw_{WIDTH}(iwin,nb)$

b) Calculate the number of bins (nbins) for the current value of δz_{pc}

$$nbins = (Zh_{max} - Zh_{min})/ \delta z_{pc}$$

It is important to verify that there are enough histogram bins for the signal finding algorithm to perform properly. If the telemetry band is very narrow and the algorithm is using a large value of δz_{pc}, it is possible that there will not be enough bins for a useful discrimination between signal and noise, as defined by the parameter Nbinmin. If there are are not enough bins at the current value of δz_{pc} then increase δt_{pc} (if not yet at the maximum value, δt_{max}) and cycle through all values of δz_{pc}. If at δt_{max} there are still not enough bins for this Δtime increment, the algorithm proceeds to the next time increment.

Assuming there are a sufficient number of bins, the algorithm proceeds to create a histogram for this time increment. Hz(j) are the number of photons in each j bin, and Hx(j) are the heights associated with the beginning of each bin j, such that

1) $Hx(j) = Zh_{min} + \delta z_{PC} \times j$ for j = 0 to nbins

2) $Hz(j) = \sum i$ where $Hx(j) \le Hp(i) < Hx(j+1)$ and $time\_h_b \le Tp(i) < time\_h_e$

c) Recompute Zh_{max} so that the height limits contain an integer number of histogram bins. One way to do this is:

$$Zh_{max} = real(Zh_{min} + dble(nbins)* \delta z_{pc})$$

where attention is paid to convert the number of bins (nbins) to double precision to insure the necessary accuracy is achieved. The effect of the formulation above is to neglect any photon counts at the top of the highest window in what would otherwise be a partial bin.

5.4.2.2 Threshold for Signal / Background Discrimination, Th_{sig}

Th_{sig} is the threshold to discriminate between bins containing background and those containing signal photons. It is calculated from the distribution of the background counts as

$$Th_{sig} = \mu_{bg\_\delta z_{pc}\_\delta t_{PC}} + e_m \times \sigma_{bg\_\delta z_{pc}\_\delta t_{PC}}$$

where:

$\mu_{bg}\_\delta z_{pc}\_\delta t_{PC}$ is the mean background photon count for the specific integration interval time_h_b to time_h_e and height bin size δz_{pc} as determined below, and

$\sigma_{bg}\_\delta z_{pc}\_\delta t_{PC}$ is the standard deviation of the background photon count for the specific integration interval time_h_b to time_h_e and height bin size δz_{pc} as determined below.

The mean and standard deviation of the number of background counts are included in the algorithm output (Table 5-4). Note that δt_{pc} = time_h_e - time_h_b and can change, as shown in Figure 5-.

1) Using the calculated time-dependent values of the mean and standard deviation of the background counts Ha_bg_μ and Ha_bg_σ (section 5.4.1.1), and the associated start and stop times, Ta_start and Ta_stop, the algorithm calculates the distribution statistics of the background counts specific to the time interval, time_h_b to time_h_e. These are labeled $\mu_{BG}\_tn\_\delta t_{BG}\_\delta z_{BG}$ for the mean and $\sigma_{BG}\_tn\_\delta t_{BG}\_\delta z_{BG}$ for the standard deviation. They pertain to an integration time, δt_{BG} and a height bin size of δz_{BG} and are associated with a specific time along the profile (section 5.4.2.2.1).

2) These values are scaled by $\delta t_{PC}\_use/\delta t_{BG}$ and $\delta z_{PC}/\delta z_{BG}$ to obtain $\mu_{bg}\_\delta z_{PC}\_\delta t_{pc}$ and $\sigma_{bg}\_\delta z_{PC}\_\delta t_{pc}$ that correspond to the integration time and height bin size used to form the histogram created in section 5.4.2.1.

where

δt_{PC}_use = actual time span over which photon events exist for δt_{PC} such that

$\delta t_{PC}\_use = \delta t_{PC}$ if there are no missing telemetry windows within δt_{PC}

otherwise δt_{PC} use = Σ t for the portions of all telemetry windows that exist within δt_{PC}

After scaling, these background count statistics can then be used to set Th_{sig} that are used to identify signal photons in an individual histogram for time_n.

Note that if $\mu_{bg}\_\delta z_{pc}\_\delta t_{PC}$ is equal to zero or so close to zero that $\sigma_{bg}\_\delta z_{pc}\_\delta t_{PC}$ is calculated as infinity or Th_{sig} is less than one then increase the integration time, δt_{pc} in steps of δt_{inc} until at the maximum integration time, δtmax. If δtmax has been reached, and Th_{sig} is still less than one, then the algorithm does not use a threshold check and instead marks the bins with photon counts > r2 * the number of counts in the bin with the most photon counts as signal. If $\mu_{bg}\_\delta z_{pc}\_\delta t_{PC}$ is < 0.0001 then it sets the confidence flags to 4, otherwise it recalculates the signal to noise ratio using $\mu_{bg}\_\delta z_{pc}\_\delta t_{PC}$ and sets the confidence flags accordingly.

5.4.2.2.1 Calculate μBG_tn_δtBG_δzBG and σBG_tn_δtBG_δzBG

These terms define the distribution of the background photon events centered at the specific time, time_$_n$, for an integration time δt_{BG}, and the height bin size, δz_{BG}. In the discussion below, k refers to the results from the kth atmospheric histogram. It is possible that at times, a given

interval (δt_{PC}) will span more than one atmospheric histogram. In these cases, the algorithm combines the two atmospheric histograms that are completely or partially within the time interval of interest. Note that if one of the two necessary atmospheric histograms are not present, use the photon cloud to determine the background statistics for this histogram.

1) Determine the elements, k, of Ha_bg_u (k) and Ha_bg_σ(k) that are partially or wholly within the time interval time_h_b to time_h_e.

   Determine all k where

   (time_$h_b \geq$ Ta_start (k) and time_$h_b \leq$ Ta_stop (k)) or

   (time_$h_e \geq$ Ta_start (k) and time_$h_e \leq$ Ta_stop (k)) or

   (time_$h_b <$ Ta_start (k) and time_$h_e \geq$ Ta_stop (k)).

If more than one element k is found, calculate μ_{BG}_tn_δt_{BG}_δz_{BG} and σ_{BG}_tn_δt_{BG}_δz_{BG} by combining the individual distributions using the equations below. Generalized notation is used for simplicity. The algorithm combines two distributions at a time until the final values are representative of all distributions within the time period.

a) To calculate the combined mean (μt) of distribution a and b:
   $\mu t = (Na * \mu a + Nb * \mu b) / Nt$
   where:
   Na,b = number of bins from distributions a and b,
   μa,b = mean of distributions a and b, and
   Nt = Na + Nb

b) To calculate the combined standard deviation, σt

$$\sigma t = \sqrt{\{[(Na - 1) * \sigma^2 a + (Nb - 1) * \sigma^2 b + Na * \mu a^2 + Nb * \mu b^2 - Nt * \mu t^2] / (Nt - 1)\}}$$

where:

$\sigma^2 a$ = square of the standard deviations of distribution a, and

$\sigma^2 b$ = square of the standard deviations of distribution b

and:

μ_{BG}_tn_δt_{BG}_$\delta z_{BG} = \mu t$, and

σ_{BG}_tn_δt_{BG}_ $\delta z_{BG} = \sigma t$

3) if only one element, k, is found then:

μ_{BG}_tn_δt_{BG}_δz_{BG} = Ha_bg_μ(k), and

σ_{BG}_tn_δt_{BG}_ δz_{BG} = Ha_bg_σ(k)

These two parameters ($\boldsymbol{\mu_{BG}\_tn\_\delta t_{BG}\_\delta z_{BG}}$ and $\boldsymbol{\sigma_{BG}\_tn\_\delta t_{BG}\_\delta z_{BG}}$) are written to the data product.

5.4.2.2.2 Calculate μbg_δzpc_δtPC and σbg_δzpc _δtPC

After calculating $\mu_{BG}\_tn\_\delta t_{BG}\_\delta z_{BG}$ and σ_{BG} $tn\_\delta t_{BG}\_\delta z_{BG}$ in section 5.4.2.2.1 above, now the algorithm calculates the mean background photon count and standard deviation corresponding to the specific values of δt_{PC} and δz_{PC} used for each histogram defined in section 5.4.2.1. They are formed by scaling $\mu_{BG}\_tn\_\delta t_{BG}\_\delta z_{BG}$ by the ratios δt_{PC}_use / δt_{BG} and δz_{PC} / δz_{BG}:

$$\mu_{bg}\_\delta z_{pc}\_\delta t_{PC} = (\delta t_{PC}\_use/\ \delta t_{BG}) \times (\delta z_{pc} / \delta z_{BG}) \times \mu_{BG}\_tn\_\delta t_{BG}\_\delta z_{BG}$$

$$\sigma_{bg}\_\delta z_{pc}\_\delta t_{PC} = \sigma_{BG}\_tn\_\delta t_{BG}\_\delta z_{BG} \times$$

$$\sqrt{(\ \mu_{bg}\_\delta z_{pc}\_\delta t_{PC}/\ \mu_{BG}\_tn\_\delta t_{BG}\_\delta z_{BG})}$$

Normally, δt_{PC_use} will equal $\delta t_{PC.}$ However, if telemetry windows within $time\_h_b$ and $time\_h_e$ are missing then δt_{PC}_use needs to be set to the width of the telemetry span actually present from $time\_h_b$ to $time\_h_{e.}$

Note that at some point in the calculation, the results may be undefined or infinite due to the mean of the background count rate for a specific δt_{pc} and δz_{PC} being near or equal to zero. The algorithm tests for this situation by calculating:

$$\sigma_{bg}\_\delta z_{pc}\_\delta t_{PC} = 0 \text{ or } (\mu_{bg}\_\delta z_{pc}\_\delta t_{PC} + e_m \times \sigma_{bg}\_\delta z_{pc}\_\delta t_{PC} <= 1)$$

In particular, this will be most likely at night. To avoid such issues, if the above test is true, the algorithm increases δt_{pc} and δz_{PC} as per section 5.4.2.4. If the maximum values for both δt_{pc} and δz_{PC} are reached and the background count rate is close to zero such that the mean is close to machine precision and the standard deviation cannot be calculated, then select all bins where the number of photons is greater than r2 * the number of photons in the bin with the highest photon count, and continue with step 5 of section 5.4.2.3, where r2 is as defined in Table 5-2.

5.4.2.3 Find All the Bins in Hz That May Contain Signal

Now that histograms have been generated for a given time interval (section 5.4.2.1) and the criteria for distinguishing signal from noise have been determined (section 5.4.2.2), the algorithm identifies bins that may contain signal photons. This is performed in four steps.

1) Find the bins, Sigbins, for which the number of photon events are both greater than the threshold, Th_{sig}, (section 5.4.2.3.1) and the signal to noise ratio (SNR) of the photon events compared to the mean background > R (the minimum ratio as input in Table 5-2).
2) Divide the values in Sigbins into groups of contiguous height bins (section 5.4.2.3.2).
3) Remove false signal (section 5.4.2.3.3)
    a) Remove spurious noise falsely selected as signal by increasing the signal threshold for any groups containing only one bin. This assumes that photons returned from a flat surface (i.e. all signal photons are in one bin) have a very large SNR. Tests on representative MABEL data showed that this removed

the vast majority of false positives (e.g. atmospheric returns) while retaining the photon events returned from the surface.

b) Remove any groups of bins if the peak signal is significantly less than the peak signal in the histogram. Tests with MABEL data showed this removed falsely-identified signal that was not connected with the surface (e.g. two or more adjacent atmospheric bins that passed the threshold test above, but have far fewer counts than the bins containing the surface return).

c) Remove any groups that are not a local maxima. The histogram should include regions that contain no photons or only background counts. If a group does not show up as a local maxima within the full histogram, then this indicates that it probably does not contain signal photon events.

4) For ellipsoidal histograms, to ensure selection of all signal photon events, identify additional bins on each side of each remaining signal group that may contain some photon signal events but not enough to have passed the threshold tests (section 5.4.2.3.4). This step is not implemented in slant histogramming.
5) Lastly (section 5.4.2.3.5), the algorithm identifies signal photons found and assigns a confidence parameter to each of them.

5.4.2.3.1 Find Individual Bins That Pass the Threshold and Ratio Test

1) Find possible signal bins. A bin, n, is defined as possibly containing signal if the number of photon events (Hz(n)) is greater than Th_{sig} (section 5.4.2.2) and the ratio of the number of photons to the mean of the noise, SNR, is greater than R.

   Find all values of n where

   $$Hz(n) > Th_{sig} \text{ and } SNR > R$$

   where $SNR = Hz(n) / \mu_{bg}\_\delta z_{pc}\_\delta t_{PC}$.

   At this point, the algorithm has identified possible signal bins, and proceeds to further evaluate them in section 5.4.2.3.2.

2) If no signal is found, then the algorithm increases δt_{PC} or δz_{PC} if possible as per section 5.4.2.4 and returns to section 5.4.2.1. If both δt_{PC} and δz_{PC} are at their maximum values then this time interval Δtime contains no signal photon events. The algorithm returns to section 5.4.2 to process the next Δtime increment.

5.4.2.3.2 Group Values in Sigbins into Groups of Contiguous Signal Bins

1) Go through Sigbins, and form groups of contiguous signal bins. For each group, ig,
   a. Store the beginning and end indices, Indxsig_beg(ig) and Indxsig_end(ig), and
   b. Store the max number of photons found in any one bin in each group, Pmax(ig).

5.4.2.3.3 Remove False Positives

This step of the algorithm checks for false positives in a different way.

1) Remove any group that contains only one height bin if

$$Pmax(ig) < Th_{sig2}$$

where

$$Th_{sig2} = \mu_{bg\_}\delta z_{pc\_}\delta t_{PC} + e_{m\_}mult \times e_m \times \sigma_{bg\_}\delta z_{pc\_}\delta t_{PC},$$

e_m = The multiplier of the standard deviation of the number of background photon events per bin used to determin if a bin possibly contains signal photons, and

$e_{m\_}mult$ = A multiplier of e_m used to increase the signal finding threshold for singleton signal bins; bins that pass the Th_{sig} test but adjacent bins do not pass the Th_{sig} test.

2) Remove any group if Pmax (ig) is significantly less than the maximum number of photon events in any bin in Hz:

If Pmax(ig) < r2 x max(Hz), then remove group ig

where r2 is defined as in Table 5-2.

3) Remove any groups that are not a local maxima:
   - Starting at Indxsig_beg(ig), go backwards through Hz until you find the second time Hz(j) ≤ μbg_$\delta z_{pc_}\delta t_{PC}$. Set jbef equal to this value of j. If the algorithm does not find any bins before indxsig_beg(ig) where the photon event count is equal to or below the background count mean and indxsig_beg(ig) is > 2 then remove the group.
   - Starting at Indxsig_end(ig) go forwards through Hz until the second time Hz(j) ≤ μbg_$\delta z_{pc_}\delta t_{PC}$, set jaft equal to this value of j. If the algorithm does not find any bins after $indxsig_{end}$(ig) where the photon event count dips below the background count mean and $indxsig_{end}$(ig) is < (nbins-2) can't be found, then remove the group.

If after these checks, no signal groups are left, then there are no signal bins found, and the algorithm increases δt_{pc} and/or δz_{pc} as per section 5.4.2.4 and returns to section 5.4.2.1. If both δt_{pc} and δz_{pc} are at their maximum values then there is no signal in this time interval (Δtime) and the algorithm proceeds to the next Δtime and returns to section 5.4.2.

5.4.2.3.4 Add Additional Bins to Get All Signal

For ellipsoidal histogramming, reset indxsig_beg(ig) = jbef and indxsig_end(ig) = jaft to include all bins on each side of the original signal bins selected until the histogram dips below or is equal to twice the mean background count noise level. This takes care of the situation where signal bleeds from the signal bins in to neighboring bins but not enough to put them over the threshold. Do not reset indxsig_beg and indxsg_end for slant histogramming.

5.4.2.3.5 Assign Confidence Parameter

Now that the bins likely to contain signal photons have been identified, the algorithm determines the height ranges of those signal bins and assigns an appropriate confidence parameter to each photon within this height range based on the signal to noise ratio of the histogram bin the photon falls in. The signal to noise thresholds for high medium and low confidence are given by snrlow and snrmed, as used below.

1) Merge any groups if the indices overlap or are immediately adjacent to each other, i.e. indxsigbeg(ig+1) ≤ (indxsigend(ig)+1)
2) For each histogram bin, l, within an ig group selected calculate the signal to noise ratio, SNRbin:
   SNRbin(l) = Hz(l) / μbg_δz_{PC}_δt_{PC}
3) For all photon events i such that Hp(i) falls within histogram bin l and time_$_n$ - Δtime/2 ≤ Tp(i) < time_$_n$ + Δtime/2
   a. Reset ***conf(i)*** based on SNRbin(l)
      i. ***conf (i)*** = 2 if SNRbin(l) < snrlow
      ii. ***conf (i)*** = 3 if snrlow ≤ SNRbin(l) < snrmed
      iii. ***conf(i) =*** 4 if SNRbin(l) ≥ snrmed

Note that if SNRbin cannot be calculated because the background mean is too low then set ***conf(i)*** = 4.

Save the parameters used for each time_n where signal photon events were selected, ***δz_{PC}_out (time_n) =*** δz_{PC}***, δt_{PC}_out(time_$_n$)*** = δt_{PC}, ***tintbeg_out(time_n)*** = time_$_n$ - Δtime/2, ***μ_{bg}_δz_{BG}_δt_{BG} _out(time_n)*** = μ_{BG}_tn_δt_{BG}_δz_{BG} , ***σ_{bg}_δz_{ATM}_δt_{ATM} _out(time_n)*** = σ_{BG}_tn_δt_{BG}_δz_{BG}. At this point, the algorithm has found signal photons in time interval Δtime, and now increments Δtime and returns to the beginning of section 5.4.2. If the last Δtime interval in the data granule has been reached, the algorithm has completed the ellipsoidal histograms, and proceeds to try to identify additional signal by histogramming the elevations relative the surface defined by the current signal found (section 5.4.2.5).

5.4.2.4 Methodology to vary δtPC and δzPC

Histogram results are dependent on two parameters; the integration time, δt, and the height bin size, δz. In order to find signal bins at the finest resolution, the algorithm begins with the smallest bin size possible. However if the signal is spread out due to a sloping or rough surface, it may be necessary to increase δz until the entire signal is concentrated in or around one bin. If the signal to noise ratio is very low or the signal is intermittent spatially due to partial cloud coverage or a weak return then increasing δt may help. Section 5.4.2.3 described the process to evaluate the histogram generated by particular values of the δt_{PC} and δz_{PC}; this section describes how to vary these parameters. The algorithm uses values in the δt_{PC}, δz_{PC} space in two passes, as

depicted in Figure 5-5, stopping as soon as signal bins have been identified for a given Δtime. In summary, the sequence is:

- Start with $\delta t_{PC} = \delta t_{min}$, $\delta z_{PC} = \delta z_{min}$ increase δz_{PC} by dz_{inc1} until $\delta z_{PC} \geq \delta z_{max1}$ where $dz_{inc1} = (\delta z_{max1} - \delta z_{min}) / (n\delta z1-1)$
- Then increase δt_{PC} by δt_{inc} and iterate through δz_{PC} from δz_{min} to δz_{max1} until $\delta t_{PC} > \delta t_{max}$ where $\delta t_{inc} = (\delta t_{max} - \delta t_{min}) / 2.0$
- Reset $\delta t_{PC} = \delta t_{min}$ and iterate through $\delta z_{PC} = \delta z_{min2}$ to δz_{max2} increasing δz_{PC} by dz_{inc2} until $\delta z_{PC} \geq \delta z_{max2}$ where:
  $dz_{inc2} = (\delta z_{max2} - \delta z_{max1}) / n\delta z2$
  $\delta z_{min2} = \delta z_{max1} + dz_{inc2}$
- Increase δt_{PC} by δt_{inc} and iterate through $\delta z_{PC} = \delta z_{min2}$ to δz_{max2} until $\delta t_{PC} > \delta t_{max}$

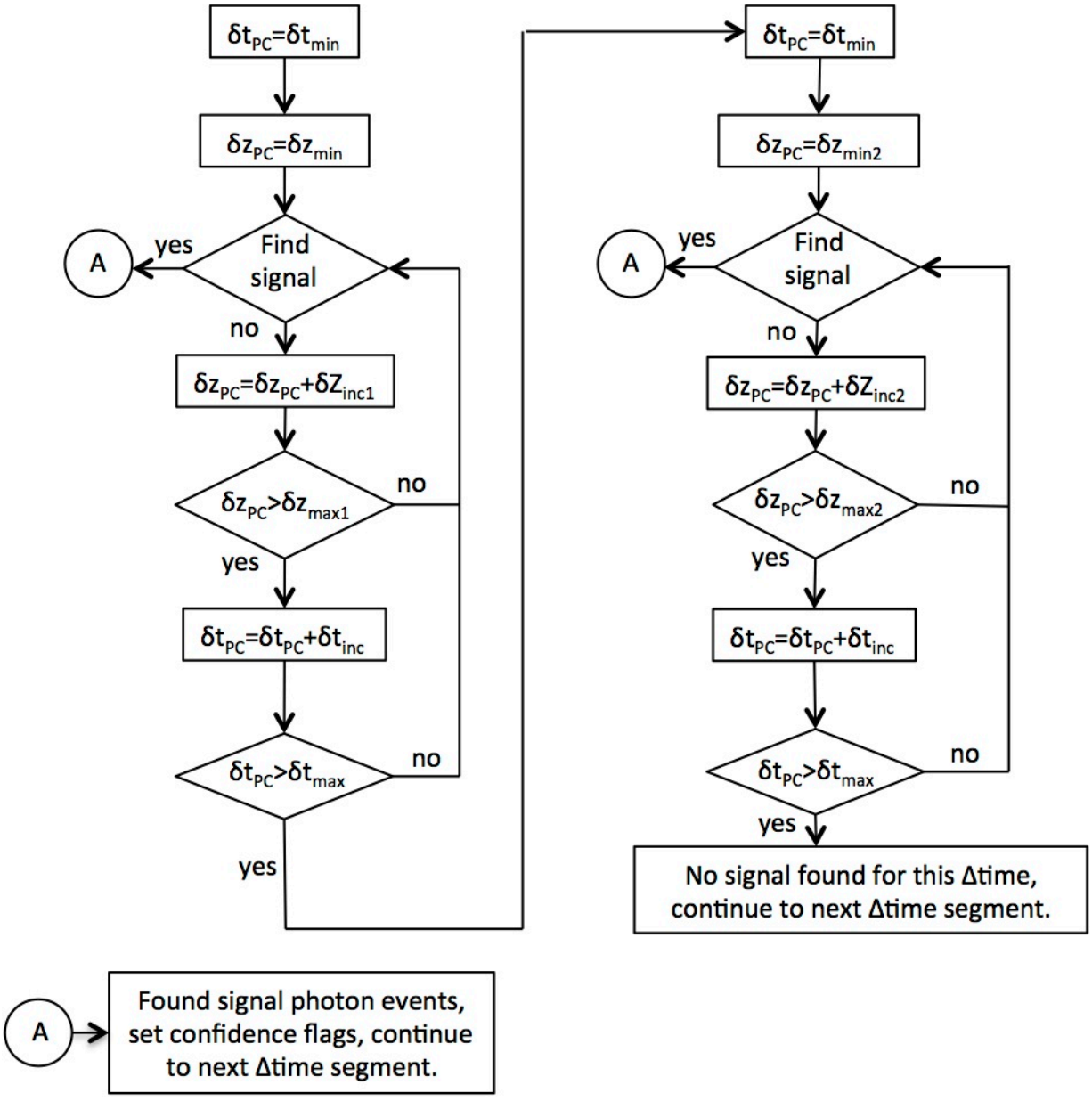

Figure 5-5. Steps to Vary δt_{PC} and δz_{PC}.

If no signal is found for the initial δt_{PC} and δz_{PC}, the algorithm first varies the histogram bin height from δz_{min} to δz_{max1}. The algorithm then increases the along-track bin width δt_{PC} and again sweeps through δz_{PC}. If δt_{max} and δz_{max1} are reached, the algorithm scans a larger range of δz_{PC}, limited by δz_{max2}. This process continues until either the maximum values of δt_{max} and δz_{max2} are reached, or signal is found. This process is shown graphically in Figure 5-5.

Figure 5-6 shows how the algorithm varies the histogram bin size, δz_{pc}, in two steps; first from δz_{min} to δz_{max1} and second from $\delta z_{max1}+\delta z_{inc1}$ to δz_{max2}. The logic of separating these two steps is that signal is most often found in the region spanned by δt_{min} to δt_{max} and δz_{min} to δz_{max1}. Therefore, the algorithm checks this region first, before examining larger values of δz.

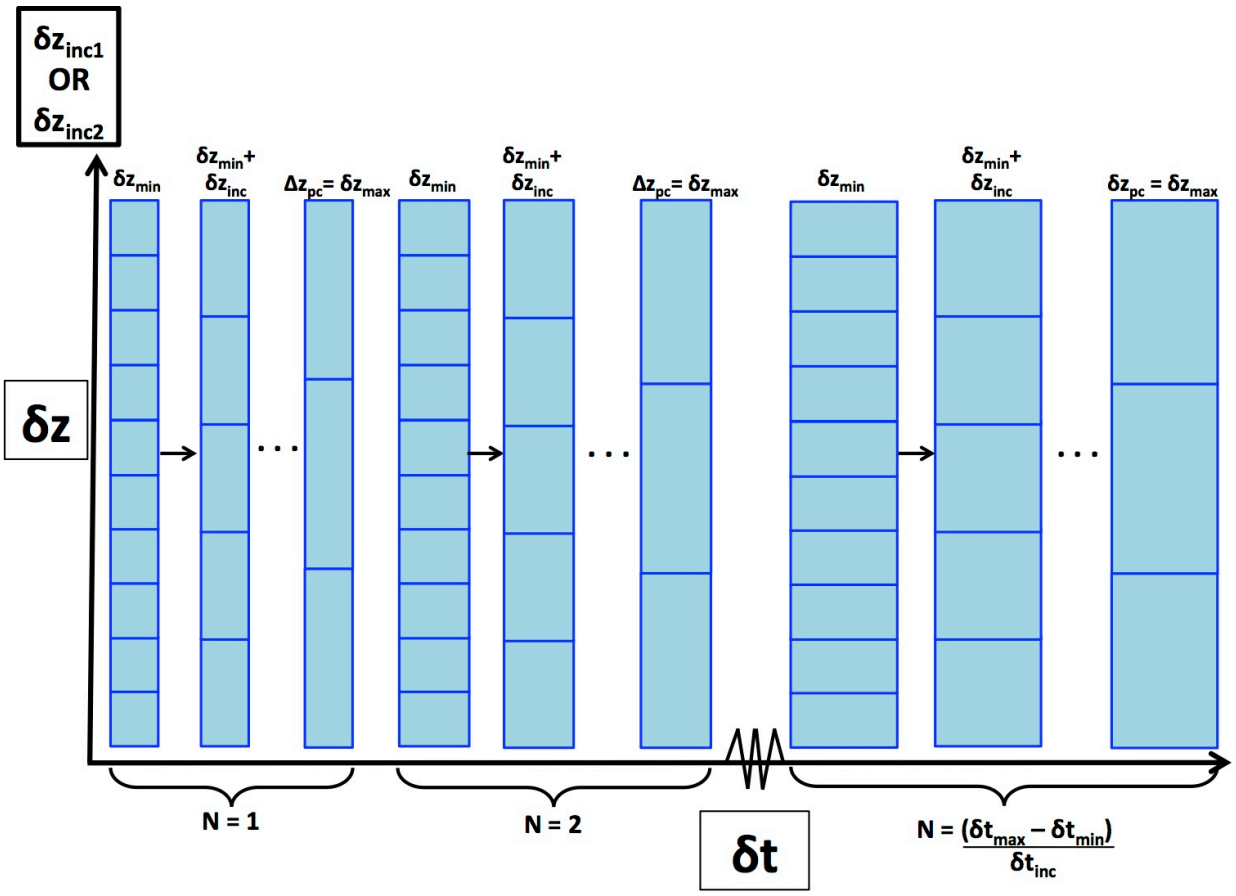

Figure 5-6. Variation of Histogram Bin Size.

The algorithm first increases the vertical bin size for a single value of δt_{PC}, as indicated on the left side of the figure for N = 1. The algorithm then increases δt_{PC}, and again sweeps through the range of δz_{PC}. The process continues until one or more bins are determined to have signal photons.

Since δt_{PC} can be greater than Δtime it is possible to find signal photons outside of Δtime although none exist inside Δtime at these larger values of δt_{PC}. If this happens continue increasing δt_{PC} and δz_{PC} until find signal photons within Δtime or the limits are reached and no signal photons are identified.

5.4.2.5 Slant Histogramming

The term "slant histogramming" is used to describe when the algorithm histograms the photon heights relative to a sloping surface. Two types of slant histogramming are performed. Type one describes where the surface slope is defined along the whole profile by performing running linear fits to the signal photons defined from the ellipsoidal histogram step (section 5.4.2.5.1); then the slant histograms are formed relative to the slopes of the linear fits (section 5.4.2.5.2) to these likely signal photon heights. Type two describes the situation when type one slant histogramming still leaves large gaps in the profile within a segment. In this case, the slope is varied through a range from $-\alpha max$ to $+\alpha max$ and the algorithm seeks the value of the slope that gives the maximum number of signal photons (section 5.4.2.5.3). Then regular slant histogramming is performed relative to the resulting slope (section 5.4.2.5.2).

5.4.2.5.1 Estimation of Surface Profile from Identified Signal

The first type of slant histogramming relies on the surface slope inferred from the signal photons identified as signal photons by ellipsoidal histogramming. Given:

- The time and ellipsoidal height of each photon Tp(i), Hp(i)
- The confidence flag for each photon, conf(i,isurf) where conf(i,isurf) ≥ 2 indicates a signal photon (section 5.4.2)
- The factor to multiply Δtime by, min_fit_time_fact(isurf,ibeamstrength) to calculate the time increment to fit over
- The beginning and end time of the granule, Timebeg_seg and Timeend_seg (section 5.4.1.2)
- The minimum number of photons over which to perform a linear fit, nphotmin
- The multiplier of the standard deviation of the linear fit used to remove outliners, e_linfit_slant

The algorithm steps through the granule in steps of min_fit_time, overlapping each step by 10%. The parameter min_fit_time is formed by multiplying Δtime by min_fit_time_fact, a multiplicative factor. This sets the duration (in time) over which to perform linear fits. Note that since both Δtime and min_fit_time_fact are functions of beam strength and surface type, min_fit_time is also a function of beam strength and surface type. The algorithm then performs an iterative linear fit to the signal photons found through ellipsoidal histogramming for each min_fit_time. If there are not nphotmin signal photons in a particular time step, no linear fit is performed. The output of this part of the algorithm are the start and end times of each fit (tbegcoef(nfit) and tendcoef(nfit), respectively; and the coefficients of the linear fits: c0(nfit) and c1(nfit), where nfit is the number of linear fits performed in each time step

1. Start at the beginning of the granule, and set the time limits (Timebeg_use(1) and Timeend_use(1)) for the time interval over which to generate linear fits to the signal photons:

Timebeg_use(1) = Timebeg_seg

Timeend_use(1) = Timebeg_seg(1) + min_fit_time

2. Set the time boundaries over which to use the first fit, Tbegcoef(1) and Tendcoef(1):

Tbegcoef(1) = Timebeg_use(1)

Tendcoef(1) = Timeend_use(1)

For the following time increments, denoted by the index m > 1, Tbegcoef(m) and Tendcoef(m) differ from Timebeg_use(m) and Timeend_use(m) because they do not include the overlap discussed in step 5.

3. Determine if sufficient signal photons (nphotmin) exist in this time interval:

find all values of k where

Conf(k,isurf) ≥ 2 and

Timebeg_use(m) ≤ Tp(k) ≤ Timeend_use(m)

If the algorithm never gets nphotmin values of k then it does not perform slant histogramming for this interval.

4. If the number of k is greater than or equal to nphotmin, perform an iterative least-squares linear fit using all signal photons in the interval, and store the coefficents of the fit, c0(m) and c1(m) and the limits of the time over which the fit was performed, Tbegcoef(m), Tendcoef(m):

(a) First, fit all values of Hp(k) and Tp(k) with a linear least-squares equation between these two time limits:

$H(m,k) = c0(m) + c1(m) \times (Tp(k) - T_{beg})$

(b) Calculate the standard deviation, σ_linfit, of the photon event heights against the resulting least-squares line, and classify any photon events with heights that differe from the fit by more than e_linfit_slant x σ_linfit as background.

(c) Recalculate the coefficients of the least-squares line as in step (a) and edit outliers as in step (b) until σ_linfit converges to within 2% or the number of iterations is greater than 4.

(d) If during this iterative editing, the number of remaining potential signal photons used in the fit falls below the nphotmin criteria, a suitable linear fit for this interval is not defined.

(e) After the solution converges, or the maximum number of iterations are reached, store the resulting c0(m) and c1(m) coefficients and the associated start and stop times to use this fit over are Tbegcoef(m) and Tendcoef(m). At each (m), these terms are calculated as:

Tbegcoef(m), for m>1 = Timebeg_use(m) + 0.1*min_fit_time
Tendcoef(m), for m>1 = Timeend_use(m)

5. Continue performing linear fits along the granule by updating Timebeg_use and Timeend_use, insuring that consecutive time segments overlap by 10%:

$$\text{Timebeg\_use}(m+1) = \text{Timeend\_use}(m) - 0.1*\text{min\_fit\_time}$$
$$\text{Timeend\_use}(m+1) = \text{Timebeg\_use}(m+1) + \text{min\_fit\_time}*1.1$$

The algorithm continues through the granule until the end of the granule is reached. Since the total time spanned by a granule may not be an integral of 0.9*min_fit_time, special consideration is needed for the last segment in the granule. For the last segment, Timeend_use should equal the time of the last photon in the granule, and Timebeg_use in this segment should be min_fit_time seconds prior to Timeend_use. In this way, some photons are used in two consecutive iterative linear fits, but all fits are predicated on using min_fit_time seconds.

6. For the last fit of the segment, define:

$$\text{Tbegcoef}(m) = \text{Timeend\_use}(m-1)$$
$$\text{Tendcoef}(m) = \text{Timeend\_seg}$$

This forces Tbegcoef to always be coincident with a Δtime boundary, and align the results from the slant and ellipsoidal histogram parts of the algorithm.

5.4.2.5.2 Slant Histogram Along a Specified Surface Slope

Now that the surface slope in signal photon have been identified throughout the granule, the algorithm now completes the type one slant histogram step along this slope by forming a histogram of photons in each time interval along the best-fit line found in the previous section. The slope α, in each segment is based on the slope from the linear fits, c1(m).

For each set of linear fits, m:

1. Calculate the surface slope, α, of each linear fit interval:
   $\alpha(m) = \arctan(c1(m))$

   Note that α is not the physical slope of the surface (i.e. meters of elevation change per meters along-track distance) but represents the change in elevation per seconds of time, and so has units of meters / second.

2. If $\alpha(m) > \alpha_{max}$ then skip this set of coefficients, otherwise continue. The purpose of this step is to avoid trying to form slant histograms on very steeply sloping surfaces where we don't expect ICESat-2 to recover coherent returns. In these regions any apparently coherent surface is very likely spurious.

3. Rotate the photon elevations in each segment, Hp, through the angle α into a slant reference frame Zsl. Note that the photon times are not rotated; the algorithm continues to use the times defined in the original ellipsoidal reference frame.

   $Zsl = Hp \times \cos(\alpha) - Tp \times \sin(\alpha)$

Figure 5-7 depicts the geometry for slant histogramming.

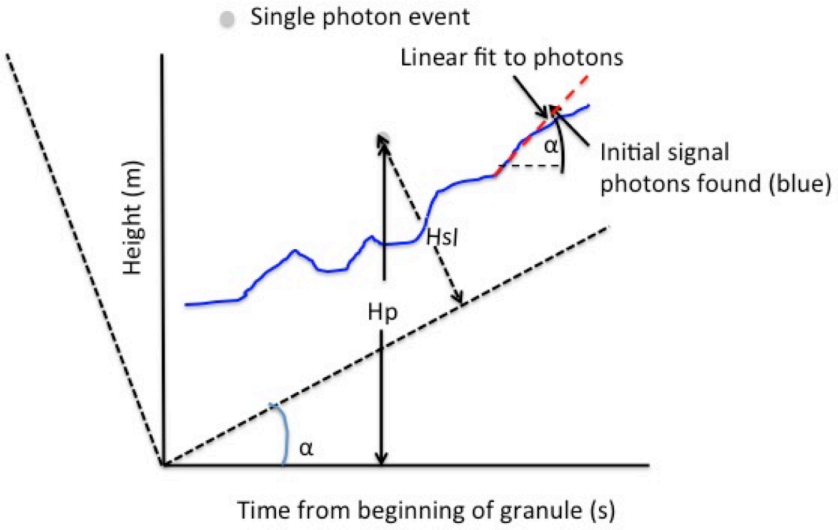

Figure 5-7. Slant Histogram Geometry Over a Single Gap.

4. For each time, time_$_n$, from time_$_n$ = Tbegcoef(m) + Δtime/2, to Tendcoef(m)_ - Δtime/2, the algorithm forms a histogram of the heights relative to the surface defined by the linear fit for that segmentor time interval, H(m). The histogram bin size, $\delta z_{pc,}$ and integration time, δt_{pc}, are set in the same manner as in section 5.4.2.4.

   (a) Calculate the beginning and end values of the elevation of the mth linear fit, noting that although this corresponds to the mth entry in the Tbegcoeff array, not all m intervals had valid linear fits:

   $$Z_{beg} = c0(m) + c1(m) \times time\_h_b$$

   $$Z_{end} = c0(m) + c1(m) \times time\_h_e$$

   where:

   $time\_h_b = time\_{}_n - \delta t_{pc}/2$

   $time\_h_e = \min(time\_{}_n + \delta t_{pc}/2, Tendcoef(m))$

(b) Rotate Z_{beg}, Z_{end} and the bin size δz_{pc} into the slant reference frame defined by α to obtain heights, Zsl_{beg}, Zsl_{end} and the corresponding times, $Tsl_{beg}(m)$, $Tsl_{end}(m)$. Again note that photon times along track are not adjusted, but carry over from the ellipsoidal-reference frame times:

$$Zsl_{beg} = Z_{beg} \times \cos(\alpha(m)) - Time\_h_b \times \sin(\alpha(m))$$
$$Zsl_{end} = Z_{end} \times \cos(\alpha(m)) - Time\_h_e \times \sin(\alpha(m))$$
$$Tsl_{beg} = Time\_h_b$$
$$Tsl_{end} = Time\_h_e$$
$$\delta z_{pc}sl = \delta z \times \cos(\alpha(m))$$

(c) Set the height window in the slant reference frame over which to select photons, $Zhsl_{min}$, $Zhsl_{max}$:

$$Zhsl_{min} = \min(Zsl_{beg}, Zsl_{end}) - nslw * \delta z_{max2}sl$$
$$Zhsl_{max} = \max(Zsl_{beg}, Zsl_{end}) + nslw * \delta z_{max2}sl$$
$$\delta z_{max2}sl = \delta z_{max2} \times \cos(\alpha(m))$$

(d) Create a histogram Hz(j) such that:

$Hx(j) = Zhsl_{min}(1) + \delta z_{pc}sl \times j$ for j=0, nbins - 1

Hz(j) = is formed by binning the photon heights in the rotated reference frame Zsl(i) into each of the Hx(j), for photons in the range spanned by $Zhsl_{min}$ to $Zhsl_{max}$ in the time period spanned by Tsl_{beg} to Tsl_{end}. E.g. where:

$$Hx(j) \le Zsl(i) < Hx(j+1)$$
$$Tsl_{beg} \le Tp(i) < Tsl_{end}$$
$$nbins = (Zhsl_{max} - Zhsl_{min}) / \delta z_{pc}sl$$

(e) Following section 5.4.2.2, calculate the signal threshold and following section 5.4.2.3, determine signal bins and the indices i in Zsl(i) that contain signal. Be sure to use the corresponding value of δz_{pc} not $\delta z_{pc}sl$ when scaling the background noise statistics, because those statistics were created using ellipsoidal (rather than slant) elevations.

(f) Update the confidence flag, conf(i,isurf), based on the value of SNRbin (as in section 5.4.2.3.5, step (2)). Always set the confidence parameter to the maximum of the previously defined value and the new value:

conf(i,isurf) = max(conf(i,isurf), 2) if SNRbin(l) < snrlow

conf(i) = max(conf(i), 3) if snrlow ≤ SNRbin(l) < snrmed

conf(i) = max(conf(i), 4) if SNRbin(l) > snrmed

(g) Save the number of photons selected from this process in **nphot_slant(time_n)**.

(h) If for any time_n, nphot_slant(time_n) is greater than nphot (time_n) then update the integration parameters such that these parameters represent those used to select the majority of the photon events at any time_n. That is, if nphot_slant(time_n) is greater than nphot(time_n), then:

Nphot(time_n) = nphot_slant(time_n)

δz_{PC}_out (time_n), δt_{PC}_out (time_n), and tintbeg_out(time_n) become the values used for slant histogramming.

If $\boldsymbol{\mu_{bg}\_\delta z_{BG}\_\delta t_{BG}}$ ***_out(time_n)*** and, $\boldsymbol{\sigma_{bg}\_\delta z_{BG}\_\delta t_{BG}}$ ***_out(time_n)*** are undefined then set them equal to μ_{BG}_tn_δt_{BG}_δz_{BG} and σ_{BG}_tn_δt_{BG}_δz_{BG}, respectively.

5. Repeat section 5.4.2.5.2 for all linear fits in this granule.

5.4.2.5.3 Identifying Remaining Gaps in the Profile

If gaps remain that cannot be filled by the type one slant histogramming steps above (sections 5.4.2.5.1 and 5.4.2.5.2), the algorithm proceeds to slant histogram with respect to a range of surface slopes in a second effort to identify signal photons in these gaps. From Timebeg_seg to Timeend_seg identify any time gaps where no signal photon events have been identified that are larger than Δtime_gapmin. First, the algorithm calculates Timebeg_gap(ig) and Timeend_gap(ig) as the time boundaries of gap ig relative to time_beg.

For every Δtime increment in each ig gap, the algorithm:

- Approximates the bias associated with each gap as the mid value of the signal photon heights for the Δtime increment preceding the gap;
- Performs slant histogramming using $\delta t_{PC} = \delta t_{max}$, $\delta z_{PC} = \delta z_{max2,}$ and δEslw = nslw $\times \delta z_{max2}$sl, δEslw_v = nslw_v × δz_{max2}sl, varying the surface slope over the range spanned by ± αmax by αinc until the value of α for which the most signal photons are identified, αopt_c, is found;
- Uses values for $\delta t_{PC} = \delta t_{max}$, $\delta z_{PC} = \delta z_{max2,}$ and δEslw = δEslw_v to perform slant histogramming varying the surface slope from αopt_c - αinc to αopt_c + αinc in steps of αinc/5 and find the value of α for which the most signal photons are identified, αopt_f. The goal of this step is to complete a finer search around the coarse slope identified in the prior step;
- For α = αopt_f, performs slant histogramming by varying δt_{PC} and δz_{PC} as per section 5.4.2.4, using δEslw = δEslw_v.

The algorithm repeats the above steps for each increment, Δtime, throughout the gap.

5.4.3 Editing Outliers

If the Ledit(isurf) flag is set then the algorithm performs an edit on identified signal photons to further remove outliers in each segment

- The algorithm first calculates a linear fit using least-squares to each group of signal photon events for each Δt_lf span of time throughout the segment, overlapping the fitting region by Δt_linfit_edit/2. The results will be a set of linear functions, Z(n), with coefficients, c0(n) and c1(n) that are used from tbeg_lf(n) to tend_lf(n), where:

  Z(n) = c1(n) * t + c0(n), for n = 1 to (tend - tbeg) / (Δt_linfit_edit/2)
  tbeg_lf (n) = Timebeg_seg + (Δt_lf/2) * n;
  tend_lf(n) = tbeg_lf(n) + Δt_linfit_edit

  and where n = 0 until tend_lf(n) is greater than Timeend_seg

- For each linear fit region, the algorithm performs an nσ edit to remove outliers by:
  - Calculating the standard deviation, σlf(n), of the signal photon heights around the fit, Z(n)
  - Recalculating the residuals for each signal photon height, editing any photon events which heights differ from the fit by more than e_linfit_edit× σlf(n) where e_linfit_edit is the multiplier of σ for performing this edit
  - Repeating the above steps until the values of σlf converge, or four iterations, whichever is first.

5.4.4 Padding the Signal Photons

Select additional photons so that the minimum height span of selected photons is ≥ htspanmin at each Δtime.

Now that all signal photons have been identified for a segment, the algorithm examines the range of signal photons in each Δtime and selects additional photons as necessary to force the height span of selected photons at each Δtime increment to be greater than or equal to Htspanmin. Any additional photons selected as padding to ensure the height span is greater than or equal to htspanmin will have the confidence flag set to 1 to indicate that the algorithm did not select it as signal but it is close in height to the signal photon events selected.

1) Calculate the minimum and maximum value of Hp(i) over each nth Δtime increment for all photon events, i, where conf(i) > 0: Zmin(n), Zmax(n).
2) If Zmax(n) - Zmin(n) is less than Htspanmin:
   a. Calculate the middle value of Z, Zmid(n) = (Zmax(n) - Zmin(n)) / 2
   b. Calculate, Zmax_slct(n) and Zmin_slct(n):
      i. Zmax_slct(n) = Zmid(n) + htspanmin / 2
      ii. Zmin_slct(n) = Zmid(n) – htspanmin / 2

For any photon event where Tp(i) is within the nth Δtime increment and Zmin_slct(n) ≤ Hp(i) ≤ Zmax_slct(n), reset conf(i) = max(1,conf(i)). This sets the confidence flag to 1 if it was not

previously selected as signal or to the confidence level already set if previously selected as signal.

At this point, all output parameters defined in Table 5-4 have been defined and the algorithm output is consistent with the needs of the higher-level data products.

6.0 GEOPHYSICAL CORRECTIONS

This section provides an outline for present-day geophysical standards and corrections that must be applied in order to fulfill science requirements for the ICESat-2 mission. It is suggested that, when applicable, the International Earth Rotation and Reference Systems Service (IERS) conventions from 2010 be used.

6.1 Introduction

From the *ATBD for ICESat-2 Receive Photon Geolocation (ATL03g)*:

"The geolocation of an ATLAS photon event is computed as a function of three complex measurements:

1. The position of the space based ranging instrument from the Precision Orbit Determination (POD);
2. The pointing of the laser pulse from the Precision Pointing Determination (PPD), and
3. The photon event round trip travel time observation measured by the ATLAS instrument."

The geolocation of ATLAS photons provides the starting point for the ATL03 science level product. Each photon event will have been placed within a geodetic coordinate system, with a latitude, longitude, and height above the WGS-84 ellipsoid based on ITRF 2000 G1150 (a_e = 6378137m, 1/f = 298.257223563) assigned to it.

In summary, each ATLAS emitted photon passes through the atmosphere and experiences delays that depend on the refractive index along the optical path. The photons ultimately encounter a surface on the Earth (terrestrial, ocean or snow/ice-covered), and are reflected back to the satellite receiver system. The round-trip time of a photon is what constitutes a base input measure for geolocation. Over oceans, sea ice and ice shelf surfaces, each photon event requires corrections to account for temporal variability in atmospheric-oceanic interactions (e.g., inverted barometer and wind field effects) as well tidal states and other corrections. Over land surfaces, each photon event requires corrections for ocean loading and solid earth tides. These constitute what are referred to as *geophysical corrections*.

In the most general of terms (omitting, e.g., precision pointing and atmospheric delay corrections), the calculation for sea surface height (*SSH*) or an analogous land surface height is conceptualized in the following manner. First, an estimate of the photon event height (H_P), having the WGS-84 ellipsoid as its reference surface, is formed by the difference:

$$H_P = H\_satellite_{ellipsoid} - H\_satellite_{surface}$$

where $H\_satellite_{ellipsoid}$ represents the satellite height above the WGS-84 ellipsoid (determined by POD) and $H\_satellite_{surface}$ is the height of the satellite above the surface upon which the photon was reflected. The latter quantity is often referred to as a *range*, intuitively understood as one half the signal photon round-trip time (consisting of a photon being transmitted at time t_T, reflected by the Earth's surface and then received at time t_R) multiplied by the speed of light, c.

$$H\_satellite_{surface} = c(t_T - t_R)/2$$

These are fundamental quantities that enter into the precision orbit determination (POD) and photon geolocation processes (ATL03g).

Very generally, the photon event height, H_P, is corrected for an i-number of temporally and spatially varying geophysical effects (tides, loading, etc., as listed below), represented by C_i which are, by convention, consistently subtracted via

$$H_{gc} = H_P - \sum C_i$$

where H_{gc} are geophysically-corrected photon event heights referring to the WGS-84 ellipsoid. Some of the corrections in C_i are only applicable over specific surface types (for example, ocean tides only apply for oceanic photon event returns). This is more explicitly desribed in the following sections.

For those interested in having, for example, oceanic photon event heights refer to a mean sea surface (MSS), then the equation becomes

$$SSH = H_{gc} - MSS = H_P - MSS - \sum C_i$$

To be perfectly clear, the photon heights reported on the ATL03 product are referenced to the WGS-84 ellipsoid based on ITRF 2000 G1150 (a_e = 6378137m, 1/f = 298.257223563). ATL03 also provides information to allow the interested user to derived geoid-referenced heights, or sea-surface heights.

By standard convention, and more generally, corrections are subtracted from height values to form corrected heights; if the correction should need to be removed (or "undone," say, to apply a differently modeled correction), the original correction is added to the corrected height.

With regard to implementation and application of the geophysical corrections, in most cases, a regional calculation (or interpolation) of each geophysical parameter is applied uniformly across a group of photons. Since the density of the photon distribution is very high (with the average along-track distance between sequential laser pulses being ~70 centimeter) and given the locally smooth nature (over ~500 meter distances) for the parameters involved, computation or interpolation of geophysical corrections at every individual photon location is computationally prohibitive. Instead, geophysical corrections are computed or interpolated along each ground track at a sampling distance of 20 meters (corresponding to the along-track segments outlined in section 3.1) and applied uniformly over the group of photons within each segment. This is performed independently for each ground track. The reference photons provide a useful regular along-track discretization in space and time. Therefore, the reference photon location and time is used to determine geophysical corrections for all photons in a given along-track segment.

While the along-track segments of section 3.1 and the reference photons provide a convenient regular set of points to evaluate these geophysical models, care was taken to insure that such a sampling interval (~20 meters) was acceptable from a geophysical standpoint. Local and regional geographical variations and sensitivities of the Dynamic Atmospheric Correction (DAC) and ocean tide geophysical correction parameters were investigated to ensure that errors arising from the uniform application of geophysical corrections remain small (sub centimeter level). For example, the DAC (section 6.3.2), as applied over oceans, possesses the most rapid geographic

variations (among the set of geophysical corrections), but with a rather small amplitude (±15 centimeters). Imposing a 20-m along-track interpolation distance upon DAC, a maximum height errors on the order of ±0.07mm (typically less) is incurred when applied to group photons within a ±10 meters zone. With regard to ocean tides, imposing a 20-m along-track computational distance incurs maximum height errors of up to ±3.0 millimeters in regions characterized by high geographic gradients (e.g., Hudson Strait, Bay of Fundy, the Yellow Sea, etc.).

6.2 List of Geophysical Corrections

The following list summarizes time-dependent geophysical corrections and static reference values required to produce the ATL03 L2 science product for ICESat-2. This list is similar to corrections and standards applied in other altimetric and geodetic satellite missions, as well as multi-national climatological investigations (e.g., ESA's Sea Level Climate Change Initiative).

The list below provides typical magnitudes expected for each parameter. A schematic diagram of associated corrections and reference values is shown in Figure 6-1. Table 6-1 presents the parameters, the inputs and outputs for each, whether a correction is to be applied or whether it serves as a reference value, and the sources for the models or data required to make the corrections or to provide reference values.

Time regularization of photon surface bounce point variations (corrections):

- **Ocean Tides** including diurnal and semi-diurnal (harmonic analysis), and longer period tides (dynamic and self-consistent equilibrium) (±5 meters)
- **Dynamic Atmospheric Correction** (DAC) which included the **inverted barometer** (IB) effect (±50 centimeters)
- **Solid Earth Tides** (±40 centimeters, max)
- **Ocean Loading** (centimeters)
- **Solid Earth Pole Tide** Deformation due to centrifugal effect from small variations in polar motion (±1.5 centimeters)
- **Ocean Pole Tide** Oceanic height correction due to centrifugal effect from small variations in polar motion (±2 millimeters amplitude)
- **Geocenter Motion** correction *not* applied to L2 science products, but accounted for in precision orbit determination (amplitude 3 to 5 millimeters in X,Y,Z).

Photon round-trip range corrections:

- **Total column atmospheric delay** (-2.6 to -0.9 meters)

Static parameter (reference value):

- **Geoid** (-105 to +90 meters, max)

Given this list and the corrections identified in Table 6-1, the previous equation for the geophysically-corrected photons events can be expressed more explicitly as:

$$H_{gc} = H_P - H_O - H_{DAC} - H_{OL} - H_{SEPT} - H_{OPT} - H_{SET} - H_{TCA}$$

where: H_P is again the photon event height, H_O are ocean tides; H_{DAC} are IB/DAC; H_{OL} are ocean loading deformations; H_{SEPT} are solid earth pole tides; H_{OPT} are ocean pole tides; H_{SET} are solid earth tides; and H_{TCA} are total column atmospheric delay corrections. The models used in ATL03 are global, with values defined everywhere on the surface of the Earth. Where such models are undefined (e.g. H_O over land surfaces) the model returns a value of zero. The photon event heights on the ATL03 output product are the geophysically-corrected photon event heights, referenced to the WGS-84 ellipsoid.

The values of the geophysical corrections described below are determined using the reference photons, nominally spaced at twenty meters along-track for each ground track. The reference photons are determined in section 3.2 and have a corresponding latitude, longitude, time, and ellipsoidal height. The interpolating functions to determine geophysical corrections at a specific point (i.e. the reference photon locations) are described below in the Implementation Plan for each correction. In the event that an along-track segment has no reference photon (i.e. there are no photons in a given segment) the geophysical corrections for that segment are given the maximum value a data type can accommodate to represent an invalid value of that parameter.

While the models selected here provide state-of-the-art corrections to the photon ellipsoidal heights, users are cautioned that small-scale features (such as bays or peninsulas) or edges of surface-specific corrections (such as ocean tides, which have meaningful values only over the world's oceans) require particular attention. Despite of the best efforts of the geodetic community to produce global models that retain fidelity at small spatial or temporal scales, such regions remain challenging to model at the fine spatial and temporal scales of interest to some users. Therefore, ATL03 provides the detail necessary to enable these users to remove corrections as they see fit, and apply whatever improved corrections are needed in these areas. The ATL03 data product also provides geiod and Mean Sea State values for informational purposes, to allow the interested user to change the photon event height reference surface.

Model Type	Input Params	Output Params	Application*	Processing/Source Candidates
Ocean Tides	lat, lon, time	ocean height correction	C	GOT4.8 – in-house support
Met Data	lat, lon, time	surface and column temperature, pressure	R	NASA GMAO GEOS5 FP-IT
IB/DAC	lat, lon, time	ocean height correction	C	MOG2D (AVISO)
Ocean Loading	lat, lon, time	ocean height correction	C	GOT4.8 – supplemental files
Solid Earth Pole Tide	lat, lon, time	solid earth deformation	C	IERS Conventions (2010)
Ocean Pole Tide	lat, lon, time	ocean height correction	C	IERS Conventions (2010)
Solid Earth Tides	lat, lon, time	solid earth deformation	C	IERS Conventions (2010)
Geoid	lat, lon	reference surface	R	EGM2008, mean tide system
Geocenter Motion	time	Cartesian shift of tracking stations	N	Via SLR/GPS estimation, applied in POD
Total Column Atmospheric correction	lat, lon, time	range correction	C	Recommendation by Luthcke & Petrov, cf. ATBD ATL03a

* C = applied as a correction; R = supplied as reference value; N = no correction to L2 science product.

Table 6-1. Table of Geophysical Corrections and Reference Model Sources for ICESat-2.

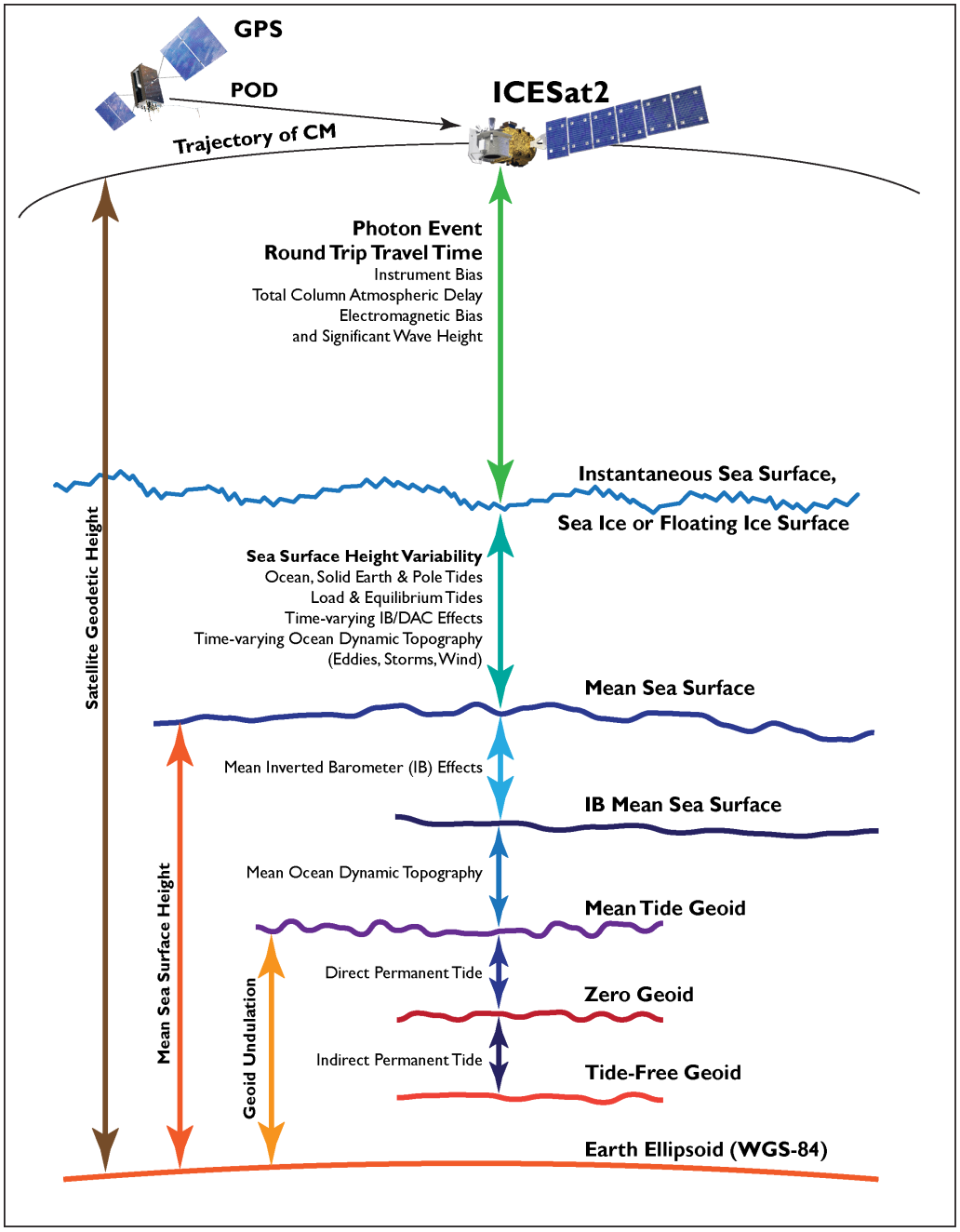

Modified from: Tapley, B. D. & M-C. Kim, Applications to Geodesy, Chapt. 10 in *Satellite Altimetry and Earth Sciences*, ed. by L-L. Fu & A. Cazenave, Academic Press, pp. 371-406, 2001.

Figure 6-1. Schematic of Geophysical Corrections Required in Satellite Altimetry.

6.3 Geophysical Corrections and Models

6.3.1 Ocean Tides

Ocean tides account for about 70% of the total variability of the ocean surface at daily and half-daily periods (diurnal and semi-diurnal). The effects of tides vary regionally; open ocean areas typically have smaller amplitudes (±0.3m r.m.s) than continental shelves and coastal regions (which can increase to several meters or more).

Ocean tide models quantitatively describe the time-variant changes of sea level due to gravitational attraction by the Sun and the Moon. The models are applicable for any point in the oceans, as well as on sea ice and on ice shelves.

Modern tide models fall into two broad categories: those which are formed on the basis of purely hydrodynamic numerical modeling; and those that assimilate the hydrodynamics with tidal observations, including satellite altimeters [Le Provost, 2001]. Assimilation models provide accurate measures of tides across all open ocean expanses.

The recent investigation by Stammer et al, (2014) compared and evaluated global ocean tide models. It provides a helpful guide to select from candidate models for use in ocean tidal corrections. Table 6-2 lists ocean tide models currently available.

Model	Type	Resolution	Authors
Modern Data-constrained Models			
GOT4.8	E	1/2°	Ray [1999, updated]
OSU12	E	1/4°	Fok [2012]
DTU10	E	1/8°	Cheng and Andersen [2011]
EOT11a	E	1/8°	Savcenko and Bosch [2012]
HAM12	H	1/8°	Taguchi et al. [2014]
FES12	H	1/16°	Lyard et al. [2006, updated]
TPXO8	H	1/30°	Egbert and Erofeeva [2002, updated]
Historical Models			
NSWC	H	1°	Schwiderski [1979]
CSR3.0	E	1°	Eanes and Bettadpur [1996]
Purely Hydrodynamic Models			
HIM	N	1/8°	Arbic et al. [2008]
OTIS-GN	N	1/8°	Green and Nycander [2013]
STORMTIDE	N	1/10°	Müller [2012]
OTIS-ERB	N	1/12°	Egbert et al. [2004]

STM-1B	N	1/12°	Hill et al. [2011]
HYCOM	N	1/12.5°	Arbic et al. [2010–updated]
E – semi-empirical adjustment to an adopted prior model.			
H – assimilation into a barotropic hydrodynamic model.			
N – purely hydrodynamic (no data constraints)			

Table 6-2. Ocean Tidal Models Currently Available.

Stammer et al. (2014) didn't identify a tide model that was superior beyond its peers across all categories. Tables 3 through 11 in Stammer et al. (2014) provide a series of quality assessment evaluations that include, for example, comparisons with tide gauges, ocean bottom pressure gauges and orbit fits to several geodetic satellites. Table 6-3 summarizes the best performing tide models by category. The assimilation models achieving the best marks are TPXO8, HAM12, GOT4.8 and EOT11a models.

Figures 8 through 11 in Stammer et al. (2014) illustrate global GRACE range-acceleration residuals for four tide constituents (M_2, K_1, O_1 and S_2). Of the six tide models represented, the maps suggest that none of them perfectly represented regions surrounding (a) Antarctica (particularly the Weddell and Ross Seas as well as the Filchner-Ronne and Ross ice shelves); (b) Greenland and (c) the Canadian archipelago. The HAM12 model best represented the tides for these regions.

Model comparison	Best performance	2nd best	3rd best
Deep Ocean bottom pressure gauges	TPXO8	HAM12	GOT4.8
Shelf water tide station	FES12 (Europe)	TPXO8 (Europe)	HAM12 (Europe)
	FES12 (elsewhere)	TPXO8 (elsewhere)	DTU10 (elsewhere)
56 Coastal tide gauges	EOT11a (rms)	DTU10 (rms)	FES12 (rms)
	EOT11a (median absolute difference)	HAM12 (median absolute difference)	TPXO8 (median absolute difference)
Arctic tide gauges	DTU10	EOT11a	TPXO8 and GOT4.8
Antarctic tide gauges	TPXO8	HAM12	GOT4.8
LAGEOS-1 satellite	TPXO8	HAM12	GOT4.8
GRACE residuals	EOT11a (M_2)	HAM12 (M_2)	GOT4.8 (M_2)
Residual SSH anomalies, shallow	FES12	DTU10	GOT4.8

Residual SSH anomalies, deep	HAM12	EOT11a and OSU12	GOT4.8
[Based on tables in *Stammer et al*. (2014)]			

Table 6-3. Performance Order of Tide Models Based on RSS over Main Constituents

Ocean tidal corrections will be made with Ray's GOT4.8 ocean tide model with long period equilibrium tides being computed via the LPEQMT.F Fortran routine where fifteen tidal spectral lines from the Cartwright-Tayler-Edden tables are summed. GOT4.8 was selected since ICESat-2's Precision Orbit Determination effort relies on the GOT4.8 model (cf. POD ATBD), and given that GOT4.8 receives "in-house" development provides an added incentive.

Comparison of a year (2011) of 6-hour global oceanic tides computed by both the GOT4.8 and TPXO8 models showed that the TPXO8 model exhibited 1-centimeter amplitude periodicities in it's global oceanic mean value; and that GOT4.8 had 5 millimeter amplitude periodicities (Figure 6-2). This is not offered in order to make a claim that one model is superior over another, but merely to point out the existence of time-dependent, global behavior of the models.

ICESat-2 altimetry will likely be important for further improving the GOT4.8 tide model initially used to correct ICESat-2 ATL03 altimetry (especially in polar oceans). Using a GOT-series tide model also allows for adoption of supplemental harmonic modeling components for ocean loading tidal effects (section 6.3.4). Long period equilibrium tides (with maximum amplitudes of ±7cm) are computed using the fifteen most relevant constituents from the Cartwright & Edden (1973) corrected tables of tidal harmonics.

6.3.1.1 Tidal Field Sensitivities

Tidal heights, at any moment in time across open oceans, are broad scale features in a geospatial sense. Along some coastlines, tidal heights can vary by more than a centimeter over rather short distances (tens of kilometers). Accurate modeling along coastal zones is particularly challenging. ICESat-2 altimetry will provide an important data resource for improving coastal zone and shallow seas tidal modeling (as well as better modeling tidal effects in polar regions and experienced on ice shelves).

Additionally, temporal variations in tidal heights can be significant over short time periods. As an example, a 24-hour tidal time series, with one minute time resolution, from Canada's Bay of Fundy, well known for its extreme tidal variability, demonstrates that tides can change by as much as 9.75 meters over a six-hour time span. The rate of change approaches ±2.7 centimeters per minute. Therefore, both geolocation position and time are critical inputs for computing and applying oceanic tidal height corrections, especially in coastal regions where high tidal variability can occur.

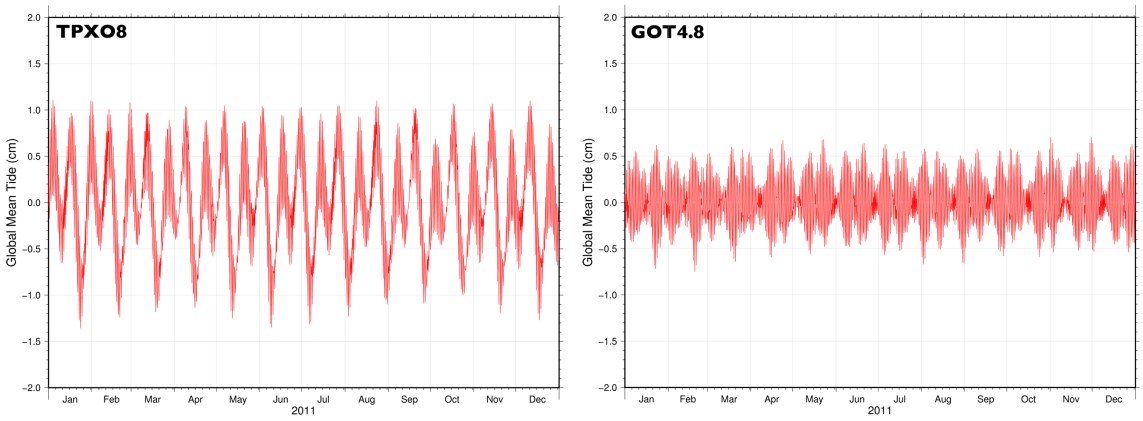

Figure 6-2. One year time series for 2011, of tide values averaged over the global oceans based on a time sequence of 1460, 1°x1° resolution global grids, computed every six hours. TPXO8 at left and GOT4.8 at right.

6.3.1.2 Implementation

The computation of ocean tidal corrections will be performed by computing a modeled tidal height at each reference photon (~20 meters along-track) latitude and longitude, with its corresponding time, *t*. The correction is subtracted from all neighboring group photon heights above the ellipsoid. This correction will be well within error limits given the geolocation and temporal sensitivities exhibited by the tide model. For locations where the ocean tide is undefined, the value of the ocean tide correction is zero.

The GOT4.8 model is given as tidal harmonic amplitude and phase files (typically in NetCDF) which requires integration into existing tidal prediction packages. Long period equilibrium tides are included via the Fortran routine, LPEQMT.F.

6.3.2 Inverted Barometer (IB) and Dynamic Atmospheric Correction (DAC)

The DAC has two main components: (1) a portion that describes the oceanic level response to variations in atmospheric pressure; and (2) a portion that describes mass momentum forcing driven by the highly variable wind stress field. IB Correction describes the first effect, whereas DAC typically describes a combination of both effects. The wind stress field is applicable over open ocean water surfaces. Mass momentum response is further complicated over ice-covered oceans and ice shelves where floating ice dramatically attenuates the influence of the wind field.

IB Correction: When atmospheric pressure is low, the ocean level will rise and when atmospheric pressure is high the ocean level is forced down. In this way, the ocean acts as an inverted barometer. The response relationship is approximately stated as: an increase in pressure of 1 mbar (= 1 hPa) will cause the ocean level to drop 1 centimeter.

Early models of the correction utilized a mean global pressure, P_{ref}, via the relationship,

$$D_h \approx -0.99484(P_i - P_{ref})$$

where P_i is the local atmospheric pressure in mbar and P_{ref} was, as used by TOPEX, a static value of 1013.3 mbar. Before the advent of global pressure fields (ECMWF or NCEP), the local pressure, P_i, was usually ascertained on the basis of the dry tropospheric correction. Andersen & Scharoo [2011] show that a seasonally variable mean, computed exclusively over the oceans, provides a better value for P_{ref}.

The source for ICESat-2 meteorological data may require re-negotiation, depending on what source is chosen. The current plan is that these data will be provided by NASA GSFC's Global Modeling and Assimilation Office (GMAO) GEOS-5 FP-IT (Forward Processing for Instrument Teams) data sets. When required, estimates of a simple IB correction can be constructed from on-record mean sea level pressure data.

DAC: Two DAC sources were considered for application to ICESat-2 L2A products, MOG2D and OMCT.

MOG2D (2 Dimensions Gravity Waves model) is available from AVISO. It is a DAC with 0.25° resolution that has been commonly adopted for use by oceanographers. The formulation of MOG2D is governed by "classical shallow water continuity and momentum equations" [http://www.aviso.oceanobs.com/en/data/products/auxiliary-products/atmospheric-corrections.html] driven by ECMWF atmospheric pressure and wind fields [Carrère & Lyard, 2003]. A map of a 13-month mean of the MOG2D_IB DAC is shown in figure 6-3. Andersen & Scharoo [2011] note reductions in the standard deviation of the residual sea surface height variations across six years of JASON-1 data when using MOG2D_IB DAC over that computed via local IB correction.

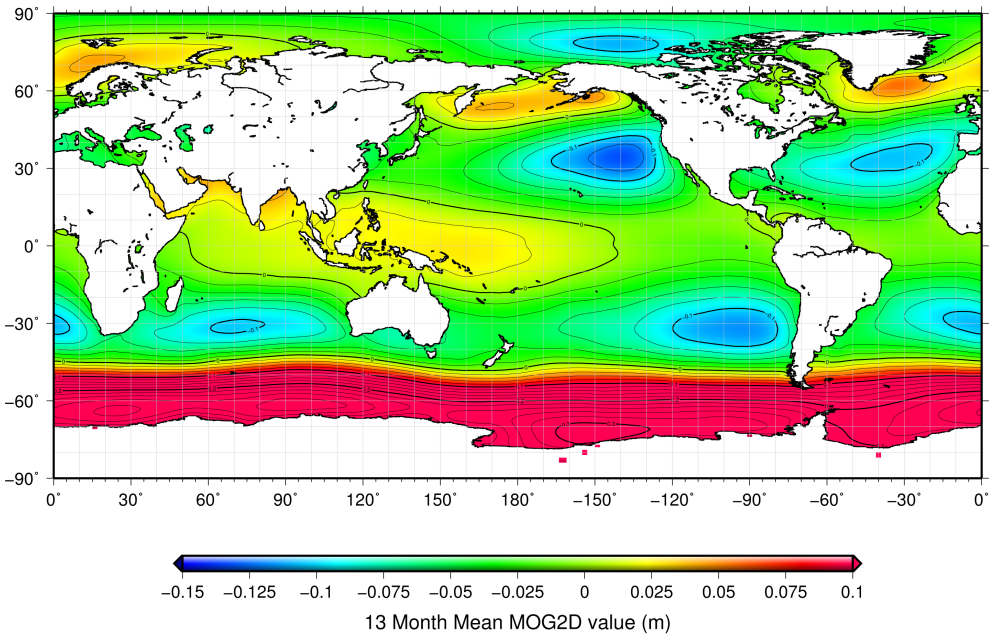

Figure 6-3. 13-Month mean of the MOG2D_IB Dynamic Atmospheric Correction.

OMCT (Ocean Model for Circulation and Tides) by Maik Thomas (GFZ, Potsdam) also models DAC with the enhancement that sea ice covered regions can also be modeled following a Hibler type thermodynamic algorithm. Thomas provided thirteen months (2007-2008) of half-degree global grids of OMCT with mean dynamic topography removed. The mean grid over the 13-month period is shown in figure 6-4. Comparisons between OMCT and MOG2D DAC indicate that the far-southern oceans are quite differently represented.

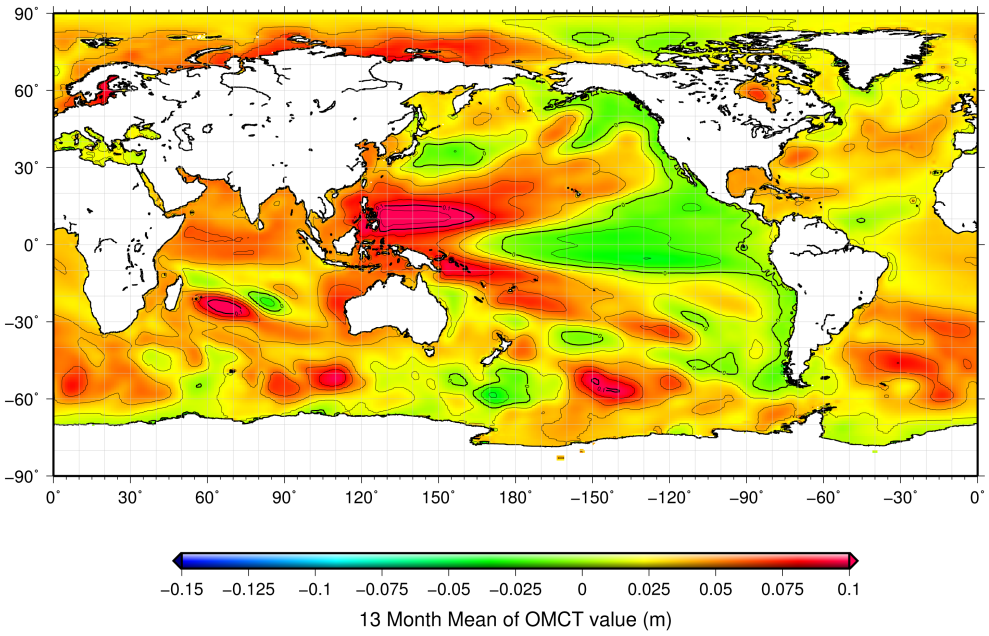

Figure 6-4. 13-Month Mean of the OMCT Dynamic Atmospheric Correction.

6.3.2.1 Implementation

The simple IB corrections of the past have developed into more sophisticated global oceanic correction fields that represent ocean surface deformations that take into account surface pressure and high frequency (< 2 weeks) wind fields. Both DAC sources considered for ICESat-2, AVISO's MOG2D and Maik Thomas' OMCT, are provided as NetCDF grids with 6-hour temporal resolution.

AVISO's MOG2D is the recommended DAC. Six-hour fields are generated daily, in near real-time and are easily accessible. Each fields is approximately 900KB in size. For ICESat-2 processing, the fields will require electronic transfer from AVISO.

For each reference photon, its corresponding time, *t*, is used to select the corresponding 6-hour DAC fields that surround time *t* ("pre" and "post"). These would each be sampled at the reference photon positions (via bi-linear or bi-cubic geographic interpolation), followed by a linear temporal interpolation. The equation,

$$DAC_{correction}(\phi\square\lambda) = DAC_{pre}(\phi\square\lambda) + [DAC_{post}(\phi\square\lambda) - DAC_{pre}(\phi\square\lambda)]/6 * (t - t_{pre})$$

describes the linear temporal interpolation where the DACs have been sampled at lat, lon, ($\phi\square\lambda$) with *t* given in hours. Given the sign convention used in MOG2D, the correction would be subtracted from all neighboring group photon heights above the ellipsoid. For regions where the DAC is undefined, the value of the DAC is zero.

6.3.3 Solid Earth Tides

The correction for solid earth tides takes into account the deformation (elastic response) of the solid earth (including the sea floor) due to the attractions of the Sun and Moon. Ninety-five percent of the tidal energy comes from the second-degree (semi-diurnal) tides. A useful summary of tidal forces, solid earth responses and tidal loading is given in Agnew [2009].

The procedure for the calculation of the displacements due to solid earth tides recommended by recent IERS Conventions 2010 [Petit and Luzum, 2010, section 7.1.1], was suggested by Mathews et al. [1997] and consists of two steps. In the first step, the displacement with frequency-independent nominal values of the Love and Shida numbers for the second and third degree of the tidal potential is computed. The vector displacement is expressed in the time domain in terms of the location and the instantaneous position of the Moon and the Sun obtainable from ephemeris (e.g., JPL Development Ephemeris DE421). In the second step, corrections to the results of the first step are computed in the frequency domain. They take account of the frequency-dependent deviations of the Love and Shida numbers and also of the variations arising from mantle anelasticity. The number of spectral components for which such computations have to be done may be minimized by appropriate choice of nominal values used in the first step (see Mathews et al., 1997). This procedure is utilized in the DEHANTTIDEINEL.F program as well as in Dennis Milbert's SOLID.F program system.

More recent developments include the consideration of lateral inhomogeneities in the elastic Earth model [Latychev et al., 2009], but inclusion of such effects cause deformations on the ±1 mm level [Fok, 2012], and are negligible for ICESat-2 altimetry. Consistency between the ICESat-2 orbit determination is desirable.

6.3.3.1 Implementation

Solid earth tides are, spatially, fairly long-wavelength effects, however, they can vary fairly quickly in time (approximately one centimeter in five minutes). In order to be consistent with the ICESat-2 Precision Orbit Determination process, ATL03 uses a process recommended by the IERS 2010 conventions. For each reference photon (about twenty meters spacing along-track) location (latitude, longitude) with its corresponding time, solid earth tide displacements are computed (in local east-north-up components) with the up-component acting as the solid earth tide correction, C_{SET}. This value is subtracted from the group photon heights above the ellipsoid. This is performed globally for all measured heights.

6.3.4 Ocean Loading

This correction removes the deformation of the Earth's crust due to the weight of overlying ocean tides. As the tides rise and fall, mass is added or lost in the water column and this mass redistribution cause loading of the ocean bottom. Conceptually, ocean loading is computed by integrating the ocean tides and applying a weighting function, G,

$$a(r) = \int_A \rho Z(r') G|r - r'| dA$$

where a is the loading displacement at the station located at r. The ocean tide at r' is given in its complex form, $Z = amplitude * \exp(i \text{ phase})$. r is the mean density of sea water and G is the Green's function for the distance $|r - r'|$. The integral is taken over all global water masses, A.

Although too simplistic for ICESat-2 requirements, a more practical formulation uses a grid [Petit and Luzum, 2010]. With the displacement component (radial, west and south) at time t denoted Δc,

$$\Delta c = \sum_j A_{cj} \cos(\chi_j(t) - \phi_{ck})$$

where the summation is carried out for a set of tidal constituents. The amplitudes, A_{cj}, and phases, ϕ_{cj} describe the loading response for a chosen site. $\chi_j(t)$ are astronomical arguments for eleven main tides consisting of: (a) four semi-diurnal waves (M_2, S_2, N_2 and K_2); (b) four diurnal waves (K_1, O_1, P_1 and Q_1); and three long-period waves (M_f, M_m and S_{sa}). Ancillary ocean loading phase and amplitude files corresponding to the GOT4.8 ocean tide model provide the basis for computing corrections for ocean loading to an accuracy sufficient for ICESat-2 (Richard Ray, personal communication). These files include ten major tidal constituents (q_1, o_1, p_1, s_1, k_1, n_2, m_2, m_4, s_2 and k_2) and sixteen minor tides ($2Q_1$, s_1, r_1, M_1, c_1, p_1, f_1, q_1, J_1, Oo_1, $2N_2$, m_2, n_2, l_2, L_2, T_2).

For more accurate modeling, an enhancement by Duncan Agnew considers 342 constituent tides whose amplitudes and phases are found by spline interpolation of the tidal admittances based on the 11 main tides. The Fortran routine, HARDISP.F, can be obtained through the IERS web site: ftp://tai.bipm.org/iers/conv2010/chapter7.

Of greatest accuracy, but well beyond the needs for geophysical corrections, is Duncan Agnew's SPOTL (Some Programs for Ocean Tidal Loading). This package produces research-level ocean loading values which may be of interest in specific ocean loading investigations, but the quality of the values are beyond the needs for altimetric geophysical corrections (Richard Ray, private communication).

6.3.4.1 Implementation

GOT4.8 loading tides will be computed by POD and transmitted to SIPS for inclusion as geophysical corrections. For each reference photon (about twenty meters spacing along-track) location (latitude, longitude) with its corresponding time, ocean load vertical displacements would be computed. This value would be subtracted for all group photon heights.

6.3.5 Solid Earth Pole Tide

The pole tide is a tidal response of both the solid earth (this section) and oceans (section 6.3.1) to the centrifugal potential caused by small perturbations of the Earth's rotational axis (polar motion). IERS2010 section 7.1.4 gives the formulation, in terms of potential, as

$$\Delta V(r, \theta, \phi) = - (\Omega^2 r^2 / 2) \sin 2\theta (m_1 \cos\lambda + m_2 \sin\lambda)$$

where m_1 and m_2 are related to the polar motion variables (x_p, y_p) by subtracting appropriate long term mean polar motion positions ($<x_p>$, $<y_p>$).

Displacement in the radial direction is given by IERS2010, using Love number values appropriate to the frequency of the pole tide (eq. 7.26 in IERS2010), as:

$$S_r = -33 \sin 2\theta (m_1 \cos\lambda + m_2 \sin\lambda)$$

where the coefficients m_1 and m_2, are given by

$$m_1 = x_p - <x_p> \; , \; m_2 = -(y_p - <y_p>)$$

with the conventional mean polar motion positions $<x_p>$, $<y_p>$ are given by a Fortran subroutine (names IERS_CMP_YYYY.f), distributed annually by the IERS (cf., ftp://tai.bipm.org/iers/convupdt/chapter7/) since 2015. The daily polar motion x_p, y_p are available from the finals.daily tables available from the USNO: http://www.usno.navy.mil/USNO/earth-orientation/eo-products/daily.

6.3.5.1 Implementation

Following IERS Conventions (2010) and with 2015 revisions, as described above, the radial component of the solid earth tide is computed based on co-latitude and longitude for the reference photon locations (about twenty meters along-track), time *t* and polar motion variables x_p and y_p. This value would be subtracted for all group photon heights.

6.3.6 Ocean Pole Tide

A formulation, similar to that given for solid earth pole tide, applies for the oceans, as well. The polar motion is dominated by the fourteen-month Chandler wobble and annual variations. At these long periods, the ocean pole tide is expected to have an equilibrium response, where the displaced ocean surface is in equilibrium with the forcing equipotential surface [*IERS2010*, sections 6.5 and 7.1.5].

A self-consistent equilibrium model of ocean pole tides developed by Desai (2002) has been adopted by the IERS. The radial component of the displacement is given by

$$u_r(\phi,\lambda) = K\{(m_1\gamma_2^R + m_2\gamma_2^I)u_r^R(\phi,\lambda) + (m_2\gamma_2^R - m_1\gamma_2^I)u_r^I(\phi,\lambda)\}$$

where:

$$K = (4\pi \, G \, a_E \, \rho_w \, H_p) / (3 \, g_e)$$

$$H_p = (8\pi / 15)^{1/2} (\Omega^2 a_E^4) / (GM)$$

and,

G = 6.67428 x 10^{-11} $m^3kg^{-1}s^{-2}$ is the constant of gravitation
GM = 3.98004418 x 10^{14} m^3s^{-2} is the geocentric gravitational constant
g_e = 9.7803253359 ms^{-2} is the mean equatorial gravity
a_E = 6378137 meters is the equatorial radius of the Earth
Ω = 7.292115 x 10^{-5} rad/s is the mean rotation rate of the Earth
ρ_w = 1025 kg/m^3 is the density of water
Based on the above values, the adopted value of K is 5340.43158233.
$\gamma = (1 + k_2 - h_2) = \gamma_2^R + i\gamma_2^I = 0.6870 + 0.0036i$ with values of k_2 and h_2 appropriate for the pole tide.

m_1 and m_2 are wobble parameters, as given in the previous section.

The real (superscript *R*) and imaginary (superscript *I*) pole tide coefficients, *u*, are found in a table available from

ftp://tai.bipm.org/iers/conv2010/chapter7/opoleloadcoefcmcor.txt.gz

This table forms a 0.5° x 0.5° grid of ocean pole load tide coefficients.

6.3.6.1 Implementation

Following IERS Conventions (2010), the ocean pole tide is computed by the above equation utilizing S. D. Desai's 0.5° x 0.5° grid of ocean pole load tide coefficients. The computation of the radial component of the ocean pole tide displacement occurs at reference photon locations (about twenty meters along-track) with the real and imaginary coefficients interpolated to the latitude and longitude of the reference photon location. This value would be subtracted for all group photon heights.

6.3.7 Geocenter Motion

Geocenter motion is broadly defined as the translational motion of the center of mass (CM) of the Earth system (solid earth, oceans, cryosphere and atmosphere) with respect to the center-of-figure (CF) of the solid earth surface, realized by the International Terrestrial Reference Frame (ITRF). Geocenter motion largely reflects global scale mass redistributions in the atmosphere and oceans, as well as continental water variations.

Geocenter motions possess definite seasonal components in all three directions: X (amplitude 2.7 mm), Y (amplitude 2.8 mm), and Z (amplitude 5.2 mm) [Cheng et al., 2013]. Secular terms along each axis have been estimated to be: -0.2 mm/yr (X), 0.3 mm/yr (Y), and -0.5 mm/yr (Z), with formal uncertainties at about those same levels.

Geocenter motions are accounted for during ICESat-2 precision orbit determination (POD). The orbit refers to CM, but the GPS and SLR tracking station locations refer to a crustal realization of CF.

Cheng et al., (2013) point out that the CF's dynamic tie to the CM is not yet a component of the conventional model of ITRF. Since the dynamic tie of the CF to the CM has not received formal, international agreement, nor has it been introduced into the ITRF by the IERS, this effect is not at a stage for empirical application as a geophysical correction.

6.3.7.1 Implementation

No geocenter motion correction is provided or included on the ATL03 data product.

6.3.8 Geoid

The geoid undulation is given on the data record as a reference parameter. This parameter permits photon heights, which typically refer to the reference ellipsoid, be translated so that they can refer to the geoid surface.

The EGM2008 geoid model given in a mean tide system (i.e., where the effects of the Earth's permanent tide are included) will be used to provide reference geoid undulations that refer to the WGS-84 reference ellipsoid [Pavlis et al., 2012]. A global grid of geoid undulations with one arc-minute resolution is used to interpolate the undulation at reference photon locations.

N. Pavlis (private communication) indicated that no further publicly available geoid development beyond EGM2008 is planned in the immediate future (2015). GOCE satellite results have demonstrated some problem regions (on the order of ±50 cm) in the EGM2008 model, particularly across parts of the Himalayas, Africa and South America. Global geoid modeling will likely improve after GOCE data have been thoroughly analyzed.

6.3.8.1 Implementation

Bi-linear geographic interpolation based on WGS-84 referenced, EGM2008 mean tide system, gridded geoid undulations will be made for reference photon locations (~20m along-track). We re-iterate that geiod values are provided for users who wish to change the reference surface of the ellipsoidal photon event heights reported on ATL03.

6.3.9 Atmospheric Delay Correction

Computation of path delay through the neutral atmosphere is a correction dependent on the state of the atmosphere, which itself is dependent on total pressure, partial pressure of water vapor, and air temperature all given as functions of three spatial coordinates and time. (Given that

nearly 25% of the range delay is in the stratosphere, we use the more general 'Neutral Atmosphere' instead of the more common'Troposphere' to describe the range delay corrections.) Output of numerical weather models does not provide the state of the atmosphere directly, but it can be deduced from that data. The GEOS-FPIT model provides output at 72 pressure layers that, among other parameters, has pressure thickness, specific humidity and air temperature at the middle of a layer. These are processed to yield the slanted path delay in processing steps that include gridding, expansion into B-spline basis functions, estimation of refractivity fields and computation of zenith delays. A comprehensive description of the theory is found in Chapter 3 and algorithm implementation is described in Chapter 5 of ATL03a ATBD for Atmospheric Delay Correction to Laser Altimetry Ranges.

7.0 ADDITIONAL PARAMETERS FOR HIGHER-LEVEL DATA PRODUCTS

7.1 Overview

This section introduces parameters that are not used by ATL03, but are required by one or more of the higher-level data products. Two of these groups are the ATLAS impulse response function and related parameters (section 7.2) and the background count parameter (section 7.3). Several of the higher-level data products (e.g. ATL07; ATL12) use a deconvolution approach to determine the precise ellipsoidal heights of the Earth's surface by deconvolving instrument effects from the distribution of signal photon events. While, in general, the time-dependent ATLAS instrument-response function is not known on orbit on a per-shot basis, section 7.2 presents an algorithm for estimating this function. In addition, several higher-level data products require an estimate of the solar background rate of photon events. The amount of photon data downlinked is not sufficient to generate a robust estimate of the background count rate. Instead, ATL03 provides histograms generated and used onboard by the flight software. Section 7.4 introduces parameters used to determine each received photon event uniquely, and allows traceability to specific detectors or timing channels within ATLAS.

7.2 ATLAS Impulse-Response Function

7.2.1 ATLAS Start Pulse Detector

The temporal distribution of signal photon events detected by ATLAS combines the temporal profile of the transmitted laser pulse shape with the effects of the ATLAS transmit optics, passage though the atmosphere, reflection off the surface of the Earth, passage through the atmosphere again, and finally passage through the ATLAS receive optics and electronics. In order to remove the effects induced by ATLAS on the temporal distribution of signal photon events, several higher-level data product algorithms use deconvolution to distinguish instrument and geophysical effects to determine the ellipsoidal height of the Earth's surface. The small-signal instrument temporal effects are collectively described as the ATLAS impulse-response function. (Effects of instrument dead time, chiefly on large signals, are treated separately.)

The ATLAS impulse-response function was characterized prior to launch during ground testing, and included measurements of the effects of the optics on the temporal distribution of the transmit and received laser pulse, and the temperature- and voltage-dependent impact of the photon-detection electronics. While it is not possible to characterize the ATLAS impulse-response function on-orbit for every transmitted laser pulse, this section presents an estimate of this function derived from on-orbit data. These data are grouped into two categories (and associated subgroups): pulse energy and impulse-response.

The transmitted pulse energy will primarily vary due to the variable laser transmitter output, at least over short (less than six month) timescales. We do not expect significant impact from

changes in the transmit optical path, though efficiency changes are possible over the life of the mission (e.g. due to cumulative contamination).

The ATLAS instrument has several methods of monitoring the output laser energy which are described in Section 5.2.1 and Section 5.2.2 of ATL02. ATL03 makes use of the transmit energy data provided by the laser internal energy. These data are described in ATL02 Section 5.2.2 and given by equation 5-4. ATL03 takes these values from the e_tx_pce{1,2,3}{s/w} parameters in the /atlas/housekeeping/laser_energy_spd group of ATL02. ATL03 uses the /orbit_info/sc_orient parameter to map the data from a particular strong or weak beam from a given pce card to the nomenclature of ATL03 (gt1l, gt1r, etc…). Since the values change slowly, ATL03 provides the mean, standard deviation, minimum and maximum values of the 1 Hz data from ATL02 on each ATL03 granule as /ancillary_data/engineering/transmit. The units are in joules, and described in the table below.

Parameter	Description	Units	Source / Input
parameters in /ancillary_data/atlas_engineering/transmit			
tx_pulse_energy	The mean, standard deviation, minimum and maximum values of the transmit energy for each beam as reported by the laser internal energy, averaged over a given ATL03 granule. A 6x4 array with values corresponding to gt1l, gt1r, gt2l, gt2r, gt3l, gt3r.	Joules	ATL02, Section 5.2.1, 5.2.2 /atlas/housekeeping/laser_energy_spd

Table 7-1. Transmitted Pulse Energy Parameters.

The temporal distribution of transmitted photons (sometimes referred to as the "pulse shape") for each beam for each shot is not known on orbit (though these data are available from pre-launch calibration products). However, there are two sources of information to estimate the on-orbit ATLAS impulse-response function: threshold crossing times from the start pulse detector (SPD) and photon events recorded from the transmitter echo pulse (TEP).

The ATLAS SPD provides the transmit energy measurement described above, as well as the time that the transmit pulse crosses two energy thresholds on both the leading edge of the pulse and on the trailing edge of the pulse; thereby providing four crossing times. In order to mitigate the effects of pulse-to-pulse variation in phase between the mode-beating peaks and the pulse envelope, these measurements are made after a low-pass filter in the SPD. These crossing times are used (along with other data) in ATL02 to generate a best-possible laser pulse transmit time. Photon event receive times are correlated with, and differenced from, the laser pulse transmit

time to calculate the photon time of flight that is a primary input to ATL03. The laser transmit time is the best estimate of the first moment (mean) of the transmit laser pulse.

The four crossing times are combined in ATL02 to make an estimate of the width of the transmit laser pulse. The differences between the lower threshold crossing times and upper threshold crossing times are provided in the ***tx_pulse_width_lower*** and ***tx_pulse_width_upper*** parameters, and have units of seconds. The associated thresholds (tx_pulse_thresh_lower and tx_pulse_thresh_upper) are also provided, in units of volts. In order to synchronize these data with the transmit pulse energy parameters, the differences described above are calculated on a per-shot basis, and then the differences are averaged over ~20 meters (~28 shots) to provide a single value for each ICESat-2 geolocation segment. The reported time of these parameters, are the same as that of the pulse energy parameters (***tx_pulse_energy_time***), and the reported time relates to the beginning of the averaging period. The averaged values are in the /gtx/geolocation/start_pulse_det group. In the event that the threshold settings change during a granule, these parameters will have two values. Due to differences in how the threshold crossing times and the along-track time of the ~20 meter segments are recorded, the averages described here may include data from 27, 28, or 29 consecutive laser shots from ATL02.

The four crossing times are also combined in ATL02 to estimate the third moment (skew) of the transmit laser pulse, also at the ~20 meter rate. The parameter ***tx_pulse_skew_est*** is the mean of the lower threshold crossing times minus the mean of the upper threshold crossing times. In this way, a positive value of tx_pulse_skew_est corresponds to a positive skew in the transmit pulse, and conversely for negative values of tx_pulse_skew_est. Note that this parameter is not the same as the pulse skew; it is an indication of pulse skew and variations of the actual pulse skew. This parameter is aligned with ***tx_pulse_width_lower*** and ***tx_pulse_width_upper***, uses the same threshold crossings, and can be found in the /gtx/geolocation/start_pulse_det group.

The parameters related to the transmit pulse provided at the geolocation segment (~20 meter) basis therefore are:

Parameter	Description	Units	Source / Input
tx_pulse_width_lower	difference between the lower threshold crossing times	seconds	ATL02, Section 3.5
tx_pulse_width_upper	difference between the upper threshold crossing times	seconds	ATL02, Section 3.5
tx_pulse_thresh_lower	lower threshold setting of the SPD	volts	ATL02, Section 3.5
tx_pulse_thresh_upper	upper threshold setting of the SPD	volts	ATL02, Section 3.5
tx_optic_eff	transmit optical efficiency	unitless	<insert ATL02 here>

Parameter	Description	Units	Source / Input
tx_pulse_distribution	fraction of transmit pulse energy per beam	unitless	ATL02, Section 3.5
tx_pulse_skew_est	difference between the means of the lower and upper threshold crossing times	seconds	ATL02, Section 3.5

Table 7-2. Transmit Pulse Parameters.

7.2.2 ATLAS Tranmitter Echo Path

An estimate of the ATLAS impulse-response function is derived from the transmitter echo path (TEP) photon events. The TEP is an optical path that provides a means to calibrate ATLAS time of flight internally, and is described in detail in ATL02. Briefly, light following the optical path of the TEP begins at the laser, travels to the laser sampling assembly where part of the transmitted laser pulse is sampled, and then via a fiber optic cable to the optical filter assembly to the detector array assembly. In this way, photons detected via the TEP traverse part of the transmit optical path, part of the receive optical path, and all of the receiver electronics that all other signal photons traverse. The TEP exists for two of the three strong beams (beam 1 and 3; as noted elsewhere, depending on the spacecraft orientation these will be the strong beam of the central pair of beams, and the strong beam of either the right or left pair).

In ATL02, section 4.0 describes how possible TEP photon events are identified, and put into a separate group within the ATL02 data product (/ATLAS/PCE{1,2}/TEP), and include the photon arrival time referenced to the correct laser transmit pulse time, among other parameters. Here, we first establish criteria for a set of TEP data, and then distinguish possible TEP photon events from the possible signal photon events determined in ATL02 section 4.0, and then develop an estimate of the ATLAS impulse response function for each of the two beams with TEP photon events.

The TEP photon events will be downlinked either when commanded to or when the TEP photon events happen to occur within the telemetry band. Pre-launch analysis indicates that the TEP will fall within the telemetry band approximately twice per orbit, for about three hundred seconds in each instance. Additional instances of TEP photon events can be captured and telemetered by manipulating parameters in the flight software.

Pre-launch data analysis shows that the number of TEP photons per shot for a particular beam varies; owing to changes in laser transmit energy, and the temperature-sensitive reflectivities of the fiber optics involved. However, the ratio of the number of TEP photons between beams 1 and 3 appears stable with a value of 0.7, with beam 1 being the stronger of the two. Averaging across a range of instrument configurations, beam 1 generates approximately 0.09 TEP photons per shot, and beam 3 generates approximately 0.07 TEP photons per shot.

Using one TEP photon event per twenty shots as the lower limit for the TEP strength, downlinking TEP photons for approximately three hundred seconds (i.e. the approximate duration TEP photons will fortuitiously appear in the telemetry band) should yield about 150,000 TEP photons. Therefore, we proceed with the following steps any time there are more than thirty seconds of contiguous possible TEP photon events identified in ATL02, which should yield at least 15,000 TEP photons. As a secondary check, there must be at least 2000 possible TEP photons in the set. All available TEP photons within a given set are used; there is no upper limit on the duration or number of TEP photons. The set is ended when the TEP photons are no longer present in the telemetry band, or five seconds have passed with no additional TEP photons.

With a sufficient number of possible TEP photon events identified, possible TEP photon events should be either background photon events, misclassified signal photon events, or TEP photon events. The time of day of the start of the TEP data used in subsequent analyses is reported on ATL03 as ***tep_tod***, while the duration of TEP data is reported as ***tep_duration***.

Using this reduced set of possible TEP photon events, we form a histogram using 50 picoseconds bin widths. Although the nominal mean finest time resolution of the ATLAS system is ~190 picoseconds, since the laser start time is the average of the four threshold crossings, we use a finer time resolution in this histogram.

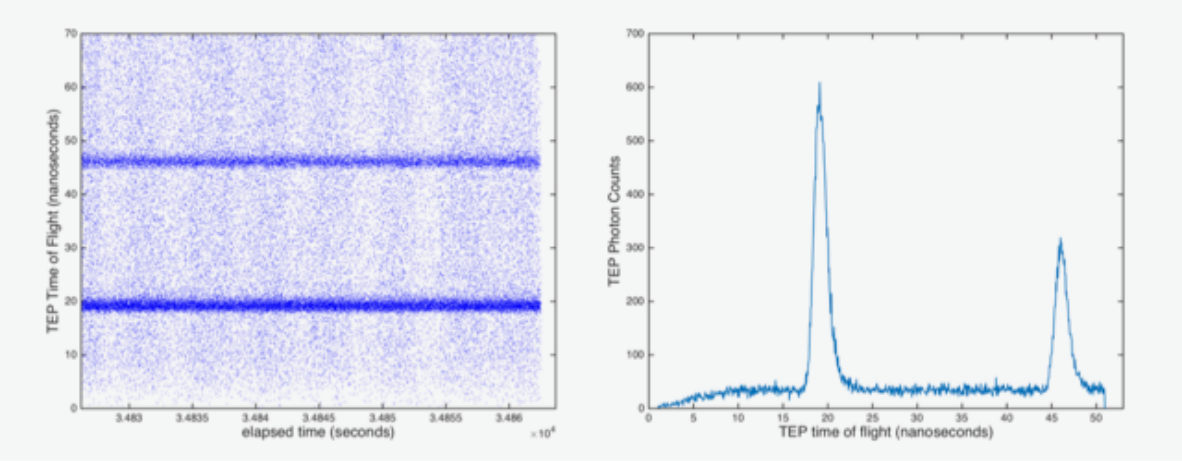

Figure 7-1. Example TEP photon cloud and TEP histogram.

Figure 7-1 shows the TEP photon cloud on the left and the histogram of that data on the right based on the test data from ATLAS. It is apparent that there is more than a single mean arrival time of TEP photons; with two primary bands being apparent (at ~ 20 nanoseconds and 46 nanoseconds). We refer to these two arrivals as the primary TEP arrivals (at ~ 20 nsec) and the secondary TEP arrivals (at ~ 46 nsec). The secondary arrival is generated by a refletion off the other end of the optical fiber. Additional noise photons are also present.

The next step is to determine the background photon event rate and subtract this number from all bins in the histogram. The TEP window width is about fifty nanoseconds (defined in ATL02 as a possibly non-symmetric region about the TEP photon events; see section 4, Equation 41 in ATL02), which result in approximately one thousand bins in the TEP histogram. We expect the

transmit pulse leaving the laser to have a width of ~1.5 ns full-width at half max, or approximately thirty bins of this histogram. In order to remove the full primary and secondary pulses from the background calculation, the mean background is determined by excluding the bins between 17 and 24 ns (the region of the primary return) and the region between 43 and 50 ns (the region of the secondary return), and calculating the mean of the remaining bins. This value is reported on the output product as ***tep_bckgrd***. Subtract tep_bckgrd from all bin counts.

After removing the background, calculate the number of counts in the remaining histogram. Report this value as ***tep_hist_sum***.

Divide the number of counts in each bin by tep_hist_sum in order to normalize the histogram to have unit area. Report the normalized values for each bin as ***tep_hist*** and the time of the bin centers (the mean of the times of the leading and trailing edges of the bins) as ***tep_hist_time***. This normalized histogram is the best on-orbit estimate of the ATLAS impulse-response function. Note that this histogram includes both the primary and secondary arrivals. It is recommended to focus on the shape of the primary TEP arrivals in subsequent downstream processing when the ATLAS impulse-response function is required.

Note that this approach will characterize only part of the overall ATLAS impulse-response function. Based on pre-launch data collected during integration and testing, we expect the pulse spreading in the portion of the optical path not sampled to be small compared with the pulse spreading in the part of the system sampled by the TEP.

The parameters derived from TEP data are part of the ATL03 data product in the groups /atlas_impulse_response/pce1_spot1/ and /atlas_impulse_response/pce2_spot3/ and are listed in the table below.

For flexibility, the TEP parameters are calculated and stored in an ancillary data product (ANC41) prior to writing them to the ATL03 data granules. Given the latency involved in generating ATL03, a full day's worth of realizations of the TEP are drawn from ATL02 and are collected into the daily ANC41 data product. ANC41 is generated any time ATL02 is generated, even if ATLAS is not in nominal science mode. Each realization of the TEP (per the rules above) and TEP-based parameters are stored in ANC41.

Each ATL03 granule contains the realization of the TEP-based parameters drawn from ANC41 that is nearest in time. It is possible that after launch, we may be better able to determine the best realization of the TEP histogram for a particular ATL03 granule, but pre-launch data do not suggest that the ATLAS impulse response will vary measurably around an orbit. The parameter ***tep_tod*** indicates when the TEP data on a given ATL03 granule was generated.

Parameter	Description	Units	Source / Input
parameters in /atlas_impulse_response/pce1_spot1/tep_histogram or /atlas_impulse_response/pce2_spot3/tep_histogram			
tep_hist_sum	the number of counts in the TEP histogram, after removing the background	counts	ATL02, Section 4.2
tep_tod	the time of day (absolute time) of the start of the data in the TEP histogram relative to the start of the granule	seconds	ATL03
tep_duration	the duration (or width) of data in the TEP histogram	seconds	ATL03
tep_bckgrd	the average number of counts in the TEP histogram bins, after excluding bins that likely contain the transmit pulse	counts	ATL03
tep_hist	the normalized number of counts in the TEP histogram	counts	ATL03
tep_hist_time	the time associated with the TEP histogram bin centers	seconds	ATL03

Table 7-3. Parameters associated with transmit echo pulse photons.

In addition, two other TEP-related parameters are included in the /ancillary_data/tep group to assist TEP data users. The first is tep_valid_spot, a 6x1 array indicating which TEP to use for each spot that does not have a TEP associated with it (e.g. which TEP to use to characterize spots 2, 4, 5, and 6). The second is tep_range_prim, a 2x1 array indicating the range of time of flight of TEP photon events to include in generating a histogram or other analaysis of the primary TEP return. The nominal values of the primary TEP return is 10 nanoseconds to 33 nanoseconds.

At this point, we have described the averaged pulse shape characteristics from the threshold crossing times posted at the nominal ~20 meters along-track segment rate. We also have described the TEP photon events and have formed a histogram and related parameters based on TEP events. Since the times of these respective groups are known, it is possible to examine how the SPD-based statistics vary during the period spanned by the TEP data. However, combining these two groups quantitatively is complicated by two aspects. First, the SPD-based data and the TEP-based data have unique paths through the instrument and so the reported times of these data will be substantially different. While these differences are characterized with pre-launch data, we have little insight into how the temporal bias between these data will evolve through time. Secondly, the SPD-based data is derived from the reported times when a filtered version of the transmitted laser pulse crosses a particular amplitude threshold (measured in volts). The TEP-based data on the other hand is a histogram of counts of a massively attenuated version of the

transmitted laser pulse. As such a quantitative correspondence between voltages and counts is problematic. A relationship could possibly be made between the standard deviation of the threshold crossing times and the apparent width of the TEP-based histogram at several points along the profile. This may allow a user to better predict how the transmitted pulse is changing between realizations of the TEP.

7.3 Background Count Parameters

As described in section 1.1, ATLAS uses a multi-step process to reduce the number of photon events that are time tagged on board, and a reduced number of photon time tags are telemetered to the ground. Since the telemetry band is relatively narrow (~30 meters to ~1000 meters), it does not typically include enough background photons for a robust determination of the background photon rate. As several of the higher-level data products require the background photon rate, ATL03 includes background parameters derived from the altimetric histograms (formed on board at 50 Hz, or every 200 shots; i.e. the major frame rate) described in section 5.3. At a finer scale, the onboard software generates and downlinks the sum of the counts in the altimetric histogram every fifty laser transmit pulses (200 Hz) for each beam. This section also includes parameters related to the telemetry bands of photons, which can be used to derive estimates of the background photon rates.

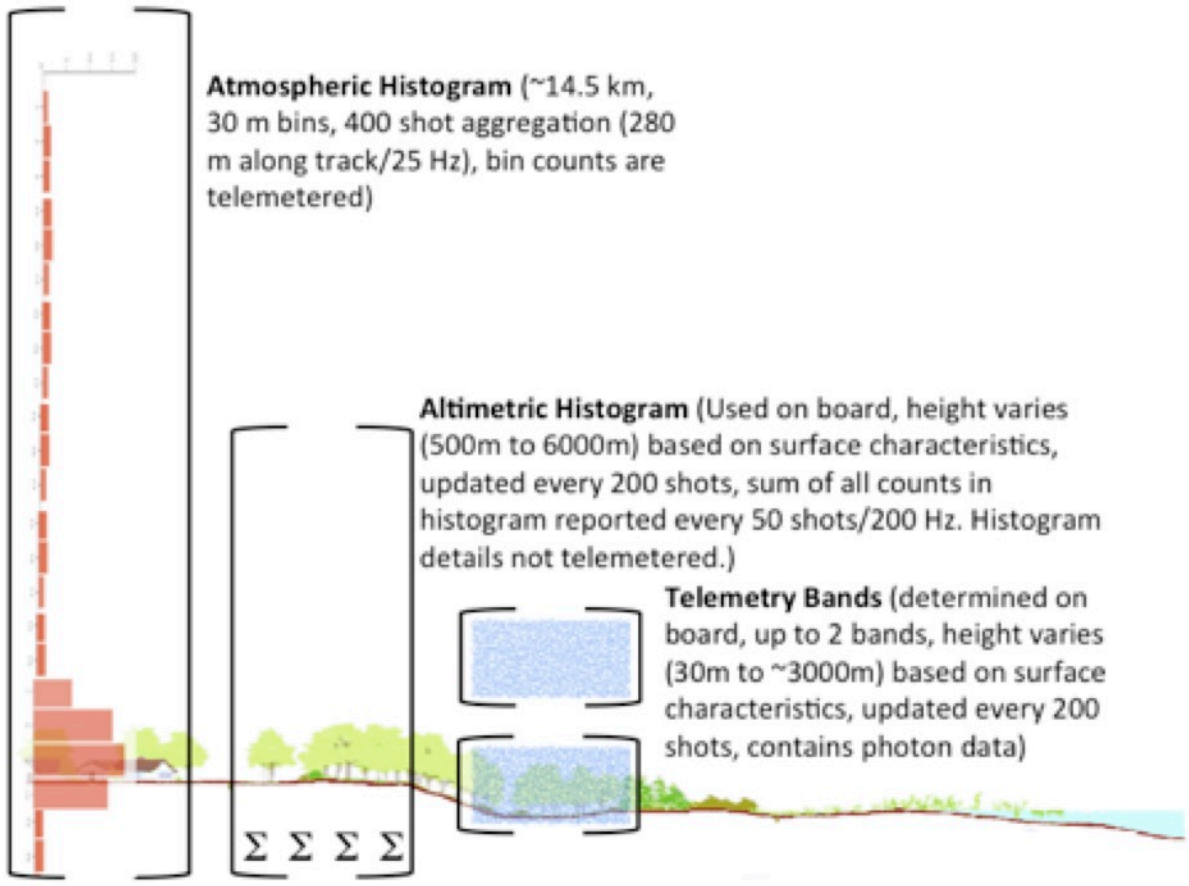

Figure 7-2. Histograms and telemetry bands used for background calculations.

7.3.1 Altimetric Histogram parameters

The altimetric histogram is formed on orbit and is used by the flight software to search for the surface echos of interest; the flight software then selects a subset of the altimetric histogram to telemeter detailed photon information to the ground. This process is described in detail in the *ATLAS Science Receiver Alogirthms Description* document. Ideally, the altimetric histogram includes the Earth's surface and extends some distance above and below it. This histogram is formed using photon event counts over a period of time (rather than range or height). The duration of the altimetric histogram varies with location around the Earth and is determined by the surface type and the precision with which the ellipsoidal height of the Earth's surface is known. Since each beam is processed separately by the onboard processing software, the altimetric histogram details can be different for each of the six beams. The histogram is formed

and used on ATLAS, while the sum of the number of counts in this histogram is telemetered to the ground every 50 shots, or at 200 Hz.

Note that ATLAS makes no accommodation on board for signal photons from either the surface of the Earth or clouds, so the sum of the altimetric histogram provided by ATLAS (***bckgrd_counts***) at 200 Hz includes background photons as well as any signal photons.

The 50-shot sum is used to derive an esimtate of the background count rate. First, subtract the number of likely signal photons (from section 5.4.2) found in this 50-shot interval. For a given 50-shot interval, the number of signal photons (n_signal_photons) is determined by summing the number of photons with signal_conf_ph == 2, 3 or 4, using the maximum value for any surface type in the interval.

Given that photons from the Transmitter Echo pulse (described in Section 7.2.2) may appear in the altimetric histogram and generate an erroneously large background rate, ATL03 determines if TEP photons are in the atlimetric histogram. TEP photons follow the laser transmit time by < 70 nanoseconds (see ATL02, Section 4), and are separated in time by the laser repetition rate (100 microseconds). The atlimeteric histogram start time is given by the ATL02 parameter /atlas/pcex/altimetry/alt_rw_start which is a time in seconds, from a given laser fire in a major frame. The duration of the altimetric histogram is the ATL02 parameter /atlas/pcex/altimetry/alt_rw_width also given in seconds, and takes values between 3 and 40 microseconds. There are several methods possible to determine if a laser transmit (and it's associated TEP photons) occur within the altimetric histogram duration. One way is to compare the modulo of the altimetric histogram start time with the laser fire interval (100 microseconds) with the altimetric histogram duration. If the modulo is less than the altimetric histogram duration, the TEP is likely in the atlimetric histogram.

Pre-launch analysis demonstrates that the TEP strength varies through time and as a function of which laser (primary or redundant) is active. Therefore, the correction to the 50-shot sum is time-dependent. Using ANC41, we determine the mean number of photons per shot in the primary TEP signal (between 17 and 24 nanoseconds; see section 7.2) and the secondary TEP signal (between 43 and 50 nanoseconds; see section 7.2) using an entire day of TEP realizations. We then scale these mean values to determine the average number of TEP photons in 50 shots for the strong beams with the TEP. The resulting values (around 8 photons for beam 1 and around 5 photons for beam 3) are subtracted from the 50-shot sum of the altimetric histogram. If subtraction would yield a negative number for the 50-shot sum, the 50-shot sum is set to zero photons.

These values are updated daily when a new ANC41 is available and are used in processing a full day of ATL03. We expect the TEP strength to change slowly through time and we will update this algorithm on-orbit if needs be. For computational efficiency, these values are generated as part of the ANC41 processing and are available in the tep_histogram group of ANC41.

With these two accomodations in mind (signal photon events and TEP photon events), the number of background photons is then given by:

bckgrd_counts_reduced *= bckgrd_counts – n_signal_photons – n_tep_photons.*

Lastly, ATL03 converts the duration of the altimetric histogram reported by ATLAS to a distance, or height, in meters:

bckgrd_int_height = /atlas/pcex/altimetry/s_w/alt_rw_width * c/2

where the alt_rw_width is the altimetric range window width from ATL02 in units of seconds. The integration height of the 50-shot sum must also be reduced by the height spanned by the signal photons. Determine the height span of the signal photons by calculating the difference in the maximum and minimum ellipsoidal heights of the signal photons with signal_conf_ph == 2, 3 or 4. This should produce a height in meters that spans the ellipsoidal heights of all signal photons in this interval. The reduced integration height is then:

bckgrd_int_height_reduced *= bckgrd_int_height – signal photon height range.*

The background photon rate is then given by

bckgrd_rate *= bckgrd_counts_reduced / (50 * bckgrd_int_height_reduced / (c/2))*

where *c* is the speed of light. We acknowledge that every fourth value could be in error by up to one part in fifty due to the potential irregular number of shots in the reported 50-shot sums.

In order to facilitate comparison between the 50-shot sum of the altimetric histogram, and the much larger atmospheric histogram (reported for strong beams every 400 shots, typically spanning 14 kilometers), we also report the height above the WGS-84 ellipsoid of the top of the altimetric histogram, as described in section 3.3. To be consistent with the photon ellipsoidal heights, this parameter (***bckgrd_hist_top***) will have the same geophysical corrections applied, per section 6.0. This allows data from the 50-shot sum to be compared with an equivalent span of data from the atmospheric histogram.

In order to maintain a consistent posting interval in a single group on the ATL03 data product, we post the two parameters naturally at 50 Hz (bckgrd_int_height and bckgrd_hist_top) at 200 Hz by repeating each value four times. This allows a single group to be formed and to allow easy combination of parameters that would otherwise have different rates.

In order to align the 50-shot sum with any other parameter, ATL03 provides the time at the start of the 50-shot integration period (***delta_time***) relative to the ATLAS Epoch Offset parameter (/ancillary_data/atlas_sdp_gps_epoch). This time is derived from every fiftieth laser transmit time, and should generate times very close (though probably not identical in all cases) to the 200-shot major frame boundaries. Due to offsets within the flight hardware, every fourth 50-shot histogram time could be +/- one laser transmit time (100 microseconds) from a major frame boundary.

All of these parameters are in the group /gtx/bckgrd_atlas/.

Parameter	Description	Units	Source / Input
bckgrd_counts	Onboard 50-shot background (200 Hz) count of photon events within the altimeter range window	counts	ATL02
bckgrd_counts_reduced	Number of photon counts in the 50-shot sum after subtracting the number of signal photon events, defined as in section 5, and potential TEP photons in that span	counts	ATL03, section 7.3.1
bckgrd_int_height	The height of the altimetric range window; this is the height over which the 50-shot sum is generated; while this value is generally available at 50-Hz, we repeat values as needed to form a 200-Hz array	meters	ATL02
bckgrd_int_height_reduced	The height of the altimetric range window after subtracting the height span of the signal photon events in the 50-shot span	meters	ATL03, section 7.3.1
bckgrd_hist_top	The height of the top of the altimetric histogram, in meters above the WGS-84 ellipsoid; while this value is generally available at 50-Hz, values are repeated as needed to form a 200-Hz array	meters	ATL02
delta_time	The time at the start of the ATLAS 50-shot sum, relative to the ATLAS_sdp_GPS-epoch reference time, measured from the start of the granule; this is based on every fiftieth laser fire time, which leads to a very close alignment with major frame boundaries (+/- 1 shot)	seconds	ATL02 laser fire times
bckgrd_rate	The background count rate from the 50-shot altimetric histogram after removing the number of likely signal photons based on section 5	counts/ sec	ATL03, section 7.3.1

Table 7-4. Altimetric Histogram Parameters.

7.3.2 Other Background Parameters

As described in section 5.4.3, the primary source of the background count estimate for the strong beams in the signal-finding algorithm is the 400-shot atmospheric histograms. For the weak beams (and for the the strong beams when the atmospheric histograms are not available), the background count rate needed in section 5.4.1.1 is nominally derived from the telemetered photon data (i.e. the photon cloud). In order to make pseudo-atmospheric histograms from the photon cloud, two pieces of information are needed:

- the ellipsoidal height of the top of the telemetry band, and
- the width of the telemetry band in meters.

The ellipsoidal height of the top of the telemetry bands with respect to WGS-84 is determined during the geolocation process, as described in section 3.3. Effectively, this treats the telemetry band top as though it were a photon event, and calculating the range and position for that imaginary photon event along with all of the other telemetered photon events. In order to make the height of the top of the telemetry bands consistent with the photon event heights, the geophysical corrections of section 6.0 are also applied to the ellipsoidal height of the top of the telemetry window. The telemetry band width in meters is determined by multiplying the telemetry band width (ATL02, /atlas/pcex/altimetry/s_w/bandx_width) in seconds by the speed of light.

These two parameters are therefore ***tlm_top_bandx*** (meters above the WGS-84 ellipsoid including the corrections of section 6.0), ***tlm_height_bandx*** (in meters). The suffix ***x*** refers to the band number (1, 2, … corresponding to the ATL02 parameter N_bands), with 1 corresponding to the first downlink band and the subsequent values corresponding to sequential downlink bands.

While these parameters are provided at 50-Hz (the major frame rate), in order to avoid forming a group at the major frame rate,values in these two parameters are duplicated and stored in the group /gtx/bckgrd_atlas/ at 200 Hz.

7.4 The Photon Identification Parameter

In order to uniquely determine the heritage of any received photon event within the ATLAS instrument, ATL03 includes parameters that can be combined to form a unique photon ID. All of these parameters are provided at the photon rate, and are therefore in the /gtx/heights/ group along with other parameters at the photon rate.

The parameter ***pce_mframe_cnt*** indicates which major frame a particular photon was recorded in. As described in the *ATLAS Science Receiver Algorithms* document, a major frame is an aggregration of two hundred consecutive shots, and is used by the onboard software to determine the downlinked telemetry band. The major frame counter is read from the digital flow controller on each photon counting electronics (PCE) card, and is unique to each PCE. Within a PCE, the major frame counter is identical for both weak and strong spots. This counter is incremented sequentially with each major frame boundary, and will roll over in approximately 2.7 years (or about 4.3 billion major frames) at a nominal laser pulse repetion frequency of ten thousand shots per second.

In order to make sense of the major frame counter, one must also know which PCE that counter is associated with. The parameter ***ph_id_channel*** provides this information, as well as additional insight into the heritage of a particular photon event. Each PCE has twenty different timing channels used to time received photon events. The channel number assigned for any received photon event is designated as ph_id_channel in the ATL02 product. In addition, it is desirable to know if a photon event was triggered by a rising or falling edge signal from the detector electronics, as the times associated with rising and falling edge signals are not necessarily identical (a subtletly used in ATL02 processing to produce the photon time of flight). Lastly,

onboard ICESat-2, there are two banks of detectors (labeled A and B). Combining all this information, we have three PCEs with twenty channels each, a corresponding rising or falling edge signal from either dector bank A or B, or 3x20x2x2 = 240 possible paths for received photon events in ATLAS. We assign a unique ***ph_id_channel*** number (between 1 and 240) according to the table below.

Detector A			Detector B		
Action	PCE Number	Channels	Action	PCE Number	Channels
rising	1	1 – 20	rising	1	121 – 140
rising	2	21 – 40	rising	2	141 - 160
rising	3	41 – 60	rising	3	161 – 180
falling	1	61 – 80	falling	1	181 – 200
falling	2	81 – 100	falling	2	201 – 220
falling	3	101 - 120	falling	3	221 - 240

Table 7-5. Table to relate ph_id_channel to a photon's path through ATLAS.

The last two parameters are ***ph_id_pulse*** and ***ph_id_count***. The first of these records the laser pulse counter within a major frame, and nominally spans 1-200 (although at times there may be 199 or 201 laser pulses, a detail described in more detail in the ATL02 ATBD). Since each major frame is unique to a given PCE, the laser pulse count may also be unique to each PCE (since major frames boundaries among the PCEs will rarely, if ever, perfectly co-align). The ***ph_id_count*** parameter records the number of photons associated with an individual laser pulse, and is reset each time the laser pulse counter is incremented. It is important to note that the ***ph_id_count*** parameter is a per-channel photon event counter, not a per-spot photon event counter. For a given channel of a given spot, this counter will record the number of photon events in that channel for the current value of the laser pulse counter. It is necessary to consider the corresponding value of ***ph_id_channel*** to determine which channel, which spot and which PCE a particular value of ***ph_id_count*** is associated with.

Combining the information in these four parameters allows a user to determine the provenance of any particular received photon event with respect to a specific ATLAS timing channel, major frame, laser shot, or detector, from ATL03 back to ATL01 if necessary. With the exception of the pce_mframe_cnt roll-over every 2.7 years, this framework establishes a unique identification for every photon in the ICESat-2 data products.

7.5 The Spacecraft Orientation Parameter

The ICESat-2 observatory can be oriented in one of two positions with respect to the direction of travel. ATL03 includes the ***sc_orient*** parameter in the group /orbit_info/ to record the observatory information. The orientation is tracked on-orbit by the Instrument Support Facility (ISF) and is passed to ATL03 via the ANC13 ancillary file. As noted above, the mapping between the strong and weak beams of ATLAS and their relative position on the ground depend on the observatory orientation (Figure 12-1 and Figure 12-2).

The forward orientation (sc_orient == 1) corresponds to ATLAS traveling along the +x coordinate in the ATLAS instrument reference frame (see ATL02). In this orientation, the weak beams lead the strong beams and a weak beam is on the left edge of the beam pattern (Figure 12-1). The table below indicates the mapping between ATLAS spots, beam strength, PCE card number, and the ground track designation used on the ATL03 data product when ATLAS is oriented in the forward orientation.

PCE	Beam strength	ATLAS spot number	ATL03 ground track designation
1	strong	1	gt3R
1	weak	2	gt3L
2	strong	3	gt2R
2	weak	4	gt2L
3	strong	5	gt1R
3	weak	6	gt1L

Table 7-6. Beam mapping when sc_orient == 1 (forward).

The backward orientation (sc_orient == 0) corresponds to ATLAS traveling along the -x coordinate in the ATLAS instrument reference frame (see ATL02). In this orientation, the strong beams lead the weak beams and a strong beam is on the left edge of the beam pattern (Figure 12-2). The table below indicates the mapping between ATLAS spots, beam strength, PCE card number, and the ground track designation used on the ATL03 data product when ATLAS is oriented in the backward orientation.

PCE	Beam strength	ATLAS spot number	ATL03 ground track designation
1	strong	1	gt1L
1	weak	2	gt1R
2	strong	3	gt2L
2	weak	4	gt2R
3	strong	5	gt3L
3	weak	6	gt3R

Table 7-7. Beam mapping when sc_orient == 0 (backward).

Lastly, when a granule contains a transition between forwards and backwards orientation, the parameter sc_orient == 2. Transitions between orientations are driven by the slowly changing beta angle between the sun and the observatory solar arrays. We expect the observatory orientation to change approximately twice a year, and take on the order of minutes. Data collected during a transition (sc_orient == 2) will not be processed beyond ATL03 since these granules contain a non-uniform mapping between ATLAS beams and the relative positions on the earth.

7.6 ATLAS Calibration Products

ATL03 includes ATLAS calibration data tables needed by higher level products. These tables are included in the group /ancillary_data/calibration in individual subgroups for each of the individual calibration products. These products were produced by the ATLAS pre-launch calibration team, and passed to ATL03 via ATL02. Each of these calibration products includedon ATL03 are described below.

7.6.1 first_photon_bias: CAL-19, First Photon Bias

The first photon bias correction consists of a table of time of flight correction values (in picoseconds) versus the apparent return strength and width for several dead-time values. This correction is added to the raw time of flight to get corrected time of flight values. Each model-generated table applies to a specific dead time. The correction is a function of the apparent return width, the dead time, and the apparent return strength (events per shot). This calibration be applied at the point of computing a surface height (for instance, an upper-level data product

such as ATL06 or ATL07). It is an additive correction to account for the effects of dead time. The uncorrected centroid is biased early in the transmit pulse, since ATLAS is more likely to detect photons on the leading edge of the return. This correction accounts for that bias.

7.6.2 low_link_impulse_response: CAL-20, System Impulse Response

On ATL03, there are two sources of system impulse response information: the transmitter echo path (TEP) photon events, which are provided as histograms and photon clouds for two of the three strong spots (spots 1 and 3), and CAL-20, which is a modeled representation of the system impulse response function developed pre-launch that can be used for spots that do not contain the TEP. The CAL-20 system impulse response data collected from the TEP (2 spots) and main alignment and altimetry target (MAAT; 6 spots) are compared to get a best estimate of per-shot impulse responses to use on-orbit.

CAL-20 provides histograms of normalized system impulse responses separated by channel and is provided as centroid-aligned histograms. As this was developed pre-launch, it is available for a number of ATLAS system states (temperature, receiver channel, PCE, laser energy mode, detector bank, return source (TEP or MAAT), and laser). As a result of using a variety of ATLAS system states, the selections span the expected range of variation of the system impulse response. Each impulse response represents roughly ten million shots, or 15 minutes of data. Small differences in histogram amplitude and shape can help determine which TEP impulse responses (spots 1 and 3) to use on-orbit for the other spots (spots 2, 4, 5, 6).

7.6.3 nominal_rx_sensitivity: CAL-30, Nominal Receiver Sensitivity (REMOVED IN FUTURE VERSIONS)

This calibration describes the overall sensitivity of each ATLAS detector to optical power expressed as a slope-and-intercept for each spot correlating the power intensity received by the ATLAS telescope to the corresponding spot return event rate (received counts/second). It is a function of which detector bank was used (A or B), as well as which spot was measured (1 through 6).

This is applied in ATL02, and there is no need for other products to apply this. This calibration is provided on ATL03 for informational purposes.

7.6.4 rx_sensitivity_vs_temperature: CAL-33, Receiver Sensitivity versus Temperature

7.6.5 dead_time_radiometric_signal_loss: CAL-34, Dead Time Radiometric Signal Loss

This calibration includes a table of dimensionless radiometric correction values versus the apparent return strength and width of the return pulse for several dead-time values. The correction is to be multiplied by the raw return strength to get the corrected return strength. Each model-generated table applies to a specific dead time. The values are a function of the apparent return width, the dead time, and the apparent return strength (events per shot).

This is a multiplicative correction to the total number of returned photon events per shot. It has the same table format and use as CAL-19. The likely users of this are ATL04 or ATL07. This calibration can be applied at the channel level or the spot level (i.e., an aggregation of channels).

7.6.6 dead_time: CAL-42, ATLAS Detector Deadtime

The ATLAS detection electronics are based on a set of multi-pixel photo-multiplier tubes (PMTs). These PMTs detect photons and convert them into electrical signals that are then timed, stored and telemetered to determine elevation in ground processing. Upon detection of a photon, there is a non-zero time period (the dead time) within which the PMT is effectively blind to additional incoming photons. The ATLAS detector design is that of a non-paralyzable detector, such that after the dead time has passed, ATLAS can detect and record additional photon arrivals.

The Cal-42 instrument calibration provides a consistent estimation of dead time for each ATLAS receiver channel accompanied by a standard deviation. This is reported as a table of estimated dead times (one per channel). Although the photon ID allows us to discriminate between photons detected on a rising clock edge from those on a falling clock edge, the differences in electronics that cause a timing difference between the edge are downstream of the PMTs and associate deadtimes. In addition, the interarrival time is inherently a difference between two consecutive photon events, and thus combines photons from rising and falling edges. The precision on the resulting dead time is 30 picoseconds.

These dead times are based on pre-launch ATLAS test data. In short, the calibration is based on photon inter-arrival times for each channel (see section 7.4 for discussion of channels). The interarrival times are histogrammed, with the bin widths and bounds of these histograms are specified as algorithm parameters. While qualitatively, the dead time could be thought of as sharp edge in photon interarrival time (with no photons exhibiting interarrival times less than the dead time), in fact there is a range of deadtimes, and the nmber of interarrival events decays to

zero as a function of apparent dead time. The mean of the bin counts of the histogram from the end of the dead time window (nominally between 2 and 3.5 nanoseconds) to the upper limit of the histogram is computed, and this value is taken as the peak value of the deadtime. By using this peak value, the range of the dead time effect is computed by including bin counts between 10% and 90% of the peak; these values are limited to be within the bounds of the dead time window. The center of the dead time effect is computed using the range determined in the previous step.

The output on ATL03 for cal_42 are the mean dead times, as defined above, and the standard deviations for each channel, for detector side that was active at the start of a given granule. Changes in detector side generate a break in ATL03 data, so we do not expect the detector side to change during a granule.

7.6.7 rx_sensitivity_to_misalignment_img/rad: CAL-47, Receiver Sensitivity as a Function of Transmit-to-IFOV Misalignments (REMOVED IN FUTURE VERSIONS)

Receiver sensitivity to surface reflectance is an important metric to This calibration is expressed in two parts: (a) radiometric loss as a function of the misalignment in azimuth and elevation angles (image version), and (b) radiometric loss as a function of the misalignment radius (radial version). The image version is expressed as a regular 2-D array of relative intensities (relative to the peak) over the alignment monitoring and control system (AMCS) azimuth and elevation misalignments, while the radial version is the relative intensity as a function of radius in the form of function points that the user can interpolate.

This is applied in ATL02, and need not be applied by higher level products. This calibration captures the sensitivity (events per joule of returned energy entering the telescope) of a misaligned transmitter and receiver in comparison with a properly aligned transmitter and receiver (e.g., the laser spot is not completely within the receiver field of view). This is a component of the overall receiver sensitivity (along with CAL-30 and CAL-61). See ATL02, Section 5.3 for a more complete description of this calibration product.

7.6.8 abs_energy_monitor: CAL-54, Absolute Energy Monitor Product

7.6.9 rx_sensitivity_vs_wtom: CAL-61, Receiver Sensitivity versus the Wavelength-tracking Optical Module (REMOVED IN FUTURE VERSIONS)

This calibration is the relative sensitivity of the receiver in which the laser wavelength does not match the center wavelength of the solar blocking filter of the receiver. This calibration provides

the degree to which the laser wavelength is off of the center pass band of the receiver filters. It is also applied on ATL02 and is described in more detail in Section 5.3. The correction is unitless and is a number between 0 and 1.

Starting with the nominal value for a particular spot (cal-30), multiply that by the effect of voltage (cal-36 perhaps). Stop there, and you have the sensitivity to background light, after applying a scaling factor to complete that. Starting with Cal-30 * Cal-36, you then multiply by values from Cal-47 and Cal-61 to get the receiver sensitivity to return light. You don't use these last two directly, to calculate a multiplicative factor. Units on the result are events per joule at a per beam.

What is reported out w.r.t the calibrations on 02 are those files actually used to generate a particular ATL02 granule.

7.7 Other ATLAS and Spacecraft Parameters

There are a number of other ATLAS and spacecraft parameters that are not associated with the sections above. These are described here along with their location on the ATL03 data product.

7.7.1 Orbit Number

The parameter **orbit_number** is included in the top_level orbit_info group. This parameter tracks the number of consecutive orbits over the life of the mission and is incremented at the equatorial crossing of the ascending node of the orbit. The corresponding RGT number of the first orbit will depend on the particulars of the launch and injection into our orbit. After orbit number one is determined, this parameter will have the same cadence as the orbit_info/rgt parameter. This section will be updated shortly after launch, when orbit number 1 is identified.

7.7.2 Uncorrelated Height Uncertainty

The sigma_h parameter in the /gtx/geolocation group is the total height uncertainty of a given reference photon, including the effects of electronics timing jitter, the transmit pulse width, radial orbit uncertainty, pointing angle uncertainty, among other terms. At times, it may be beneficial to have an estimate of the uncorrelated height uncertainty that averages out over lengths scales of tens meters. These are the uncertainty components that are random at the laser transmit rate, such as electronics timing jitter or the effects of the transmit pulse width.

The Transmitter Echo Path photon events provide an on-orbit assessment of the photon height uncertainity. Pre-launch analysis combined the individual timing uncertainties of the transmitter components, the receiver components, and the laser pulse width. Since the TEP photons time of flight combine all of these aspects, the standard deviation of the TEP photons provide the best estimate of the photon height uncertainty.

For the two beams with the TEP (beams 1 and 3), the 1-sigma pulse width is based on the standard deviation of the width of the TEP histogram. To determine this, calculate the standard deviation of the normalized bin counts (i.e. tep_hist values) for bins between 17 and 24 nanoseconds (the region of the primary return). If there is more than one TEP realization for a given beam on a given granule, an average of the 1-sigma pulse widths are used. For the four other beams, an average of the 1-sigma pulse width of the two TEP beams is used.

Note that this is the nominal case. At times, one or more of the components used to determine the start pulse time may be missing. The accommodation for these eventualities is TBD.

The resulting one sigma values are the best estimate for the total timing uncertainty in nanoseconds. This timing uncertainty is multiplied by 1e-9 * c/2 to convert this value to a height uncertainty in meters. The resulting 6 x 1 parameter is called ***ph_uncorrelated_error*** and is in the /ancillary_data/atlas_engineering group on ATL03.

8.0 THE QUALITY ASSESSMENT GROUP

In order to assess the usability of ATL03 granules, a number of quantitative metrics are provided in order to make automated decisions regarding data quality, and browse images provide simple images to assess the usability of a given ATL03 granule.

Three primary statistics will be generated for each ground track and for each surface type and included in the /quality_asssessment/ group on the product. These parameters are grouped by ground track into the /gtx/ subgroups.

The total number of low-, medium- and high-confidence signal photons for each surface type present in a particular ATL03 granule are provided in qa_total_signal_conf_ph_low, qa_total_signal_conf_ph_med, and qa_total_signal_conf_high, respectively. Each of these are 1 x 5 arrays, corresponding to the 5 surface types ordered as land, ocean, sea ice, land ice, inland water. These values correspond to the total number of low-, medium-, or high-confidence signal photons for a given surface type, where the surface type is determined at the along-track geolocation segment rate (~20m along track). Any particular along-track geolocation segment can be classified as more than one surface type, owing to the overlap between surface masks, as described in Section 4.

The percentage of low-, medium- and high-confidence signal photons for each surface type present in a particular ATL03 granule are provided in qa_perc_signal_conf_ph_low, qa_perc_signal_conf_ph_med, and qa_perc_signal_conf_high respectively. Each of these are 1 x 5 arrays, corresponding to the 5 surface types ordered as land, ocean, sea ice, land ice, inland water. They are the ratio of the number of signal photons of a particular confidence to the total number of photons from all geolocation segments similarly classified. For example if there are 171 along-track geolocation segments classified as ocean, qa_perc_signal_conf_ph_low is the ratio of the number of low-confidence signal photons across the 171 geolocation segments (qa_total_signal_conf_ph_low) to the total number of photons in those 171 geolocation segments.

Lastly, the parameter qa_perc_surf_type is the percent of the granule that is classified as land, ocean, sea ice, alnd ice, or inland water, and is also a 1 x 5 array for each ground track. These values are simply the ratio of the number of along-track geolocation segments of a particular surface type to the total number of along-track geolocation segments in the granule.

Additionally, images are included in the browse image file associated with each granule as a visual representation of data quality, and a means to quickly assess data location and quality. Note that these browse image files are not embedded in the data file and are separate. This was done to facilitate the ingest and easy transfer of browse imagery between SIPS, NSIDC, and end users.

(1) Maps of medium- and high-confidence reference photon locations for each of the three strong beams. The existence of medium- and high-confidence reference photons is a good predictor of additional medium- or high-confidence signal photons. These three maps are an indication of

where the signal-to-noise ratio in a given granule is good. Since these photon classifications are surface-type dependent, these three maps use the highest confidence for a given photon as the basis for the photon confidence plotted here. For example, if a photon is classified as high-confidence signal for surface type A and as medium confidence for surface type B, the higher confidence is used in these plots.

(2) Plots of the low-, medium-, and high-confidence signal photon ellipsoidal elevations for the entire granule versus geolocation segment id number for each surface type, for each of the three strong beams. There can be up to 15 such images per granule; 3 for each of the 5 surface types potentially present. These images give a user a depiction of what the low-, medium-, and high-confidence photon cloud looks like for each of the three strong beams. The low-confidence photons are plotted first, then the medium confidence, then the high-confidence. Consequently, the low confidence photons are generally only prominently visible if there are few high or medium confidence photons in a particular segment.

(3) Plot of background rate (/gtx/bckgrd_atlas/bckgrd_rate) for the entire granule versus time since the start of the granule, for the three strong beams. This image provides a sense of the variation in the background photon rate, based on the 50-shot sums described in Section 7.2.

In total, the above will generate up to 21 images for each granule. Given that there are 14 granules per day, this results in up to 294 images per day. It is envisioned that a particular use case will either focus on one particular surface type (land ice, for example) resulting in ~ 9 images for consideration.

In addition, there are two additional browse images (generally used as browse images through the National Snow and Ice Data Center and/or ICESat-2 Science Computing Facility). The first (Figure) is shown below and includes the elevations of the low-, medium-, and high-confidence signal photons plotted in three dimensions. Since the photon classification is surface-type dependent (see Section 5), the classification used here are the highest-level classification across surface types. The goal is to allow the user a qualitative assessment of data quality and topography in a given granule.

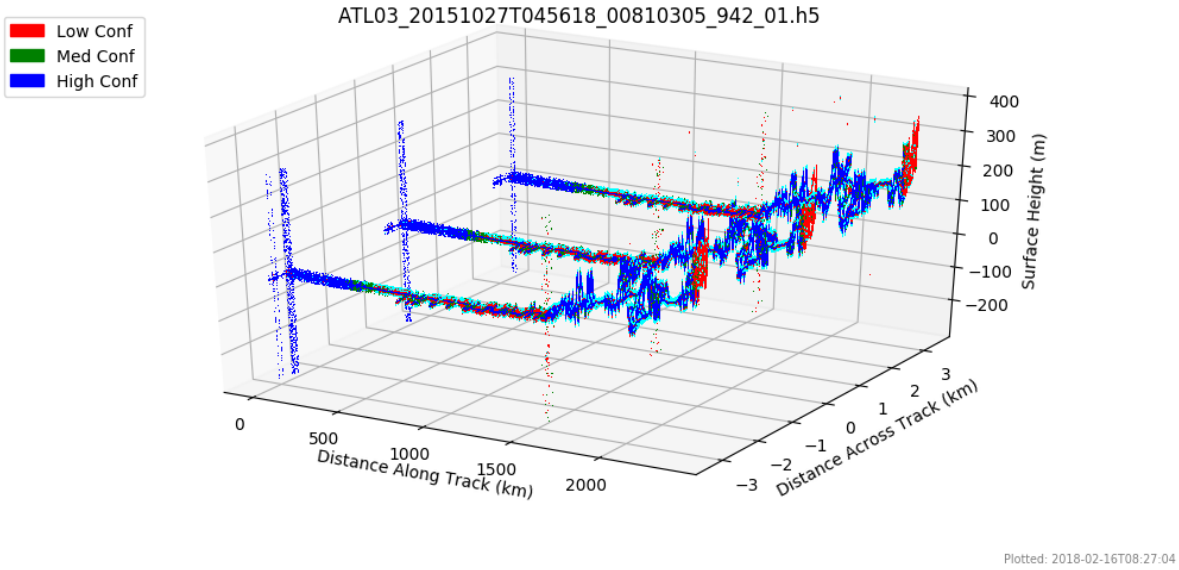

Figure 8-1. Plot of the elevation of the low-, medium-, and high-confidence signal photons for each of the strong beams in the three ground tracks.

The second (Figure) is a general location map of the granule. At this scale, it's not possible to distinguish the six ground tracks or assess the data quality.

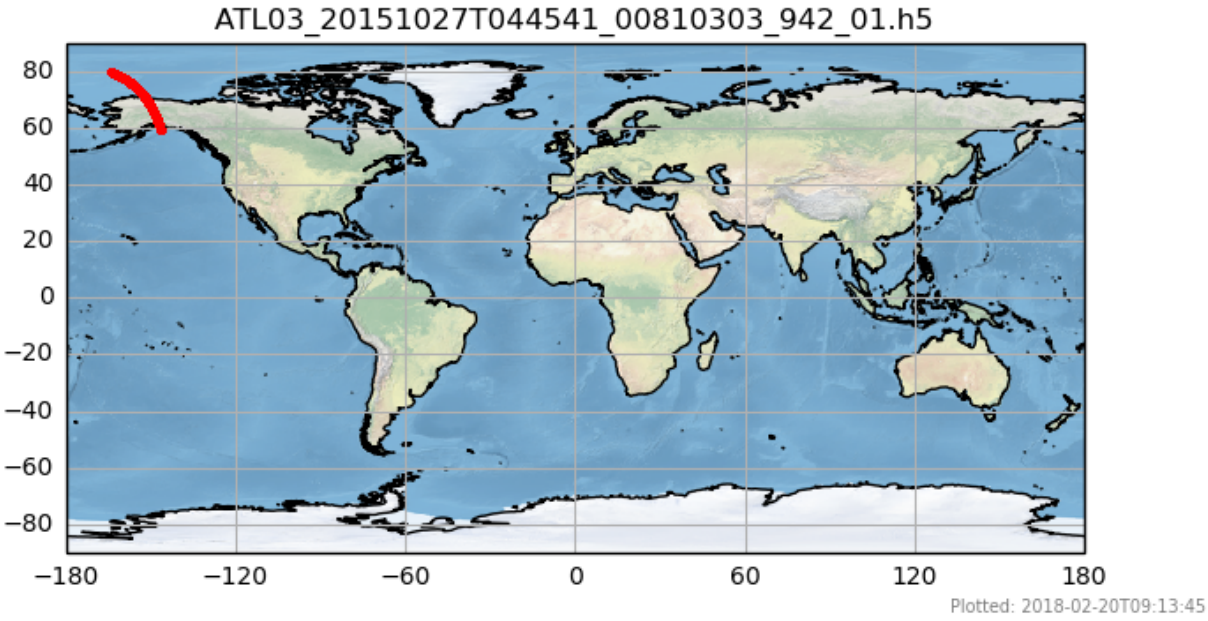

Figure 8-2. General granule location map included in browse image group.

9.0 TEST DATA

10.0 CONSTRAINTS, LIMITATIONS, AND ASSUMPTIONS (TBD)

Discussion of issues passed through from ATL02, including beam steering mechanism effects, impact of lost packets, height and geolocation uncertainty. MABEL description, and its relationship to ATLAS.

11.0 METADATA

The following metadata structure is planned for the ATLAS data within this product:

1) HDF structure overview
2) Each of the six ATLAS ground tracks (GT) have common data
    - reference ground track and cycle number
    - instrument performance / status parameters
    - background photon counts
    - signal finding algorithm (section 5.4) and associated quality assessment statistics
    - geolocation assessment (those parameters common to all beams, such as orbit)
    - geophysical corrections (section 6.0)
3) Associated metadata for all ground tracks
4) Associated ancillary data for all ground tracks

This version of ATL03 incorporates lessons learned from the GLAS_HDF development process. The development team has incorporated code written for the GLAS_HDF effort into the ATLAS codebase to 1) ensure CF-compliance, 2) to make the ATLAS products NetCDF-compatible, and 3) provide necessary metadata in accordance with current standards (https://earthdata.nasa.gov/about-eosdis/requirements). The ATL03 product design continues to evolve and we welcome comments on the design of the HDF5 files.

In ATL03, attributes (rather than datasets) are used for non-science data parameters because of HDFGroup recommendations. Attributes are significantly more efficient for containing small amounts of data. The primary information affected by this change is metadata and ancillary data. The development team realizes this may require changing existing software by the user community, but such ancillary data should improve processing efficiency.

ATLAS metadata was designed to match the existing ICESat GLAS_HDF metadata implementation. CF-style global metadata has been enhanced to contain much more information. The structured metadata in the initial release of ATL03 has adopted GLAS_HDF's pseudo-ECHO style of grouped collection and inventory-level metadata. There is a significant amount of information duplicated between the global and structured metadata. This is intentional since the different styles of metadata serve different purposes.

The global metadata is intended for CF-compliance and human-readability. ATLAS product users are encouraged to use the CF-style global metadata (rather than the structured metadata) whenever possible within their code. However, please report any useful information contained within the structured metadata that is currently not present in the global metadata for consideration in future updates.

The structured metadata is designed to instrument the ATL03 product with information required for an ECHO-based Data Center using ECS-compliant detached metadata files. We will use ISO19115-compliant metadata in the initial release.

ATL03's ancillary_data is designed to bridge the gap between metadata and product parameters. It utilizes group-attached attributes that contain constants and variables used during processing that may prove useful for data users. Examples of information contained within ancillary data include the ATLAS clock frequency, geolocation parameters, and various data quality measures. Of particular importance is the granule epoch time (atlas_sdp_gps_epoch) that is directly attached to the ancillary_data group.

The ATL03 product is NetCDF-4 compliant. Through the incorporation of CF metadata and dimension scales, all the ATLAS products should be compatible with NetCDF-based tools. NetCDF-compliance testing is limited to verifying that the ncdump utility can read the ATLAS products without incident. IDL and Fortran sample product readers will be available from the ICESat-2 website at NSIDC. These are the same readers previously used for MABEL but will have periodic updates to use evolving ATLAS data structures (as needed).

The ATL03 /metadata/ group includes a number of ATLAS-specific parameters passed on from the ATL02 processing, and are included in the /metadata/atlas/ subgroup. Among them are:

range_bias_atlas: A 1x6 dimension array of the beam-specific ATLAS range bias. This is developed through the geolocation process, and consideration of changes in the two strong beams with TEP data. This is passed through from ATL02.

atlas_sdp_gps_epoch: The reference GPS time for the ATLAS instrument. Absolute GPS times of any event in ATL03 can be computed by combining the atlas_sdp_gps_epoch with the relevant delta_time value.

12.0 APPENDICIES

12.1 Appendix A – ATL03 Output Parameter Table.

Name	Data Type	Long Name	Units	Description	Parameter ATBD Source
/gtx		Each group contains the segments for one ground track. As ICESat-2 orbits the Earth, sequential transmit pulses illuminate six ground tracks on the surface of the Earth. The track width is approximately 14 meters. Each ground track is numbered, according to the laser spot number that generates a given ground track. Ground tracks are numbered from the left to the right in the direction of spacecraft travel as: 1L, 1R in the left-most pair of beams; 2L, 2R for the center pair of beams; and 3L, 3R for the right-most pair of beams.			
/gtx/heights		Contains arrays of the parameters for each received photon.			
delta_time	DOUBLE	GPS elapsed time	seconds	The transmit time of a given photon, measured in seconds from the atlas_sdp_gps_epoch. Use the metadata parameter atlas_sdp_gps_epoch to compute full GPS time. Note that multiple received photons associated with a single transmit pulse will have the same delta_time.	
pce_mframe_cnt	UINT_4	PCE major frame counter	counts	The major frame counter is read from the digital flow controller in a given PCE card. The counter identifies individual major frames across diagnostic and science packets. Used as part of the photon ID.	ATL02 ATL03, Section 7.4
ph_id_pulse	INTEGER_4	laser pulse counter	counts	The laser pulse counter is part of photon ID and counts from 1 to 200 and is reset for each new major frame.	ATL02 ATL03, Section 7.4
ph_id_count	INTEGER_2	photon event counter	counts	The photon event counter is part of photon ID and counts from 1 for each channel until reset by laser pulse counter.	ATL02 ATL03, Section 7.4

Name	Data Type	Long Name	Units	Description	Parameter ATBD Source
ph_id_channel	INTEGER_2	photon channel id	counts	Channel number assigned for received photon event. This is part of the photon ID. Values 1 to 240 to span all channels and all detectors. For the A side detectors, values 1 to 60 are for rising edge PCE1 (1 to 20), PCE 2 (21 to 40) and PCE3 (41 to 60). Values 61 to 120 are for falling edge PCE1 (61 to 80), PCE 2 (81 to 100) and PC3 (101 to 120). For the B side detectors, values similarly span from 121 to 240.	ATL03, Section 7.4
signal_conf_ph	UINT_1_LE	photon signal confidence	counts	Confidence level associated with each photon event selected as signal (0-noise. 1-added to allow for buffer but algorithm classifies as background, 2-low, 3-med, 4-high).	ATL03, Section 5, Conf
dist_ph_across	FLOAT	distance off RGT	meters	Across-track distance projected to the ellipsoid of the received photon from the reference ground track. This is based on the along-track segment algorithm described in section 3.1.	ATL03, Section 3.1.2, Step 3
dist_ph_along	FLOAT	along-track distance	meters	Along-track distance in a segment projected to the ellipsoid of the received photon, based on the along-track segment algorithm. Total along-track distance can be found by adding this value to the sum of segment lengths measured from the most recent equatorial crossing.	ATL03, Section 3.1.2, Step 3
lat_ph	FLOAT	latitude of photon	degrees	Latitude of each received photon. Computed from the ECEF Cartesian coordinates of the bounce point.	ATL03g, Section 3.4, ϕ^N
lon_ph	FLOAT	longitude of photon	degrees	Longitude of each received photon. Computed from the ECEF Cartesian coordinates of the bounce point.	ATL03g, Section 3.4, λ^N

Name	Data Type	Long Name	Units	Description	Parameter ATBD Source
h_ph	FLOAT	height of photon	meters	Height of each received photon, relative to the WGS-84 ellipsoid including the geophysical corrections noted in section 6.0.	ATL03g, Section 3.4, h^N
/gtx/geolocation		Contains parameters related to geolocation. The rate of all of these parameters is at the rate corresponding to the ICESat-2 geolocation along-track segment interval (nominally 20 meters along-track).			ATL03g
reference_photon_index	INTEGER_4	index for the reference photon	n/a	Index *j* of the reference photon from the group of geolocated received photons that is closest to the middle of the time period and nearest to the mean of the signal photons.	ATL03, Section 3.2.
reference_photon_lat	DOUBLE	reference photon latitude	degrees	Latitude of each reference photon. Computed from the ECEF Cartesian coordinates of the bounce point.	ATL03g, Section 3.4, ϕ^N
reference_photon_lon	DOUBLE	reference photon longitude	degrees	Longitude of each reference photon. Computed from the ECEF Cartesian coordinates of the bounce point.	ALT03g, Section 3.4, λ^N
delta_time	DOUBLE	reference photon time	seconds	Along-track transmit time of the reference photon, measured in seconds from the atlas_sdp_gps_epoch. If there is no reference photon, this time corresponds to the approximate transmit time associated with the along-track start time of the segment edge.	
ref_azimuth	FLOAT	azimuth	radians	Azimuth of the unit pointing vector for the reference photon in the local ENU frame in radians. The angle is measured from north and positive towards east.	ATL03g, Section 3.3
ref_elev	FLOAT	elevation	radians	Elevation of the unit pointing vector for the reference photon in the local ENU frame in radians. The angle is measured from east-north plane and positive towards up.	ATL03g, Section 3.3

Name	Data Type	Long Name	Units	Description	Parameter ATBD Source
neutat_delay_total	FLOAT	total neutral atmospheric delay	meters	Total neutral atmosphere delay correction (wet+dry).	ATL03a
neutat_delay_derivative	FLOAT	(neutral atmosphere delay)/dh	meters/meter	Change in neutral atmospheric delay per height change.	ATL03a
neutat_ht	FLOAT	neutral atmosphere ref height	meters	Reference height of the neutral atmosphere range correction.	ATL03a
sigma_lat	DOUBLE	latitude uncertainty	degrees	Estimated geodetic latitude uncertainty (1-sigma), for the reference photon bounce point.	ATL03g, Section 3.6, $\Delta\phi$
sigma_lon	DOUBLE	longitude uncertainty	degrees	Estimated geodetic east longitude uncertainty (1-sigma), for the reference photon bounce point.	ATL03g, Section 3.6, $\Delta\lambda$
sigma_along	DOUBLE	along-track geolocation uncertainty	meters	Estimated cartesian along-track uncertainanty (1-sigma) for the reference photon bounce point.	ATL03g, Section 3.6, sigma_along
sigma_across	DOUBLE	across-track geolocation uncertainty	meters	Estimated Cartesian across-track uncertainty (1-sigma) for the refrerence photon bounce point.	ATL03g, Section 3.6, sigma_across
sigma_h	FLOAT	height uncertainty	m	Estimate height uncertainty (1-sigma) for the reference photon bounce point. For other photons in a geolocation segment, use this value since the spatial derivative of this value is very small (see ATL03g, Section TBA).	ATL03g, Section 3.6, Δh
surf_type	INTEGER_1	surface type	unitless	Flags describing which surface types this interval is associated with. 0=not type, 1=is type. Order of array is land, ocean, sea ice, land ice, inland water.	ATL03, Section 4

Name	Data Type	Long Name	Units	Description	Parameter ATBD Source
velocity_sc	FLOAT	spacecraft velocity	meters /second	Spacecraft velocity components (east component, north component, up component) an observer on the ground would measure. While values are common to all beams, this parameter is naturally produced as part of geolocation.	ATL03g, Step 3 in Section 3.1, via POD ICD.
bounce_time_offset	FLOAT	ground bounce time offset	seconds	The difference between the transmit time and the ground bounce time of the reference photon.	ATL03, Section 3.3
segment_ID	UNIT_32	along-track segment ID number	unitless	A seven-digit number uniquely identifying each along-track segment. These are sequential, starting with one for the first segment after an ascending equatorial crossing node.	ATL03, Section 3.1.2, step 5
segment_length	DOUBLE	along-track segment length	meters	The along-track length of the along-track segment. Nominally these are 20 meters, but they vary from 19.8 meters to 20.2 meters.	ATL03, Section 3.1.2, step 5
solar_azimuth	FLOAT	solar azimuth	degrees	The azimuth of he sun position vector from the reference photon bounce point position in the local ENU frame. The angle is measured from North and is positive towards East. ATL03g provides this value in radians; it is converted to degrees for ATL03 output.	ATL03g, Section 3.3, solar_azimuth
solar_elevation	FLOAT	solar elevation	degrees	The elevation of the sun position vector from the reference photon bounce point position in the local ENU frame. The angle is measured from the East-North plane and is positive Up. ATL03g provides this value in radians; it is converted to degress for ATL03 output.	ATL03g, Section 3.3, solar_elevation

Name	Data Type	Long Name	Units	Description	Parameter ATBD Source
segment_dist_x	DOUBLE	cumulative along-track distance	meters	The cumulative along-track distance from the start of the rgt (the ascending node equatorial crossing point) to the start of the segment. Note that this distance is directly related to the delta_time value, which correspondes to the bounce time of a reference photon within a segment.	ATL03, Section 3.1.2, step 3.3
ph_index_beg	INTEGER_4	first photon index	n/a	The index of the first photon in a given segment.	ATL03, Section 3.2
segment_ph_cnt	UINT_16	segment photon counter	n/a	Number of photons in a given along-track segment.	ATL03, Section 3.2
range_bias_corr		range bias correcton	n/a	ATL03 ingests the photon time of flight data from ATL02 and the range-bias corrections from ANC04 to produce our best estimate of photon range in the geolocation processing. (THIS DEF NEEDS HELP)	ATL03, Section 3.3.1
tx_pulse_width_upper	FLOAT	upper threshold crossing time difference	seconds	The difference between the two crossing times of the transmit pulse's upper thresholds; a component in estimating the width of the transmit pulse.	ATL02, described in ATL03 Section 7.2.1
tx_pulse_width_lower	FLOAT	lower threshold crossing time difference	seconds	The difference between the two crossing times of the transmit pulse's lower thresholds; a component in estimating the width of the transmit pulse.	ATL02, described in ATL03 Section 7.2.1
tx_pulse_skew_est	FLOAT	transmit pulse shape skew	seconds	The difference between the means of the lower and upper threshold crossing times; a positive value corresponds to a positive skew in the pulse, and conversely for a negative value.	ATL02, described in ATL03 Section 7.2.1
tx_optic_eff	FLOAT	transmit optics efficiency	unitless	The transmit optical efficiency, based on pre-launch calibration. This is common to all beams.	ATL03, Section 7.2

Name	Data Type	Long Name	Units	Description	Parameter ATBD Source
tx_pulse_distribution	FLOAT	transmit pulse energy distribution	unitless	The fraction of the transmit pulse energy in a given beam, based on pre-launch calibration. This is a six-valued array with the order corresponding to beam naming convention used elsewhere in ATL03 (GT1L, GT1R, etc…).	ATL03, Section 7.2
tx_pulse_thresh_lower	FLOAT	transmit pulse lower threshold	volts	The lower threshold setting of the start pulse detector. The threshold crossing times are used to determine the start pulse time, and estimate the start pulse shape. If this setting changes during a given granule, this parameter becomes two-valued.	ATL03, Section 7.1
tx_pulse_thresh_upper	FLOAT	transmit pulse upper threshold	volts	The upper threshold setting of the start pulse detector. The threshold crossing times are used to determine the start pulse time, and estimate the start pulse shape. If this setting changes during a given granule, this parameter becomes two-valued.	ATL03, Section 7.1
/gtx/geophys_corr		Contains parameters used to correct photon heights for geophysical effects, such as tides. These parameters are posted at the same interval as the ICESat-2 geolocation along-track segment interval (nominally 20 meters along-track).			ATL03, Section 6
dac	FLOAT	dynamic atmosphere correction	meters	Dynamic atmospheric correction (DAC) includes inverted barometer (IB) effect (±5 cm).	Section 6.3.2
tide_earth	FLOAT	earth Tide	meters	Solid earth tides (±40 cm, max).	Section 6.3.3
tide_load	FLOAT	load Tide	meters	The load tide is the local displacement due to ocean Loading (-6 to 0 cm).	Section 6.3.4
tide_ocean	FLOAT	ocean Tide	meters	Ocean tides including diurnal and semi-diurnal (harmonic analysis), and longer period tides (dynamic and self-consistent equilibrium) (±4 m).	Section 6.3.1

Name	Data Type	Long Name	Units	Description	Parameter ATBD Source
tide_pole	FLOAT	solid earth pole tide	meters	The solid earth pole tide is the rotational deformation due to polar motion (-1.5 to 1.5 cm).	Section 6.3.5
tide_oc_pole	FLOAT	ocean pole tide	meters	Oceanic surface rotational deformation due to polar motion (-2 to 2 mm).	Section 6.3.6
geoid	FLOAT	geoid	meters	Geoid height above WGS-84 reference ellipsoid (range -107 to 86 meters). Not applied on the product; requested by higher-level products.	Section 6.3.8
delta_time	DOUBLE	delta time	seconds	Time along-track, measured from the atlas_sdp_gps_epoch reference time, corresponding to the transmit time of the reference photon.	
/gtx/bckgrd_atlas/		Contains parameters related to the ATLAS altimetric histogram (200 Hz, 50-shot) data. For those parameters not naturally at 200-Hz, values are repeated as needed to form a 200-Hz array.			ATL03, Section 7.3.1, 7.3.2
bckgrd_counts	INTEGER_4	ATLAS 50-shot background count	counts	Onboard 50-shot (200 Hz) background sum of photon events within the altimetric range window.	ATL02
bckgrd_counts_reduced	INTEGER_4	reduced ATLAS 50-shot background coutn	counts	Counts from the onboard 50-shot background sum of photon events within the altimetric range window after subtracting the number of high- medium- and low-confidence likely signal photon events and potential TEP photons in that interval.	ATL03, Section 7.3.1
bckgrd_int_height	FLOAT	altimetric range window width	meters	The height of the altimetric range window. This is the height over which the 50-shot sum is generated. Parameter is ingested at 50-Hz, and values are repeated to form a 200-Hz array.	ATL03, Section 7.3.1
bckgrd_int_height_reduced	FLOAT	reduced altimetric range window width	meters	The height of the altimetric range window minus the height span of high-, medium- and low-confidence signal photon events.	ATL03, Section 7.3.1

Name	Data Type	Long Name	Units	Description	Parameter ATBD Source
bckgrd_hist_top	FLOAT	top of the altimetric range window	meters	The height of the top of the altimetric histogram, in meters above the WGS-84 ellipsoid, with all geophysical corrections applied. Parameter is ingested at 50-Hz, and values are repeated to form a 200-Hz array.	ATL03g, Section 3.2, Section 7.3.1
delta_time	DOUBLE	time at the start of ATLAS 50-shot sum	seconds	The time from the atlas_sdp_gps_epoch reference time of the ATLAS 50-shot sum, referenced to the start of the 50-shot sum. This is based on every fiftieth laser fire time, which leads to a very close alignment with major frame boundaries (+/- 1 shot).	ATL02 laser fire time array
pce_mframe_cnt	UINT_4	PCE major frame counter	counts	The major frame counter is read from the digital flow controller in a given PCE card. The counter identifies individual major frames across diagnostic and science packets. Used as part of the photon ID. Since this parameter is nominally at 50 Hz (200 shot cadence) values are repeated to form a 200Hz (50 shot cadence) array.	ATL02 ATL03, Section 7.4
bckgrd_rate	FLOAT	background count rate based on the ATLAS 50-shot sum	counts per second	The background count rate from the 50-shot altimetric histogram after removing the number of likely signal photons based on section **Error! Reference source not found.**.	Section 7.3.1
tlm_top_bandx	FLOAT	ellipsoidal height of the top of the telemetry band	meters	The ellipsoidal heights with repsect to WGS-84 of the top of the telemetry bands, with all geophysical corrections applied. x = 1 for the first telemetry band, =2 for the second, and so on.	Section 3.2, 7.3.2

Name	Data Type	Long Name	Units	Description	Parameter ATBD Source
tlm_height_band x	FLOAT	height of the telemetry band	meters	The height in meters of the telemetry band. May be multi-valued if there is more than one telemetry band. x = 1 for the first telemetry band, =2 for the second, and so on.	Section 7.3.2
/gtx/signal_find_output/ surf_type		Contains surface-type-specific parameters related to vertical and horizontal bin information used in the signal classification procedure. There are up to five subgroups; one for each surface type present in an ATL03 granule.			ATL03, Section 5, Table 5-4
delta_time	DOUBLE	time interval begin	seconds	The photon classification strategy use regular time intervals to discretize the photon cloud. This parameter is the time, in seconds, of the start of a given histogram interval measured from the metadata parameter atlas_epoch. Values are transmit times, in order to make array consistent with the /gtx/heights/delta_time parameter.	ATL03, Section 5, $tint_{beg}$
t_pc_delta	FLOAT	bin width size	seconds	The histogram bin width (integration time) along-track used to find signal photons.	ATL03, Section 5, δt_{PC}
z_pc_delta	FLOAT	bin height size	meters	Height bin size of the histogram used to find signal photons.	ATL03, Section 5, δz_{PC}
bckgrd_mean	FLOAT	background counts per bin	counts	Mean of the number of background counts for the specific integration interval (δt_{pc}) and height bin size (δz_{pc}).	ATL03, Section, 5, $\mu_{bg}\_\delta z_{pc}\_\delta t_{PC}$
bckgrd_sigma	FLOAT	background counts per bin	counts	Standard deviation of the background photon count for the specific integration interval (δt_{pc}) and height bin size (δz_{pc}).	ATL03, Section 5, $\sigma_{bg}\_\delta z_{pc}\_\delta t_{PC}$
/atlas_impulse_response/pce1 _spot1/tep_histogram -or- /atlas_impulse_response/pce2 _spot3/tep_histogram		Contains parameters derived from transmitter echo photon events. There are two groups corresponding to the two ATLAS strong beams with the TEP. These groups are populated generally once per granule. If a granule has two (or more) sets of TEP events, subsequent subgroups are labeled with tep_2, tep_3 etc. as needed.			ATL03, Section 7.2

Name	Data Type	Long Name	Units	Description	Parameter ATBD Source
tep_hist_sum	DOUBLE	TEP histogram sum	counts	The total number of counts in the TEP histogram, after removing the background.	
tep_bckgrd	DOUBLE	TEP background	counts	The average number of counts in the TEP histogram bins, after excluding bins that likely contain the transmit pulse.	
tep_tod	DOUBLE	TEP time of day	seconds	The time of day (absolute time) of the start of the data in the TEP histogram relative to the atlas_sdp_gps_epoch reference time.	
tep_duration	DOUBLE	TEP duration	seconds	The duration (or width) of data in the TEP histogram. Will generally be greater than 10 seconds.	
tep_hist	DOUBLE	TEP histogram	counts	The normalized number of counts in each bin of the TEP histogram.	
tep_hist_time	DOUBLE	TEP histogram time	seconds	The times associated with the TEP histogram bin centers, measured from the laser transmit time.	
/ancillary_data/atlas_ engineering		Group for ATLAS engineering products that are generated once per granule.			ATL02; ATL03 Section 7
/ancillary_data/atlas_ engineering/transmit		ATLAS engineering parameters dealing with the laser transmit pulse.			
tx_pulse_energy		ATLAS Transmit Energy	joules	A 6x4 array containing the mean, standard deviation, minimum, and maximum values of the per-beam transmit energy measured by the Start Pulse Detector and mapped onto gt1l, gt1r, gt2l, gt2r, gt3l, gt3r using the sc_orient parameter.	ATL03 Section 7.2.1
/ancillary_data/atlas_ engineering/receiver		ATLAS engineering parameters dealing with the receiver.			
rx_bckgrd_ sensitivty		Receiver background sensivitiy	events/ joule	Per-beam receiver background sensitivity and mapped onto gt1l, gt1r, gt2l, gt2r, gt3l, gt3r using the sc_orient parameter.	ATL02, Sections 5.3.2

Name	Data Type	Long Name	Units	Description	Parameter ATBD Source
rx_return_ sensitivity		Receiver return sensitivity	events/ joule	Per-beam receiver return sensitivity and mapped onto gt1l, gt1r, gt2l, gt2r, gt3l, gt3r using the sc_orient parameter.	ATL02, Section 5.3.3
/ancillary_data/calibrations		Group for ATLAS calibration products needed by higher level data products.			
first_photon_bias		Cal-19 is a correction for the first photon bias. This group contains dead time values, a first photon bias correction, spot strength, and apparent pulse width per spot.			
low_link_impulse_response		Cal-20 is a modeled representation of the system impulse response function that can be used for spots that do not contain the TEP. It provides histograms of normalized system impulse responses separated by channel and is provided as centroid-aligned histograms.			
nominal_rx_sensitivity		Cal-30 is the receiver radiometric sensitivity, in an absolute measurement, with all variables set to nominal values. This group contains a slope and intercept that, for each spot (1 through 6) on each detector side (A and B) of the receiver, as well as an RMS residual.			ATL02, Section 5.3.1.1
rx_sensitivity_vs_temperature		Cal-33 is the normalized receiver counting efficiency's sensitivity to temperature, represented by the slopes of response versus temperature. It is expressed as a value matrix of slopes to be used in computing the spot-relative counting efficiency from the PMT temperature.			
dead_time_radiometric_ signal_loss		Cal-34 provides a measure of counting efficiency loss as a function of first photon bias for received photons. This group contains dead time values, radiometric corrections, spot strength, and apparent pulse width.			
dead_time		Cal-42 is the ATLAS per-channel detector dead times. This group contains the mean and standard deviation of detector dead times, per channel, per detector bank (or side).			ATL03 Section 7.6.1
rx_sensitivity_to_misalignment _img/_rad		Cal-47 is expressed in two parts: (a) radiometric loss as a function of the misalignment in azimuth and elevation angles (image version), and (b) radiometric loss as a function of the misalignment radius (radial version).			
rx_sensitivity_vs_wtom		Cal-61 is the relative sensitivity to the wavelength tracking optical module (WTOM) for each spot, provided through a quadratic curve.			
/ancillary_data/tep		Group containing information pertaining to computing TEP histograms; data is generated once per granule.			ANC41
min_tep_ph	INTEGER_ 4	minimum TEP photons	seconds	Minimum number of TEP photons required for computing a TEP histogram	

Name	Data Type	Long Name	Units	Description	Parameter ATBD Source
min_tep_secs	DOUBLE	minimum TEP seconds	seconds	Minimum seconds of data required for computed a TEP histogram	
n_tep_bins	INTEGER_4	number of bins	counts	Number of bins in each TEP histogram	
tep_bin_size	FLOAT	TEP bin size	seconds	Size of each TEP histogram bin	
tep_gap_size	DOUBLE	TEP gap size	seconds	Minimum number of seconds separating each TEP histogram instance	
tep_normalize	INTEGER_4	TEP normalization flag	unitless	Flag indicating if the TEP histogram was normalized (1 if normalized, 0 if not normalized)	
tep_peak_bins	INTEGER_4	number of peak TEP bins to remove	counts	Number of peak TEP bins to remove for the TEP background calculation	
tep_rm_noise	INTEGER_4	noise removal normalization flag	unitless	Flag indicating if noise was removed from the TEP histogram (1 if background noise was removed, 0 if background noise was note removed)	
tep_start_x	FLOAT	TEP starting bin time	seconds	Value at the left edge of the first TEP histogram bin	
tep_valid_spot	INTEGER_4	Recommended TEP spot	unitless	A 6x1 array indicating which TEP to use for each spot that does not have an associated TEP	
tep_range_prim	DOUBLE	Recommended range of TEP photons	seconds	A 2x1 array indicating the range of times of flight of the primary TEP return, nominally 10 to 33 x 10^9 seconds.	
/ancillary_data/gtx/signal_find_input		Group contains the setup parameters for the signal finding algorithm. All parameters have dimension of 5,1 corresponding with the 5 different surface types.			ATL03, Section 5, Table 5-2
alpha_max	FLOAT	maximum slope	radians	Maximum slope allowed for slant histogram; if larger than this then don't attempt to fill gap.	ATL03, Section 5, αmax
alpha_inc	FLOAT	slope increment	radians	Increment by which the slope is varied for slant histogramming over large gaps.	ATL03, Section 5, αinc

Name	Data Type	Long Name	Units	Description	Parameter ATBD Source
sig_find_t_inc	FLOAT	histogram time increment	seconds	Time increment the algorithm uses to step through the photon cloud in a granule. Histograms are formed at each Δtime to identify signal photon events.	ATL03, Section 5, Δtime
delta_t_gap_min	FLOAT	minimum delta time gap	seconds	Minimum size of a time gap in the height profile over which to use variable slope slant histogramming.	ATL03, Section 5, Δtime_gapmin
delta_t_lin_fit	FLOAT	linear fit time increment	seconds	Time span over which to perform a running linear fit to identified signal photon events when editing outliers. Surface type dependent.	ATL03, Section 5, Δt_linfit_edit
delta_Eslw	FLOAT	half height for slant histogramming	meters	Half of the value of the height window used for slant histogramming relative to the surface defined by the linear fit to the surrounding photons at slope, alpha. Surface-type dependent.	ATL03, Section 5, δEslw
delta_eslw _v	FLOAT	half height for variable slope slant histogramming	meters	Half the value of the height window used for slant histogramming relative to the surface used when varying the surface slope, alpha, to fill large gaps. Surface-type dependent.	ATL03, Section 5, δEslw_v
delta_t_min	FLOAT	histogram minimum time	seconds	Minimum time interval over which photons are selected to histogram. Surface-type dependent.	ATL03, Section 5, δt_{min}
delta_t_max	FLOAT	histogram maximum time	seconds	Maximum time interval over which photons are selected to histogram. Surface-type dependent.	ATL03, Section 5, δt_{max}
delta_zmin	FLOAT	minimum height bin size	meters	Minimum height bin size for histogramming for first sweep. Surface-type dependent.	ATL03, Section 5, δz_{min}
delta_zmax2	FLOAT	maximum height bin size 2	meters	Maximum height bin size for histogramming for second sweep. Surface-type dependent.	ATL03, Section 5, δz_{max2}

Name	Data Type	Long Name	Units	Description	Parameter ATBD Source
delta_z_bg	FLOAT	histogram height bin size for noise calculation from photon cloud	seconds	Width of a height bin in each atmospheric histogram, Ha, if calculating Ha from the photon cloud. Surface-type dependent.	ATL03, Section 5, δz_{BG}
addpad_flag	INTEGER	additional photon flag	unitless	Binary (logical) flag: if true (=1) then identify additional photon events as padding to achieve htspanin for each time interval sig_find_t_inc.	ATL03, Section 5, Addpad
e_a	FLOAT	multiplier of Ha_sigma	unitless	Multiplier of Ha_sigma used to determine which bins in the atmospheric histogram may contain signal photon events. Surface-type dependent.	ATL03, Section 5, e_a
e_gap	FLOAT	multiplier of sigma gapfit	unitless	Multiplier of sigma_gapfit, the standard deviation of the residuals between the signal photons used to estimate the surface across a signal photon gap, and that surface estimate, using a linear fit. Used in slant histograms. Surface-type dependent.	ATL03, Section 5, e_linfit_slant
e_lfit	FLOAT	multiplier of STD of linear fit	unitless	Multiplier of standard deviation of linear fit to signal photons used to edit out noise during running linear fit edit of outliers.	ATL03, Section 5, e_linfit_edit
e_m	FLOAT	multiplier of STD of background	unitless	Multiplier of standard deviation of the number of background photon events per bin used in determining signal photon threshold. Surface-type dependent.	ATL03, Section 5, e_m
e_m_mult	FLOAT	multiplier of STD of e_m	unitless	Multiplier of e_m used to determine Th_{sig2}, threshold for singular bins. Surface-type dependent.	ATL03, Section 5, e_m_mult

Name	Data Type	Long Name	Units	Description	Parameter ATBD Source
htspanmin	FLOAT	minimum height span	meters	Minimum height span for each time interval of photons with confidence flag > 0. If the height span is < htspanmin then all photons not previously selected within +/- htspanmin/2 of the median height of the signal photons selected are marked with a confidence flag of 1. Surface-type dependent.	ATL03, Section 5, Htspanmin
out_edit_flag	INTEGER	flag to request outlier editing	unitless	Binary (logical) flag: if true (=1) then perform an nσ edit on a running linear fit to identified signal to remove outliers. Surface-type dependent.	ATL03, Section 5, Ledit
pc_bckgrd_flag	INTEGER	flag to request using photon cloud to calculate background rate	unitless	Binary (logical) flag: if true (=1) then always use the photon cloud to calculate the background photon rate, if false only use the photon cloud in the absence of the atmospheric histogram. Surface-type dependent.	ATL03, Section 5, Lpcbg
lslant_flag	INTEGER	flag to request slant histogramming for strong beams	unitless	Binary (logical) flag: if true (=1) then perform slant histogramming for the strong beam. Surface-type dependent.	ATL03, Section 5, lslant
min_fit_time	FLOAT	minimum fit time	seconds	The minimum time over which to fit a line to a height profile to calculate the local slope using running linear fits. This must be an integer of sig_find_t_inc.	ATL03, Section 5, min_fit_time
n_delta_z1	INTEGER_2	number of increments in z1	unitless	The number of increments between delta_zmin and delat_zmax1. Surface-type dependent.	ATL03, Section 5, nδz1
n_delta_z2	INTEGER_2	number of increments in z2	unitless	The number of increments between delta_zmax1 and delta_zmax2. Surface-type dependent.	ATL03, Section 5, nδz2

Name	Data Type	Long Name	Units	Description	Parameter ATBD Source
nbin_min	INTEGER_2	minimum number of bins	unitless	Minimum number of bins in a histogram required for the algorithm to be able to process the histogram.	ATL03, Section 5, $Nbin_{min}$
nphot_min	INTEGER_2	minimum number of photons to fill gap	unitless	The minimum number of photons over which to perform a linear fit to estimate the surface profile across a gap. Surface-type dependent.	ATL03, Section 5, $Nphot_{min}$
r	FLOAT	minimum ratio	unitless	Minimum ratio of max number of photons in histogram bin to mean noise value that must exist to consider a bin a signal bin.	ATL03, Section 5, R
r2	FLOAT	minimum ratio2	unitless	Minimum ratio of maximum number of photons in any one bin of contiguous signal bins to maximum number of photons in largest bin in order to accept a group of potential signal bins as signal. Surface-type dependent.	ATL03, Section 5, R2
snrlow	FLOAT	signal to noise ratio low	unitless	Signal to noise ratio below which all selected signal has low confidence.	ATL03, Section 5, snrlow
snrmed	FLOAT	signal to noise ratio medium	unitless	Signal to noise ratio above which all selected signal has high confidence. Selected signal with signal to noise ratio between snrlow and snrmed is marked as medium confidence.	ATL03, Section 5, snrmed
t_gap_big	FLOAT	gap size criteria	seconds	For time gaps less than this value, slant histogramming is performed relative to the linear slope calculated from the surrounding signal. For time gaps greater than or equal to this value the slope is varied when performing slant histogramming. Surface-type dependent.	ATL03, Section 5, t_{gapbig}
/orbit_info		Contains data that are common among all ground tracks for the granule. These are constants for a given granule.			

Name	Data Type	Long Name	Units	Description	Parameter ATBD Source
delta_time	DOUBLE	orbit change time	seconds	The time at which the orbit information in this group has changed most recently, measured in seconds from the metadata parameter atlas_sdp_gps_epoch.	
cycle_number	INTEGER_4	cycle number	unitless	Tracks the number of 91-day cycles in the mission, beginning with 01. A unique orbit number can be determined by subtracting 1 from the cycle_number, multiplying by 1,387 and adding the RGT value.	
rgt	INTEGER_2	reference ground track	unitless	The reference ground track (RGT) is the track on the Earth at which a specified unit vector within the observatory is pointed. Under nominal operating conditions, there will be no data collected along the RGT, as the RGT is spanned by GT2L and GT2R. During slews or off-pointing, it is possible that ground tracks may intersect the RGT. The ICESat-2 mission has 1,387 RGTs.	
orbit_number	INTEGER_4	orbit number	unitless	The orbit number counts consecutively from the first mission orbit (value TBD depending on launch) and incremented at equatorial crossings of the ascending node of the orbit, as the the RGT is incremented.	ATL03, Section 7.7.1
sc_orient	INTEGER_4	spacecraft orientation	unitless	This parameter tracks the spacecraft orientation between ‘forward’ and ‘backward’ orientations, to allow mapping between ATLAS hardware and the beam orientation on the ground. Forward == 1; backward == 0; transition ==2.	Section 7.5, ANC13

Name	Data Type	Long Name	Units	Description	Parameter ATBD Source
sc_orient_time	DOUBLE	time of last S/C orientation change	second	Time of the most recent orientation change, measured in seconds from the metadata parameter atlas_sdp_gps_epoch.	ANC13
/quality_assessment/along_track		Placeholder for along-track QA parameters.			
qa_total_signal_conf_ph_low	SINGLE	counts	unitless	Total number of low-confidence signal photons for each surface type	ATL03, Section 8
qa_total_signal_conf_ph_med	SINGLE	counts	unitless	Total number of medium-confidence signal photons for each surface type	ATL03, Section 8
qa_total_signal_conf_ph_high	SINGLE	counts	unitless	Total number of high-confidence signal photons for each surface type	ATL03, Section 8
qa_perc_signal_conf_ph_low	SINGLE	percentage	unitless	Percentage of low-confidence signal photons for each surface type	ATL03, Section 8
qa_perc_signal_conf_ph_med	SINGLE	percentage	unitless	Percentage of medium-confidence signal photons for each surface type	ATL03, Section 8
qa_perc_signal_conf_ph_high	SINGLE	percentage	unitless	Percentage of high-confidence signal photons for each surface type	ATL03, Section 8
qa_perc_surf_type	SINGLE	percentage	unitless	Percent of each surface type present in a particular ATL03 granule	ATL03, Section 8
/quality_assessment/summary		Placeholder for summary QA metrics.			ATL03, Section 8
/metadata				Incomplete description	
/metadata/ATLAS					

Name	Data Type	Long Name	Units	Description	Parameter ATBD Source
range_bias_atlas				A 1x6 dimension array of the beam-specific ATLAS range bias. This is developed through the geolocation process, and consideration of changes in the two strong beams with TEP data. This is passed through from ATL02.	

Table 12-1. ATL03 Output Parameter Table.

12.2 Appendix B – ATL03 Input Parameter Table

put it right here…

Table 12-2. ATL03 Input Parameter Table.

12.3 ATL03 Users Notes

12.3.1 Tracing between higher-level products and the photon cloud

In many applications, it is desirable to directly compare the photons that were included in a higher-level product or parameter. Depending on the upper-level product being considered, there are three potential methods for making such a connection.

(1) Using Geolocation Segment IDs. Many higher level products include the segment_ID parameter from ATL03. This parameter is in the group /gtx/geolocation/ on ATL03 and is a seven-digit number uniquely identifying each along-track segment. These are sequential, starting with one for the first segment after an ascending equatorial crossing node, and are defined in Section 3.1.2, step 5. To find the photons in a given segment, use the parameter /gtx/geolocation/ph_index_beg corresponding to that segment, which provides the index of the first photon in a given segment. This index, and the index of the subsequent along-track segment, can be used to bracket the indicies of photon data in the /gtx/heights/ group. For example, if the ph_index_beg is *i* and the following ph_index_beg is *j* for two particular along-track segments, the corresponding photon heights are /gtx/heights/h_ph(i:j). **Caveat:** the ph_beg_index parameter (and the reference_photon_index parameter) are unique to a specific granule, since the index counts sequentially from the first photon in the granule. If a granule is subsetted, care must be taken to either preserve the utility of the indexes, or they should be handled with caution.

(2) Using time. Many higher-level products include the cumulative time since the last equatorial crossing of an ascending node of an orbit (i.e. the cumulative time since the beginning of a particular RGT). Each major group in ATL03 includes the delta_time parameter, at the appropriate rate, that can be used to connect higher level parameters to ATL03 parameters. For example, to find all the photons in a given along-track geolocation segment, extract the beginning and end times of the segment in question from the /gtx/geolocation/delta_time parameter, and find the indexes of all photon between those start and stop times in the /gtx/heights/delta_time parameter.

(3) Using along-track distance. Several higher-level products include parameters that define the cumulative along track distance since the last ascending node equatorial crossing. The group /gtx/geolocation/ includes the segment_dist_x parameter which defines the

starting along-track distance for each along-track geolocation segment. The cumulative along-track distance for a photon in the ith segment can be determined by adding the sum of the preceeding along-track segments (sum(/gtx/geolocation/segment_length)) to the distance along-track for a given photon in a segment (dist_ph_along).

12.3.2 Apparent Return Pulse Width and Strength

At times, a user may have a need to know the width and strength of the laser pulse reflected off the surface of the earth as measured by ATLAS. ATL03 provides the information needed to determine this. The photon classification algorithm indicates which photons are most likely reflections from the surface of the Earth. Depending on a uer's needs, the high- medium- and/or low-confidence signal photons can be aggregated for some distance along track (or some number number of consecutive shots). The standard deviation of the heights of these photons provides a metric for the return pulse width, although other metrics are of course possible to calculate. The return pulse strength can be estimated by dividing the number of high- medium- and low-confidence photons by the number of laser shots in the aggregation. Care should be taken in determeining a suitable along-track aggregation, as surface topographic variation will broaden the apparent width of the returned pulse. A longer aggregation time will improve the statistics on the signal strength, but decrease the resolution of the return pulse width. ATL04 uses the ATL03 medium- and high-confidence signal photons aggregated every 400 shots along with a radiometric correction algorithm to account for photons missed as a result of the detector dead time (see Cal-34: Dead time dependent radiometric signal loss) in order to estimate the surface reflectance in the ATL04 data product. See the ATL04 ATBD for complete details.

12.3.3 Use of the TEP as the system impulse-response function

ATL03 provides the normalized TEP histograms for the two strong beams which receive TEP photons. At times, these TEP histograms could be contaminated by cloud returns or photon events reflected off the earth's surface into the window of possible TEP photon events. If the surface photon events (or photons from clouds) have a constant radiometery during the time they overlap with the TEP, the background removal steps described in section 7.2 should remove these non-TEP photon events. However, if the radiometery changes during the TEP window, it is possible that the resulting TEP histogram will have non-zero bin counts between the primary and secondary TEP return regions. We therefore suggest the following checks before a higher-level algorithm uses the TEP:

(a) If the TEP histogram is to be used as a proxy for the system impulse response function, we recommend using the region between 15 and 30 nanoseconds to avoid the secondary TEP return.

(b) if the primary TEP return has a full-width at half max value greater than 3 nanoseconds, we recommend not using this particular realization of the TEP as a proxy for the system impulse response.

With sufficient on-orbit TEP data, we intend to refine these guidelines to automate rejection of spurious TEP realizations.

12.4 Appendix D - Lexicon for ATBD Writing

Lexicon for ICESat-2 ATBD Writing 26 June 2014

The purpose of this document is to provide naming conventions for ATBD writers that define aspects of the instrument, data, and geometry. Some naming conventions are borrowed from **Spots, Channels and Redundancy Assignments** (ICESat-2-ATSYS-TN-0910) by P. Luers. Some conventions are different than those used by the ATLAS team for the purposes of making the data processing and interpretation simpler.

Spots. The ATLAS instrument creates six spots on the ground, three weak and three strong, where strong is defined as approximately four times brighter than weak. These designations apply to both the laser-illuminated spots and the instrument fields of view. The spots are numbered as shown in figure 1. At times, the weak spots are leading (when the direction of travel is in the ATLAS +x direction) and at times the strong spots are leading. However, the spot number does not change based on the orientation of ATLAS. Not: beams, footprints.

Laser Pulse. Individual pulses of light emitted from the ATLAS laser are called laser pulses. As the pulse passes through the ATLAS transmit optics, this single pulse is split into six individual transmit pulses by the diffractive optical element. The six pulses travel to the Earth's surface (assuming ATLAS is pointed to the Earth's surface). Some attributes of a laser pulse are the wavelength, pulse shape and duration. Not: transmit pulse, laser shot, laser fire.

Laser Beam. The sequential laser pulses emitted from the ATLAS instrument that illuminate spots on the earth's surface are called laser beams. ATLAS generates six laser beams. The laser beam numbering convention follows the ATLAS instrument convention with strong beams numbered 1, 3, and 5 and weak beams numbered 2, 4, and 6 as shown in the figures. Not: beamlet.

Transmit Pulse. Individual pulses of light emitted from the ICESat-2 observatory are called transmit pulses. The ATLAS instrument generates six transmit pulses of light from a single laser pulse. The transmit pulses generate six spots where the laser light illuminates the surface of the earth. Some attributes of a given transmit pulse are the wavelength, the shape, and the energy. Some attributes of the six transmit pulses may be different. Not: laser fire, shot, laser shot, laser pulse.

Reflected Pulse. Individual transmit pulses reflected off the surface of the earth and viewed by the ATLAS telescope are called reflected pulses. For a given transmit pulse, there may or may not be a reflected pulse. Not: received pulse, returned pulse.

Photon Event. Some of the energy in a reflected pulse passes through the ATLAS receiver optics and electronics. ATLAS detects and time tags some fraction of the photons that make up the reflected pulse, as well as background photons due to sunlight or instrument noise. Any photon that is time tagged by the ATLAS instrument is called a photon event, regardless of source. Not: received photon, detected photon.

Reference Ground Track (RGT). The reference ground track (RGT) is the track on the earth at which a specified unit vector within the observatory is pointed. Under nominal operating conditions, there will be no data collected along the RGT, as the RGT is spanned by GT2L and GT2R (which are not shown in the figures, but are similar to the GTs that are shown). During spacecraft slews or off-pointing, it is possible that ground tracks may intersect the RGT. The precise unit vector has not yet been defined. The ICESat-2 mission has 1,387 RGTs, numbered from 0001xx to 1387xx. The last two digits refer to the cycle number. Not: ground tracks, paths, sub-satellite track.

Cycle Number. Over 91 days, each of the 1387 RGTs will be targeted in the polar regions once. In subsequent 91-day periods, these RGTs will be targeted again. The cycle number tracks the number of 91-day periods that have elapsed since the ICESat-2 observatory entered the science orbit. The first 91-day cycle is numbered 01, the second 91-day cycle is 02, and so on. At the end of the first 3 years of operations, we expect the cycle number to be 12. The cycle number will be carried in the mid-latitudes, though the same RGTs will (in general) not be targeted more than once.

Sub-satellite Track (SST). The sub-satellite track (SST) is the time-ordered series of latitude and longitude points at the geodetic nadir of the ICESat-2 observatory. In order to protect the ATLAS detectors from damage due to specular returns, and the natural variation of the position of the observatory with respect to the RGT throughout the orbit, the SST is generally not the same as the RGT. Not: reference ground track, ground track.

Ground Tracks (GT). As ICESat-2 orbits the earth, sequential transmit pulses illuminate six ground tracks on the surface of the earth. The track width is approximately fifteen meters wide. Ground tracks are always numbered with 1L on the far left of the spot pattern and 3R on the far right of the spot pattern. Not: spots, tracks, paths, reference ground tracks, footpaths.

Reference Pair Track (RPT). The reference pair track is the imaginary line half-way between the planned locations of the strong and weak ground tracks that make up a pair. There are three RPTs: RPT1 is spanned by GT1L and GT1R, RPT2 is spanned by GT2L and GT2R (and may be coincident with the RGT at times), RPT3 is spanned by GT3L and GT3R. Note that this is the planned location of the midway point between GTs. We will not know this location very precisely prior to launch. Not: tracks, paths, reference ground tracks, footpaths, pair tracks.

Pair Track (PT). The pair track is the imaginary line half way between the actual locations of the strong and weak ground tracks that make up a pair. There are three PTs: PT1 is spanned by GT1L and GT1R, PT2 is spanned by GT2L and GT2R (and may be coincident with the RGT at times), PT3 is spanned by GT3L and GT3R. Note that this is the actual location of the midway

point between GTs, and will be defined by the actual location of the GTs. Not: tracks, paths, reference ground tracks, footpaths, reference pair tracks.

Pairs. When considered together, individual strong and weak ground tracks form a pair. For example, GT2L and GT2R form the central pair of the array. The pairs are numbered 1 through 3: Pair 1 is comprised of GT1L and GT1R, pair 2 is comprised of GT2L and GT2R, and pair 3 is comprised of GT3L and 3R.

Along-track. The direction of travel of the ICESat-2 observatory in the orbit frame is defined as the along-track coordinate, and is denoted as the +x direction. The positive x direction is therefore along the Earth-centered Earth-fixed velocity vector of the observatory. Each pair has a unique coordinate system, with the +x direction aligned with the reference pair tracks.

Across-track. The across-track coordinate is y and is positive to the left, with the origins along the reference ground track.

Segment. An along-track span (or aggregation) of received photon data from a single ground track or other defined track is called a segment. A segment can be measured as a time duration (e.g. from the time of the first received photon to the time of the last received photon), as a distance (e.g. the distance between the location of the first and last received photons), or as an accumulation of a desired number of photons. Segments can be as short or as long as desired.

Signal Photon. Any photon event that an algorithm determines to be part of the reflected pulse.

Background Photon. Any photon event that is not classified as a signal photon is classified as a background photon. Background photons could be due to noise in the ATLAS instrument (e.g. stray light, or detector dark counts), sunlight, or mis-classified signal photons. Not: noise photon.

h_.** Signal photons will be used by higher-level products to determine height above the WGS-84 reference ellipsoid, using a semi-major axis (equatorial radius) of 6,378,137 meters and a flattening of 1/298.257223563. This can be abbreviated as ‘ellipsoidal height’ or ‘height above ellipsoid’. These heights are denoted by h; the subscript ** will refer to the specific algorithm used to determine that elevation (e.g. is = ice sheet algorithm, si = sea ice algorithm, etc…). Not: elevation.

Photon Cloud. The collection of all telemetered photon time tags in a given segment is the (or a) photon cloud. Not: point cloud.

Background Count Rate. The number of background photons in a given time span is the background count rate. Therefore a value of the background count rate requires a segment of received photons and an algorithm to distinguish signal and background photons. Not: Noise rate, background rate.

Noise Count Rate. The rate at which the ATLAS instrument receives photons in the absence of any light entering the ATLAS telescope or receiver optics. The noise count rate includes received photons due to detector dark counts or stray light from within the instrument. Not: noise rate, background rate, background count rate.

Telemetry band. The subset of received photons selected by the science algorithm on board ATLAS to be telemetered to the ground is called the telemetry band. The width of the telemetry band is a function of the signal to noise ratio of the data (calculated by the science algorithm onboard ATLAS), the location on the earth (e.g. ocean, land, sea ice, etc…), and the roughness of the terrain, among other parameters. The widths of telemetry bands are adjustable on-orbit. The telemetry band width is described in section 7 or the *ATLAS Flight Science Receiver Algorithms* document. The total volume of telemetred photon events must meet the data volume constraint (currently 577 GBits/day).

Window, Window Width, Window Duration. A subset of the telemetry band of received photons is called a window. If the vertical extent of a window is defined in terms of distance, the window is said to have a width. If the vertical extent of a window is defined in terms of time, the window is said to have a duration. The window width is always less than or equal to the telemetry band.

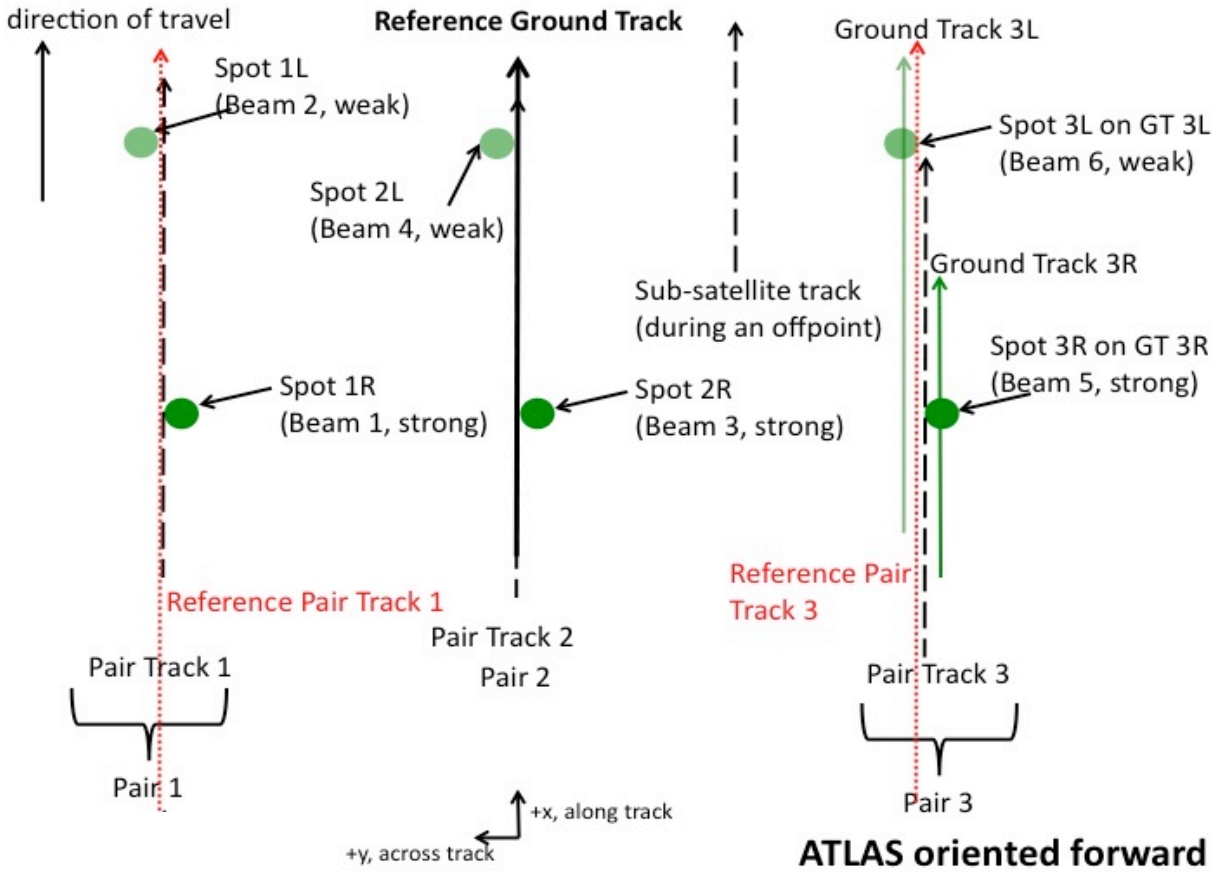

Figure 12-1. Spot and track naming convention with ATLAS oriented in the forward (instrument coordinate +x) direction.

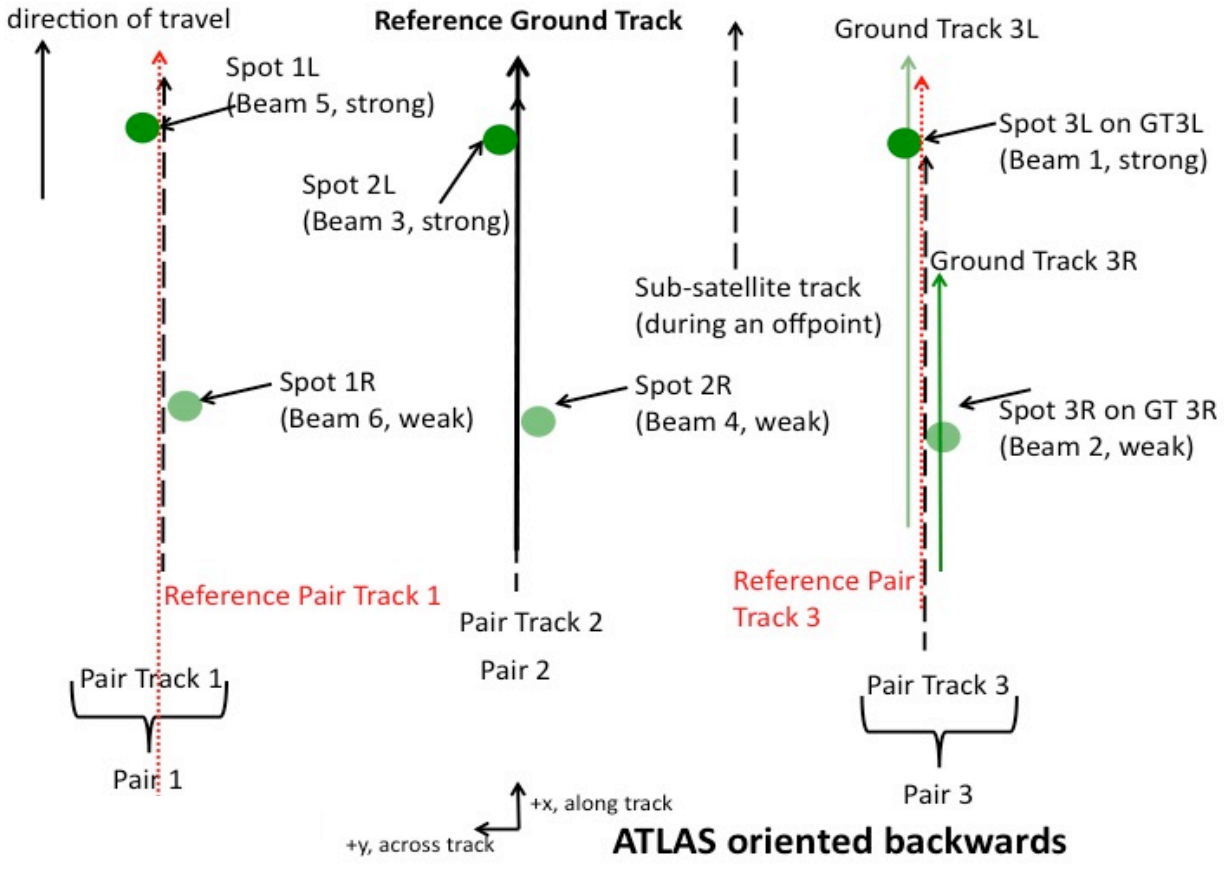

Figure 12-2. Spot and track naming convention with ATLAS oriented in the backward (instrument coordinate -x) direction.

13.0 REFERENCES

Agnew, D. C., Earth Tides, in *Treatise on Geophysics: Geodesy*, ed. By T. A. Herring, pp. 163-195, 2009.

Andersen, O. B. and R. "Scharoo, Range and Geophysical Corrections in Coastal Regions: And Implications for Mean Sea Surface Determination," Chapter 5, pp.103-145, in *Coastal Altimetry*, ed. By S. Vignudelli, et al., Springer-Verlag, Berlin, 2011.

Birkett, Charon M. and Ian M. Mason, **A New Global Lakes Database for a Remote Sensing Program Studying Climatically Sensitive Large Lakes,** *Journal of Great Lakes Research*, Volume 21, Issue 3, 1995, Pages 307–318, http://dx.doi.org/10.1016/S0380-1330(95)71041-3

Brown, J., O.J. Ferrians, Jr., J.A. Heginbottom, and E.S. Melnikov. 1998, revised February 2001. **Circum-arctic map of permafrost and ground ice conditions**. Boulder, CO: National Snow and Ice Data Center/World Data Center for Glaciology. Digital media.

Carrère, L and F. Lyard, Modeling the barotropic response of the global ocean to atmospheric wind and pressure forcing–comparisons with observations, *Geophys. Res Lett.*, V.30, doi:10.1029/2002GL016473, 2003.

Carroll, M.L, J. R. Townshend, C. M. DiMiceli, P. Noojipady, and R. A. Sohlberg, A new global raster water mask at 250 m resolution, *Int. J. Digit. Earth*, vol. 2, no. 4, pp. 291-308, Dec. 2009, doi: 10.1080/17538940902951401.

Cartwright, D. E. and A. C. Edden, Corrected Tables of Tidal Harmonics, *Geophys. J. Royal Astron. Soc.*, V.33, 253-264, 1973.

Cartwright, D. E. and R. J. Tayler, New Computations of the Tide-Generating Potential, *Geophys. J. Royal Astron. Soc.*, V.23, 45-74, 1971.

Cheng, M., J. C. Reis and B. D. Tapley, Geocenter Variations from SLR, paper presented to the Reference Frames for Applications in Geosciences (REFAG2010) meeting, Marne-Le-Vallee, France, October 4-8, 2010.

Cheng, M. K., J. C. Reis and B. D. Tapley, Geocenter Variations from Analysis of SLR Data, in *Reference Frames for Applications in Geosciences*, IAG Symp., V138, 19-25, ed. by Z. Altamimi and X. Collilieux, Springer-Verlag, DOI: 10.1007/978-3-642-32998-2_4, 2013.

Desai, S. D., Observing the pole tide with satellite altimetry, *J. Geophys. Res.* 107(C11), 3186, doi:10.1029/2001JC001224, 2002.

ESA, Geophysical Correction Application in Level 2 CryoSat Data products, IDEAS-VEG-IPF-MEM-1288, Version 1, 19 June 2013.

Fok, H. S., Ocean Tides Modeling using Satellite Altimetry, *OSU Report* 501, 2012.

Howat, I., A. Negrete, and B. Smith. 2015. The Greenland Ice Mapping Project (GIMP) land classification and surface elevation data sets. *The Cryosphere* 8: 1509-1518.

Jakobsson, M., L. A. Mayer, B. Coakley, J. A. Dowdeswell, S. Forbes, B. Fridman, H. Hodnesdal, R. Noormets, R. Pedersen, M. Rebesco, H.-W. Schenke, Y. Zarayskaya A, D. Accettella, A. Armstrong, R. M. Anderson, P. Bienhoff, A. Camerlenghi, I. Church, M. Edwards, J. V. Gardner, J. K. Hall, B. Hell, O. B. Hestvik, Y. Kristoffersen, C. Marcussen, R. Mohammad, D. Mosher, S. V. Nghiem, M. T. Pedrosa, P. G. Travaglini, and P. Weatherall, 2012, The International Bathymetric Chart of the Arctic Ocean (IBCAO) Version 3.0, *Geophysical Research Letters*, doi:10.1029/2012GL052219.

Jason-2 Product Handbook, Version 1.8, 2011. www.aviso.oceanobs.com/fileadmin/documents/data/tools/hdbkj2.pdf

Latychev, K., J. X. Mitrovica, M. Ishii, N. Chen and J. L. Davis, Body tides on a 3-D elastic Earth: Towards a tidal tomography, *Earth Planet Sci. Lett.*, 277, 86-90, 2009.

Lehner, Bernhard, and Petra Döll, **Development and validation of a global database of lakes, reservoirs and wetlands**, *Journal of Hydrology*, Volume 296, Issues 1–4, 20 August 2004, Pages 1–22. http://dx.doi.org/10.1016/j.jhydrol.2004.03.028

Leigh, H.W, L.A. Magruder, C.C. Carabajal, J.L. Saba, and J.F. McGarry. Development of onboard digital elevation and relief databases for ICESat-2. *IEE Trans. on Geosci and Rem. Sci.* 3(4), 2011-2020, doi:10.1109/TGRS.2014.2352277.

Le Provost, C., Ocean Tides, chapter 6 in *Satellite Altimetry and Earth Science*, ed. By L. L. Fu & A. Cazenave, Academic Press, 2001.

Mathews, P. M., V. Dehant and J. M. Gipson, Tidal Station Displacements, *J. Geophys. Res.*, V.102, B9, 20,469-20,477, 1997.

Obligis, E., M. Ablain, J.-F. Legeais and J. Fernandez, WP2300 & WP2700 Wet Tropospheric Correction RRDP and Validation Reports, http://www.esa-sealevel-cci.org/webfmsend/79, 2012.

Padman, L. and H. A. Fricker, Tides on the Ross Ice Shelf observed with ICESat, *Geophys. Res. Lett.*, 32, L14503, doi:10.1029/2005GL023214, 2005.

Padman, L. and S. Erofeeva, A barotropic inverse tidal model for the Arctic Ocean, *Geophys. Res. Lett.*, 31(2), L02303, doi:10.1029/2003GL019003, 2004.

Pavlis, N. K., S. A. Holmes, S. C. Kenyon and J. K. Factor, The development and evaluation of the Earth Gravitational Model 2008 (EGM2008), J. Geophys. Res., 117, B04406, doi:10.1029/2011JB008916, 2012.

Petit, G. and B. Luzum (eds.), *IERS Conventions 2010*, IERS TN-36, 2010.

Pfeffer, W. Tad, Anthony A. Arendt, Andrew Bliss, Tobias Bolch, J. Graham Cogley, Alex S. Gardner, Jon-Ove Hagen, Regine Hock, Georg Kaser, Christian Kienholz, Evan S. Miles, Geir Moholdt, Nico Molg, Frank Paul, Valentina Radic, Philipp Rastner, Bruce H. Raup Justin Rich, Martin J. Sharp, and THE RANDOLPH CONSORTIUM, 2014, The

Randolph Glacier Inventory: a globally complete inventory of glaciers. *Journal of Glaciology* **60**:537-552,

Phillips, H. A., J. R. Ridgway, J.-B. Minster, D. Yi, and C. Bentley, 1999, Tidal Corrections, ICESat GLAS ATBD Version 2

Stammer, D & 26 others, Accuracy Assessment of Global Ocean Tide Models, *Rev. Geophys. 52*, 243-282, doi:10.1002/2014RG000450, 2014.

Tapley, B. D. and M-C. Kim, Applications to Geodesy, Chapt. 10 in *Satellite Altimetry and Earth Sciences*, ed. by L-L. Fu & A. Cazenave, Academic Press, pp. 371-406, 2001.

Topex/Poseidon (T/P) User's Handbook, Version 2.0, July 30, 1997, JPL D-1007 http://woce.nodc.noaa.gov/wocev3/wocedata2/satsl/topex/docs/html/usrtoc.htm

Wessel, P., and W. H. F. Smith, A Global Self-consistent, Hierarchical, High-resolution Shoreline Database, *J. Geophys. Res.*, 101, 8741-8743, 1996.

Zwally, H. J. et al, ICESat's laser measurements of polar ice, atmosphere, ocean, and land, *J. Geodyn.*, 34, 405-445, 2002.

Glossary/Acronyms

AN	Ascending node
ASAS	ATLAS Science Algorithm Software
ATBD	Algorithm Theoretical Basis Document
ATLAS	ATLAS Advance Topographic Laser Altimeter System
BP	Bounce point
CF	Center-of-Figure
CM/CoM	Center of Mass
CM	Configuration Manager
DAAC	Distributed Active Archive Center
DAC	Dynamic Atmospheric Correction
DEM	Digital Elevation Model
DOT	Dynamic Ocean Topography
ECF	Earth-centered, fixed
ECEF	Earth-centered, Earth-fixed
ECMWF	European Center for Medium-Range Weather Forecasts
ENU	Easting, Northing, Up
EOSDIS	Earth Observing System Data and Information System
GEUS	Geological Survey of Denmark and Greenland
GLAS	Geoscience Laser Altimeter System
GLIMS	Global Land Ice Measurements from Space
GPS	Global Positioning System
GSFC	Goddard Space Flight Center

GMAO	Global Modeling and Assimilation Office
GMT	Greenwich Mean Time
GOCE	Gravity field and steady-state Ocean Circulation Explorer
GSHHG	Global Self-consistent, Hierarchical, High-resolution Geography database
GT	Ground Tracks
HDF	Hard Data Format
IB	Inverted Barometer
IBCAO	The International Bathymetry Chart of the Arctic Ocean
ICESat-2	Ice, Cloud, and Land Elevation Satellite-2
IDL	Interactive Data Language
IERS	International Earth Rotation and Reference Systems
ITRF	International Terrestrial Reference Frame
JPL	Jet Propulsion Laboratory
MABEL	Multiple altimeter Beam Experimental Lidar
MDT	Mean Dynamic Topography
MIS	Management Information System
MOA	Mosaic of Antarctica
MOD44W	MODIS 250-m resolution water mask
MODIS	Moderate Resolution Imaging Spectroradiometer
MOG	Mosaic of Greenland
MOG2D	2 Dimensions Gravity Waves Model
MSS	Mean Sea Surface
NASA	National Aeronautics and Space Administration

NCEP	National Center for Environmental Prediction
NSIDC	National Snow and Ice Data Center

OMCT	Ocean Model for Circulation and Tides
RFA	Request for Action
RGI	Randolph Glacier Inventory
RGT	Reference Ground Track
POD	Precision Orbit Determination
PPD	Precision Pointing Determination
PSO	ICESat-2 Project Science Office
QA	Quality Assessment
RGI	Randolph Glacier Inventory
RGT	Reference Ground Track
SCoRe	Signature Controlled Request
SDMS	Scheduling and Data Management System
SIPS	ICESat-2 Science Investigator-led Processing System
SLA	Sea Level Anomaly
SLP	Sea level pressure
SLR	Satellite Laser Ranging
SNR	Signal to Noise Ratio
SPD	Start Pulse Detector
SSH	Sea Surface Height
SSMI/SMMR	Special Sensor Microwave / Imager; Scanning Multichannel Microwave Radiometer

TBD	To Be Determined
TEP	Transmitter echo pulse
TMR	TOPEX Microwave Radiometer
TOPEX	Topography Experiment
UNSO	United States Naval Observatory
UTC	Coordinated Time Universal
UTM	Universal Transverse Mercator
WFF	Wallops Flight Facility
WGS-84	World Geodetic System - 1984